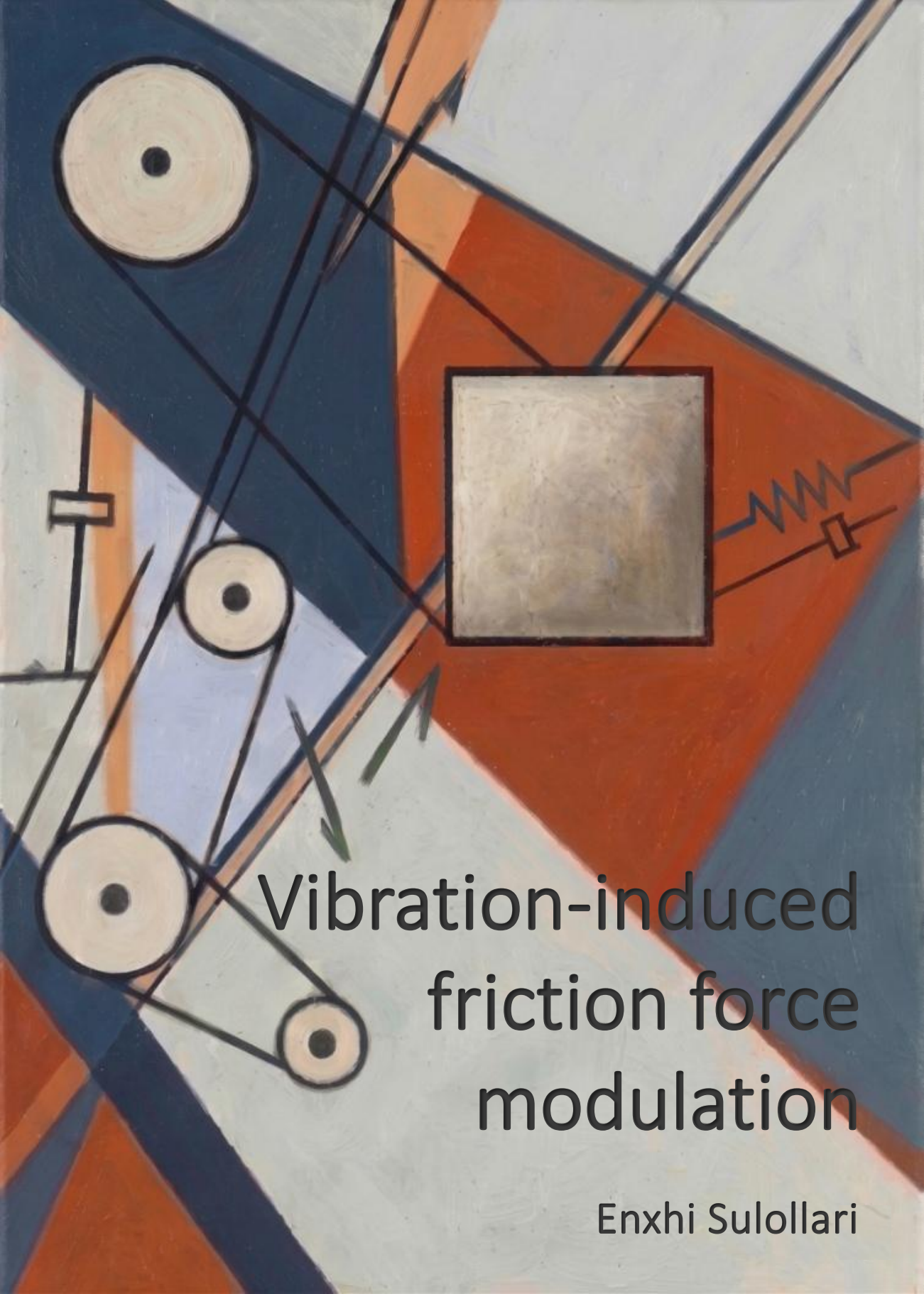

Vibration-induced friction force modulation

Enxhi Sulollari

Vibration-induced friction force modulation

Vibration-induced friction force modulation

Dissertation

for the purpose of obtaining the degree of doctor
at Delft University of Technology
by the authority of the Rector Magnificus Prof. dr. ir. H. Bijl;
Chair of the Board for Doctorates
to be defended publicly on
Thursday 7 May 2026 at 12.30 pm

by

Enxhi SULOLLARI

This dissertation has been approved by the promoters.

Composition of the doctoral committee:

Rector Magnificus,	chairperson
Dr. ir. K. N. van Dalen,	Delft University of Technology, promotor
Dr. A. Cabboi,	Delft University of Technology, copromotor

Independent members:

Prof. dr. P. G. Steeneken,	Delft University of Technology, Netherlands
Dr. M. Wiertlewski,	Delft University of Technology, Netherlands
Prof. dr. N. Hoffmann,	Technische Universität Hamburg, Germany
Prof. dr. A. Le Bot,	École Centrale de Lyon, France
Prof. dr. Z. Li,	Delft University of Technology, Netherlands, reserve member

This thesis was made possible by Delft University of Technology.

Keywords: average friction, external excitation, stick–slip, nonlinear contact, friction–induced oscillations, negative damping, dynamic friction, stability analysis, numerical analysis

Printed by: Uitgeverij U2pi BV. – Den Haag

Front & Back: designed by E. Sulollari using A.I

ISBN 978 94 9343 783 8

An electronic version of this dissertation is available at
`https://repository.tudelft.nl/`.

Here's to friction, and to friction.
Without the one we would all slip away,
and without the other we seldom would.

A.J. Schaar

CONTENTS

SUMMARY

Friction is a phenomenon we encounter daily, often without noticing, except in moments of inconvenience: the slipperiness on a wet floor, the difficulty of pushing a heavy object or the squeak of a bicycle brake. Besides these familiar experiences, friction plays a vital role in natural systems, mechanical devices, transportation networks and other processes. For many of these processes, friction is essential, allowing them to operate safely. At the same time, it can cause inefficiency, wear, energy loss and unpredictable nonlinear behaviours. Due to these adverse effects, understanding and controlling friction has become a key focus in engineering and scientific research.

Traditionally, lubrication has been used to control and reduce friction. However, this approach has several drawbacks. Lubrication must be applied at the right time, and removing and replacing it when needed can be challenging. Moreover, lubricants raise sustainability concerns. They often leak into the environment, where their toxic, non-degradable, and persistent nature causes long-term ecological harm. Exploiting the effects induced by a deliberately applied oscillatory force is another method that can be used to alter friction forces. This flexible alternative can be considered as a form of lubrication that can be controlled and removed quickly by changing the amplitude and frequency of the oscillatory force. Experiments dating back to the 1950s have demonstrated that external vibrations, particularly ultrasonic, could significantly reduce friction forces, with the extent of reduction depending on factors such as excitation amplitude, frequency, and application direction. To understand the mechanism of vibration-induced friction force modulation, various modelling approaches have been developed, and analytical and numerical methods have been employed to deal with simple and complex systems or friction models.

Despite the experimental and practical evidence on vibration-induced friction force modulation, several important aspects remain insufficiently understood. Most existing studies focus on the effect of so-called high-frequency excitation, while the influence of factors such as the excitation phase, load application location, multiple simultaneous loads, and the ambiguous distinction between “high” or “low frequency” in relation to the system’s dynamic response remains inadequately addressed. Moreover, the existing literature focuses specifically either on the effect of applied vibration on friction or on the effect of friction in inducing self-excited vibrations, rarely addressing their coupled nature, the possibility that external vibrations may destabilise otherwise stable systems, or the effect self-excited vibrations have on modulating friction.

While the aspects mentioned are related to the characteristics of the external loads, the way the system is modelled, and its dynamic response also strongly influence friction modulation. Many studies considered the bodies in contact to be rigid, overlooking the role of system flexibility. Furthermore, instead of addressing the role and interplay of external loads and system dynamics, much of the existing research relies on systems

that use phenomenological models, which reproduce experimental results often through parameter calibrations. This focus risks neglecting the effect of structural and dynamic complexity of real-world systems on the friction force, limiting the generalisation of research findings and the predictive capabilities of existing models.

To this end, this dissertation aims to investigate the effect of external excitation on friction modulation by adopting a modelling strategy that increases system complexity without relying on overly complex friction laws. The research addresses this objective from multiple perspectives, focusing on both the properties of the applied excitation and the influence of system dynamics, while also considering the practical relevance of these effects. Specifically, it examines how excitation frequency relates to system dynamics, with an emphasis on clarifying the notion of "high frequency" in this context; how the phase, location and presence of multiple simultaneously applied loads influence the results and how linear and nonlinear contact properties, as well as system flexibility, contribute to friction modulation. In addition, the study explores the coupled friction-vibration interaction by assessing whether external excitation can destabilise stable systems and how such instabilities affect friction modulation. Finally, the work bridges theoretical modelling and experimental observations by embedding the analysed systems in real-life scenarios.

The dissertation begins with an overview of the current state of knowledge on friction–vibration interaction, presented in Chapter 2. The chapter first introduces a broad range of examples, from natural phenomena to industrial applications, followed by a review of experimental evidence and modelling approaches within these contexts. It concludes with a detailed discussion of the research gaps and objectives, highlighting the specific contributions of this work to the field. The chapters that follow present the core research contributions. Chapter 3 investigates vibration-induced friction modulation for a general frequency of excitation, using an extended version of the Method of Direct Separation of Motions, applied to both 1-DOF and 2-DOF systems. Building on this, Chapter 4 examines the influence of transverse stiffness in friction modulation through combined tangential and transverse loading, with results compared against analytical predictions and experimental studies. Chapter 5 introduces a nonlinear Hertz-Damp contact model within the 2-DOF framework, showing how normal–tangential coupling and external excitation lead to parametric excitation and friction-induced oscillations, and how the latter affects friction modulation. Chapter 6 shifts the focus to a moving oscillator in contact with an elastic rod, analysing how support flexibility and excitation influence friction modulation and connecting the findings to vibration-assisted decommissioning tests and experimental studies. Finally, Chapter 7 summarises the conclusions drawn, and suggests potential paths for extending the study in terms of both theoretical advancements and practical applications.

SAMENVATTING

Wrijving is een fenomeen dat we dagelijks tegenkomen, vaak onopgemerkt, behalve op momenten van ongemak: de gladheid van een natte vloer, de moeite van het verplaatsen van een zwaar voorwerp of het piepen van een fietsrem. Naast deze vertrouwde ervaringen speelt wrijving een cruciale rol in natuurlijke systemen, mechanische apparaten, transportnetwerken en andere processen. Voor veel van deze processen is wrijving essentieel om ze veilig te laten functioneren. Tegelijkertijd kan het leiden tot inefficiëntie, slijtage, energieverlies en onvoorspelbaar niet-lineair gedrag. Vanwege deze nadelige effecten is het begrijpen en beheersen van wrijving een belangrijk aandachtspunt geworden in de techniek en wetenschappelijk onderzoek.

Traditioneel worden smeermiddelen gebruikt om wrijving te beheersen en te verminderen. Deze aanpak heeft echter verschillende nadelen. Smeermiddelen moeten op het juiste moment worden aangebracht, en het verwijderen en vervangen ervan kan een uitdaging zijn. Bovendien roepen smeermiddelen vragen op over duurzaamheid. Ze lekken vaak in het milieu, waar hun toxische, niet-afbreekbare en persistente aard langdurige ecologische schade veroorzaakt. Het benutten van effecten veroorzaakt door een doelbewust aangebrachte oscillerende kracht is een andere methode die kan worden gebruikt om wrijvingskrachten aan te passen. Dit flexibele alternatief kan worden beschouwd als een vorm van smering die controleerbaar is en snel kan worden verwijderd door de amplitude en frequentie van de oscillerende kracht aan te passen. Experimenten die teruggaan tot de jaren vijftig hebben aangetoond dat externe trillingen, met name de ultrasone, de wrijvingskrachten aanzienlijk kunnen verminderen, waarbij de mate van reductie afhangt van factoren zoals excitatie-amplitude, frequentie en de richting van de belasting. Om het mechanisme van trillingsgeïnduceerde wrijvingsmodulatie te begrijpen, zijn verschillende modelleringsbenaderingen ontwikkeld, waarbij analytische en numerieke methoden zijn ingezet om eenvoudige en complexe systemen of wrijvingsmodellen te analyseren.

Ondanks het experimentele en praktische bewijs voor trillingsgeïnduceerde wrijvingsmodulatie, blijven verschillende belangrijke aspecten onvoldoende begrepen. De meeste bestaande studies richten zich op het effect van zogenaamde hoogfrequente excitatie, terwijl de invloed van factoren zoals de excitatie-fase, de locatie van de belasting, meerdere gelijktijdige belastingen en het ambigue onderscheid tussen “hoge” of “lage frequentie” in relatie tot de dynamische respons van het systeem onvoldoende aan bod komen. Bovendien richt de bestaande literatuur zich specifiek op ofwel het effect van aangebrachte trillingen op wrijving, ofwel op het effect van wrijving bij het induceren van zelfgeëxciteerde trillingen. De gekoppelde aard hiervan wordt zelden behandeld, evenals de mogelijkheid dat externe trillingen anderszins stabiele systemen kunnen destabiliseren, of het effect dat zelfgeëxciteerde trillingen hebben op het moduleren van wrijving.

Hoewel de genoemde aspecten verband houden met de kenmerken van de externe belastingen, hebben ook de manier waarop het systeem wordt gemodelleerd en de bijbehorende dynamische respons een sterke invloed op de wrijvingsmodulatie. Veel studies beschouwen de lichamen in contact als star, waarbij de rol van systeemflexibiliteit over het hoofd wordt gezien. Bovendien vertrouwt veel van het bestaande onderzoek, in plaats van de rol en wisselwerking tussen externe belastingen en systeemdynamica aan te pakken, op systemen die gebruikmaken van fenomenologische modellen, die experimentele resultaten vaak reproduceren via parametercalibraties. Deze focus brengt het risico met zich mee dat het effect van structurele en dynamische complexiteit van systemen op de wrijvingskracht wordt verwaarloosd, wat de generalisatie van onderzoeksresultaten en het voorspellende vermogen van bestaande modellen beperkt.

Hiertoe beoogt dit proefschrift het effect van externe excitatie op wrijvingsmodulatie te onderzoeken door een modelleringsstrategie te hanteren die de systeemcomplexiteit verhoogt zonder te vertrouwen op overmatig complexe wrijvingswetten. Het onderzoek benadert dit doel vanuit meerdere perspectieven, waarbij de focus ligt op zowel de eigenschappen van de toegepaste excitatie als de invloed van de systeemdynamica, terwijl ook de praktische relevantie van deze effecten in overweging wordt genomen. Concreet wordt onderzocht hoe de excitatiefrequentie zich verhoudt tot de systeemdynamica, met de nadruk op het verduidelijken van het begrip "hoge frequentie" in deze context; hoe de fase, locatie en aanwezigheid van meerdere gelijktijdig toegepaste belastingen de resultaten beïnvloeden en hoe lineaire en niet-lineaire contacteigenschappen, evenals systeemflexibiliteit, bijdragen aan wrijvingsmodulatie. Daarnaast verkent de studie de gekoppelde wrijving-trilling interactie door te beoordelen of externe excitatie stabiele systemen kan destabiliseren en hoe dergelijke instabiliteiten de wrijvingsmodulatie beïnvloeden. Ten slotte slaat het werk een brug tussen theoretische modellering en experimentele waarnemingen door de geanalyseerde systemen in realistische scenario's te plaatsen.

Het proefschrift begint met een overzicht van de huidige stand van de kennis over wrijving-trilling interactie, gepresenteerd in Hoofdstuk 2. Het hoofdstuk introduceert eerst een breed scala aan voorbeelden, van natuurverschijnselen tot industriële toepassingen, gevolgd door een overzicht van experimenteel bewijs en modelleringsbenaderingen binnen deze contexten. Het sluit af met een gedetailleerde bespreking van de kennishiaten en de onderzoeksdoelstellingen, waarbij de specifieke bijdragen van dit werk aan het vakgebied worden belicht. De hoofdstukken die volgen presenteren de kernbijdragen van het onderzoek. Hoofdstuk 3 onderzoekt trillingsgeïnduceerde wrijvingsmodulatie voor een algemene excitatiefrequentie, gebruikmakend van een uitgebreide versie van de "Method of Direct Separation of Motions", toegepast op systemen met 1 of 2 vrijheidsgraden. Voortbouwend hierop beschouwd Hoofdstuk 4 de invloed van transversale stijfheid bij wrijvingsmodulatie door gecombineerde tangentiale en transversale belasting, waarbij de resultaten worden vergeleken met analytische voorspellingen en experimentele studies. Hoofdstuk 5 introduceert een niet-lineair Hertz-Damp contactmodel binnen het 2 vrijheidsgraden raamwerk, waarbij wordt aangetoond hoe normaal-tangentiale koppeling en externe excitatie leiden tot parametrische excitatie en door wrijving geïnduceerde trillingen, en hoe dit laatste de wrijvingsmodulatie beïnvloedt. Hoofdstuk 6 verlegt de focus naar een bewegende oscillator in contact met een elastische staaf, waarbij wordt

geanalyseerd hoe de flexibiliteit van de ondersteuning en excitatie de wrijvingsmodulatie beïnvloeden, en waarbij de bevindingen worden gekoppeld aan trillingsgeassisteerde ontmantelingstests en experimentele studies. Ten slotte vat Hoofdstuk 7 de getrokken conclusies samen en worden de vervolgmogelijkheden benoemd voor deze studie, zowel op het gebied van theoretische vooruitgang, als op de praktische toepassingen.

PREFACE

This dissertation chronicles the evolution of my PhD journey, a journey that, a long time ago, I wanted to take because others thought I should, that some years later I hesitated to start because I wasn't certain, and that I eventually embarked upon and have now reached its end. As often happens at the end of a journey, I look back now to before its beginning: to my time as a student. While there were various fields I explored that didn't quite hold my interest, there was one that always resonated with me: Dynamics. I loved dynamics not only because of its use in engineering, but because it relates to everything around us, the rhythm of a heartbeat, the sway of a tree, the cadence of music, our whole world. This PhD gave me the chance to encounter another omnipresent force: Friction.

As I embarked on this journey, I came across the intricate, often stubborn and unstable dialogue between motion and resistance, specifically pursuing a better understanding of vibration-induced friction modulation. One might expect that this modern dissertation would delve into the quantum interaction of surfaces in contact or involve high-tech measurement systems, but the path I followed was a bit different. There is perhaps a bit of irony in the fact that, five centuries after Leonardo da Vinci[1] sketched a mass on an inclined plane to understand the nature of resistance, I spent a good part of my research also studying a mass, now over a moving belt. I watched as harmonic loads of different frequencies and directions acted on this mass, I saw single-degree-of-freedom systems transform into multi-degree-of-freedom ones, I even encountered the mass oscillating over a continuous body, all while witnessing how the resistance transformed its value and shape under these shifting dynamics. What's more, I often experienced plenty of friction outside my models: with myself, with others, and simply with the unpredictable nature of life. While the road branched into others, some of which are not even described in this dissertation, the main path remained focused on investigating the effect of external loads on the friction force by adopting a modelling strategy that increases complexity without resorting to overly complex friction laws. Some paths compared my results to those of existing experimental studies, while others explored the implications of these findings in relation to various industrial applications.

As you move through these chapters, dear reader, I hope you find some answers amidst the many questions that arise. May the findings presented here serve not only as a collection of results, but also as a catalyst for new ways of thinking about how we overcome the obstacles in our path, turning the very forces that slow us down into the drivers that set us in motion.

Enxhi Sulollari
Delft, March 2026

[1] A salute to the cover letter I wrote for this PhD position, where Da Vinci first appeared, bringing the journey full circle.

1

INTRODUCTION

"No one could say why a thing in motion should stop anywhere; for why should it stop there rather than here? So that a thing will either be at rest or must be moved ad infinitum, unless something more powerful gets in its way."

Aristotle raised these fundamental questions in his book Physics around 300 BC [1]. Friction, however, has been a topic of curiosity and technological attention long before the dawn of science, though the earliest exploitations of the awareness of friction were not accompanied by scientific explanation. Perhaps the earliest and most significant of such explorations was the advent of fire-making, which was achieved by scratching or knocking flint on pyrite and by rubbing wood. In the periods that followed, key historical milestones included the development of tools, sledges, and the wheel, with friction awareness influencing human evolution and societal progress. While essential for many technologies, friction has also presented significant disadvantages. For example, the friction surfaces in mechanical products play a decisive role in the equipment's efficiency, noise, accuracy, corrosion, reliability, and life. According to statistics, friction causes 30 % of primary energy waste worldwide [2](see Fig. 1.1). The most significant quantities of energy are used by industry and in transportation. Recent studies on energy use on the latter stated that saving as much as 17.5 % of the energy used in road transport in the short term (5 - 9 years) is possible by implementing new tribological solutions. These numbers equal annual energy savings of 11.6 exajoules, fuel savings of 330 billion litres and a reduction in CO_2 emissions by 860 million tonnes [3]. Such figures represent the energy that drives nations, the fuel that powers daily life, and the emissions that challenge global climate efforts. Therefore, understanding and controlling friction is not just a technical challenge; it is a societal necessity with broad economic and environmental impacts.

1.1. BACKGROUND AND CONTEXT

Controlling and reducing friction has commonly been done through lubrication, which improves the performance and adds value in terms of cost savings and expenses arising from wear and tear, repair, and maintenance of parts in contact. However, timely lubrication is required to ensure the proper functioning of tools, automotive and machines, and removing and replacing the lubricant (if needed) can be challenging. In some other

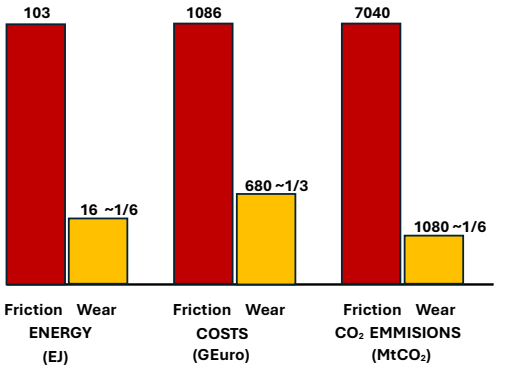

Figure 1.1: Energy consumption, costs and CO2 emissions due to friction and wear globally. Adopted from [4].

cases, it might not even be possible to remove and replace lubricant materials within the inaccessible confines of a contact. Another downside of lubricants is that they are not sustainable. It is almost impossible to avoid lubricants leaking into the environment. In general, 20% – 40% of them enter into the environment with altered appearance and physical properties [5]. Thus, lubricants can pose environmental concerns as they can be toxic, non-degradable and persistent in ecosystems, leading to long-term ecological harm.

Exploiting the effects induced by a deliberately applied oscillatory force is another method to alter friction forces. This flexible alternative can be considered as a form of lubrication that can be controlled and removed very quickly by changing the amplitude and frequency of the oscillatory force. Similar to the case of lubricants, the application of an oscillatory source to alter friction forces has its disadvantages as well. An additional power source is needed to apply the external vibration, meaning more energy needs to be spent. Moreover, the vibration can affect the system dynamics and even cause surface fatigue and wear. Despite the drawbacks, this technique can be practically efficient if designed and optimised while accounting for the additional energy required for the applied excitation.

The effect of vibrations on friction forces has been observed from early experiments dating back to the 1950s. The results of experimental investigations demonstrated that the friction forces could be significantly reduced under the effect of external vibrations, more specifically ultrasonic vibrations, with some studies reporting reductions approaching even zero [6]. Later on, the effect of excitations acting tangentially or normally on both static and kinetic friction was investigated, with the results of friction change shown to depend on factors such as excitation amplitude, frequency, and application direction [7, 8, 9, 10]. To understand the mechanism of vibration-induced friction force modulation, various modelling approaches have been developed, with simple models often based on Amonton-Coulomb's law. These simple models, typically solved analytically, can

sometimes overestimate results because they neglect dynamic effects. Therefore, more complex systems, or those with complicated friction laws, are considered and analyzed using numerical methods.

The interaction between friction and vibration is observed not only experimentally but also in nature, where it aids, for example, in insect locomotion and also in phenomena like fault slips, where vibrations can reduce frictional resistance and trigger earthquakes. The principle of friction reduction is also applied in different industrial fields, such as metal forming processes like wire drawing and forging [11], where ultrasonic oscillations help in reducing forming forces and improving surface quality. It is also utilised for positioning control in robotics and medical procedures like vibration-assisted needle insertion [12], ultrasonic friction-modulating catheters [13], and in the offshore industry for gentle pile driving [14], installation, and decommissioning of slip joints in wind turbines [15], see Fig. 1.2. Conversely, the unintentional presence of vibrations can lead to issues like the self-loosening of bolts in engineering applications [16].

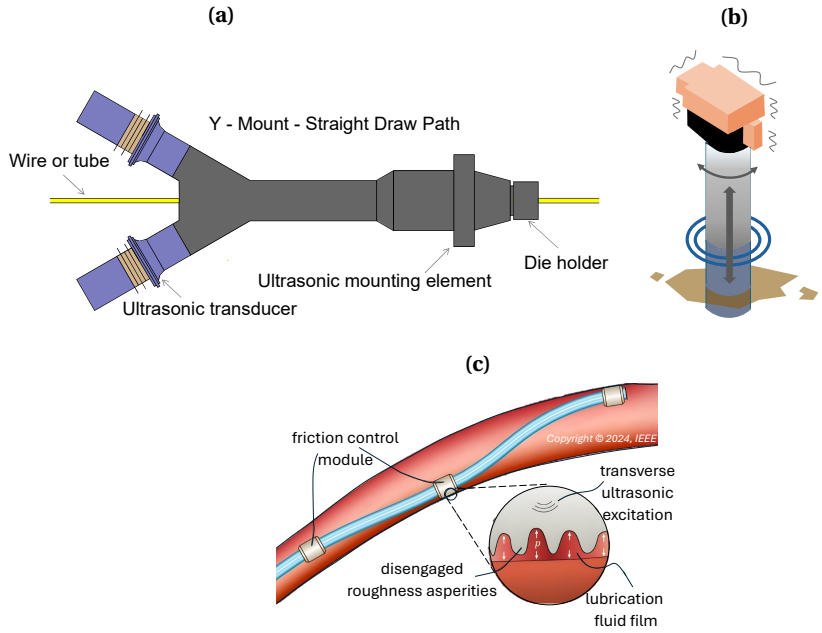

Figure 1.2: Vibration-assisted friction modulation examples in applications: (a) ultrasonic metal drawing; (b) gentle pile driving; (c) ultrasonic friction-modulating catheter. Images adopted from: Aktive Arc Ultrasonics, Grow to Go, and from [13], respectively.

The relationship between friction and vibrations is interactive and coupled. While vibrations modulate the friction force, the friction force can influence the vibrational response. With reference to the latter, several mechanisms have been identified experimentally as drivers of friction-induced vibrations, some of which include the decreasing friction force with increasing relative sliding velocity (creating a negative damping effect), sprag-slip, mode coupling and the presence of a follower force [17, 18, 19, 20, 21]. Both

analytical and numerical models are used to study these mechanisms, which, similar to the vibration-induced friction modulation case, appear in natural systems, like insect stridulation and aquatic courtship songs, and in industry, where they can cause issues such as brake squeal, chatter, and surface damage. Considering these examples, it is therefore relevant to study the mutual interaction between friction and vibrations to better understand, predict, and control their effects in various systems.

1.2. RESEARCH OBJECTIVE

Friction-vibration interaction presents complex dynamic behaviours that are crucial to understand for both the advancement of practical applications and the proper interpretation of experimental investigations. Despite the experimental and practical evidence on the effect of vibration on friction, several important aspects remain insufficiently understood. This section first outlines these knowledge gaps, followed by the formulation of the research objective.

In existing research, investigations on the effect of vibrations on the friction force often overlook several critical factors. When it comes to the characteristics of the external excitation, most existing studies focus on the effect of so-called high-frequency excitation applied in a certain direction. However, important aspects such as the influence of the applied excitation phase and application location, the effect of multiple simultaneous external loads, the ambiguous characterisation of excitation frequency as “high" or “low frequency", as well as the relation of these frequencies to the system’s dynamic response remain insufficiently addressed. Moreover, while the relationship between friction and vibrations is coupled, the existing literature focuses specifically either on the effect of applied vibration on friction or on the effect of friction in inducing self-excited vibrations. The possibility that such external vibrations may destabilize otherwise stable systems and the self-excited vibration’s effect on changing friction is rarely addressed.

While the aspects discussed so far are primarily related to the characteristics of the external loads, the way the system is modelled and its dynamic response also play a crucial role in the change of friction due to external excitation. In this regard, many studies considered the bodies in contact to be rigid, an idealization that may fail to capture essential dynamic interactions. The presence of system stiffnesses (e.g., directional stiffnesses in discrete models) as well as the consideration of flexible bodies in contact (deformability in continuous models) are also aspects that are not adequately explored. Furthermore, instead of addressing the role and interplay of external loads and system dynamics, much of the existing research relies on systems that use phenomenological models (e.g. Stribeck, Dahl, Dupont models). While such models have shown to reproduce experimental results with good accuracy, these agreements typically require parameter calibrations. Thus, the focus on sophisticated friction laws often overlooks the effect of the real-world systems’ structural and dynamic complexity on the friction force, which may lead to inaccurate or misleading interpretations. These limitations hinder the generalisation of research findings and limit the predictive capabilities of existing models, especially in experimental or industrial settings.

To this end, this dissertation aims to address the identified research gaps with its main objective being:

To investigate the effect of external excitation on changing the friction force by adopting a modelling strategy that increases system complexity without resorting to overly complex friction laws.

This objective is pursued by examining the problem from multiple perspectives, focusing on both the properties of the external excitation and the effect of system dynamics on the change of the friction force, while also considering the relevance of these effects in practical scenarios. To achieve this, the research is structured around four main aspects:

(1) In terms of the system dynamics, this work aims to investigate how linear and nonlinear contact properties (through their impact on the system dynamics), as well as system flexibility, contribute to friction change.

(2) With regard to excitation properties, the aim is to examine how the phase and location of the applied load affect friction change and to clarify the relationship between excitation frequency and dynamic system response, including a more precise characterisation of "high frequency" in this context.

(3) Furthermore, this study seeks to explore friction-vibration interaction by investigating the potential of external excitation in destabilising initially stable systems and understanding how such instabilities affect friction forces.

(4) Lastly, the work aims to bridge the gap between theoretical models and existing experimental observations by embedding the analysed systems in the context of real-life scenarios.

Finally, as the main focus of this work is investigating the effect of vibration on changing friction forces, it is important to describe what is meant by friction change. The calculation of the friction change in this study is based on the averaging approach already adopted in the literature. Specifically, the effect of vibration on friction force is evaluated by analysing the variation of friction force over one period of oscillation. In the systems considered in this study, governed by Amonton-Coulomb's law, the friction force variation corresponds to a reversal in direction depending on the sign of the relative velocity. This variation is integrated over the cycle of oscillation, resulting in the averaged friction force. It should be noted that in this work, the terms average friction and effective friction describe the same concept and are used interchangeably. The same applies to the terms friction change and friction modulation, which are likewise used synonymously throughout the study.

Moreover, it is important to acknowledge that this modulation might not always lead to an actual friction reduction in real-world systems. For instance, as discussed in Popov's work, the system may remain confined within a single potential well even when oscillations are present, resulting in minimal or no change in macroscopic friction [22]. This observation highlights the importance of the characteristic slip length, a key length scale over which microscopic displacements can occur before macroscopic sliding begins. More specifically, this length is linked to the period of the interfacial interaction potential, which is the energy landscape that governs how asperities on two surfaces interact. When the oscillation amplitude is much smaller than the slip length, the contact points remain within a single potential well and the static friction is essentially unchanged. Amplitudes

comparable to or larger than the slip length allow the system to traverse multiple wells, and the static friction reduces [22]. Thus, while analytical and numerical analysis can predict vanishing friction under sufficient vibration amplitudes, some experimental results have shown that static friction may still persist. In this thesis, it is assumed that whenever the friction force changes direction and/or magnitude (averaged friction force is computed), a modulation of the friction force occurs. An investigation of the existence and identification of a hypothetical characteristic slip length is out of the scope.

1.3. RESEARCH SCOPE

The problem of friction-vibration interaction is inherently multidisciplinary, involving expertise from different research fields. The field of nonlinear dynamics, for example, is essential for analysing the complex system behaviours that arise from friction and vibration interaction. Material science contributes to understanding surface interaction, material properties and wear behaviour at contact interfaces. Acoustics becomes relevant when friction-induced vibrations lead to noise (e.g. squeal, squeak). Computational mechanics provides tools for performing finite element simulations, experimental mechanics plays a key role in designing, conducting and interpreting lab experiments, etc. Naturally, this dissertation addresses only a few of these aspects, and this subsection presents the chosen focus.

As stated in Section 1.2, this work investigates the effect of external excitation on friction modulation by adopting a modelling strategy that increases system complexity without resorting to overly complex friction laws. To explore how system dynamics influence friction modulation and how excitation frequency relates to the dynamic response, the study begins with the classic single-degree-of-freedom mass on moving belt model (1-DOF). For this system, vibration-induced friction modulation is investigated for a general frequency of excitation. Building on this foundation, 2-DOF models are introduced to increase system complexity by incorporating either normal or transverse contact stiffness, in addition to the tangential stiffness of the system. These models are subjected to loading in one or two directions, and the focus is on studying the effect of the loads and system stiffnesses on friction reduction by comparing the results to those of the classical 1-DOF model. Moreover, the 2-DOF system allows the investigation of friction-vibration interaction by examining how vibrations can destabilise otherwise stable systems and how resulting instabilities can, in turn, alter friction forces.

In addition to these discrete models, to investigate the influence of external excitation in the presence of support flexibility on friction modulation, this work considers a continuous system. Specifically, it examines a moving oscillator in frictional contact with an elastic rod of finite length subjected to distributed damping. Unlike the discrete models, where the load is always applied to the mass, the continuous system allows for loading either on the mass or on the rod. For the load-on-rod scenario, large deformations are observed close to and above resonance, and geometric nonlinearity is accounted for to accurately describe the system dynamics.

Regarding methodology, both analytical and numerical approaches are employed. Analytical methods offer the advantage of providing an explicit expression of friction change, revealing how system and excitation properties influence the results. However,

such analyses are only feasible for simple discrete systems (1-DOF and 2-DOF). For more complex systems (2-DOF and continuous), numerical simulations using MATLAB solvers are performed to study friction modulation.

For all the systems considered, Amontons-Coulomb's law is assumed. No experiments are conducted in this work, however, the results in terms of friction modulation obtained using different models and analytical and numerical methods are compared to related existing experimental and theoretical outcomes from the Dahl and Dupont models. The aim of the comparisons is to explore whether the presence of normal or transverse stiffness and that of support flexibility can reproduce experimental trends despite using Amontons-Coulomb's law. Finally, to link theoretical results to applications, the findings are used to qualitatively interpret vibration-assisted decommissioning tests on a slip-joint application. A visual representation of the research framework, including the aim and objectives, is provided in Fig. 1.3.

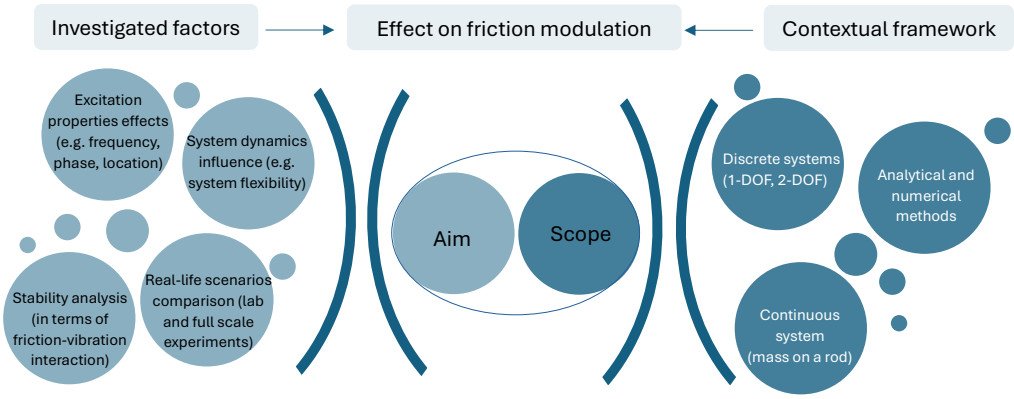

Figure 1.3: Visual representation of the research aim and scope.

Lastly, as mentioned in Section 1.1, friction is a major source of energy loss across various industries. It is important to acknowledge that, as this study investigates the effect of vibration on friction change, an additional power source is needed to apply the external vibration, meaning more energy needs to be spent. While this thesis does not determine the amount of energy needed to achieve friction modulation, practical implementations should consider the overall energy balance to ensure a net energy saving. A quantitative framework for this analysis can be derived from the energetic considerations established by Littmann and coworkers [23]. Their research indicated that the energy dissipated in the contact zone under vibration can be compared to the energy dissipated without vibration through an energetic coefficient which depends on the ratio of the macroscopic sliding velocity to the vibration velocity amplitude. The analysis of energetic considerations showed that, for certain velocity ratios, macroscopic friction can be reduced by 40%, while requiring less than 10% additional energy input. In contrast, achieving a more aggressive friction reduction up to 75% at lower velocity rations requires approximately 75% more energy. For cases where the macroscopic sliding velocity equals the vibration velocity amplitude, the dissipated energy with vibration is equal to the

energy dissipated without vibration; in this regime, no friction reduction occurs, but no extra energy is wasted in the contact zone. By identifying these specific regimes, it is possible to drive a system in a state that provides considerable friction reduction while avoiding excessive additional energy supply. It should be noted that while these specific calculations by Littmann and coworkers are validated for ultrasonic vibrations, a similar methodology can be applied to general frequencies of excitation.

1.4. THESIS OUTLINE

This thesis starts by providing an overview of the current state of knowledge related to friction-vibration interaction presented in Chapter 2. In this chapter, first, a plethora of examples on this interaction, ranging from natural phenomena to industrial applications, is presented. Then, a review on experimental evidence followed by modelling approaches in the context of applications and systems mentioned is given. Lastly, a more detailed discussion than in Section 1.2 on the research gaps and objectives is provided, highlighting the contribution of the work to the field.

Chapter 3 explores the vibration-induced effect on friction modulation using an extended version of the Method of Direct Separation of Motion (MDSM). The results obtained through this method are compared with those obtained by exploiting the velocity response function of the system. This analysis is conducted for two discrete systems: a 1-DOF and a 2-DOF system (with tangential and normal stiffness), both consisting of a mass on a moving belt and subjected to general excitation frequencies. In the 2-DOF system, loads are applied in both the normal and tangential direction and the influence of these loads and the choice of the normal contact force expression (including either inertia or damping-stiffness effects) is investigated. In this chapter and the rest of the thesis, the friction force is modelled using Amontons–Coulomb's law. This chapter has been published as: Sulollari, E., van Dalen, K.N., and Cabboi, A. (2024). Vibration-induced friction modulation for a general frequency of excitation. Journal of Sound and Vibration, 573, 118200.

Chapter 4 also considers a 2-DOF system, now incorporating stiffness in both the tangential and transverse directions. The influence of transverse stiffness on friction modulation is investigated by subjecting the system to combined tangential and transverse loading. The numerical results obtained in this chapter are compared to those obtained analytically from the 1-DOF system analysed in Chapter 3 and to existing experimental studies where complex friction models have been employed to align theoretical prediction with experimental observation. The work presented in this chapter has been expanded and published as: Sulollari, E., van Dalen, K.N., and Cabboi, A. (2026). On the effect of planar dynamics and resonance on vibration-induced friction modulation. International Journal of Non-Linear Mechanics, 187, 105362.

Chapter 5 builds upon the 2-DOF system introduced in Chapter 3 by employing a nonlinear Hertz-Damp contact model, while again considering external loads in both tangential and normal directions. The combined presence of the normal–tangential coupling through friction and of the external excitation results in a parametric excitation and triggers friction-induced oscillations. A numerical analysis is conducted to investigate the underlying mechanism driving these oscillations. Additionally, a linearised stability

analysis of the steady sliding state is employed to predict the bifurcation point as a function of system parameters and to identify conditions under which friction-induced oscillations occur. Lastly, the effect of the observed friction-induced oscillations on the friction modulation is studied and the results are qualitatively compared with findings from related experimental studies. This chapter has been published as: Sulollari, E., van Dalen, K.N., and Cabboi, A. (2025). Parametric excitation and friction modulation for a forced 2-DOF system. Nonlinear Dynamics, 113, 12793–12816.

Chapter 6 shifts the focus from discrete systems to a moving oscillator in frictional contact with an elastic rod of finite length subjected to distributed damping. This system allows the investigation of how external excitation, in combination with support flexibility, influences friction modulation. The study also compares the effect of applying the load on the mass versus on the rod, in terms of their effect on friction change. The results are compared to those obtained using the 1-DOF system analysed in Chapter 2. To link the findings to applications, they are used to qualitatively interpret slip-joint vibration-assisted decommissioning tests and are further compared with existing experimental results in which friction force reduction is explained through the use of elasto-plastic friction models that account for surface deformability. This chapter has been published as: Sulollari, E., van Dalen, K.N., and Cabboi, A. (2025). Vibration-induced friction modulation for an oscillator moving on an elastic rod. International Journal of Solids and Structures, 2025, 113572.

In the last chapter, Chapter 7, the conclusions drawn in this research are summarized, and several directions for future investigations are provided.

2

STATE OF THE ART

This chapter provides an overview of the current state of knowledge related to friction-vibration interaction. First, to illustrate the broader relevance of the topic, examples from nature and industry are provided. These examples lead into a discussion of the interactive and coupled relationship between friction and vibration. Vibrations modulate friction, and in turn, friction also influences vibrations. Therefore, following the introductory examples, the chapter is structured in two main sections: vibration-assisted friction modulation and friction-induced vibration. In each section, a review of the experimental evidence is first presented, followed by a discussion on the modelling approaches and solution methods within the context of the applications and systems mentioned. Each section concludes by identifying the research gaps, establishing the motivation for this dissertation, and highlighting its contribution to the field.

2.1. Applications: From nature to industry

To illustrate the ubiquity and importance of friction-vibration interactions, this chapter begins with examples drawn from nature and industry. Rather than acting as direct foundations for the present research, these cases highlight how the relations between friction and vibrations play an important role in a wide range of systems. From biological phenomena to engineered processes, these examples show how the coupling between friction and vibrations can lead to desired or disruptive effects. By presenting these cases, the aim is to illustrate the broader relevance of the topic and to suggest potential contexts where a deeper understanding of friction-vibration interaction, such as that pursued in this work, can be applied.

2.1.1. Natural phenomena

Deep in the leaf litter of a humid forest, tiny leaf-cutting ants harvest vegetation not with brute strength, but with rhythm and precision. These ants are one of the organisms that utilise vibration to harvest fresh vegetation that they use as food for symbiotic fungi. They have a special organ located in their gaster, which produces high-frequency vibrations. These vibrations lead to movements of the mandibles (at about 1000 hertz), and when tender leaves are cut, the vibrations appear to stiffen the material to be cut, reduce force fluctuations, ultimately allowing for a smoother cut to be made, Fig. 2.1(a). Thus, vibrations lower the cutting resistance during leaf cutting, resulting in reduced energy consumption and a smoother cutting process [1].

Microvibrations are observed on dolphin skin as well, and inspired by them, researchers have hypothesised that the microstructure on the dolphin skin is not static but dynamically oscillates in the form of Longitudinal Micro-Ultrasonic Waves (LMUWs) [2]. Dolphins have cutaneous ridges on their skin that are believed to reduce friction drag effectively. However, these skin ridges are aligned perpendicular to the swimming direction, an orientation that can generate additional drag, raising questions about how the forces generated due to the specific arrangement and structure of the ridges influence swimming performance overall. Building on the skin's characteristics, such as high sensitivity and flexibility [3, 4], as well as its acoustic behaviours, including the emission of high-intensity, ultrasonic-frequency click signals from the melon [5, 6], researchers proposed that skin oscillations, in the form LMUWs, exists on dolphin skin as shown in Fig. 2.1(b). These oscillations lead to a novel near-wall force distribution and flow pattern, presenting significant potential for reducing total drag (composed of both pressure and friction drag).

Plants also utilise oscillations which can play a crucial role in facilitating seed dispersal. An example of such behaviour is observed in tumbleweeds. By the onset of frost, these rounded-shaped plants break away from their roots and, with the wind's help, begin to roll. While the plant is dead, its thousands of seeds are mature and survive for months. As the tumbleweed rolls, it does not simply glide along the ground. Instead, it frequently bounces and jostles over uneven terrain. The bouncing motion and the vigorous tumbles help in reducing the friction between the seeds and their homes on the plant. When the seeds fall in an ideal location, they wait for favourable conditions to germinate.

The mechanism of friction modulation due to vibrations has been observed not only in living organisms but also in other natural systems such as fault slips. In fault zones,

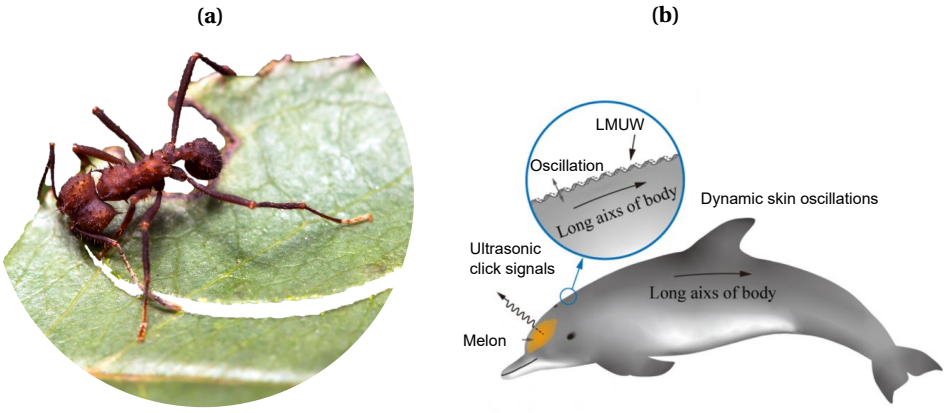

Figure 2.1: (a) Leaf-cutting ant using its vibrating mandibles to cut the leaf. Image credit: Rainforest Alliance; (b) Dynamic skin oscillations on dolphin skin, in the form of LMUWs. Reprinted from [2].

vibrations can lead to a significant reduction in frictional resistance, a phenomenon crucial for understanding events such as earthquake triggering. In 1979, Melosh was the first to propose that when a fault slips seismically, some of the energy released may excite strong, short-wavelength vibrations near the fault core [7]. Such vibrations can temporarily reduce the normal stress on the fault, allowing it to slip at lower shear stresses than predicted by laboratory coefficients of friction [7, 8]. This mechanism of frictional weakening by vibrations was further invoked to explain the remote triggering of earthquakes or the abnormally large runout of landslides or pyroclastic flows.

The preceding examples highlight the effect of vibration on friction. The relationship between friction and vibrations, however, is interactive and coupled with friction forces generating vibrations, and nature also offers its own friction-induced vibration examples. For instance, pleural and pericardial friction sounds or friction rubs are two forms of friction sounds developed in humans. Pleural friction rub occurs when the two layers of tissue lining the lungs become inflamed or when they lose the lubrication between them. When these inflamed tissues rub together, due to the presence of friction, a loud grating lung sound is generated, similar to the squeaking of a shoe on wet surfaces. These sounds can be heard during inspiration and expiration as they occur whenever the patient's chest wall is moving. Pericardial friction sounds are related to the cardiac cycle and are created similarly from the rubbing of inflamed tissues that surround the heart. These sounds are also often described as grating or scratching, and like the sound of sandpaper rubbed on wood.

While the friction sounds generated in humans are a sign of health issues, in the ecology of many insects across the globe, acoustics play a vital role in facilitating defence, information transfer, and mate finding. The sounds of grasshoppers and singing cicadas are familiar to many, yet insects can produce sounds that might not even be perceptible to human ears. The sound production mechanism in insects is called stridulation, which relies on friction-based processes. For stridulation to work effectively, many insects, like

crickets, grasshoppers and some beetle species, have two specialised body parts called a scraper and a file, each located in one of the insect's wings, Fig. 2.2(a). To generate the sounds, the scalper strikes the file, as shown in Fig. 2.2(b). The song's length and frequency depend on the morphological and mechanical structure of the body parts rubbing against each other and the speed at which the strikes are occurring [9]. Thus, every mating call within a species differs because the neuronal networks controlling the process vary between individuals [10]. Terrestrial insects and animals are not the only ones producing sounds. Many aquatic species also produce a variety of sounds. The water boatman Micronecta scholtzi, for example, produces courtship songs to attract mates by rubbing a scraper against a ridge on its body. Despite the small size, the sound generated is extremely loud, up to 100 dB SPL at 1 m [11].

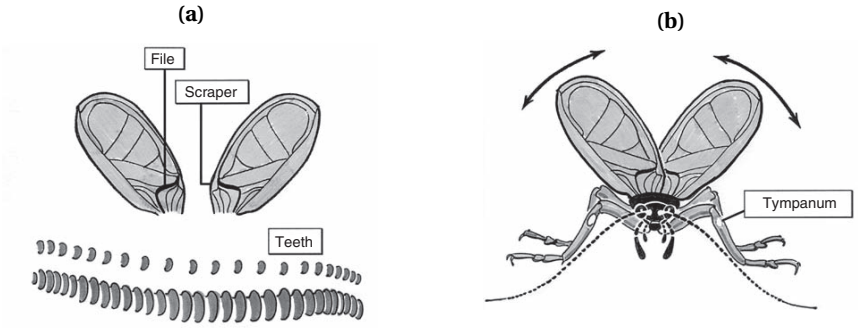

Figure 2.2: (a) The scraper is on the right wing and the file on the left wing; (b) The wings move back and forth, causing the file to strike the scraper. Reprinted from [12] with permission from Elsevier.

Similar friction sounds can also be observed in non-biological systems within nature, such as the creaking of glaciers, the humming of sand dunes and the grinding of tectonic plates. Some of these sounds constituted nature's most puzzling phenomena and have been the subject of art, poetry, legends and desert folklore for centuries. For instance, in the 13th century, the explorer Marko Polo witnessed strange noises on his journey through the Gobi desert and described them as voices of evil spirits that "at times fill the air with the sounds of all kinds of musical instruments, and also of drums and the clash of arms" [13]. Charles Darwin also mentioned these sand sounds in his classic Voyages of the Beagle [14]. Two types of sand produce sound when the grains rub past one another. The most common sand type, known as whistling sand, can be found at numerous lake shores, riverbeds and beaches across the world and produces a short, high-frequency (500 – 2500 Hz) squeak when sheared. The rarer type called booming sand occurs in large isolated dunes in deserts and produces long, low-frequency (typically 50 – 300 Hz) sounds upon avalanching. The difference in the sounds generated by booming and whistling sand is a result of several physical properties, including the surface roughness, the sphericity of the grains and the looseness of their packing [15].

2.1.2. INDUSTRIAL APPLICATIONS

As is often the case, engineering systems draw inspiration from nature, with mechanisms observed in natural systems adapted for engineering applications. For instance, similar to leaf-cutting ants using high-frequency vibrations to lower the cutting resistance during leaf cutting, ultrasonic vibrations are used to cut paper sheet stacks in the print and paper industry. The same mechanism is used in metal cutting, drawing and forming, positioning control in robotics, pile driving and decommissioning in the offshore industry, vibration-assisted needle insertion in the medical field, and the development of touch-sensitive interfaces. In these applications, vibrations are intentionally applied and controlled; however, there are scenarios where unintentional vibrations result in friction reduction, such as in the self-loosening of bolts. Moreover, as illustrated in the nature-related examples, the relationship between friction and vibration is coupled, and friction itself can generate vibrations. Examples include machining chatter and squeal generated by the wheel-rail interaction. This section provides a more detailed exploration of these examples, illustrating how vibrations and friction interact in engineering systems.

In metal forming processes, the application of ultrasonic oscillating has shown to reduce the forming forces, reduce the friction between the die and the workpiece and achieve higher form precision and better surface qualities [16]. In 1953, Garskii and Efromov were the first to use ultrasonic or vibrational energy on metals [17]. Blaha and Langenecker followed in 1955 and observed a considerable stress reduction as a result of ultrasound in a drawing experiment [18]. After that, several studies were conducted, and different techniques were used to excite the die. In some cases in tube and wire drawing, the die was excited longitudinally, in others, the die was excited in a radial mode, with some examples of ultrasonics applied to metal forming processes shown in Fig. 2.3. Furthermore, the influence of varying the vibration direction has been studied. If the vibration direction is parallel to the drawing direction, the influence on the friction force is the greatest. If the vibration direction is perpendicular to the drawing direction, the influence is greatest on the forming properties of the workpieces [16].

The effect of vibrations on friction has been utilised in the medical field as well, such as in vibration-assisted needle insertion. Wenhao and colleagues explored this technique in deep brain stimulation of the subthalamic nucleus surgery, a treatment proven to improve motor symptoms of movement disorders like Parkinson's disease [20]. This surgical procedure must satisfy the highest accuracy and safety standards to improve patients' postoperative life quality. An important source of error in the needle insertion procedure is the deformation of the soft tissue that occurs as the needle is inserted. The main factor affecting the degree of tissue damage and the accuracy of target location is the friction between the tissue and the needle shaft. In their work, Wenhao and colleagues investigated the influence of longitudinal vibration on the friction force during needle insertion under different vibration parameters. The experiments conducted showed that the vibration can change the friction force by affecting the equivalent friction coefficient, and the cause of the decrease in the equivalent friction coefficient is the change of relative velocity in vibration.

Another field where the effect of vibrations is leveraged is the offshore industry, particularly in slip joint applications, Fig. 2.4(a). In essence, a slip joint for wind turbines enables the connection between the monopile and the transition piece by simply overlapping the

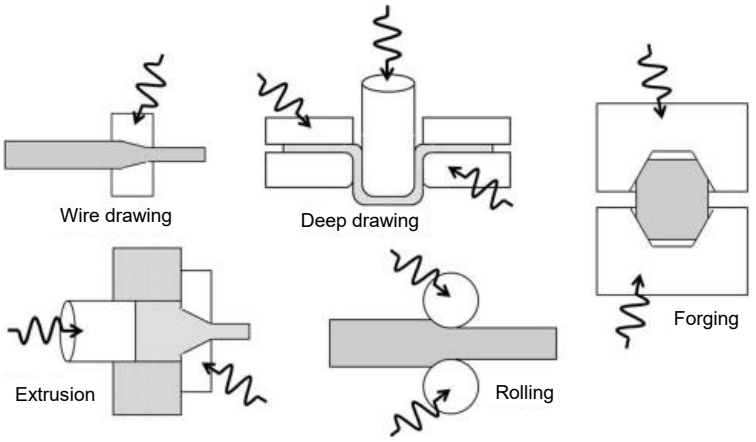

Figure 2.3: Ultrasonics applied to metal forming processes. Reprinted from [19] with permission from Elsevier.

two cylindrical structures. The entire connection relies on the frictional forces between the two surfaces in contact. In the first study of Cabboi and coworkers on the slip joint application, the effectiveness of applying a harmonic excitation during the installation and decommissioning procedure was experimentally investigated using a 1:10 scaled model of the slip joint [21]. In a follow-up study, the vibration-assisted decommissioning of the slip joint was applied to a full-scale wind turbine. In both studies, the load was applied in either horizontal or vertical direction utilising a shaker, whereas the static pushing load was applied at the top cone [22]. The results of the tests performed during the experimental campaigns showed that settlements were observed for excitation frequencies that, in general, corresponded well with the identified natural frequencies.

Remaining in the offshore field, vibrations are also utilised in the Gentile Driving of the Piles (GDP) process, a new vibratory technology for the installation of tubular monopiles, Fig 2.4(b). During the installation process, low-frequency axial and high-frequency torsional vibrations are applied simultaneously to achieve high installation performance, reduced underwater noise emissions, and reduced overall driving loads required to install the pile. In their study, Tsetas and coworkers conducted a medium-scale onshore field campaign to demonstrate the concept of GDP experimentally and showcase the potential of the method in terms of installation and post-installation performances [23]. They studied the driving process numerically as well, to further comprehend the mechanics of the method, by considering a novel pile-soil method. The comparison of the experimental data and numerical results highlighted the potential of the numerical framework for analysing the GDP. Lastly, the mechanics of the installation process were analysed, revealing that the redirection of the friction force vector, driven by high-frequency torsion, is the primary mechanism behind GDP.

Vibration-induced friction change is also leveraged in the field of surface haptics, which

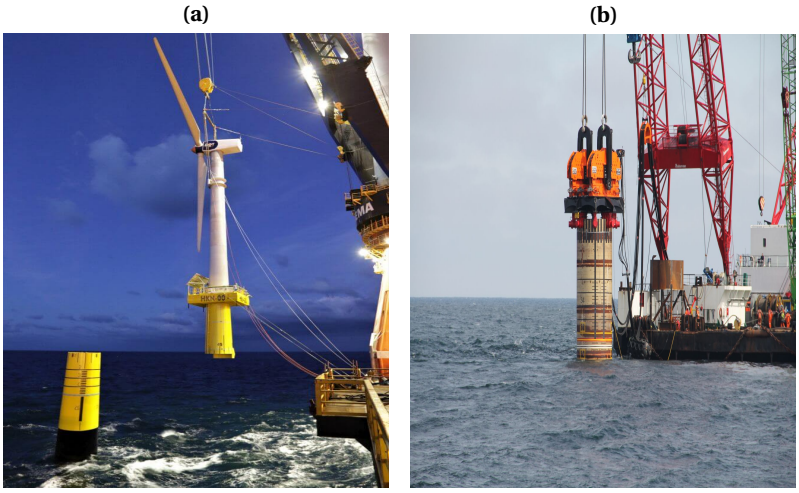

Figure 2.4: (a) Slip joint application. Image credit: hmc.heerema.com; (b) Gentle pile driving application. Image credit: CAPE-Holland.

focuses on designing and developing new devices that provide tactile feedback to the users by modulating the interaction between a touch surface and the user's finger. Friction modulation between surfaces in contact relies on waves outside the perceptual window of touch in the order of micrometres. These waves can create a near-field acoustic levitation that reduces friction. Therefore, using ultrasonic friction modulation, surface haptic devices can provide artificial tactile sensations by producing the illusion of shape and texture on a two-dimensional plate. For instance, the sensation of pressing a button can be simulated, not through physical movement of the button but by dynamically altering the friction between the skin and the surface [24, 25, 26]. Meyer and coworkers also studied the dynamic behaviour of the finger friction using amplitude-modulated electrostatic and ultrasonic friction modulation devices. It was found that ultrasonic devices offer a significantly broader range of friction modulation compared to electrostatic displays, achieving coefficients of friction ranging from as high as 1 to nearly frictionless contact, thereby enabling the simulation of a wide variety of stickiness sensations [27].

Lastly, the self-loosening bolts example is described as a scenario where friction reduction results from unintentional vibrations. Bolted joints are essential components in engineering, acting as critical connectors in mechanical assemblies and structural applications. Despite their often small size, they are crucial in ensuring structural integrity and operational reliability. Loosening is a critical challenge for threaded fasteners. In engineering applications, these fasteners are often exposed to harsh environments and periodic external loadings, increasing the risk of loosening. This phenomenon is mainly caused by the slippage and friction behaviours on the thread and bearing surfaces. In a review article, Gong and coworkers summarised the causes and mechanisms of nonrotational and rotational loosening [28]. Specifically, nonrotational loosening is primarily influenced by plastic deformation, fretting wear, and stress redistribution, while periodic transverse vibration mainly results in large-scale rotational loosening. With

regard to rotational loosening under a transverse vibration, the research indicates that local slippage accumulation is the key mechanism driving this type of loosening.

While vibration can be used to change friction in industrial applications, friction itself can also induce vibrations. For instance, chatter, a low-frequency noise, is an example of an unwanted friction-related sound phenomenon occurring during machining operations. A source of this phenomenon is mode coupling. Besides the excessive noise, chatter occurrence has several other adverse effects, including machine tool damage, inaccuracy, and waste of materials and energy. An example of marks on machined surfaces due to chatter is shown in Fig. 2.5(a).

Figure 2.5: (a) Marks on the machined surfaces due to chatter. Image credit: Richconn; (b) Steel railway wheel in contact with a steel rail. Image credit: Gary T. Fry / Railway Age.

Another well-known friction phenomenon of audible nature is squeal, a high-frequency noise. One of the industries where squeal occurs is the railway industry, where the squeal is generated by the wheel-rail interaction, Fig. 2.5(b). To explain the occurrence of squeal, different mechanisms are proposed. One of them occurs as a train takes a curve and the outer wheel travels a longer distance than the inner one. This difference in distance leads to lateral creepage [29]. In such a case, it can occur that, as lateral creepage increases, the resisting lateral force does not increase, but it can decrease instead. This creates a negative slope in the friction–velocity relationship, leading to negative damping, which is the mechanism behind squeal noise generation. Other mechanisms include mode coupling, where vibrations in the rail and wheel interact and amplify each other, leading to instability and squealing. Another type of squeal is the disk brake squeal, a high-pitched noise between 1000 – 18000 Hz, common in vehicle braking systems, railway brakes, and brake draw systems. In this case as well, the mechanisms describing break squeal include stick-slip, sprag-slip (geometrically-induced instability with constant friction coefficient), and modal coupling of structure involving sliding parts and negative friction-velocity slope causing self-excited vibration [29].

2.2. VIBRATION-ASSISTED FRICTION MODULATION

This section examines vibration-assisted friction modulation through a combination of experimental results and theoretical predictions. The discussion concludes by identifying the research gap that emerges, pointing to areas where further investigation is needed.

2.2.1. EXPERIMENTAL EVIDENCE

The fact that friction forces can be significantly reduced by applying external excitation has been known since at least the 1950s. One of the most dated and available published results was provided by Fridman and Levesque in 1959 [30] who studied how static friction is influenced by an induced vibratory motion. They observed that sonic vibration significantly reduced the estimated static friction force compared to initial static tests, and the coefficient of static friction could virtually be reduced to zero as a result of increased vibration levels. Focusing on the reduction of static friction force again, Tolstoi carried out a seminal work on friction force reduction, showing the influence of normal vibration [31]. Key findings revealed that the negative friction-velocity slope and self-excited vibrations were linked to the freedom of the normal displacement of the slider. This study highlighted the sensitivity of frictional force to normal displacements, demonstrating that natural microvibrations influence both frictional force magnitude and stability. Moreover, a friction force reduction between 35–85% was observed, with the main results portrayed in Fig. 2.6(a) and Fig. 2.6(b). It is worth noting that, in these studies, the concept of friction force reduction was defined as the decrease in the maximum force required to initiate sliding. More specifically, in the case of Friedman and Lavesque, this reduction was calculated using the difference in the angle of inclination needed for motion with and without vibrations, while in Tolstoi's study, it referred to the decrease in the maximum force required to start the rotation of a system comprising a slider and a rotating ring.

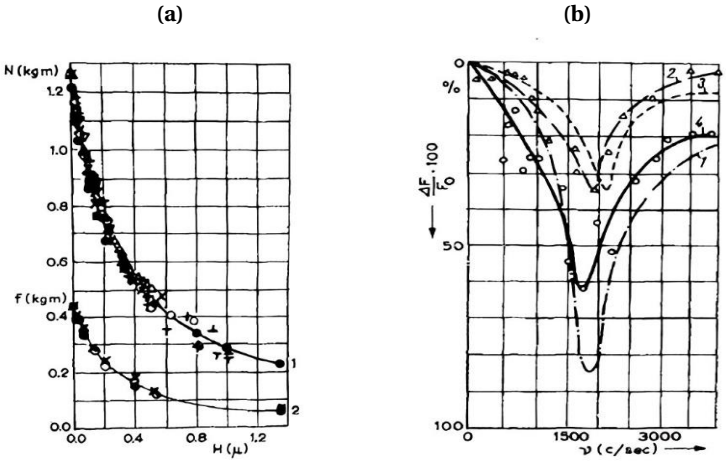

Figure 2.6: (a) Net normal load and static friction force reduction curves with respect to the normal displacement; (b) Percentage friction drop as a function of vibration frequency. The variable f stands for the static friction force, N for the net normal load, H indicates the normal displacement in micron induced by the oscillatory normal force, v is the frequency and $\Delta F/F_0$ defines the force reduction ratio with reference to the static friction force F_0. Reprinted from [31] with permission from Elsevier.

Godfrey also conducted experiments to determine the effect of periodic vibrations on friction force, focusing this time on the kinetic friction force [32]. He observed that

vibrations reduced the apparent friction force during lubricated and unlubricated sliding. Similarly to what was hypothesised by previously mentioned studies, Godfrey suggested that a temporary reduction in the normal load between the objects in contact may cause possible ruptures of the micro-welds, and hence a reduction of the friction force. In addition to the studies focusing on the effects of normal load on friction force, experimental campaigns studying the influence of tangential horizontal loading were also performed. In [33], the results of a testing campaign were reported showing variations of the static and kinetic friction force with respect to an applied harmonic tangential force. The results showed a decrease of the kinetic and static friction force, with the latter reduction values exceeding 80%. Interestingly, the static friction drop observed at higher frequencies of excitation (at 200 Hz) was almost independent of the amplitude of excitation, while for lower frequencies, the excitation amplitude had a significant effect: a large amplitude led to a larger decrease of the static friction force.

Within the structural joint community, one of the first relevant studies on friction was conducted by Nolle, who performed some experiments to assess the change of static friction force subjected to a harmonic in-plane loading [34]. A drop of the static friction force was observed from 0.19 to 0.13 (40%), without any dependency on the frequency of excitation. In addition, during some tests, an increase of the static friction force for an increasing number of cycles (probably due to wear) was observed. Later studies provided further evidence of a non-trivial dependency between the friction force and an applied harmonic oscillatory force. The results showed a general decrease of the static friction force between 40-60%, but no correlation regarding the frequency of excitation was provided [35]. Broniec and Lienkewicz hypothesised that an applied harmonic force at an interface could cause changes in the molecular interaction in the elastoplastic deformation regime of the interface, triggering possible localised losses of contact.

Inspecting the experimental results published in the time period mentioned above, no clear pattern can be observed between friction force reduction and parameters characterising the excitation force, such as frequency and vibration amplitude. The majority of the results seem to be dependent on the test setup, and unfortunately, not much information is provided concerning the dynamic behaviour of the adopted test rigs. The latter aspect also raises concerns regarding the inertial force compensation (inertial contribution of the specimen is measured and subtracted from the recorded friction force) necessary to obtain "trustworthy" readings of the friction force. In the studies mentioned below, starting from the late-80s, a higher relevance is placed on how the dynamics of the test setup may influence the friction change results. Regarding the latter aspect, in 1987, Lehtovaara carried out an investigation on the effect of normal vibration on kinetic friction [36]. A reduction of the kinetic friction force was observed only at low frequencies, specifically at the resonance frequency (11.8 Hz) of the first mode of the clamped beam. The author's claim that at higher frequencies, for instance at 54 and 70 Hz (also linked to structural modes of the test setup), no friction reduction was observed.

A few years later, Skare and Stahl published the results of an extensive testing campaign meant to determine the variation of the static and kinetic friction forces between two contact surfaces subject to different contact pressures, frequencies and amplitudes of excitation [37]. The results showed that either an increase or a decrease in the kinetic friction force can be obtained when one of the parameters, such as normal load, fre-

quency or amplitude, is changed. In 1995, Matunaga and Onoda used a high-frequency signal (also called dither) to reduce friction for gravity compensation [38]. Tests were performed by applying the excitation parallel and perpendicular to the sliding direction, and friction force reduction was observed for both directions, as shown in Fig. 2.7(a) and Fig. 2.7(b). The authors stressed that the observed reduction is not linked to the actual friction coefficient, but rather to the time-averaged value over a cycle of fast vibration of the friction force divided by the normal force (hence expressed as an averaged friction coefficient). It is worth highlighting that the concept of identifying the reduction of friction through a time-averaged quantity performed over the cycle of fast vibration was already discussed by Blekhman, whose main findings can be found in the English version of his book published a few years later in 2000 [39].

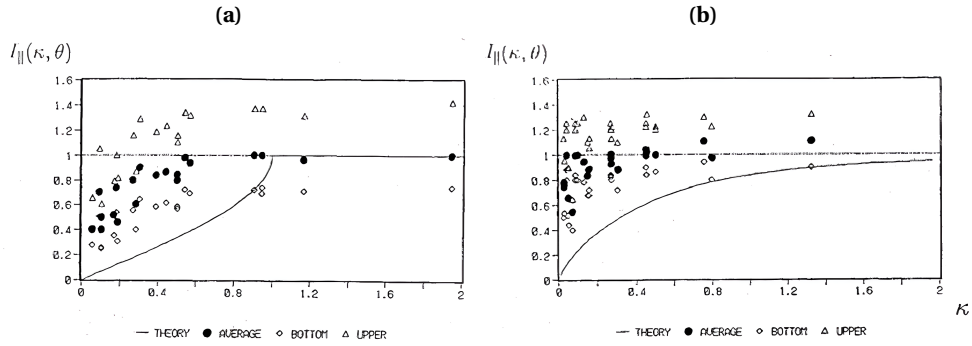

Figure 2.7: Comparison between the predicted time-averaged coefficient of friction (continuous line) and measured experimental data. The solid black markers defined the averaged values from experiments, while the triangles and rhombuses correspond, respectively, to the upper and bottom values of the experimental results. (a) Excitation applied parallel to the sliding direction; (b) Excitation applied perpendicularly to the sliding direction. Reprinted from [38] with permission from AIAA.

Similarly to what was shown in [38], Storck and coworkers conducted experimental tests with the ultrasonic vibration direction oriented either parallel or perpendicular to the sliding direction, illustrating a reduction in friction force using the same concept of time-averaged friction [40]. Later on, Kumar performed similar experiments studying the effect of ultrasonic vibration in tangential and perpendicular directions [41]. Significant reduction in sliding friction force was observed (up to 80%) with longitudinal vibration producing greater reduction in friction force than transverse vibration at the same amplitude and frequency. In addition to experimental investigations, Matunaga and Onoda, Storck and coworkers and Kumar and Hutchings developed simple models to explain the mechanism of friction force reduction by vibration, to calculate the friction reduction and compare the results to those obtained experimentally. The theoretical results confirmed the reduction effect, and good qualitative agreements were found between the experimental and theoretical results, with the latter generally overestimating the friction force reduction. Discrepancies between experimental and theoretical results could be due to the omission of system dynamic effects in the theoretical analysis. A detailed description

of the models is presented in Section 2.2.2.

In the 2000s, Chowdhury and Helali conducted a series of experiments to assess the influence of vibration applied in different directions on the friction coefficient. In their study in 2006, they investigated the variation of the friction force with the variation of the frequency of vibration [42]. It was found that the friction force under no vibration conditions is higher than that under vibration conditions, and the values of the friction force linearly decrease with the increase of the frequency of vibration. To explain the observed friction force reduction due to normal vibration, Chowdhury assumes that the applied normal vibration leads to a reduction in the mean contact area between the two sliding objects. Further follow-up experiments, extended to different material pairs and aimed at assessing the influence of different amplitudes of normal vibration of friction, were published later on, see [43]. During the experiments, the effects of sliding velocity, roughness, normal load and duration of rubbing were also investigated. The main results of this study indicate that the friction coefficient exhibits an approximately linear decrease with the increase of amplitude of vibration for every material pair (mild steel, ebonite, rubber) except PTFE for which the relationship between friction reduction and amplitude was nonlinear. Another series of results obtained by Chowdhury were published in 2009, see [44, 45]. One of these studies experimentally investigated the effect of horizontal vibration on friction. Friction forces were lower under longitudinal vibration (parallel to sliding) than under transverse vibration (perpendicular to sliding) [44]. The other study investigated experimentally the effect of external vertical vibration on the friction property and found again that vibration affects the friction force of different materials considerably. The friction force decreased with the increase of frequency and amplitude of vibration [45].

Starting from 2010, a set of systematic experimental and theoretical studies was published by Popov's research group on the influence of vibration on the averaged friction force over one cycle of vibration. Popov and coworkers [46, 47, 48] also studied the effect of ultrasonic vibrations on the static and kinetic friction, both experimentally and theoretically, considering in-plane and out-of-plane oscillatory excitation separately and different tribological pairings. They observed that the frictional force typically decreases with increasing oscillation amplitude, Fig. 2.8(a), and the decrease of the force is larger at smaller sliding velocities, Fig. 2.8(b). For small sliding velocities, the measured friction coefficient tends to a finite value, contradicting theoretical results that predict the averaged friction force to approach zero as sliding velocity goes to zero [46]. To explain the latter discrepancy, Popov and his coworkers stressed out the relevance of introducing a tangential contact stiffness and any interface dynamic process in the model [49, 50]. A description of the theoretical models developed and the comparisons of the theoretical and experimental results is discussed in Section 2.2.2.

In parallel to the research studies published by the group led by Popov, complementary experimental and theoretical work has been carried out by Gutowski and Leus. In the two papers, published in 2012 [51] and 2015 [52], the main scope was to analyse the influence of an external harmonic vibration applied parallel and perpendicular to the sliding direction, respectively, on the averaged friction force. The experimental observations showed deviations from theoretical results obtained using the Amonton-Coulomb's law, prompting the use of more advanced friction models such as Dahl and Dupont ones. A

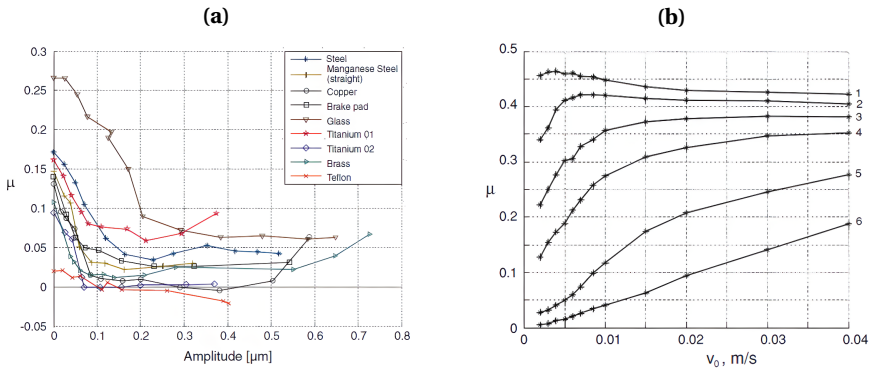

Figure 2.8: (a) Variation of static friction coefficients due to an increase of the vibration amplitude for different friction pairs; (b) Variation of the kinetic friction coefficient of a steel–steel friction pair as a function of sliding velocity, v_0, and for an excitation frequency of 45 kHz. The different curves correspond to the following vibration amplitudes: (1) 0.023 μm, (2) 0.056 μm, (3) 0.095 μm, (4) 0.131 μm, (5) 0.211 μm, (6) 0.319 μm. Reprinted from [46] with permission from Springer Nature.

description of their computational models is given in Section 2.2.2.

Besides systems and applications present in mechanical engineering, the geomechanics scientific community shared the same interest concerning the variation of friction force due to an oscillatory force. The correct understanding of such interaction could be relevant to shed light on the dynamic triggering of earthquakes due to small ground perturbations. Worth noting studies in this field were published by Wang and coworkers [53, 54], in which the variation of the friction force between surfaces of different materials such as steel, sandstone and shale, sliding against a steel sample and subjected to different in-plane oscillatory forces was studied. Overall, the friction force reduction with reference to the velocity ratio seems to exhibit a quite analogous pattern as the one shown in previous studies [38, 40, 41, 46, 51].

One of the latest detailed experimental campaigns was carried out and described by Kapelke and Seemann, analysing the effect of longitudinal vibrations on dry friction [55]. Measurements performed showed the hysteretic behaviour of the contact as well as the reduction of average friction forces in the presence of vibrational excitation. A comparison of experimental and theoretical results using the elasto-plastic Dupont model yielded good agreement for moderate excitation frequencies, see Fig. 2.9(a). However, when high-excitation frequencies were used, to catch the behaviour of the friction force accurately, a significantly different value of tangential stiffness was needed for the Dupont model, as shown in Fig. 2.9(b). A detailed description of the system used to obtain the numerical results is given in Section 2.2.2.

More recently, Gutowski and Leus performed experiments to investigate the effect of external oscillatory vibration on friction reduction. In their 2020 study, they considered vibrations applied in tangential, transverse, and arbitrary directions [56], while their 2023 study focused on transverse and tangential loading directions [57]. The results demonstrated that external vibrations in the tangential direction could effectively reduce

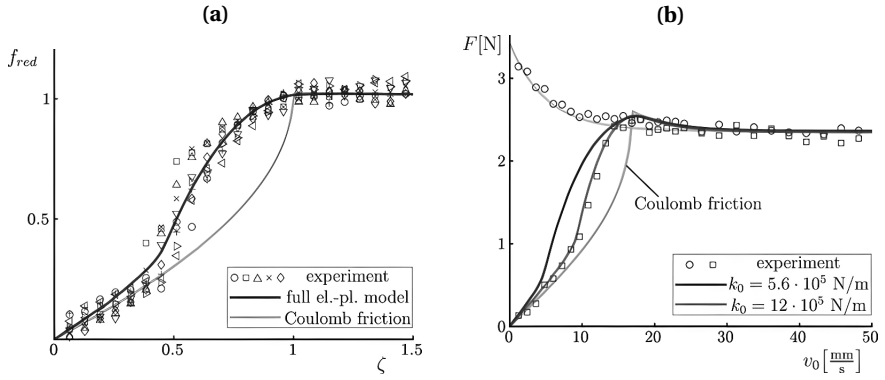

Figure 2.9: (a) Friction reduction observed at a harmonic force of 40 Hz, and comparison with the Amonton-Coulomb and elasto-plastic Dupont friction model to compute the corresponding averaged friction reduction; (b) Friction reduction observed at a harmonic force of 350 Hz (square markers), and comparison with the Amonton-Coulomb and elasto-plastic Dupont friction model to compute the corresponding averaged friction reduction. The circle markers refer to experiments performed with no applied excitation. Reprinted from [55] with permission from Springer Nature.

friction forces if the amplitude of the velocity response exceeded the constant sliding velocity. However, this condition was not necessary for diagonal and transverse vibrations to achieve friction reduction. Additionally, computational models were developed to simulate friction force reduction under arbitrary vibration directions, with further details provided in Section 2.2.2.

2.2.2. THEORETICAL STUDIES

In the previous section, experimental evidence on the effect of external excitation on friction was presented. In this section, theoretical studies aimed at predicting the experimental results, understanding the underlying mechanism and performing parametric studies are described. This section is divided into two parts. The first part describes simple models, primarily 1-DOF models for which average friction results can often be obtained analytically. The second part discusses more complex models, including MDOF or continuous ones, for which the average friction results are obtained numerically.

SIMPLE MODELS

As briefly mentioned in Section 2.2.1, Matunaga and Onoda developed a simple model to explain the mechanism of friction force reduction by vibration, to calculate the friction reduction and compare the results to those obtained experimentally [38]. The model consisted of a mass moving with a constant velocity on a sinusoidally shaken table. The friction force was assumed to follow the Amonton-Coulomb model. Thus, as the relative velocity rapidly changed direction in accordance with the vibration of the table, the direction of the Amonton-Coulomb friction force also changed. While the amplitude of relative velocity changed, the amplitude of the friction force remains constant. Consequently,

the frictional force in the direction of the constant velocity decreased on time average. The results obtained analytically were compared to those obtained experimentally. The friction ratios obtained in the experiment had the same form as those obtained from the analytical analysis, but they had higher values. The most important reason for this result is thought to be the omission of dynamic effects in the analytical method.

Stock and coworkers also developed a simple model to predict friction reduction and compare it to experimental results [40]. The system in their study consisted of a rigid body sliding over a rigid flat plane with a prescribed velocity consisting of two components. The first one was a macroscopic constant velocity and the second one was a harmonic representing the ultrasonic vibration, Fig. 2.10(a). The macroscopic and harmonic velocity components were parallel or perpendicular to each other. Amonton-Coulomb's friction law was assumed, and to calculate the friction change, the component of the friction force in the direction of the macroscopic movement was averaged over one period of vibration, with the results for each loading direction shown in Fig. 2.10(b) and Fig. 2.10(c). Similar models were developed by Kumar and Hutchings, where a body was assumed to slide with a constant velocity over another body performing an oscillatory motion [41]. The friction reduction was calculated using the averaging mechanism as in the previously mentioned studies.

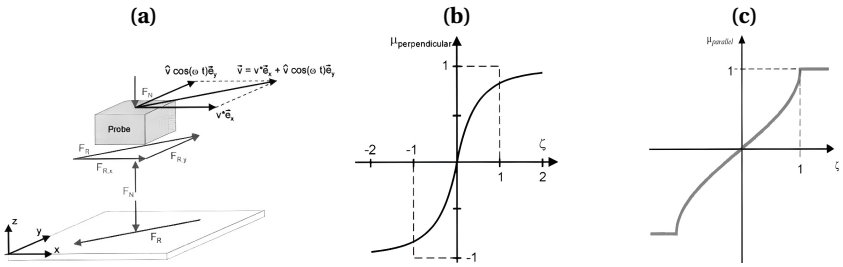

Figure 2.10: (a) The considered system with indicated forces and velocities; (b) Friction reduction for perpendicular velocity component; (c) Friction reduction for parallel velocity component. ξ is the ratio of the macroscopic constant velocity to the velocity amplitude of the harmonic component. Reprinted from [40] with permission from Elsevier.

In parallel to the aforementioned works from the friction research community, studies originating from the structural dynamics community also focused on the interaction between the global dynamics of the system and the vibration-induced friction reduction. These studies explored a different computational route to friction reduction. For example, in the research conducted by Thomsen [58], the Method of Direct Separation of Motion (MDSM) was used (see [39] for more details on the MDSM). The main idea of MDSM lies in separating the motion of a dynamic system arising due to high-frequency excitation into two components of motion, a "slow" and a "fast" one. The slow component is usually of primary interest and equations describing it are simpler than the initial equations. Approximations are involved only for solving the equations of fast motion and do not strongly affect the accuracy of the resulting equations for the slow motion, because only averaged fast components are employed in their formulation [59]. Plots of the total motion and of the slow motion component from the response of the system studied by

Thomsen are presented in Fig. 2.11. It should be noted that using MDSM, an analytical expression of the friction change expression can be obtained, however, the motions in Fig. 2.11(a) and Fig. 2.11(b) are obtained by numerical integration of the full and slow equations of motion. The responses correspond to a single-degree-of-freedom oscillator

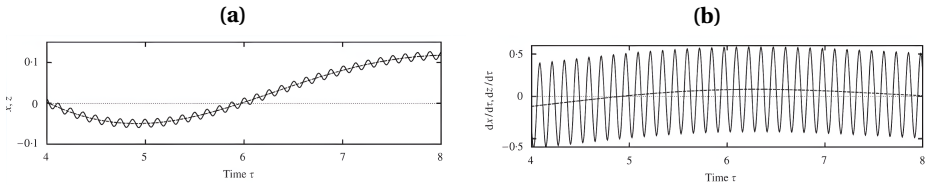

Figure 2.11: (a) Displacement responses in the presence of fast harmonic excitation. (——) Full motion x; (– – –) slow component of motion z. The slow component traces the moving fast-time-average of the full motion; (b) Velocity responses showing the same trend. Reprinted from [58] with permission from Elsevier.

sliding over a rigid belt, Fig. 2.12(a). To investigate the effect of high-frequency excitation on quenching self-exited oscillation, the Stribeck law was used. It was shown that high-frequency excitation could prevent self-excited oscillations by effectively cancelling the negative slope in the assumed friction-velocity relationship, with the results of friction change plots for different intensities of excitation shown in Fig. 2.12(b).

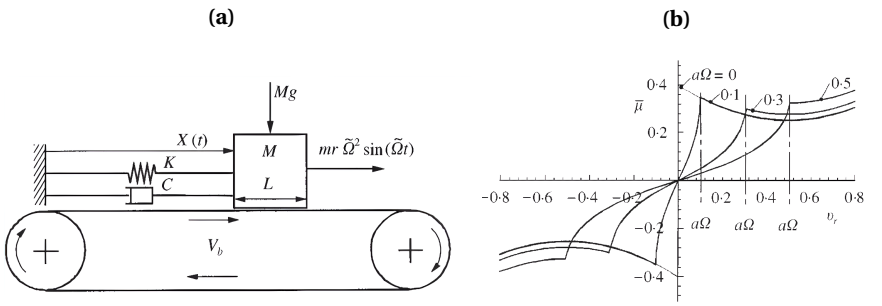

Figure 2.12: (a) The system considered: a mass on a moving belt; (b) Average friction plots for different intensities of fast excitation. Fast excitation smoothness the plots, and at sufficiently large intensity, cancels the negative slope. Reprinted from [58] with permission from Elsevier.

Using a similar SDOF mass on a moving belt system and two different models of friction, Amonton-Coulomb and Stibeck law, in 2008, Michaux and coworkers investigated the effect of the waveform of different periodic signals on the effectiveness of tangential high-frequency excitation to cancel friction-induced oscillation [60]. Hoffmann and coworkers also used the MDSM to quench mode-coupling friction-induced instability using high frequency in a 2-degree-of-freedom system with Amonton-Coulomb friction law [61] . In their work, they not only investigated the effect of external tangential excitation on the friction force change, but also showed that excitation can stabilise the mode-coupling instability, with the stability analysis performed numerically.

To interpret the experimental data for both static and sliding friction, Popov and coworkers considered a phenomenological macroscopic model [46]. The model represente the pin-on-disk setup, considering an object over a disk. The motion of the contact points is assumed to be the superposition of a constant sliding velocity and harmonic oscillations. By assuming Amonton-Coulomb's friction law, the macroscopically measured (averaged over the oscillation period) friction coefficient was calculated. The theoretical predictions fitted well with the measurements of friction coefficients vs sliding velocity for different amplitudes of the oscillation velocity for sliding velocities larger than the actuation velocity. For small sliding velocities, the measured friction coefficient tended to a finite value, contradicting theoretical results that predict the averaged friction force to approach zero as sliding velocity goes to zero [46]. Similar models and conclusions were reached in the follow-up study [47]. To explain the latter discrepancy, Popov and his coworkers stressed the relevance of introducing a tangential contact stiffness and any interface dynamic process in the model [49, 50].

MORE COMPLEX MODELS

Most of the models described so far consisted of a rigid body moving with a constant velocity over an oscillating body or of a rigid body oscillating with a prescribed constant and harmonic velocity over a rigid plane. Moreover, in most cases, the friction force was assumed to follow Amonton-Coulomb's model. For these systems, it was possible to calculate the change in relative velocity and eventually in the friction force analytically. As the systems become more complex, incorporating factors such as contact stiffness, additional degrees of freedom, and complex friction laws, determining frictional change analytically becomes increasingly challenging or even impractical. Therefore, numerical methods have been used to calculate the effect of vibrations on friction. For instance, at the beginning of the '90s, numerical attempts to study the effect of vibrations on friction were made by Hess and Soom [62, 63, 64]. Their studies showed that normal oscillations applied on top of a Hertzian and adhesion-like contact lead to a reduction of contact deflection and consequently of the average area of contact and the average friction force.

Later on, Leus and Gutowski [65] showed that using the Dahl model [66], in which asperities are modelled by means of micro-springs characterised by a shear stiffness, see Fig. 2.13(a)-(b), the above-mentioned averaged friction force could be reduced independently of whether a change in the direction of the net friction force vector is observed, Fig. 2.13(c). Grudzinski and Kostek also considered the surfaces in friction contact to be rough, creating an elastic interface modelled by non-linear springs [67]. In this model, the external force applied was a constant one instead of a harmonic one. The study showed that the main cause of the decrease in the friction force could be due to complex non-linear dynamic processes occurring at the asperity level.

In more recent works [55, 68], the effect of vibration on friction has been investigated using a simple 1-DOF friction oscillator. In [55] the analysis used both the Amonton–Coulomb law and the elasto-plastic Dupont accounting for stiction and the transition to sliding motion. The average friction was calculated numerically, and as previously mentioned in Section 2.2.1, good agreement was found between the numerical results from the elasto-plastic model and the experimental data at moderate excitation frequencies. At higher frequencies, however, the tangential stiffness of the friction model required

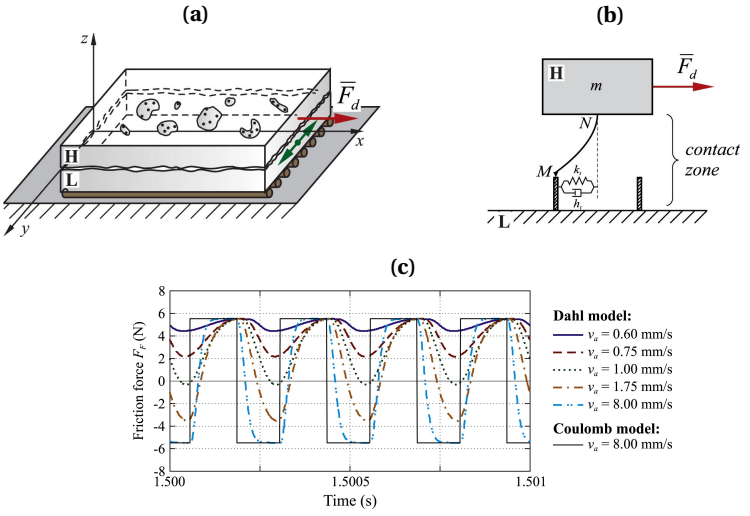

Figure 2.13: (a) A scheme of contact of two surfaces; (b) Its model; (c) Friction force for the Amonton-Coulomb and Dahl models for different values of amplitude of vibration velocity v_a. (a) and (b) reprinted from [52] with permission from Elsevier and (c) reprinted from [51] with permission from Elsevier.

adjustment to maintain this agreement.

Similarly, to back up and corroborate experimental results from applications such as gentle pile driving, or pile installation and decommissioning, numerical methods are used. For instance, to comprehend the mechanics of the GDP method, Tsesas and coworkers developed a novel pile-soil model in which the pile is treated as a thin cylindrical shell via a Semi-Analytical Finite Element (SAFE) approach, Fig. 2.14(a) [23]. At the same time, the Thin-Layer Method (TLM) coupled with Perfectly Matched Layers (PMLs) was used for the linear elastic layered soil half-space, Fig. 2.14(b). A frictional interface was used for the pile-soil coupling, and the redirection of the friction force vector due to the high-frequency torsion was identified as the main driving mechanism of GDP. Cabboi and coworkers also developed a finite element model of the slip joint in Abaqus FEA to link experimental results to physical insights [22]. The model allowed for the computation of natural frequencies and mode shapes, which were then compared with experimental results. It is important to note that this study did not model the interaction between vibration and friction. Instead, the focus was on exploring how exciting the modes may have contributed to facilitating the installation and decommissioning process.

Lastly, as already mentioned in Section 2.2.1, Gutowski and Leus developed computational models to stimulate friction force change under longitudinal, transverse and arbitrary forcing direction. They incorporated the Dahl, Dupont, and LuGre dynamic friction models to describe the friction force as a function of contact elastic deformation, as these models incorporate parameters like tangential stiffness and damping of the contact zone. The simulation results showed good qualitative and quantitative agreement with the experimental findings.

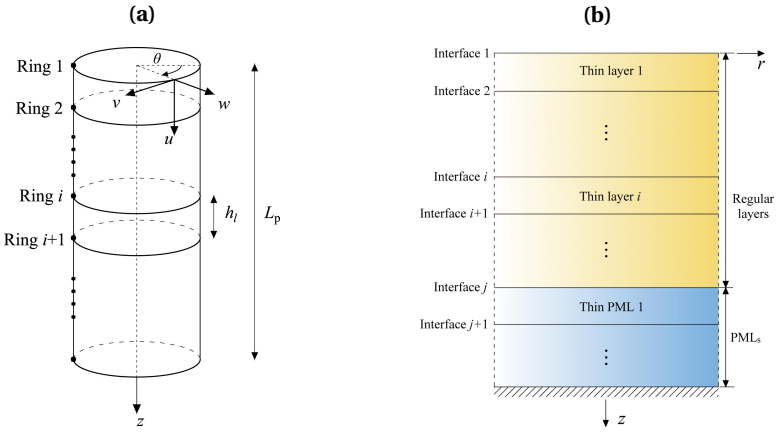

Figure 2.14: (a) A thin cylindrical shell discretized axially into nodal rings based on the SAFE method; (b) A layered soil half-space modelled via the TLM+PMLs. Reprinted from [23].

2.2.3. RESEARCH GAP

In the studies discussed in this chapter so far and in the existing literature, in general, despite the experimental and theoretical evidence on the effect of external excitation on friction force, several important aspects are overlooked or remain insufficiently understood. Specifically, when it comes to the external excitation properties, the existing studies focus on the effect of fast or high-frequency oscillations on friction forces, while a clear definition of "high frequency" is lacking, hindering the generalisation of research findings. Moreover, the effect of excitation phase and location (on the moving mass versus the supporting structure) and the influence of multiple simultaneous external loads remain largely unexplored, despite their significant impact on the system's dynamic response and the resulting friction modulation.

Additionally, much of the existing research does not address the role of system dynamics and the interplay of the latter with external load properties (in the context of friction modulation). In this regard, many studies consider the bodies in contact to be rigid, an idealization that may fail to capture essential dynamic interaction. The presence of directional system stiffnesses in discrete models and the consideration of flexible bodies in contact (continuous models) are also underexplored aspects. Instead, the existing studies predominantly focus on simplified discrete systems (e.g. single or two-degree-of-freedom systems) where phenomenological friction models, such as the Stribeck, Dahl, or Dupont models, are considered. While the results in terms of friction modulation obtained using these friction models have been shown to align with experimental results, this often comes at the cost of adjusting model parameters. Thus, past research that focuses on using more sophisticated friction laws often neglects the complexities and the dynamics of the system itself. This approach leads to inaccurate predictions and potentially misleading interpretations when applied to real-world scenarios such as experimental investigations or industrial applications.

Lastly, it is important to note that, since this section focuses on the effect of vibra-

tions on friction, the research gaps identified here represent only a subset of the broader gaps addressed in this study. The interaction between vibration and friction is coupled—friction can induce vibrations, which in turn influence friction modulation. These aspects are discussed in the following section, which outlines additional research gaps and completes the framework underpinning the rationale for the research conducted.

2.3. FRICTION-INDUCED VIBRATIONS

The previous section explored how vibration affects friction forces. In this section, the focus shifts to the role of friction in inducing vibrations. Unlike the previous section, which provided a detailed chronological overview of studies on vibration-induced friction force modulation due to the absence of comprehensive review papers on the topic, this section maintains the same structure but focuses the content in each subsection on distinct mechanisms that excite friction-induced oscillations. For further details, one can refer to the existing review papers on this topic [29, 69, 70, 71, 72].

2.3.1. EXPERIMENTAL EVIDENCE

In literature, several types of friction-induced vibrations have been reported together with the distinct mechanisms that can excite these oscillations. One of the most studied mechanisms that leads to friction-induced oscillations is based on the presence of a decreasing friction force or friction coefficient linked to the corresponding increase in relative sliding velocity, naturally triggering a negative damping-like effect. If such "negative damping" is higher than the bulk or structural damping of the system, instability occurs, characterised by the growth of the oscillatory motion during sliding. Experimentally, this mechanism was investigated by Yokoi and Nakai, who considered a contact rod clamped at one end and pressed on a rotating disk [73]. A rubbing noise was generated when the friction coefficient between the rod and the disk was small and the contact surface had a lot of rough areas. With increasing sliding distance, the tip of the rod became worn, the coefficient of friction increased, and the rod vibrated in the lateral direction at its fundamental mode. In this case, the frictional noise changed to a squeal. To reveal the mechanism behind the squeal noise, they investigated the experimentally measured friction-velocity curves, which showed a negative slope until a certain sliding velocity, after which the slope turned positive, as shown in Fig. 2.15(a). This mechanism was studied theoretically as well as described in Section 2.2.2.

Friction-induced oscillations may also occur for a constant value of the friction coefficient if phenomena such as sprag-slip or mode coupling characterise the system dynamics. The sprag-slip mechanism was proposed by Spurr and is known as a geometrically induced or kinematic constraint instability [74]. This phenomenon occurs due to the locking action of a slider into a sliding surface and was observed on a system involving a rigid member loaded at a specific angle against a moving surface, Fig. 2.15(b). If the member is mounted rigidly, the frictional resistance can rise to extremely high values, causing the system to sprag or lock. If the member is mounted flexibility, stick-slip motion occurs instead.

Mode coupling is another mechanism that leads to self-excited vibrations. A characteristic of this instability is that the oscillation frequencies of two structural modes of an

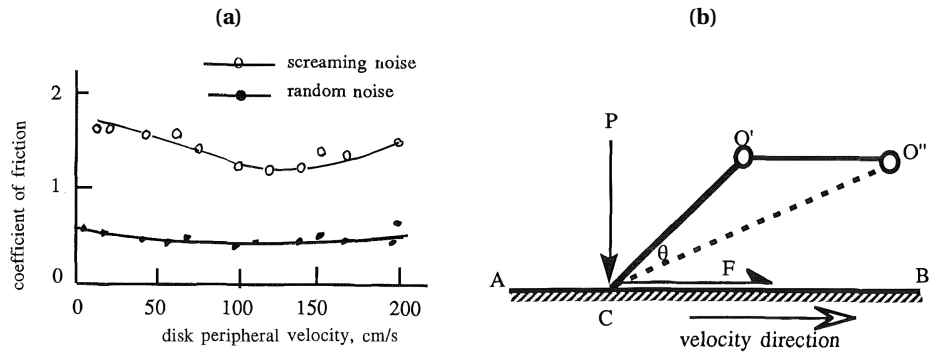

Figure 2.15: (a) Coefficient of friction versus the circumferential speed of the disc; (b) Rigid member at a specific angle with a moving surface. Reprinted from [29] respectively, with permission from ASME.

undamped system approach each other (as a function of a control parameter) and merge, resulting in a pair of an unstable and a stable mode. Experimentally, these vibrations were observed in metal cutting and are known as machine tool chatter. During metal cutting, the tool usually moves in an elliptical path, and the cutting force varies with time. Due to mode coupling, vibration in the cutting force direction generates vibrations in the cutting direction and vice versa. The frequency of chatter is equal to the dominant mode of the natural vibrations of the mechanical structure involved [29]. Similarly, mode coupling can also influence self-excited vibrations in other systems, such as rubber bearings. Figure 2.16(a) illustrates how normal load and sliding speed define the transition between different vibration regimes, such as squeal and chatter, in water-lubricated rubber bearings [29].

Another mechanism that causes instability is the presence of a follower force for structures resembling the Pflüger or Ziegler column. This mechanism was experimentally demonstrated for the first time by Bigoni and Noselli [75]. In the classical Ziegler column, the follower load is imposed and remains tangent to the rod. Using a two-degree-of-freedom structure, inspired by the Ziegler column, the authors showed that the tangential follower load can be generated by the frictional force, which is produced by dry Coulomb friction through a wheel sliding on a rigid plane. Thus, a follower force realised by Coulomb friction leads to observable flutter (blow-up oscillations) and divergence (exponentially growing motion). Some of the experimental results showing the measured acceleration versus time during the flutter test are illustrated in Fig. 2.16(b). Alongside experiments, the authors employed a theoretical study to investigate flutter and divergence instabilities, as described in Section 2.2.2.

2.3.2. THEORETICAL STUDIES

This section introduces the modelling approaches used in the experiments and applications discussed above. It begins with simple models and progresses to more complex ones, all developed to better understand the mechanisms behind friction-induced vibrations.

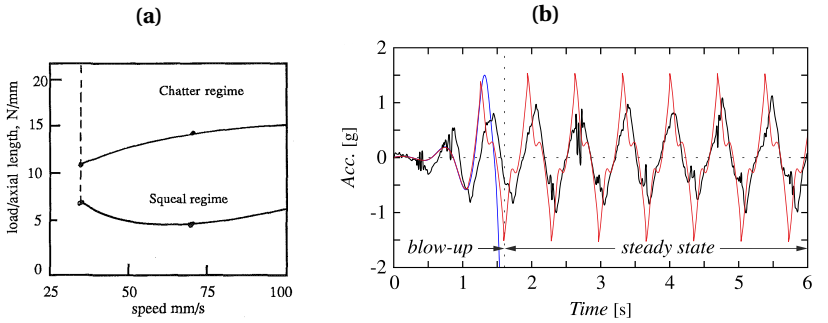

Figure 2.16: (a) Squeal and chatter regimes for curved soft rubber; (b) Measured acceleration versus time during the flutter test. The solution of the linear equations(blue curve) has been interrupted at 1.5s since the blow-up was too high.The initial increase in the amplitude of the acceleration denotes flutter. Reprinted from [29] and [75] with permission from ASME and Elsevier, respectively.

Simple models

In the context of mode-coupling instabilities, Hoffmann and coworkers analytically investigated a two-degree-of-freedom model of a mass over a moving belt connected with a vertical and two diagonal springs, as shown in Fig. 2.17(a) [76]. The findings revealed that simultaneous out-of-phase oscillations of the friction force and displacement tangential to the friction force can lead to energy transfer from the frictional system to vibrational energy, emphasising the significance of the phase shift between in-plane and out-of-plane motions in friction-induced oscillations. Mode-coupling phenomenon in terms of the merging of natural frequencies and the appearance of non-zero growth rates is shown in Fig. 2.17(b)-(c). While this study focused on physical mechanisms underlying the mode-coupling instability, others investigated the influence of system parameters on this instability [77, 78], and also the role of excitation on quenching this instability as already described in Section 2.2.2 [61].

Analytical studies were also performed by Thomsen and Fidlin, who investigated the classical mass on moving belt model with a friction force-velocity curve that has a negative slope at low velocities, corresponding to negative damping and potentially causing oscillations that grow in amplitude [79]. Approximate analytical expressions were derived for the cases of friction-induced stick-slip and pure slip oscillation. Similar to the previous case, to quench friction-induced stabilities, high-frequency excitation was used to cancel the negative slope in the friction-velocity relationship [58]. Regarding the sprag-slip mechanism, Spurr not only observed the phenomenon but also derived the condition at which the locking behaviour or “spragging” occurs, an expression which depends on the friction coefficient and the angle between the strut member and the surface [29]. Lastly, as for flutter and divergence instability, as mentioned in Section 2.3.1, other than performing experimental studies, Bigoni and Noselli also used an analytical approach to perform a linearised stability analysis to determine the conditions for instabilities to occur [75].

As the applications involving friction-induced vibrations, such as brake components,

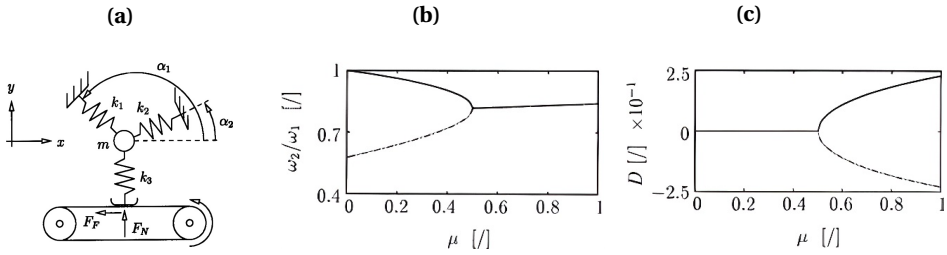

Figure 2.17: (a) The two-degree-of-freedom model considered; (b) Mode-coupling phenomenon in terms of the merging of natural frequencies; (c) The appearance of non-zero growth rates. Reprinted from [76], respectively, with permission from Elsevier.

involve continuous media of complicated geometrical shapes, for these systems, more complicated models were introduced, including multiple degrees of freedom or continuous systems for which the application of analytical methods was cumbersome or impossible. Therefore, when studying friction-induced vibrations, numerical methods were employed, some of which are described in the next section.

MORE COMPLEX MODELS

In the context of negative damping, as mentioned in Section 2.3.1, Yokoi and Nakai studied the generating mechanisms of frictional force not only experimentally but also theoretically. Experimental results showed that the noise was mainly generated by the lateral vibration of the rod [73]. Thus, the model they considered was a rod with the contact load and friction force acting at its tip. Using this model, they obtained and solved the nonlinear differential equations derived from only the lateral vibration of the rod using the Runge-Kutta-Gill method. The numerical results showed that when the gradient of the loop (friction vs relative velocity curve) was inclined to the right (was smaller than zero) and was above a certain negative value (depending on the damping coefficient), self-excited vibrations were generated and responsible for the squeal noise.

Concerning the mode-coupling mechanism, Friets and coworkers studied the effect of damping on brake squeal coalescence patterns. To compute the brake model behaviour, instead of considering discrete systems, they built a finite element model of a brake system encompassing the disk, pads, calliper, hub, knuckle and anchor bracket, as shown in Fig. 2.18(a) [80]. To assess the brake stability as a function of the friction coefficient, a complex eigenvalue analysis was performed, and the effect of damping distribution across modes on stability was investigated, Fig. 2.18(b)-(c). It was found that unequal damping can, under certain conditions, lead to instability. Similar conclusions were drawn by Hoffmann and coworkers [77], Sinou and coworkers [81], and Charroyer and coworkers [82] on the role of damping on mode coupling instability. While most of the studies have focused on the role of damping on friction-induced vibrations, others have investigated the influence of contact stiffness on stability as well, as done by Li and coworkers, who revealed that increased preload and nonlinear stiffness can, in some cases, destabilise the system [78]. Regarding sprag-slip, Bigoni and Noselli also used numerical methods to solve the full nonlinear differential equations. The numerical simulations

allowed them to study the effects of nonlinearities on the development of the instabilities and to compare the theoretical predictions with experimental observations [75].

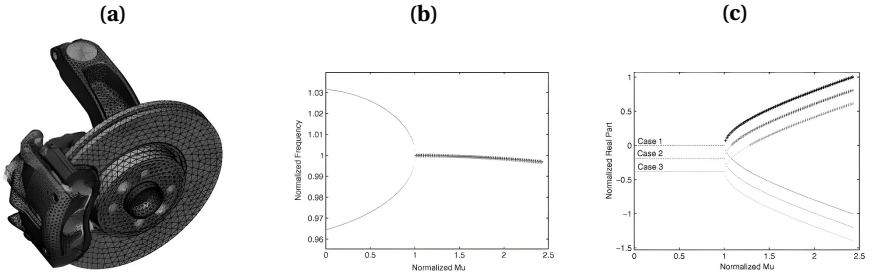

Figure 2.18: (a) Finite Element Model of the brake system; (b) Frequencies of the two modes; (c) Real parts of the two modes as a function of the friction coefficient, highlighting the mode coupling phenomenon. Reprinted from [80] with permission from Elsevier.

The mechanisms explaining the causes of friction-induced vibrations are not limited to negative gradient of the coefficient of friction versus the relative velocity, stick–slip vibration, follower force, mode coupling and the sprag–slip vibration. Other mechanisms proposed include hammering [83], the moving couple [84], feed-in energy [85] etc. Berger and coworkers, for instance, showed that parametric excitation was the mechanism behind the friction-induced instability, more specifically, the dynamic coupling of tangential and normal modes of the slider, arising in a system with non-constant normal forces and a velocity-dependent friction coefficient [86]. The combination of the oscillating normal force and the non-zero slope of the friction curve led to large-amplitude oscillations and, in some cases, to stick–slip responses.

2.3.3. RESEARCH GAP

Most existing studies, whether experimental, numerical or analytical, focus on identifying the underlying mechanism and providing physical explanations for friction-induced vibrations. Additionally, they investigate the effect of system parameters, such as damping or contact stiffness, on initiating or suppressing these vibrations with the ultimate goal of establishing effective means to control friction-induced vibrations in engineering and daily life. Beyond the effect of system parameters, another approach to mitigating friction-induced vibrations involves the application of high-frequency excitation. Consequently, many studies considering the effect of external excitation have primarily focused on stabilising systems that are initially unstable. However, in the research area of friction modulation, the potential for external excitation to destabilize an initially stable system and the mechanisms underlying such instability remain largely unexplored.

Furthermore, existing research predominantly aims at analysing or mitigating friction-induced vibrations, while the influence of these vibrations in friction modulation has received little attention. The impact of instabilities on frictional changes in the context of experimental results also lacks thorough investigation. This gap could lead to the misinterpretation of data in vibration-assisted friction reduction experiments, where the presence of instability may significantly affect the observed changes in friction. At

the same time, the effect of these instabilities on friction modulation may represent a phenomenon that can be deliberately exploited to control or manipulate frictional behaviour. This dissertation addresses these gaps to provide a deeper understanding of the interplay between vibration-induced instabilities and friction modulation and improve the interpretation of experimental results in this context.

3

VIBRATION-INDUCED FRICTION MODULATION FOR A GENERAL FREQUENCY OF EXCITATION

This chapter begins with the classical mass-on-a-moving-belt model and examines how external excitation of a general frequency influences friction modulation. Building on the one-degree-of-freedom system, a two-degree-of-freedom model is introduced to investigate how the presence of normal contact stiffness affects friction modulation under excitation. Through the analysis of these systems, the study directly addresses the dissertation's objectives: exploring the relationship between excitation frequency and dynamic system response, characterizing the definition of "high-frequency" in this context, and assessing the influence of multiple simultaneous loads as well as their relative phases on friction change. Readers familiar with the background presented in the "State of the art" chapter may skip the introduction section if desired.

This chapter has been published as: Sulollari, E., van Dalen, K.N., and Cabboi, A. (2024). Vibration-induced friction modulation for a general frequency of excitation. Journal of Sound and Vibration, 573, 118200.

ABSTRACT

Applying an oscillatory load is one of the most efficient ways to alter friction forces. Several theoretical and experimental studies on the influence of oscillatory loads on friction have been conducted, investigating the effect of both in-plane and out-of-plane oscillations for different tribological pairings. However, in the literature, the effect of an oscillatory load on the friction force has been studied with an emphasis on dynamic loads characterized by a high-frequency content, while a clear statement as to what is considered high frequency is missing. Moreover, the effect of a combination of load directions on the friction reduction is not accounted for. Therefore, this study aims to determine the vibration-induced effect on friction regardless of the frequency range and direction of harmonic force for a single and multi-degree-of-freedom system. Analytical methods are used to obtain the friction modulation due to harmonic loads, considering a classical mass-spring-dashpot system on a moving belt and the Amontons-Coulomb law. It is found that, in the case of continuous slip, a general relation for the vibration-induced friction modulation is obtained utilizing the velocity response function of the investigated system. The latter is used to highlight a threshold from which the high-frequency regime starts and to determine the stick-slip boundaries. Moreover, through the velocity response function, the influence of different external harmonic forces is investigated and discussed. This includes considerations of phase, excitation frequency, system characteristics, and the choice of the normal contact force expression.

3.1. INTRODUCTION

Friction control is crucial for the satisfactory operation of systems in many fields of applied science. Lubricants are commonly used as a way to control and reduce friction between surfaces in contact, improving their performance and adding value in terms of cost savings and expenses that arise due to wear and tear, repair, and maintenance of parts in contact. However, timely lubrication is required to ensure the proper functioning of tools, automotive and machines, and the removal and replacement (if needed) of the lubricant can be quite a challenging task. Exploiting the effects induced by a deliberately applied oscillatory force is another method used to alter friction forces. This is a flexible alternative that can be considered as a form of lubrication that can be controlled and removed very quickly by changing the amplitude and the frequency of the oscillatory force. Examples of applications in which a vibration-assisted technique is used to alter friction can be found for positioning control in robots [1], decommissioning of joints [2], pile driving [3], needle insertions [4] and drilling operations [5]. Ultrasonic oscillations, for example, are used to alter friction in wire drawing and cutting, metal working [6], in nanotribological devices by means of atomic force microscopes [7], for rendering texture on haptic surfaces [8] and in friction stir welding [9]. However, despite the technique successfully being used for specific applications, a universally accepted physical interpretation of how static and kinetic friction forces change and react to externally applied excitation is still missing. This is mainly due to the absence of a universal law of friction and the missing link between surface property variation and externally applied forces, but also because most of the current applications are specifically focused on the use of applied oscillatory forces characterized by a high-frequency content.

The fact that friction forces can be significantly reduced by applying external excitation

has been known since at least the 1950s [10, 11]. In the '60s and '70s, most of the experimental results obtained seem to be strongly dependent on the characteristics of each test rig. Thus, no general law explaining the observed behavior was identified. Since then, several experimental and theoretical studies have been conducted to understand the effect of external excitation on friction and exploit it in practical applications. At the beginning of the '90s, analytical and numerical attempts were made by Hess and Soom [12, 13, 14]. Their studies showed that normal oscillations applied on top of a Hertzian and adhesion-like contact lead to a reduction of contact deflection and consequently of the average area of contact and the average friction force. Matunaga and Onoda [15] investigated the effect of vibration on friction on a mass sliding on an in-plane vibrating table. To illustrate the mechanism of friction reduction by means of vibration, they proposed the concept of effective, time-averaged frictional forces. Based on this concept, Storck and coworkers [16] and Kumar and Hutchings [17] studied the reduction of the friction force due to ultrasonic vibrations applied parallel and perpendicularly to the sliding direction. For each loading case, qualitative good matches between theoretical predictions and measurements were obtained. These studies assume Amonton-Coulomb's law, and the friction force varies due to the change of direction of the resultant sliding velocity vector. Hence, the "friction reduction" results from the average frictional force over a whole vibration cycle.

Later on, Leus and Gutowski [18] showed that using the Dahl model [19], in which asperities are modelled by means of micro-springs characterized by a shear stiffness, the above-mentioned averaged friction force could be reduced independently of whether a change in the direction of the net friction force vector is observed. Grudzinski and Kostek [20] also considered the surfaces in friction contact to be rough, creating an elastic interface modeled by non-linear springs. In this model, the external force applied was a constant one instead of an harmonic one. The study showed that the main cause of the decrease in the friction force could be due to complex non-linear dynamic processes occurring at the asperity level. Popov and coworkers [21, 22, 23] also studied the effect of ultrasonic oscillations on the averaged friction force, both experimentally and theoretically, considering in-plane and out-of-plane oscillatory excitation separately and different tribological pairings [21]. By assuming Amonton-Coulomb's friction law, the measurements of friction coefficients vs sliding velocity for different amplitudes of the oscillation velocity fitted well with theoretical predictions for sliding velocities larger than the actuation velocity. For small sliding velocities, the measured friction coefficient tends to a finite value, contradicting theoretical results that predict the averaged friction force to approach zero as sliding velocity goes to zero [21]. To explain the latter discrepancy, Popov and his coworkers stressed out the relevance of introducing a tangential contact stiffness and any interface dynamic process in the model [24, 25].

In parallel to the aforementioned works from the friction research community, studies originating from the structural dynamic community also focused on the interaction between the global dynamics of the system and the vibration-induced friction reduction. These studies explored a different computational route to friction reduction. For example, in the research conducted by Thomsen [26], the Method of Direct Separation of Motion (MDSM) was used (see [27] for more details on the MDSM). The main idea of MDSM lies in separating the motion of a dynamic system arising due to high-frequency excitation

into two components of motion, a “slow” and a “fast” one. The slow component is usually of primary interest and equations describing it are simpler than the initial equations. Approximations are involved only for solving the equations of fast motion and do not strongly affect the accuracy of the resulting equations for the slow motion, because only averaged fast components are employed in their formulation [28]. In 2014, Sorokin [29] suggested a modification of the MDSM. This version of the MDSM allows for solving a broader range of problems, namely problems that do not imply restrictions on the spectrum of excitation frequencies. In problems with friction, MDSM has been applied in cases of harmonic excitation of small amplitude and very high frequency only. Michaux and coworkers [30], for example, investigated the effect of the waveform of different periodic signals on the effectiveness of tangential high-frequency excitation to cancel friction-induced oscillation using a single degree of freedoms system. Hoffmann and coworkers [31] also used the MDSM to quench mode-coupling friction-induced instability using high frequency in a 2-degree of freedom system. In more recent works [32, 33], the effects of longitudinal high-frequency excitation on contact compliance considering different dynamic friction models were studied, performing analytical, numerical and experimental investigations.

In both research communities described above, the effect of external load on friction force has been studied with an emphasis on loads characterized by a high-frequency content (i.e. ultrasonic vibration over 20 kHz). However, in the literature, a clear statement as to what is considered high frequency with reference to vibration-induced friction modulation is still missing. Blekhman [28] provided a rule of thumb for applied problems, indicating that an excitation frequency around 3-5 times the natural frequency could be considered as high frequency, without showing any explicit demonstration. Moreover, the applied load directions in all the aforementioned studies is either normal or tangential to the sliding direction. The effect of a combination of load directions on the friction behavior is also missing. Lastly, the nature of the normal contact force (stiffness or inertia driven) and how the tangential friction force depends on it is also seldomly discussed. Therefore, the first aim of this study illustrated in Section 3.2 aims at extending the existing investigations on the effect of a high-frequency harmonic load to friction to a general excitation frequency range and define a threshold starting from which a high-frequency regime can be identified.

For this purpose, the MDSM will be extended considering initially a single load case. In the same section, the second aim is to unify and explain the similar results in terms of friction reduction due to vibrations (only with reference to Amonton-Coulomb’s friction law) obtained by both the aforementioned research communities, even though different methods were used from both sides (without ever cross-referencing each other). To bridge this gap, it will be shown that the underlying physical mechanism of friction reduction due to vibration resides in the velocity response function of the dynamic system. Moreover, while in some studies it is mentioned that the effect of excitation on sliding friction is investigated, none of these works (with the exception of Teidelt’s and Mao’s studies, see [23] and [25], respectively) distinguish the presence of the stick-slip and sliding regimes. To compute vibration-induced friction reduction, however, it is important to know whether the system is stick-slipping or not. Thus, in Section 3.3, it is pointed out that in order to get analytical solutions for the vibration-assisted friction

modulation, the analysis has to be framed with reference to the identification of stick-slip boundaries. To such regard, it is shown that the velocity response function is not only crucial to compute the friction modulation due to vibration, but it also provides a more intuitive insight to the identification of the stick-slip regime, compared to the analysis shown in other seminal works on such topics [34, 35, 36]. Besides the extension to a general frequency of excitation, in Section 3.4 the vibration-assisted friction reduction is also investigated for a two-degree-of-freedom system, assessing the influence of different harmonic load combinations: tangential and normal ones with reference to contact surface. Lastly, the effect of introducing a different expression of the normal contact force, dependent either on the contact stiffness and damping or on the inertial force, is investigated and its consequences on the vibration-assisted friction reduction are discussed.

3.2. METHOD OF DIRECT SEPARATION OF MOTION FOR A FORCED SINGLE DEGREE OF FREEDOM SYSTEM

In this section, a single-degree-of-freedom system will be considered to investigate the effect of external excitation on the friction force. At first, the method of direct separation of motion is illustrated to quantify such effect, limited to the case of high-frequency excitation. The vibration-induced friction reduction results are then compared with the ones obtained using alternative methods available in the literature. Lastly, the MDSM will be extended to include the effect of a general frequency of excitation.

3.2.1. ILLUSTRATIVE EXAMPLE OF THE METHOD OF DIRECT SEPARATION OF MOTION FOR HIGH-FREQUENCY EXCITATION

To illustrate the procedure of applying the MDSM, the single degree of freedom system (SDOF) characterized by a mass-spring-damper configuration in contact with a moving belt is considered, as shown in Fig. 3.1. The non-dimensional equation of motion for this system is

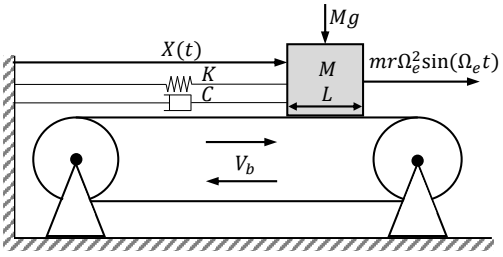

Figure 3.1: Mass-spring-damper system on a moving belt, subject to a friction force and applied harmonic loading.

$$\ddot{x} + 2\beta\dot{x} + x + \gamma^2\mu_s \text{sgn}(v_r) = \alpha\Omega^2 \sin(\Omega\tau) \tag{3.1}$$

where $\dot{x} = \frac{dx}{d\tau}$ is the non-dimensional velocity of the mass at non-dimensional time τ, μ_s is the coefficient of static friction and

$$\tau = \omega_n t, \quad \omega_n^2 = \frac{K}{M}, \quad x = \frac{X}{L}, \quad 2\beta = \frac{C}{\sqrt{KM}}, \quad \gamma^2 = \frac{g/L}{K/M}, \quad \Omega = \frac{\Omega_e}{\omega_n}, \quad \alpha = \frac{mr}{ML}, \tag{3.2}$$
$$v_r = \dot{x} - v_b, \quad v_b = \frac{V_b}{\omega_n L}.$$

For the chosen model setup, we consider the kinetic friction to be the same as the static friction. The adopted friction law for this illustrative example is the Amontons-Coulomb's law. Throughout the paper, the following formulation is used

$$\mu(v_r) = \mu_s \text{sgn}(v_r), \tag{3.3}$$

which defines the friction coefficient as a function of the relative velocity's sign. To clarify the parameters in Eq. (3.2), the belt's motion is represented by the speed V_b, the mass M is a rigid body with a characteristic length L and position $X(t)$ at time t, subjected to gravity loading Mg, a linear spring force KX, a damping force CdX/dt and a friction force $Mg\mu(V_r)$. Time is normalised by the natural frequency ω_n of the undamped system. The damping ratio is described by β and γ^2 defines the ratio between the gravity force and the spring force. Parameters v_b, Ω and α represent the non-dimensional speed of the belt, the non-dimensional frequency of harmonic excitation and the non-dimensional amplitude of excitation, respectively. The SDOF system is forced by a time-harmonic loading, characterized by a frequency Ω_e and an amplitude $mr\Omega_e^2$ (e.g., load arising from a horizontally unbalanced mass m at eccentricity r [26]). The baseline parameter values considered (unless otherwise stated in the figure captions) are shown in Table 3.1.

Table 3.1: Baseline parameter values for the 1-DOF system.

Symbol	β	μ_s	α	γ^2
Value	0.1	0.4	10	1.0

In previous works [26, 27], it was shown that if the external forcing is characterized by a high-frequency oscillation and by a small amplitude ($\Omega >> 1$ and $\alpha << 1$, respectively), the MDSM allows to quantify the reduction of the friction force, averaged over one vibration cycle, governed by the high-frequency excitation. To do so, the MDSM separates the motion $x(\tau)$ into its slow and fast components as follows

$$x(\tau) = z(\tau) + \Omega^{-1}\phi(\tau, \Omega\tau) \tag{3.4}$$

where $z(\tau)$ describes the slow motion at the time scale of free oscillation of the given SDOF system, and ϕ describes the fast motion at the rate of the external excitation. Thus, τ represents the slow time scale whereas $\Omega\tau$ defines the fast time scale. Note that these time scales are considered independent. Typically, for engineering applications (e.g.

see [3]), the effects induced by the fast motion ϕ on the motion z would be of primary interest. As discussed in [27], to make the transformation of variables from x to z and ϕ unique, the following constraint is necessary

$$\langle \phi(\tau, \Omega\tau) \rangle = \frac{1}{2\pi} \int_0^{2\pi} \phi(\tau, \Omega\tau) \mathrm{d}(\Omega\tau) = 0 \tag{3.5}$$

where <> defines the average operator over the period of the rapidly oscillating component. The transformation of variables is carried out by substituting Eq. (3.4) into Eq. (3.1), and imposing the constraint given by Eq. (3.5). The resulting expression reads as follows

$$\ddot{z} + 2\beta\dot{z} + z + \gamma^2 \langle \mu(\dot{z} + \phi' + \Omega^{-1}\dot{\phi} - v_b) \rangle = 0 \tag{3.6}$$

where $\dot{z} = \frac{dz}{d\tau}$, $\dot{\phi} = \frac{\partial\phi}{\partial\tau}$, and $\phi' = \frac{\partial\phi}{\partial(\Omega\tau)}$.

Since the purpose of this example is to quantify the effect of the external forcing on the friction force, the expression representative of the fast motion ϕ should be retained. As shown in [26, 27], to isolate the fast motion, the equation of slow motion z shown in Eq. (3.6) is subtracted from the main governing equation defined by Eq. (3.1), resulting in

$$\begin{aligned} &\Omega\phi'' + 2\dot{\phi}' + \Omega^{-1}\ddot{\phi} + 2\beta(\phi' + \Omega^{-1}\dot{\phi}) + \Omega^{-1}\phi + \\ &\gamma^2 \left(\mu(\dot{z} + \phi' + \Omega^{-1}\dot{\phi} - v_b) - \langle \mu(\dot{z} + \phi' + \Omega^{-1}\dot{\phi} - v_b) \rangle \right) = \alpha\Omega^2 \sin(\Omega\tau). \end{aligned} \tag{3.7}$$

At this stage, it is important to anticipate that when using Amontons–Coulomb's law and in the absence of a stick regime ($v_r \neq 0$), the averaged friction coefficient $\langle \mu(v_r) \rangle$ present in the equation of slow motion average acts as a constant parameter. For instance, in the case of unidirectional sliding, this constant is equal to μ_s. In this case, Eqs. (3.6)–(3.7) are simplified to

$$\ddot{z} + 2\beta\dot{z} + z + \gamma^2\mu_s = 0, \tag{3.8}$$

and

$$\Omega\phi'' + 2\dot{\phi}' + \Omega^{-1}\ddot{\phi} + 2\beta(\phi' + \Omega^{-1}\dot{\phi}) + \Omega^{-1}\phi = \alpha\Omega^2 \sin(\Omega\tau). \tag{3.9}$$

The solutions of Eq. (3.8) and Eq. (3.9) each have a transient and a steady-state response. At steady-state motion, the displacement response of the motion z is just a constant, meaning its velocity response will be zero. Since sinusoidal forcing is present on the right-hand side of Eq. (3.9), the displacement and velocity response in the steady state will be harmonic. Thus, only the solution of ϕ contributes to the steady-state velocity response. In subsection 3.2.3, a more detailed discussion concerning the link between the transient/steady-state solutions and the fast/slow components of motion will be provided.

To isolate the high-frequency vibration-induced effect on friction, we exploit the underlying assumption that $\Omega >> 1$, meaning that all the terms in Eq. (3.7) multiplied by Ω^{-1} and Ω^{-2} are small, and the equation of the fast motion can be expressed in the following compact form

$$\phi'' = \alpha\Omega \sin(\Omega\tau) + O(\Omega^{-1}) + O(\Omega^{-2}) \tag{3.10}$$

where $O(\Omega^{-1})$ and $O(\Omega^{-2})$ denote terms significantly smaller than 1. The solution of fast motion ϕ and its corresponding derivative ϕ' are

$$\phi = -\alpha\Omega\sin(\Omega\tau) \quad \text{and} \quad \phi'(\tau,\Omega\tau) = -\alpha\Omega\cos(\Omega\tau). \tag{3.11}$$

Hence, substituting this solution into the equation of the slow motion given by Eq. (3.6) results in

$$\ddot{z} + 2\beta\dot{z} + z + \gamma^2\left\langle\mu(\dot{z} - \alpha\Omega\cos(\Omega\tau) - v_b)\right\rangle = 0. \tag{3.12}$$

The following term from Eq. (3.12)

$$\bar{\mu} = \left\langle\mu(\dot{z} - v_b - \alpha\Omega\cos(\Omega\tau))\right\rangle \tag{3.13}$$

enables to quantify the vibration-induced effect on friction. Therefore, the term "effective friction" is used for $\bar{\mu}$. In this study, the expression of the effective friction force is obtained for steady-state vibratory motion only. Thus, no information is provided for the vibration-induced effect on friction during the transient response. Since steady-state motion is considered, there is no contribution due to $\dot{z}$, so the expression of relative velocity, $\dot{z} - v_b$, reduces to $-v_b$. Since the continuous-sliding regime is assumed, it should be checked that for each v_b value considered, the system remains in the sliding regime.

In case of interest, the slow motion z can be found by solving Eq. (3.12). However, to study the effect induced by the high-frequency excitation on the averaged friction force, it is sufficient to evaluate $\bar{\mu}(v_b)$. It is worth highlighting that the effective friction expression defined in Eq. (3.13) holds for any constitutive law of friction characterized by a dependence on the relative velocity. Dynamic friction laws of the rate-and-state types [37, 38] were not tested so far. On such regards, the reader might be interested in [32], where numerical solutions were provided for Eq. 3.13, while accounting for an elasto-plastic friction law. With reference to the Amontons-Coulomb's law defined in Eq. (3.3), the effective friction expression reads as follows

$$\bar{\mu}(v_b) = \left\langle\mu(-v_b - \alpha\Omega\cos(\Omega\tau))\right\rangle = \mu_s\left\langle\operatorname{sgn}(-v_b - \alpha\Omega\cos(\Omega\tau))\right\rangle, \tag{3.14}$$

$$\bar{\mu}(v_b) = \begin{cases} \mu_s(1 - \frac{2}{\pi}\arccos(-\frac{v_b}{\alpha\Omega})) & \text{for } |v_b| \le \alpha\Omega \\ \mu_s\operatorname{sgn}(-v_b) & \text{for } |v_b| \ge \alpha\Omega. \end{cases} \tag{3.15}$$

Figure 3.2 shows the effective friction defined by Eq. (3.15) as a function of the belt velocity v_b. It should be noted that, while negative signs are present in Eq. (3.14), suggesting negative friction values for positive belt velocities, the plot follows an opposite sign convention, to be comparable and in line with other studies on such topic (see [16, 17, 26]). The black dashed lines in Fig. 3.2 mark the following equality $v_{b,c} = \alpha\Omega$. The index c refers to the value of v_b from which the effective friction coefficient becomes the constant μ_s again. Two conclusions can be drawn by inspecting the $\bar{\mu}(v_b)$ vs. v_b graph. First, for $|v_b| \le \alpha\Omega$, the typical discontinuity of the coefficient of friction observed at $v_b = 0$ is smoothed, since the effective friction expression is characterized by a shape governed by the arc-cosine function. Secondly, for $|v_b| > \alpha\Omega$, the effective friction characteristic $\bar{\mu}(v_b)$ equals μ_s which is the friction value for the case of $\alpha\Omega = 0$. In other words, no effect on the averaged friction force due to the high-frequency excitation is observed.

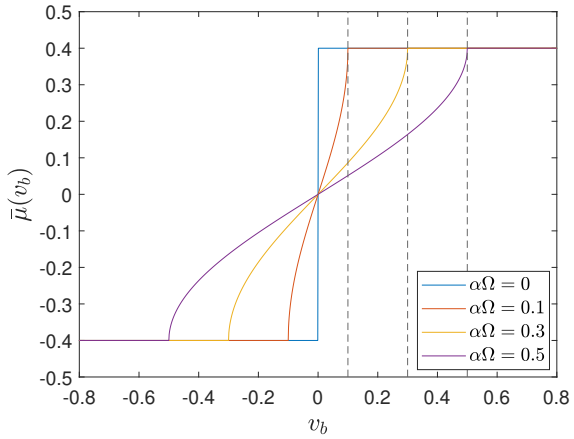

Figure 3.2: Effective friction $\bar{\mu}(v_b)$ behaviour as given by Eq. (3.15) for different values of $\alpha\Omega$.

In the next subsection, the method is compared to an alternative one used to obtain the effective friction under high-frequency excitation. Comparing the MDSM with the alternative method will allow to unify and explain the similar results in terms of friction reduction obtained by different research communities, even though different approaches were used from each side.

3.2.2. ALTERNATIVE METHODS FOR HIGH-FREQUENCY EXCITATION

In the literature, alternative models exist that predict the effect of excitation on friction. Studies by [15, 16, 17] were devoted to giving an explanation to the friction force reduction when ultrasonic vibrations were superimposed to macroscopic motions. The ultrasonic excitation was applied either parallel or perpendicular to the sliding direction. The reduction on friction was analyzed both experimentally as well as theoretically, and for the latter, Amontons-Coulomb's law was considered.

Figure 3.3(a) shows the model considered by [16, 17], with the excitation applied parallel to the sliding direction. Body A is assumed to slide with a constant velocity V_b over body B, which has an oscillatory motion of amplitude α and angular frequency Ω_e along the same line of action as that of V_b. When the instantaneous velocity of B, $V(t)$, is greater than V_b, the friction force on body A, F_f, will reverse its direction and act in the same direction as V_b. In Fig. 3.3(b), the corresponding variation of frictional force with time over one cycle is shown. The friction force, F_f, first changes from positive to negative and then to positive again (interval OC, CD and DG, respectively). The time t_b taken for the vibration velocity to reach the sliding velocity V_b is given by

$$t_b = \frac{1}{\Omega_e} \sin^{-1}\left(\frac{V_b}{\alpha\Omega_e}\right). \tag{3.16}$$

The time CD for which the friction force is negative is equal to the time EF over which it is positive. While averaging over one cycle, these two will cancel each other out. The

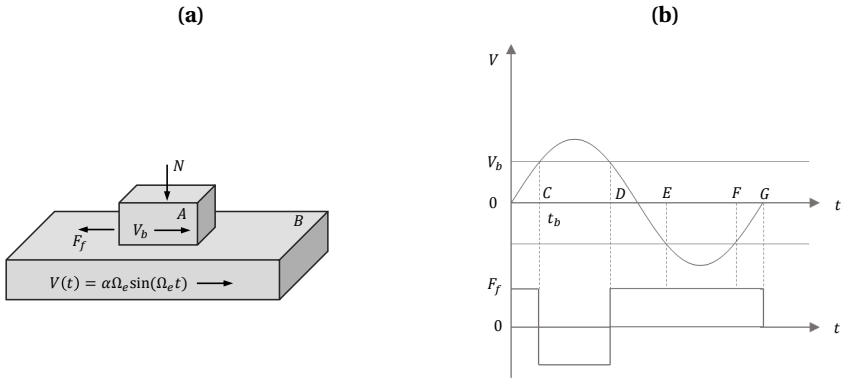

Figure 3.3: (a) The model considered for sliding motion and subjected to an excitation along the sliding direction; (b) Variation of vibration velocity with time and the corresponding change in direction of frictional force.

resultant average frictional force over the whole cycle F_a is thus given by

$$F_a = \frac{F_f}{T} 4 t_b = F_f \frac{2}{\pi} \sin^{-1}\left(\frac{V_b}{\alpha\Omega_e}\right). \tag{3.17}$$

where $T = \frac{2\pi}{\Omega_e}$ is the period of vibration.

Equation (3.17) is valid only for $\alpha\Omega_e > V_b$, so the amplitude of the velocity of body B should be bigger than the constant velocity V_b. If the sliding velocity V_b is higher, Eq. (3.17) ceases to apply because, in that case, the friction force opposes the direction of macroscopic sliding during the whole duration of a cycle of vibration. Since the friction force does not change direction, no reduction in friction is predicted. Considering the friction force, $F_f = \mu_s N$, and the constant sliding velocity V_b to be either positive or negative, the effective friction under the effect of ultrasonic oscillation can be written as

$$\mu_a = \begin{cases} \mu_s \frac{2}{\pi} \sin^{-1}\left(\frac{V_b}{\alpha\Omega_e}\right) & \text{for } |V_b| \leq \alpha\Omega_e \\ \mu_s \text{sgn}(V_b) & \text{for } |V_b| \geq \alpha\Omega_e. \end{cases} \tag{3.18}$$

where $\mu_a = F_a / N$.

Equation (3.18) portrays the effect of ultrasonic oscillations on the friction force, thus, it should be possible to compare it with the effective friction expression obtained in Eq. (3.15). Firstly, it is important to realize that the constant belt velocity v_b and the excitation frequency Ω used in subsection 3.2.1 are non-dimensional terms. Thus, for $\omega_n = 1$ and $L = 1$, v_b and Ω correspond to V_b and Ω_e (see Eq. (3.2)), respectively. From both expressions (Eqs. (3.15) and (3.18)), it is inferred that for belt velocities higher than the amplitude of the oscillation velocity, no change in friction force is observed. To compare the equations for belt velocities lower than $\alpha\Omega_e$, both expressions are plotted in Fig. 3.4 for $\alpha\Omega_e = 0.3$. From the figure, it is observed that the plots coincide, proving that both methods give the same results.

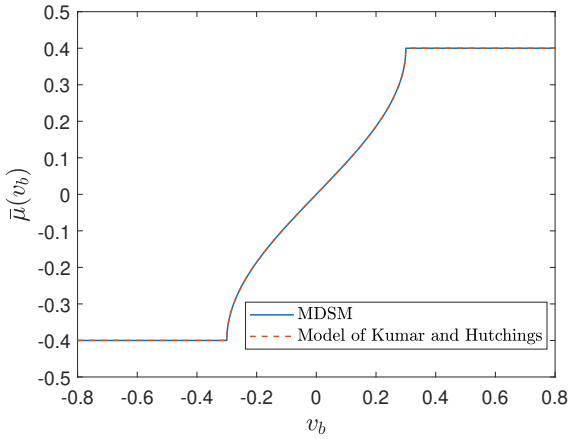

Figure 3.4: Comparison of $\bar{\mu}(v_b)$ obtained using MDSM and the model of [17].

It is worth highlighting again that these results (using MDSM and by [17]) are reached considering steady-state vibratory motion within a continuous-sliding regime. For certain combinations of belt velocity, excitation amplitude and frequency, stick-slip might occur, making the analytical expressions of the effective friction force invalid. However, none of the studies explicitly mention such limitation. Moreover, while it is possible to straightforwardly get the effective friction force using the rationale depicted in Fig. 3.3, see also [16, 17], this model gives the same results as the MDSM for the case of Amontons-Coulomb's law and high-frequency vibration. If another friction law or a general frequency of excitation is considered, it becomes hard or even impossible to obtain the effective friction characteristic with this approach. Moreover, the MDSM is more versatile, since it can be applied to systems with more than just one degree of freedom.

The rationale depicted in [16, 17] was also used to evaluate a friction change considering the Dahl model, see [18], which accounts for the asperity's compliance along the sliding direction. To solve for this model, however, a numerical procedure was implemented, and the friction force reduction was calculated over one period of oscillation. While in the case of the Amontons-Coulomb's law, the change in friction force direction occurs instantaneously, Fig. 3.3(b), when using the Dahl model, the change of friction force direction is not abrupt and depends on the value of the tangential contact stiffness. In the latter model, like [16, 17], a friction reduction was observed only for $V_b < \alpha\Omega_e$. As the value of the tangential contact stiffness increases, the Dahl model reduces to Eq. (3.18).

3.2.3. EXTENSION OF THE MDSM FOR A GENERAL FREQUENCY OF EXCITATION

In subsections 3.2.1 – 3.2.2, the effect of high-frequency excitation on friction was presented. To seek a more general expression able to quantify the vibration-induced effect on friction, the following subsection aims at extending the MDSM procedure illustrated above to a general frequency of excitation of the system. A modification of the MDSM

aiming at relaxing the restriction on the spectrum of excitation frequencies was already proposed in previous studies [28, 29]. However, its application to a friction-driven system has never been investigated. To illustrate the procedure, the system shown in Fig. 3.1 is considered again. As already discussed in subsection 3.2.1, to compute the effective friction expression, the equation for the fast motion ϕ, Eq. (3.7), is needed.

In subsection 3.2.1, since $\Omega >> 1$, all the terms multiplied by Ω^{-1} and Ω^{-2} were small terms and could be ignored. To find the effect caused on the averaged friction force by a general frequency of excitation, the condition $\Omega >> 1$ does not hold anymore, meaning that all the terms in Eq. (3.7) should be retained. It is worth highlighting that the assumption $\Omega >> 1$ is relevant if the interest resides in computing the effect of excitation on the slow motion term $z(\tau)$. However, if the interest lies only in computing an averaged friction force reduction during a steady-state oscillatory motion, an analytical expression of the friction reduction can be obtained for a general harmonic forcing.

To solve Eq. (3.7), the rationale used in [28, 29] is adopted. It is worth highlighting that the extension of the MDSM to a general harmonic forcing presented in this section differs from the one shown in [28, 29], as it considers the original MDSM. The solution is sought in the form of a harmonic series by means of the method of varying amplitude (MVA) proposed in [39] and also applied in [28, 29]. A possible harmonic series solution is

$$\phi = B_{11}(\tau)\sin(\Omega\tau) + B_{12}(\tau)\cos(\Omega\tau) + B_{21}(\tau)\sin(2\Omega\tau) + B_{22}(\tau)\cos(2\Omega\tau) + ... \tag{3.19}$$

In the leading-order approximation, only the first two terms are needed, resulting in

$$\phi = B_{11}(\tau)\sin(\Omega\tau) + B_{12}(\tau)\cos(\Omega\tau). \tag{3.20}$$

Note that as continuous sliding is considered and no nonlinearities are present in the system, Eq. (3.20) provides the closed-form solution. Moreover, the time-scale τ of the varying amplitude of the B_{11} and B_{12} parameters do not need to vary slowly with reference to the time-scale of the sinusoidal function $\Omega\tau$, as discussed in [39].

Inserting Eq. (3.20) into Eq. (3.7), and gathering the coefficients of the involved harmonics $\sin(\Omega\tau)$, $\cos(\Omega\tau)$, results in one expression for $\ddot{B}_{11}$ and one for $\ddot{B}_{12}$. Using some cumbersome mathematical manipulations, the solution for ϕ in Eq. (3.7) can be obtained analytically. Both $B_{11}(\tau)$ and $B_{12}(\tau)$ approach to a constant value as τ increases, thus reaching a steady-state condition. At steady state, $B_{11}(\tau)$ and $B_{12}(\tau)$ are described by

$$B_{11} = -\frac{\alpha\Omega^3(\Omega^2-1)}{(4\beta^2-2)\Omega^2+1+\Omega^4}, \quad B_{12} = -\frac{2\beta\alpha\Omega^4}{(4\beta^2-2)\Omega^2+1+\Omega^4}. \tag{3.21}$$

Using these expressions for B_{11} and B_{12}, the solution in terms of ϕ in the steady state (same symbol used for notational brevity) becomes

$$\phi = \frac{\alpha\Omega^3}{\sqrt{4\beta^2\Omega^2+(1-\Omega^2)^2}}\sin(\Omega\tau+\theta) = \hat{V}\sin(\Omega\tau+\theta) \tag{3.22}$$

and its derivative with respect to $\Omega\tau$ leads to

$$\phi' = \frac{\alpha\Omega^3}{\sqrt{4\beta^2\Omega^2+(1-\Omega^2)^2}}\cos(\Omega\tau+\theta) = \hat{V}\cos(\Omega\tau+\theta) \tag{3.23}$$

where

$$\hat{V} = \frac{\alpha\Omega^3}{\sqrt{4\beta^2\Omega^2 + (1-\Omega^2)^2}} \quad \text{and} \quad \theta = \arctan(2\beta\Omega, \Omega^2 - 1). \tag{3.24}$$

At steady state, ϕ is only a function of $\Omega\tau$, hence the expression of the effective friction function, Eq. (3.6), simplifies to

$$\bar{\mu}(v_b) = \mu_s \langle \text{sgn}(-v_b + \phi' + \Omega^{-1}\dot{\phi}) \rangle = \mu_s \langle \text{sgn}(-v_b + \phi') \rangle , \tag{3.25}$$

where $\dot{z}$ is omitted as it has no contribution in steady-state motion. By inserting Eq. (3.23) into Eq.(3.25), the equation of the effective friction function for harmonic excitation with arbitrary frequency becomes

$$\bar{\mu}(v_b) = \mu_s \langle \text{sgn}(-v_b + \hat{V}\cos(\Omega\tau + \theta)) \rangle = \begin{cases} \mu_s \left(1 - \frac{2}{\pi} \arccos\left(\frac{v_b}{\hat{V}}\right)\right) & \text{for } |v_b| \le \hat{V} \\ \mu_s \text{sgn}(v_b) & \text{for } |v_b| \ge \hat{V}. \end{cases} \tag{3.26}$$

Equation (3.26), combined with Eq. (3.24), highlights that for large values of Ω, the parameter $\hat{V}$ approaches asymptotically the value of $\alpha\Omega$, which is the amplitude of the harmonically varying term in Eq. (3.13). Concurrently, the phase angle θ in Eq. (3.24) tends to vanish. To clarify this observation, Fig. 3.5(a) compares the relation between the parameter $\hat{V}$ as a function of Ω, with the linear and monotonic trend defined by the amplitude $\alpha\Omega$ of the harmonic varying term in Eq. (3.13). Figure 3.5(b) displays the behaviour of θ for increasing values of Ω. The values to generate the plot are reported in the caption of Fig. 3.5.

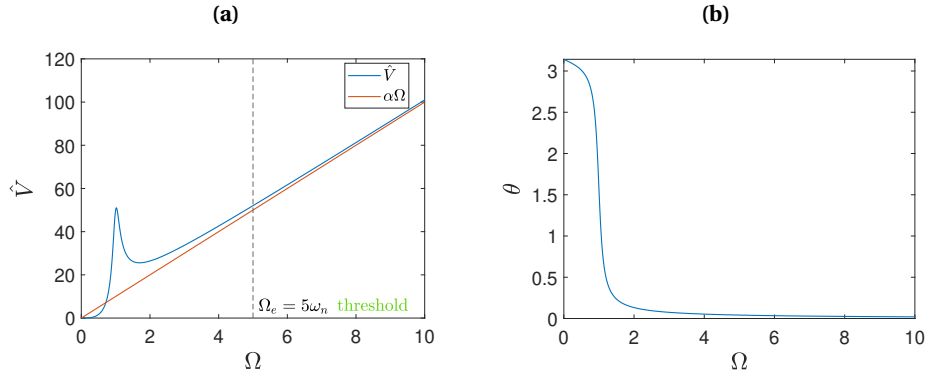

Figure 3.5: (a) Coefficient $\hat{V}$ versus Ω; (b) θ versus Ω. Plots obtained for $\beta = 0.1$ and $\alpha = 10$.

From Fig. 3.5, it can be concluded that if Ω lies in the high-frequency regime, the solution of ϕ' provided in Eq. (3.23), matches the solution shown for ϕ' given in Eq. (3.11). The comparison highlighted in Fig. 3.5a also allows to identify a non-dimensional threshold frequency of excitation that discriminates between a high-frequency and near-resonant or low-frequency region. The value of $\Omega_e = 5\omega_n$ could be considered as a possible minimum value of excitation frequency for the high-frequency band. The relative error between $\hat{V}$ and $\alpha\Omega$ at such threshold is 3.9%. It is worth mentioning that the MDSM technique

is commonly used for systems subject to high-frequency excitation. However, in the literature, an explicit and proven statement on what the minimum frequency starting from which a high-frequency regime can be defined has never been provided.

While the trend of $\hat{V}$ over the high-frequency regime resembles a linear one, a nonlinear trend is observed near resonance. A rapid increase and decrease can be noticed as soon $\hat{V}$ approaches and exceeds, respectively, the resonance frequency $\Omega_e = \omega_n = 1$. Figure 3.6(a) examines closely the latter regime, and specifically, four colored markers were placed to inspect the behaviour of the corresponding effective friction expression. Figure 3.6(b) shows the trend of $\bar{\mu}(v_b)$ with reference to the colored markers in Fig 3.6(a). Similarly to what was discussed with reference to Fig. 3.2, the value of $v_{b,c}$ corresponds to the value of $\hat{V}$ which marks the point after which the effective friction coefficient becomes μ_s and remains constant. As the magnitude of Ω increases from 0, the value of $v_{b,c}$ ($= \hat{V}$) that separates the constant region from the varying one of $\bar{\mu}(v_b)$, increases as well, until the resonance condition is reached (see the red marker and the red line in Figs. 3.6(a),(b) respectively). For $\Omega \approx 1$ (small damping present), the threshold value of $v_{b,c}$ is $|v_{b,c}| \approx 50$, and it decreases for the further selected points at $\Omega = 1.2$ and $\Omega = 4$ (orange and purple markers and lines, correspondingly). For the high-frequency range, the value of $v_{b,c}$ (or $\hat{V}$) only increases with an increase in Ω.

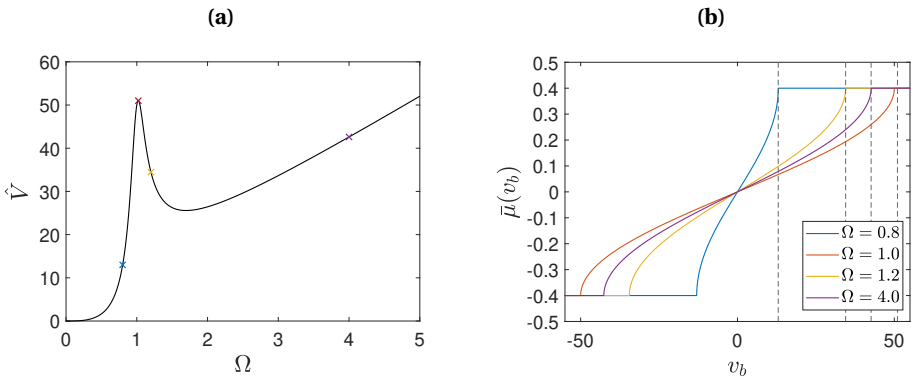

Figure 3.6: (a) $\hat{V}$ versus Ω; (b) $\bar{\mu}(v_b)$ behaviour for different excitation magnitudes. Plots obtained for $\beta = 0.1$ and $\alpha = 10$. The colored markers in (a) are linked to the corresponding colored lines in (b).

In subsection 3.2.1, it was mentioned that in the case of Amontons-Coulomb's law and during a full-slip regime (absence of stick-slip), the solution of the equation of motion for z has no contribution in the steady-state velocity response. Thus, the velocity response can be found by solving the equation of motion for ϕ. This kind of correspondence has never been explicitly pointed out in any previous study with reference to the MDSM technique. It is shown here that such correspondence holds also for the case of the extended version of the MDSM, valid for a general excitation with arbitrary frequency. For the considered system, Eq. (3.1), the steady-state solution x_{ss} (for $\dot{x} > v_b$) is

$$x_{ss} = \frac{\alpha\Omega^2}{\sqrt{4\beta^2\Omega^2 + (1-\Omega^2)^2}} \sin(\Omega\tau + \theta) + \mu_s \tag{3.27}$$

and its derivative then becomes

$$\dot{x}_{ss} = \frac{\alpha\Omega^3}{\sqrt{4\beta^2\Omega^2 + (1-\Omega^2)^2}}\cos(\Omega\tau+\theta) = \hat{V}\cos(\Omega\tau+\theta) = \phi' \tag{3.28}$$

The expression of $\dot{x}_{ss}$ would be the same for $\dot{x} < v_b$ as well, as the contribution of the friction force within the particular solution given in Eq. (3.27) is provided by a constant ($\pm\mu_s$). Therefore, Eq. (3.28) exactly corresponds to the derivative of motion ϕ' given in Eq. (3.23). The expression $\hat{V}$ corresponds to the amplitude of the velocity response function of the system (Eq. (3.1)), subject to the Amontons-Coulomb's friction force and considering a sliding regime (absence of stick-slip motion). The correspondence between $\hat{V}$ and the system's velocity response function facilitates the interpretation of the vibration-induced effects on the friction force, hence, avoiding cumbersome calculations to find the expression of ϕ' for an arbitrary frequency using the extended MDSM. The effective friction force function $\bar{\mu}(v_b)$ and the expression for ϕ' can be straightforwardly found by means of the velocity response function of the given system. Comparing the cases presented in subsections 3.2.1- 3.2.2 (MDSM and the model used in [16, 17]), the effective friction force expression seemed to come out mainly from mathematical considerations, while, as revealed here, it is actually part of a physical process related to the velocity response of the system. While for high frequencies the effective friction expression is driven by the velocity solely induced by inertial effects, as the frequency of excitation decreases, the influence of damping and stiffness forces comes into play.

Lastly, to validate the analytical results numerically, a comparison of the analytical solution of $\bar{\mu}(v_b)$ (solid line) versus the numerical solution of $\bar{\mu}(v_b)$ (dashed line), for the case of a low-frequency and high-frequency excitation (high and low relative to the natural frequency of the system) is shown in Fig. 3.7(a) and Fig. 3.7(b), respectively. Note that the numerical solution (steady state) of ϕ', Eq. (3.19), is obtained for a set of parameter values in which no stick-slip occurs. In both figures, it can be observed that the analytical solution matches the numerical one, proving that the analytical solutions of ϕ' and $\bar{\mu}(v_b)$ are correct. The following section will demonstrate that the velocity response function can not only be exploited to calculate the effective friction expression but also to define the boundaries of the transition between the stick and slip regimes.

3.3. IMPLICATIONS TO STICK-SLIP ANALYSIS FOR AN OSCILLATOR AND BELT SYSTEM

As highlighted in this study, the expression of the effective friction force for a generic harmonic excitation is obtained for the steady-state oscillatory motion in continuous sliding. However, for certain belt velocities, excitation amplitudes and frequencies, stick-slip might occur, making the analytical expressions, such as Eq. (3.26), invalid. Thus, it is crucial to define the boundaries of the transition from the stick-slip to the slip regime. To achieve this, the analysis performed by den Hartog [40] in his seminal work is first considered. The investigated model is a single mass-spring-damper system with Amontons-Coulomb's law, similar to the one presented in Fig. 3.1, but without the moving belt. For this system, the stick-slip boundaries are defined by the graph shown in Fig. 3.8(a), as a function of the ratio between forcing and natural frequency $\Omega = \Omega_e/\omega_n$

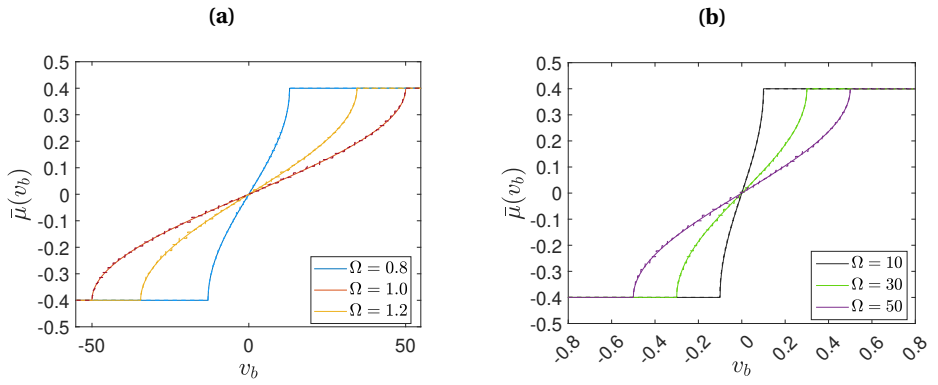

Figure 3.7: (a) Comparison of numerical (dashed line) and analytical (solid line) solutions of effective friction for the case of low-frequency excitation; (b) Same comparison for the case of high-frequency excitation ($\beta = 0.1$ and $\alpha = 10$).

and the ratio between friction force and excitation amplitude $\mu_s N/mr\Omega_e^2$ for different values of damping ratio β. The region below the lines defines the continuous-slip regime and the one above indicates the stick-slip regime.

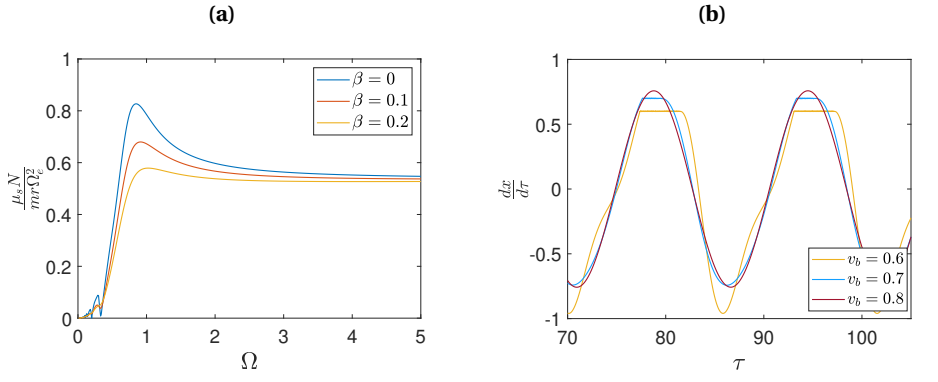

Figure 3.8: (a) Stick-slip boundary for a damped SDOF system subjected to harmonic excitation (see [40]); (b) Velocity response for different belt velocities, $\beta = 0.1$, $\alpha = 10$, and $\Omega = 0.4$.

Using the graph for specific values of μ_s, β and excitation amplitude, the range of frequencies for which the mass is in continuous-slip motion can be determined. For these frequencies, regardless of the presence of the moving belt and the corresponding belt velocity, the mass will always be characterized by a continuous-slip motion, provided no dependency between friction force and slip velocity magnitude is assumed. The presence of a moving belt only shifts the equilibrium position around which the mass oscillates. For the range of frequencies for which stick-slip is present in den Hartog's model, the presence of the belt and its corresponding velocity plays an important role in

eliminating stick-slip. For the latter case, the condition presented below is necessary

$$V_b > |\hat{V}|. \tag{3.29}$$

If the belt velocity is larger than $|\hat{V}|$, the relative velocity between the mass and the belt will not cross zero, hence stick-slip will not occur. This finding was already discussed in [35], and it is important to highlight here that $|\hat{V}|$ simply corresponds to the amplitude of the velocity response function. Therefore, if for a certain excitation frequency stick-slip is present for $V_b = 0$, to eliminate stick-slip, V_b should simply be bigger than the magnitude of the velocity response function (obtained assuming continuous slip) for that excitation frequency.

As an example, Fig. 3.8(b) shows the velocity responses of a SDOF system for different V_b values. The tangential excitation frequency is the same for all cases and, when assuming continuous slip, the corresponding amplitude of $\hat{V} = 0.76$ is identified. Figure 3.8(b) shows that for $V_b < \hat{V}$ stick-slip is present while for $V_b > \hat{V}$, the motion is continuous. Thus, to prevent stick-slip, a belt velocity $V_b > \hat{V}$ is necessary. With reference to the effective friction expression, see Eq. (3.26) and Fig. 3.6(b), and for the specific case of assuming Amontons-Coulomb's law, the condition of $V_b > \hat{V}$ results in no variation of the friction force. Thus, before performing an analysis to calculate the effective friction for a specific excitation frequency, the first step is to check whether stick-slip or continuous-slip motion is present for the case with a non-moving belt (den Hartog's model). If the latter system is in continuous-slip motion, the effective friction of the actual system can be calculated for any belt velocity. If den Hartog's model is in stick-slip regime for a specific excitation frequency, a belt velocity higher than the amplitude of the velocity response function (obtained assuming continuous slip) will eliminate stick-slip. In the case of Amontons-Coulomb's law (no dependence between friction force and magnitude of slip velocity), this also leads to no variation of the friction force due to the high belt velocity. While the illustrative example presented here only refers to a single-degree-of-freedom system, as it will be shown in the next section, the same conclusion holds for a multi-degree-of-freedom system as well.

3.4. VIBRATION-INDUCED FRICTION MODULATION FOR A HARMONICALLY FORCED 2-DOF SYSTEM IN SLIDING REGIME

The following section makes use of the extended MDSM to quantify the vibration-induced effect on friction for a multi-degree-of-freedom system in the absence of any stick regime. Different load directions and combinations are considered. The results are then compared to each other and to the ones obtained by exploiting the velocity response function of the system, which allows bypassing the cumbersome mathematical steps needed for the extended MDSM.

3.4.1. DESCRIPTION OF THE HARMONICALLY FORCED 2-DOF SYSTEM

To illustrate the procedure, a two-degree-of-freedom (2-DOF) model is investigated as shown in Fig. 3.9. The system consists of a mass M positioned on a belt moving at

a constant speed V_b. The mass is being held in position by two linear springs with stiffnesses K_1 and K_2, and by two linear dashpots with damping coefficients C_1 and C_2, for which subscripts 1 and 2 refer to the parallel and normal direction with respect to the belt surface, respectively. The spring K_2 and the dashpot C_2 are respectively considered as the normal contact stiffness and damping between the objects in relative sliding motion. Regarding the external load, three cases will be studied: tangential loading only, normal loading only, and the combination of these two, as shown in Fig. 3.9. For all the considered loading scenarios, the external harmonic loading is characterized by a frequency Ω_e and amplitude $Ma\Omega_e^2$.

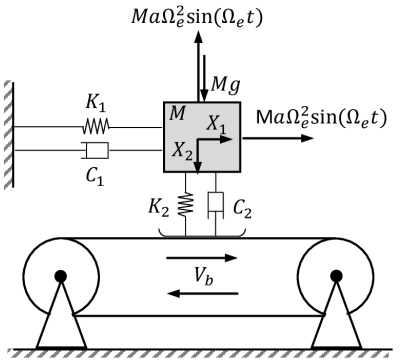

Figure 3.9: Layout of the 2-DOF system subject to external harmonic loads in the normal and tangential directions.

If no external loading is present, the equations of motion for the 2-DOF system read as follows

$$M\ddot{X}_1 + C_1\dot{X}_1 + K_1X_1 + F_f = 0 \tag{3.30}$$

$$M\ddot{X}_2 + C_2\dot{X}_2 + K_2X_2 - Mg = 0 \tag{3.31}$$

where F_f is the frictional force. As mentioned earlier, the frictional force F_f is assumed to obey Amontons-Coulomb's law, given by $F_f = \mu(V_r)F_n$ with $\mu(V_r)$ referring to the dimensional form of Eq. (3.3). In this study, we assume the normal force, F_n, to be dependent on the contact stiffness and the damping in the X_2 direction. Therefore, the expression of the friction force becomes

$$F_f = \mu(V_r)F_n = \mu(V_r)(C_2\dot{X}_2 + K_2X_2). \tag{3.32}$$

This expression for F_f is chosen to demonstrate the effect of the contact resonance on the effective friction expression. The equations of motion of the system in the absence of

an external load can be rewritten in a more generic form as

$$\begin{bmatrix} 1 & 0 \\ 0 & 1 \end{bmatrix} \begin{pmatrix} \ddot{X}_1 \\ \ddot{X}_2 \end{pmatrix} + \begin{bmatrix} 2\beta_1\omega_1 & 0 \\ 0 & 2\beta_2\omega_2 \end{bmatrix} \begin{pmatrix} \dot{X}_1 \\ \dot{X}_2 \end{pmatrix} + \begin{bmatrix} \omega_1^2 & 0 \\ 0 & \omega_2^2 \end{bmatrix} \begin{pmatrix} X_1 \\ X_2 \end{pmatrix} + \begin{pmatrix} \mu(V_r)(2\beta_2\omega_2\dot{X}_2 + \omega_2^2 X_2) \\ -g \end{pmatrix} = \begin{pmatrix} 0 \\ 0 \end{pmatrix} \tag{3.33}$$

where $\beta_i = \frac{C_i}{2M\omega_i}$ and $\omega_i^2 = \frac{K_i}{M}$ and $i = 1,2$. The baseline parameter values considered (unless otherwise stated in the figure captions) are shown in Table 3.2. In the following

Table 3.2: Baseline parameter values for the 2-DOF system.

Symbol	ω_1	ω_2	β_1	β_2	μ_s	a	γ^2
Value	1.0	0.5	0.1	0.15	0.4	10	1.0

subsection, the first loading case, that of tangential load only will be investigated.

3.4.2. TANGENTIAL HARMONIC LOADING

If only a tangential harmonic load is considered, the right-hand side of Eq. (3.33) containing the external loading $\mathbf{F}_{ext}$ becomes

$$\mathbf{F}_{ext} = \begin{pmatrix} \alpha\Omega_e^2 \sin(\Omega_e t) \\ 0 \end{pmatrix}. \tag{3.34}$$

As mentioned in Section 3.3, the first step is to define the stick-slip boundary. According to [40], the boundary is defined by the graph shown in Fig. 3.8(a), as a function of the ratio between forcing and natural frequency $\Omega = \Omega_e/\omega_1$ and the ratio between friction force and excitation amplitude (the latter being $\mu_s N/mr\Omega_e^2$ for the SDOF) for different values of damping ratio β. In this case, since no external load is present in the X_2 direction, no motion will occur in this direction. The system then reduces to a SDOF one, and the ratio between the friction force and the excitation amplitude becomes $\mu_s g/\alpha\Omega_e^2$. Figure 3.10 shows the graph defining the stick-slip boundary and the graph of $\mu_s g/P_t$, where $P_t = \alpha\Omega_e^2$ is the amplitude of the tangential external force in Eq. (3.34). As shown in Fig. 3.10, for frequencies $\Omega = \Omega_e/\omega_1$ higher than approximately 0.78, the mass will be in the sliding regime. For these frequencies, analytical expressions for the effective friction are valid.

Having defined the stick-slip boundary, the effective friction expression $\bar{\mu}(V_b)$ can be derived using the extended MDSM. However, since the loading is applied in the tangential direction only and the system reduces to a single degree of freedom one, the effective friction characteristic is the same as in subsection 3.2.2 (valid for Ω higher than approximately 0.78). This correspondence holds since the value of $\omega_1 = 1$ and the used values of β_1 and α are the same for both cases. In the next subsection, the 2-DOF system subject to a normal harmonic loading only (index n referring to the latter) is considered.

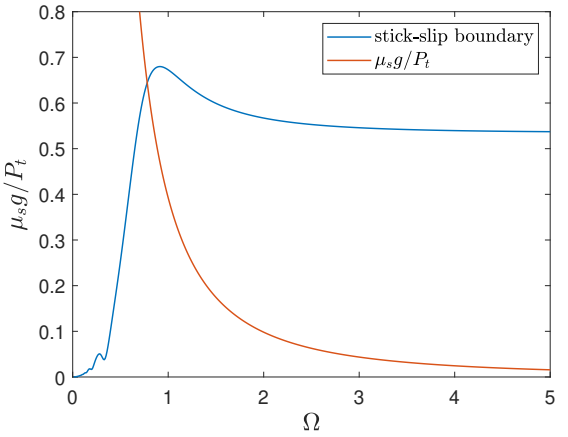

Figure 3.10: Stick-slip boundary for the 2-DOF system with external loading applied in tangential direction only ($\alpha = 10$ and $\mu_s = 0.4$).

3.4.3. NORMAL HARMONIC LOADING

When the system represented in Fig. 3.9 is only subject to the normal loading, the right-hand side of Eq. (3.33) containing the external loading $\mathbf{F}_{ext}$ becomes

$$\mathbf{F}_{ext} = \begin{pmatrix} 0 \\ -\alpha\Omega_e^2 \sin(\Omega_e t) \end{pmatrix}. \tag{3.35}$$

Since motion is present in the X_2 direction and since the tangential friction force F_f, Eq. (3.32), depends on X_2 and $\dot{X}_2$, mode coupling is present due to the friction force and motion is expected to be exhibited in both directions. To ensure an analytical solution for full vibration cycles, it should be noted that the amplitude of oscillation in the X_2 direction should be smaller than the static contact compression given by

$$X_{2,0} = \frac{Mg}{K_2} = \frac{g}{\omega_2^2}, \tag{3.36}$$

in which case the mass is always in contact with the belt. For amplitudes of vertical oscillation higher than $X_{2,0}$, the belt is in a state of intermittent contact (jumping case). Figure 3.11 shows a comparison of the limit $X_{2,0}$ with the amplitude of displacement in the X_2 direction for a range of α and Ω_e. As the displacement values are below the limit, for the parameters considered in the study, the mass is always in contact with the belt. It should be noted that different parameters such as a higher amplitudes of excitation or lower damping will result in higher amplitudes of displacement in the X_2 direction, and eventually in jumping scenarios for which the analytical results on friction modulation are not valid.

To ensure that stick-slip is not occurring, the same analysis as described in Section 3.3 for the SDOF should be performed now considering the 2-DOF system. As mentioned in Section 3.3, the first step is to check whether slick-slip or continuous sliding is present

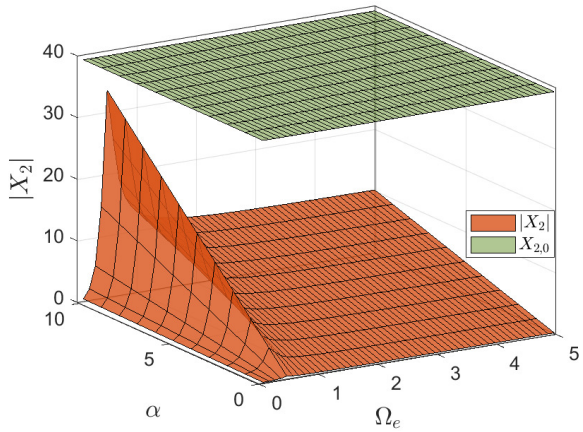

Figure 3.11: Comparison of the amplitude of displacement $|X_2|$ (orange), and the static contact compression $X_{2,0}$ (green) for a range of α and Ω_e ($\omega_1 = 1$, $\omega_2 = 0.5$, $\beta_1 = 0.1$, $\beta_2 = 0.15$, $\alpha = 10$ and $\mu_s = 0.4$)

for the case with a non-moving belt (den Hartog's model). For the 2-DOF system with normal load only, and with friction force described as in Eq. (3.32), if a non-moving belt is present, no motion is occurring in the tangential direction. For oscillations to be present in this direction, a moving belt is necessary. Then, a belt velocity higher than the amplitude of the velocity response function (obtained assuming continuous slip) will ensure continuous sliding. Since Amontons-Coulomb's law is assumed (no dependence between the friction force and the magnitude of the slip velocity), this also leads to no variation of the friction force due to the high belt velocity. Thus, for the 2-DOF system with normal loading only, the mass will be in continuous sliding only for belt velocities higher than the amplitude of the velocity response function (obtained assuming continuous slip), for which no friction change will be observed. Since this loading case leads to no friction change, there is no need to neither solve for the equations of motion for Φ (see Appendix A.1) nor to compute the velocity response function. In the next subsection, these analyses are performed for a general setup subjected to harmonic loads in different directions.

3.4.4. GENERAL HARMONIC LOAD SETUP

When both tangential and normal loading is present, the right-hand side of Eq. (3.33) containing the external loading $\mathbf{F}_{ext}$ becomes

$$\mathbf{F}_{ext} = \begin{pmatrix} \alpha\Omega_e^2 \sin(\Omega_e t) \\ -\alpha\Omega_e^2 \sin(\Omega_e t) \end{pmatrix}. \tag{3.37}$$

which is a superposition of the tangential force, Eq. (3.34), and the normal force, Eq. (3.35). Since the normal loading is the same as in subsection 3.4.3, the mass is in continuous contact (provided the parameter values chosen are the same). The next step is to define

the stick-slip boundary, for which the ratio between the friction force and the excitation amplitude for the motion in the X_1 direction should be calculated. Considering a non-moving belt and $\dot{X}_1 < 0$ (as in [40]), the equation of motion is

$$\ddot{X}_1 + 2\beta_1\omega_1\dot{X}_1 + \omega_1^2 X_1 - \mu_s(2\beta_2\omega_2\dot{X}_2 + \omega_2^2 X_2) = \alpha\Omega_e^2 \sin(\Omega_e t). \tag{3.38}$$

The expressions for X_2 and $\dot{X}_2$ can be found by solving the equation of motion in the vertical direction. Equation (3.38) then becomes

$$\ddot{X}_1 + 2\beta_1\omega_1\dot{X}_1 + \omega_1^2 X_1 - \mu_s g = -\frac{\mu_s\alpha\Omega_e^2(\omega_2^2\sin(\Omega_e t+\theta) + 2\beta_2\omega_2\Omega_e\cos(\Omega_e t+\theta))}{\sqrt{4\beta_2^2\omega_2^2\Omega_e^2 + (\omega_2^2-\Omega_e^2)^2}} + \alpha\Omega_e^2\sin(\Omega_e t) \tag{3.39}$$

and the excitation amplitude is found using the terms on the right-hand side. Note that the static contribution of the contact force, i.e. the $\mu_s g$ term, is written on the left-hand side of the equation. Figure 3.12(a) shows the graph defining the stick-slip boundary and the graph of $\mu_s g / P_{tn}$, where P_{tn} is the amplitude of the harmonic force on the right-hand side in Eq. (3.39). As it is shown in the figure, for frequencies $\Omega = \Omega_e/\omega_1$ higher than ≈ 0.84, the mass will be in the sliding regime. For these frequencies, the analytical expressions for the effective friction will be valid.

To obtain the effective friction expression, first the extended MDSM is used and the equations of motion for Φ are solved analytically as shown in Appendix A.1. All expressions of the coefficients of the harmonics (i.e., $B_{11}(\tau)$, $B_{12}(\tau)$, $B_{21}(\tau)$ and $B_{22}(\tau)$) approach to a constant value as τ increases reaching a steady-state condition (see Appendix A.1) and the expression for Φ_1' in steady state is

$$\Phi_1' = \hat{V}_{tn}\cos(\Omega_e\tau + \theta_{tn}), \tag{3.40}$$

where

$$\hat{V}_{tn} = \frac{\alpha\Omega_e^3\sqrt{4\beta_2^2\omega_2^2\Omega_e^2(\mu_s+1)^2 + (\omega_2^2-\Omega_e^2)^2 + \mu_s\omega_2^2(\mu_s\omega_2^2 - 2\Omega_e^2 + 2\omega_2^2)}}{\sqrt{(4\beta_1^2\omega_1^2\Omega_e^2 + (\omega_1^2-\Omega_e^2)^2)(4\beta_2^2\omega_2^2\Omega_e^2 + (\omega_2^2-\Omega_e^2)^2)}}. \tag{3.41}$$

for which index tn refers to tangential-normal loading. Since coupling between the two degrees of freedom is present due to the assumed friction law, differently from the tangential loading case, there is a dependence between $\hat{V}_{tn}$ and μ_s. Moreover, since oscillations are occurring in both directions, $\hat{V}_{tn}$ depends also on the system characteristics (mass, stiffness and damping values) in both directions and on the amplitude and frequency of excitation.

Next, the velocity response function $\hat{Y}_1(\Omega_e)$ is found using Eqs. (A.6)– (A.10), Appendix A.2, with $\mathbf{F}_{ext}$ represented as in Eq. (3.37). In Fig. 3.12(b), a comparison of $|\hat{Y}_1(\Omega_e)|$ with $\hat{V}_{tn}$ for a range of μ_s values is shown. The plot of $|\hat{Y}_1(\Omega_e)|$ coincides with that of $\hat{V}_{tn}$, and both of them approach the trend of the velocity amplitude given by the high-frequency excitation only as the frequency increases. The stick-slip regime is also indicated in the figure in magenta. An increase in μ_s value results in an increase in the stick-slip regime. While oscillations occur in both directions, the first peak is very small due to the used damping and excitation amplitude values. For lower damping values, or

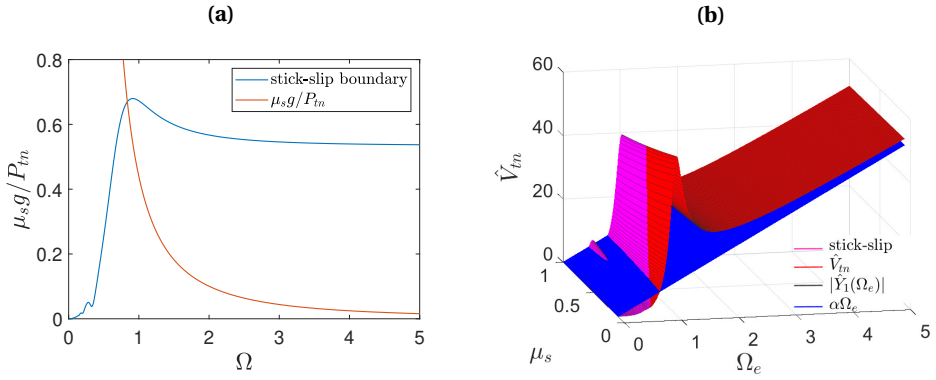

Figure 3.12: (a) Stick-slip boundary for the 2DOF system with external loading applied in tangential and normal directions ($\mu_s = 0.4$); (b) Comparison of $|\hat{Y}_1(\Omega_e)|$ (black lines), $\hat{V}_{tn}$ (red surface) and amplitude of the Φ_1' for high-frequency excitation (blue plane) for a range of μ_s values. Parameters as in Table 3.2. The magenta color defines the parameter space for which stick-slip occurs.

higher oscillation amplitudes, the first peak would be more visible, however the mass might be in intermittent contact.

If the phase of the harmonic tangential load changes by 180° (a switch from an initial positive $+X_1$ to an initial negative direction $-X_1$ with respect to the considered reference system), the stick-slip boundary, the velocity response function, and eventually the effective friction, change as well. Figure 3.13(a) shows the graph defining the stick-slip boundary for this case. As it is shown in the figure, for frequencies $\Omega = \Omega_e/\omega_1$ higher than ≈ 0.72, the mass will be in the sliding regime and the analytical solutions for the effective friction force expression will be valid. Compared to Fig. 3.12(a), the sliding regime occurs in a slightly larger parameter space, meaning that the initial loading phase has an influence on the stick-slip regime as well. In Fig. 3.13(b), the plots of $|\hat{Y}_1(\Omega_e)|$ and $\hat{V}_{tn}$ for an initial negative tangential loading are illustrated. The stick-slip boundary is displayed as well. Again, the graph of $|\hat{Y}_1(\Omega_e)|$ coincides with that of $\hat{V}_{tn}$, and both of them approach the trend of the velocity amplitude given by the high-frequency excitation only as the frequency increases.

A comparison of the amplitudes of the velocity response functions for the three loading cases (tangential, general with initial tangential loading in $+X_1$, and general with initial tangential loading in $-X_1$) for $\mu_s = 0.4$ is presented in Fig. 3.14(a). From the figure, it can be observed that as the excitation frequency increases, the amplitudes of the velocity response function coincide. Thus, for high frequencies, the results of the effective friction expression are the same, independent of the loading configuration. While the plot in Fig. 3.14(a) is obtained for one value of μ_s, from the 3D plots shown in Fig. 3.12(b) and in Fig. 3.13(b), it can be observed that this conclusion holds for any μ_s value. Looking at low frequencies, however, the plots obtained for each loading case do not coincide, meaning that nearby resonance, the effective friction expression depends on the type of loading applied. Figure 3.14(b) shows the comparison of the effective friction expression

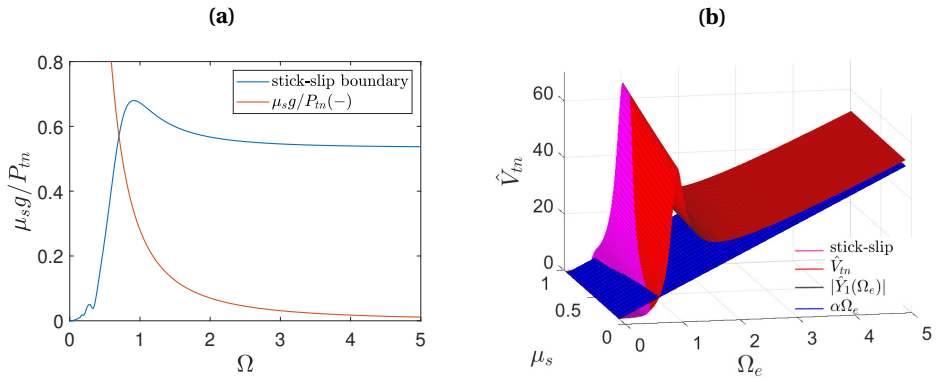

Figure 3.13: (a) Stick-slip boundary for the 2-DOF system with external loading applied in tangential and normal directions. Tangential loading initially applied in the $-X_1$ direction ($\mu_s = 0.4$); (b) Comparison of $|\hat{Y}_1(\Omega_e)|$ (black lines), $\hat{V}_{tn}$ (red surface) and amplitude of the Φ_1' for high-frequency excitation (blue plane) for a range of μ_s values. Tangential loading initially applied in the $-X_1$ direction. Parameters as in Table 3.2. The magenta color defines the parameter space for which stick-slip occurs.

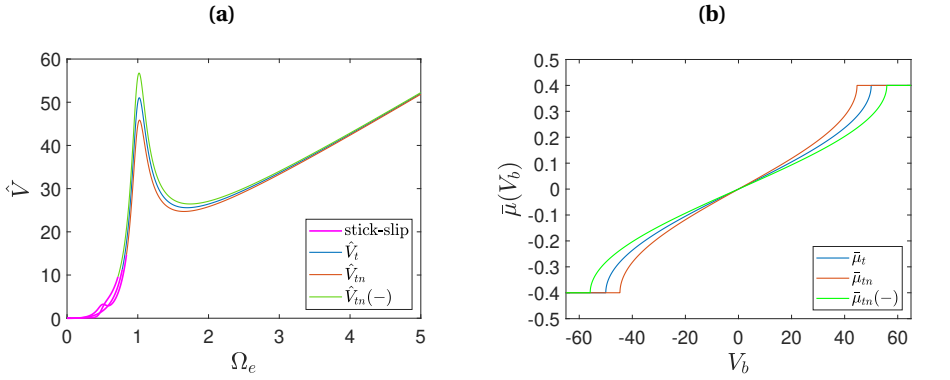

Figure 3.14: (a) Comparison of $\hat{V}$ for all 3 loading cases, tangential (blue), normal-tangential ($+X_1$) (orange), normal-tangential ($-X_1$) (green), for $\mu_s = 0.4$; (b) Comparison of $\bar{\mu}(V_b)$ for the same loading cases and $\Omega_e = 1$. Parameters as in Table 3.2. The magenta line defines the parameter space for which stick-slip occurs.

for these three loading cases and $\Omega_e = 1$. For this value of the excitation frequency, from Fig. 3.14(a), it can be observed that the normal-tangential loading case ($-X_1$) will result in a higher amplitude of the velocity response function, followed by the tangential loading case and lastly by the normal-tangential loading ($+X_1$). This trend is confirmed by the effective friction plots portrayed in Fig. 3.14(b). The loading case with higher amplitude in the velocity response is characterized by a slightly larger parameter space of V_b for which a friction force decrease can be observed.

For the parameter values used so far, from Fig. 3.12(a) and Fig. 3.13(a), it can be seen

that for excitation frequencies near the contact resonance, the mass is stick-slipping. If other parameter values are considered, however, it would be possible to obtain an effective friction graph near contact resonance as well. For example, for $\mu_s = 0.1$, $\omega_2 = 2$, $\alpha = 1$, and a vertical preload of $P = Mg$ acting on the mass in X_2 direction, at contact resonance, the 2 DOF system will be in continuous sliding contact. As the ω_2 value has increased, the amplitude of the displacement response in X_2 direction increases as well. That is why a preload and lower α values are necessary to prevent an intermittent contact. However, lower values of α lead to stick-slip in the horizontal direction. To prevent the latter, a lower μ_s value is used. For this parameter space, the stick-slip boundary shows that excitation frequencies $\Omega_e > 1.15$ result in sliding. Figure 3.15 shows the velocity response function of the 2-DOF system subjected to both normal and tangential load (in $+X_1$ direction) for $\omega_2 = 2$, $\alpha = 1$ and for $\mu_s = 0.1$ (left) and a range of μ_s (right). The rest of the parameters remain the same as in Fig. 3.11. The stick-slip regime is also shown in magenta, indicating that higher μ_s values result in stick-slip. Moreover, since different ω_2 and α values are used, both peaks are clearly visible in the figure.

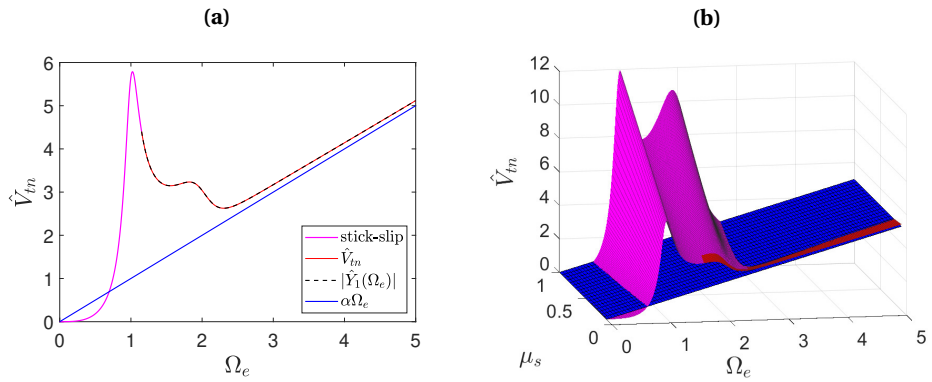

Figure 3.15: (a) Comparison of $|\hat{Y}_1(\Omega_e)|$ (black dashed line), $\hat{V}_{tn}$ (red continuous line) and amplitude of the Φ_1' for high-frequency excitation (blue continuous line) for $\mu_s = 0.1$; (b) Comparison for a range of μ_s values. $\omega_2 = 2$, $\alpha = 1$ and the rest of parameters as in Table 3.2. The magenta color defines the parameter space for which stick-slip occurs.

A comparison between the amplitudes of the velocity response functions for the three loading cases (tangential, general with initial tangential loading in $+X_1$, and general with initial tangential loading in $-X_1$) for $\mu_s = 0.1$ is presented in Fig. 3.16(a). The stick-slip parameter space is always defined by the magenta line. It can be seen that, as the excitation frequency increases, the amplitudes of each case approach each other, showing the same trend as in Fig. 3.14(a). However, moving towards the resonance peaks, the behavior changes. Figure 3.16(b) shows the effective friction plots for each loading case and $\Omega_e = \omega_2 = 2$, so that a continuous sliding regime is ensured for each load case. For this value of the excitation frequency, from Fig. 3.16(a), it can be observed that the normal-tangential loading case ($+X_1$) will result in a higher amplitude of the velocity response function, followed by the tangential loading only and lastly by the normal-tangential loading ($-X_1$) case. This trend is confirmed by the effective friction

plots portrayed in Fig. 3.16(b). Note that the effective friction changes if a different excitation frequency is considered. The effective friction trend is also different from that in Fig. 3.14(b). While in Fig. 3.14(b), the normal-tangential loading ($-X_1$) results in the highest friction decrease (comparing for $\Omega_e = 2$), in Fig. 3.16(b) the normal-tangential loading ($+X_1$) gives the largest friction change. Thus, a different dynamic characteristic of the system and different forcing parameters result not only in different stick-slip/sliding regimes but also in different effective friction values.

Furthermore, upon examining Fig. 3.16(a), it is evident that the $\hat{V}$ values for the three loading scenarios exhibit the greatest discrepancy at $\Omega_e \approx 1.8$, which is in proximity to the contact resonance frequency. This suggests that the dissimilarity in effective friction values between each load case would be most notable at this specific frequency. Hence, it can be concluded that incorporating a friction force that somehow depends on the normal contact stiffness into the model, has a considerable impact on the effective friction values, particularly when the excitation frequencies are near the contact resonance. Besides the modelling implications, the pattern shown in Fig. 3.16 nearby the contact resonance for different loading cases, can also be used as a characteristic feature during experiments to eventually confirm (or disprove) for a given friction pair, the dependence of the friction force on the normal contact stiffness and damping.

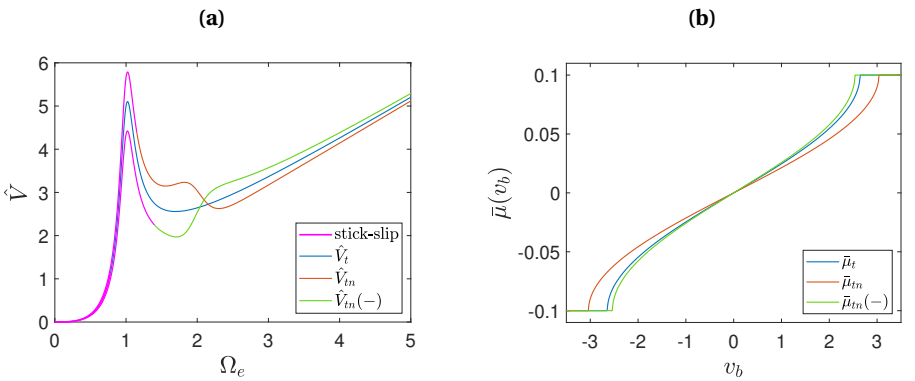

Figure 3.16: (a) Comparison of $|\hat{Y}_1(\Omega_e)|$ for all 3 loading cases, tangential (blue), normal-tangential ($+X_1$) (orange), normal-tangential ($-X_1$) (green), for $\mu_s = 0.1$; (b) Comparison of $\bar{\mu}(V_b)$ for the same loading cases and $\Omega_e = 2$. $\omega_2 = 2$, $\alpha = 1$ and the rest of parameters as in Table 3.2. The magenta line defines the parameter space for which stick-slip occurs.

It is worth highlighting that the conclusions drawn so far for the effective friction expression of the 2-DOF system subjected to different load configurations are dependent on the choice of the friction force F_f. The friction force F_f as a function of F_n, Eq. (3.32), was chosen to demonstrate the effect of the contact resonance. If F_n is assumed to be proportional to the inertial force in the vertical direction, the F_f expression becomes

$$F_f = \mu(V_r) M \ddot{X}_2 = \mu(V_r)(-\alpha\Omega^2 \sin(\Omega\tau) + g), \tag{3.42}$$

where $M\ddot{X}_2$ is found using the equation of motion in X_2 direction after neglecting the stiffness and damping terms. Considering this friction force expression, the velocity

response functions are calculated again. A comparison of their amplitudes for two loading cases and for $\mu_s = 0.4$ is presented in Fig. 3.17(a) where the continuous-line plots are obtained using F_f as in Eq. (3.32) and the dashed-line plots using F_f as in Eq. (3.42). Note that the tangential loading case is not portrayed in the figure because when only tangential loading is present both expression of F_f (Eq. (3.32) and Eq. (3.42)) are the same, i.e. $F_f = Mg\mu(V_r)$, as there is no displacement in the X_2 direction.

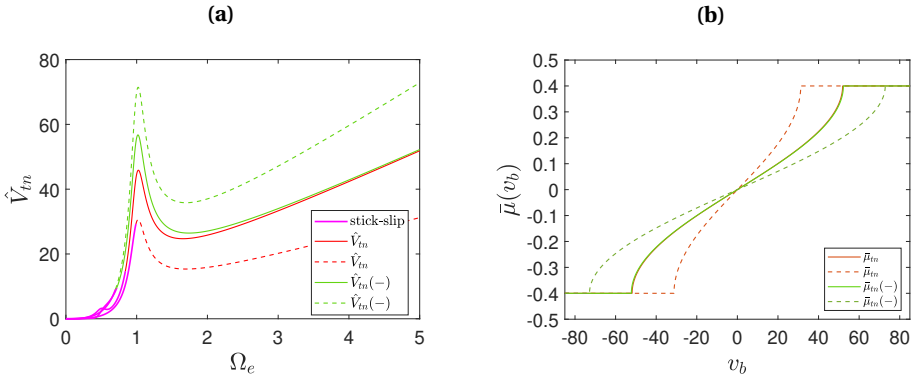

Figure 3.17: (a) Comparison of $|\hat{Y}_1(\Omega_e)|$ for 2 loading cases where continuous lines obtained using F_f as in Eq. (3.32) and dashed line using F_f as in Eq. (3.42), for $\mu_s = 0.4$; (b) Comparison of $\bar{\mu}(V_b)$ for the same loading cases and $\Omega_e = 5$. Parameters as in Table 3.2. The magenta line defines the parameter space for which stick-slip occurs.

From the figure, it can be observed that when the friction force depends only on the inertial force in the normal direction (dashed lines), as the excitation frequency increases, the amplitudes of the velocity response function do not coincide anymore. This is to be expected because the inertial force prevails at high frequencies. Figure 3.17(b) shows the comparison of the effective friction expression for these loading cases and for $\Omega_e = 5$. While the continuous lines coincide, the dashed lines display different effective friction plots, complying to the velocity response function trends portrayed in Fig. 3.17(a). This enforces the fact that the nature of the contact normal force affects the results of the effective friction expression, especially as we go towards the high-frequency regime. To reconnect to the conclusion drawn for Fig. 3.16, to assess whether a contact normal force is mainly driven by a compliant force (characterized by a contact resonance and contact damping) or by the inertial contribution in the vertical direction, the measurement of the velocity response functions for different loading cases would enable such discrimination, as shown in Fig. 3.16(a) and Fig. 3.17(a).

Note that, if the 2-DOF system considered so far included a diagonal spring (oriented at an oblique angle of 45° relative to the normal direction), mode coupling will always be present. Different values of the diagonal spring's stiffness would result in different shapes and trends of the velocity response functions. The latter can then be used to calculate the friction change. However, in such case, the system could be prone to mode coupling instabilities [31], that should be taken into account before assessing the effective friction characteristic at steady state.

To conclude the analysis done so far, it can be stated that the velocity response function can be used to obtain the effective friction expression for a multi-degree-of-freedom system and for a general frequency range of excitation. The influence of the external loadings on friction depends on the combination of loading phase, excitation frequency, system characteristics (mass, stiffness and damping values) and the value of the static friction coefficient. Depending on these parameters, applying two loads does not necessarily result in a higher friction change compared to the application of only one type of load. Lastly, the values of effective friction greatly depend on the choice of the friction force expression, inclusive of the normal contact force.

3.5. CONCLUSIONS

In this work, the Method of Direct Separation of Motion (MDSM) was extended to quantify the vibration-induced effect on the average friction force for a single and a multi-degree-of-freedom system, subject to different combinations of dynamic load directions and valid for any frequency of excitation (low- and high-frequency regime). The systems considered are influenced by a friction force represented by the Amonton-Coulomb's law, using different expressions of the normal contact force, representing a compliant and a rigid contact case. The extension enabled to identify a threshold, $\Omega = 5\omega_n$, limiting the so-called "high-frequency" regime for vibration-induced friction modulation. The MDSM results were then compared to the ones obtained by exploiting the velocity response function of the system. It is found that, instead of the MDSM, the velocity response function can be used to obtain the effective friction expression, facilitating so the interpretation of the vibration-induced effects on the averaged friction force and avoiding the cumbersome mathematical steps needed for the extended MDSM. An equivalence was also shown between the aforementioned results and the alternative rationale used by Matunaga, Storck and coworkers and Kumar and Hutchings to compute the friction force reduction, based on the variation of friction force direction within one cycle of vibration.

The expression of the effective friction for a generic harmonic excitation is obtained for steady-state and continuous-slip motion. A procedure was proposed to define the boundaries of the transition from stick-slip to a continuous-slip regime, merging the rationale used by den Hartog and the velocity response function of a forced mass-spring system in contact with a moving belt. It is important to note that if the system is already in a slip regime (regardless of the presence of a moving belt), a friction reduction can be observed due to vibration. On the contrary, if the system is in a stick-slip regime at a specific excitation frequency as per den Hartog's stick-slip plane, a belt velocity higher than the amplitude of the velocity response function (assuming sliding) will eliminate stick-slip, but no friction reduction will be observable according to the investigated system. It was also shown that the influence of the external loadings on friction depends on the combination of the loading phase, excitation frequency, system characteristics (mass, stiffness and damping values), and the value of the static friction coefficient. The choice of the normal contact force expression (including either inertia or damping-stiffness effects) also influences the results concerning the effective friction, and the velocity response function allows to shed light on the main mechanism (e.g. inertia or damping-stiffness) driving the contact normal force.

4

THE EFFECT OF TRANSVERSE STIFFNESS AND LOADING ON VIBRATION-ASSISTED FRICTION MODULATION

This chapter builds on the previous one by considering a two-degree-of-freedom model, focusing this time on the influence of transverse stiffness and oscillation on friction modulation. The single-degree-of-freedom model considered in the previous chapter serves as a basis for comparison, highlighting how different values of transverse stiffness affect the response. Through the analysis of this system, the study contributes to the dissertation's objectives: exploring the effect of system stiffness through its impact on the system dynamics and eventually on friction modulation and comparing the results to existing related experimental studies. Readers familiar with the background presented in the "State of the art" chapter may skip the introduction section if desired.

The work presented in this chapter was expanded and published as: Sulollari, E., van Dalen, K.N., and Cabboi, A. (2026). On the effect of planar dynamics and resonance on vibration-induced friction modulation. International Journal of Non-Linear Mechanics, 187, 105362.

ABSTRACT

Numerous theoretical and experimental studies have explored the effect of external excitation in modulating friction forces. To align with experimental findings, various friction models have been employed, with dynamic models often showing better correlations, though parameter tuning was required in certain studies to achieve these correlations. In this work, the focus is shifted to enhancing the overall system dynamics rather than increasing the complexity of the friction model, with the aim of providing a better understanding of how system dynamics influence friction modulation under vibration. Specifically, the influence of transverse stiffness on friction modulation is investigated in a two-degree-of-freedom system subjected to combined tangential and transverse loading. The results indicate that the characteristic concave shape in average friction plots, commonly associated with dynamic friction models, can also arise when employing Amonton-Coulomb's law. This concave shape occurs at excitation frequencies near or at resonance in the tangential direction (when the friction force is strong), irrespective of transverse stiffness values, or at higher excitation frequencies when transverse stiffness is low. These findings emphasise the importance of accurately accounting for system dynamics in friction modulation analysis.

4.1. INTRODUCTION

In many applied science fields, friction control is essential to guaranteeing satisfactory performance of systems. Controlling and reducing friction between surfaces in contact helps in improving their performance and adding value in terms of cost savings and expenses that arise due to wear and tear, repair, and maintenance of parts in contact. One of the methods used to change friction forces is the vibration-assisted technique. Applications for this technique include wire drawing [1], cutting [2], press forming [3], and other machining processes, slip-joint decommissioning [4, 5], pile driving [6] and surface haptics technologies [7].

Since the 1950s, several studies on the effect of vibrations on friction have been performed, including experimental and theoretical ones. Some of them investigated the reduction of the friction force due to ultrasonic vibrations applied parallel and/or perpendicularly to the sliding direction and developed simple models used to match the experimental results to theoretical predictions [8, 9, 10]. These models consisted of two bodies sliding over each other, with the friction force assumed to follow Amonton-Coulomb's law. Other studies considered more complex friction laws. Thomsen, for example, considered the Stribeck law and studied the effect of harmonic excitation on changing friction forces and quenching self-excited vibrations [11]. Michaux and coworkers also considered the Stribeck law and investigated the effect of the waveform of different periodic signals on the effectiveness of tangential high-frequency excitation to cancel friction-induced oscillations [12].

A series of numerical and experimental investigations have been performed by Leus and Gutowski. In the early 2000s, considering the presence of excited tangential contact vibration, they showed that using the Dahl model, in which the interface shear stiffness contribution provided by the asperities is modelled by means of micro-springs, the friction force could be reduced independently of whether a change in the direction of the net friction force vector is observed [13]. Later on, considering again tangential vibrations, they compared numerical results on average friction, obtained assuming the Dahl's and

Dupont's models and the classical Amonton-Coulomb's friction law, with experimental data. The best correlations were observed using the Dahl's friction model [14]. Numerical and experimental studies were performed to investigate the effect of transverse vibrations as well [15]. More recently, a computational model was developed to study friction force reduction under longitudinal loading applied at an arbitrary direction, assuming again dynamic friction models and comparing the numerical results to experimental ones [16].

As mentioned above, in the existing studies, dynamic friction models, such as the Dahl or Dupont models, are incorporated for theoretical predictions to better correlate with experimental results. These dynamic friction models account for the contact surface deformation by linking the friction force during the pre-sliding phase to an empirical tangential contact stiffness parameter. However, such empirical contact stiffness parameters cannot always be physically linked to measurable surface properties and need to be constantly updated to match new measurements. In this study, rather than using a dynamic friction model, a different approach focused on enhancing the system dynamics is explored, which can qualitatively lead to similar average friction results as the ones observed in the above-mentioned studies of Leus and Gutowski. Specifically, instead of limiting the analysis to a single-degree-of-freedom system, the study incorporates the influence of tangential and transverse stiffnesses, offering a more comprehensive representation of the system's behaviour. In this work, first, the system considered is presented. Then, a numerical analysis is performed to investigate the effect of tangential loading only on friction modulation. The numerical results are compared to analytical ones obtained in Chapter 3 [17], and a limitation of the latter is found. Afterwards, different transverse stiffness values are considered, and their influence on vibration-assisted friction modulation under the effect of both tangential and transverse external loading is investigated. Lastly, a discussion relating the results of this study to those obtained using the Dahl and Dupont models is provided.

4.2. THE MODEL SYSTEM

To reveal the effects of transverse stiffness on vibration-induced friction modulation, the system illustrated in Fig. 4.1 is considered. The system consists of an oscillator composed of a mass M positioned on a belt, moving at a constant speed V_b in the tangential direction X_1. In both directions, a linear spring and dashpot are present, with stiffnesses K_1 and K_2 and damping coefficients C_1 and C_2, in the tangential and transverse directions, respectively. Regarding the external load, both tangential and transverse loading, characterised by a frequency Ω_e and amplitude $mr\Omega_e^2$ (e.g., load arising from a horizontally unbalanced mass m at eccentricity r [11]), are applied as shown in Fig. 4.1.

For the chosen model setup, the kinetic friction is considered to be the same as the static friction. The adopted friction law is the Amontons-Coulomb's law [18, 19], since the corresponding friction force is directly linked to a constant coefficient of friction, μ_s and proportional to the normal force. As the aim of this study is to capture the effect of transverse stiffness on vibration-induced friction modulation, the assumption of Amontons-Coulomb's law is deemed most appropriate, since it avoids the complexity of more realistic friction laws, which are case-study and material pair dependent [20, 21].

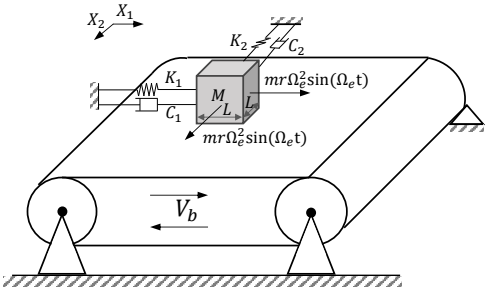

Figure 4.1: Two-degree-of-freedom mass-spring-damper system sliding over a belt moving with constant velocity V_b.

The non-dimensional equations of motion of the system at non-dimensional time τ then become

$$\begin{bmatrix} 1 & 0 \\ 0 & 1 \end{bmatrix} \begin{pmatrix} \ddot{x}_1 \\ \ddot{x}_2 \end{pmatrix} + \begin{bmatrix} 2\beta_1 & 0 \\ 0 & 2\beta_2\omega_r \end{bmatrix} \begin{pmatrix} \dot{x}_1 \\ \dot{x}_2 \end{pmatrix} + \begin{bmatrix} 1 & 0 \\ 0 & \omega_r^2 \end{bmatrix} \begin{pmatrix} x_1 \\ x_2 \end{pmatrix} + \begin{pmatrix} \frac{\mu_s\gamma^2(\dot{x}_1-v_b)}{\sqrt{(\dot{x}_1-v_b)^2+\dot{x}_2^2}} \\ \frac{\mu_s\gamma^2\dot{x}_2}{\sqrt{(\dot{x}_1-v_b)^2+\dot{x}_2^2}} \end{pmatrix} = \begin{pmatrix} \alpha\Omega^2\sin(\Omega\tau) \\ \alpha\Omega^2\sin(\Omega\tau) \end{pmatrix}, \tag{4.1}$$

where

$$\tau = \omega_1 t, \quad x_1 = \frac{X_1}{L}, \quad x_2 = \frac{X_2}{L}, \quad \beta_1 = \frac{C_1}{2M\omega_1}, \quad \beta_2 = \frac{C_2}{2M\omega_2}, \quad \omega_1^2 = \frac{K_1}{M},$$
$$\omega_2^2 = \frac{K_2}{M}, \quad \omega_r = \frac{\omega_2}{\omega_1}, \quad \gamma^2 = \frac{g/L}{K_1/M}, \quad \Omega = \frac{\Omega_e}{\omega_1}, \quad \alpha = \frac{mr}{ML}, \quad v_b = \frac{V_b}{\omega_1 L}, \tag{4.2}$$

and the friction force is defined as follows:

$$\mathbf{F}_f = -\mu_s\gamma^2 \frac{\mathbf{v}_r}{\|\mathbf{v}_r\|} = -\mu_s\gamma^2 \frac{1}{\sqrt{(\dot{x}_1-v_b)^2+\dot{x}_2^2}} \begin{pmatrix} \dot{x}_1 - v_b \\ \dot{x}_2 \end{pmatrix}. \tag{4.3}$$

As shown from the equations of motion, this system consists of two nonlinear subsystems coupled through the friction force. The baseline parameters values considered in the study (unless otherwise stated in the specific figure captions) are summarized in Table 4.1. It is important to note that the tangential and transverse excitation applied to the system

Table 4.1: Baseline parameter values used in the study.

Symbol	β_1	β_2	ω_r	μ_s	α	γ^2
Value	0.1	0.1	0.5	0.4	10	1.0

have the same magnitude and frequency, with no phase shift between them. This type of

loading can occur, for example, if an external force is applied at a 45-degree angle relative to the tangential direction of the mass. The effect of different loading phase shifts is not considered in the scope of this study.

4.3. TRANSVERSE STIFFNESS EFFECT ON FRICTION MODULATION

4.3.1. TANGENTIAL LOADING ONLY

In this section, a numerical analysis is performed to obtain the average friction plots versus the belt velocity for the case of tangential loading only. This allows for a comparison with the analytical results presented in Chapter 3 [17], as the equations of motion in this chapter reduce to those of a single-degree-of-freedom (SDOF) system on a moving belt studied therein. Before demonstrating the effect of vibration on friction modulation, it is important to define how the average friction is calculated. As described in Chapter 3, the average friction is evaluated by averaging the variation in the friction force over one cycle of oscillation corresponding to the excitation frequency. In the case of a SDOF system with loading in the tangential direction and friction force modelled using Amontons-Coulomb's law, the friction force depends on the sign of the relative velocity. The average friction is computed by integrating the time signature of the friction force over one oscillation period. Considering this approach, for the SDOF system described in Chapter 3, the equation of the average friction function for harmonic excitation with arbitrary frequency is

$$\bar{\mu}(v_b) = \begin{cases} \mu_s \left(1 - \frac{2}{\pi} \arccos\left(\frac{v_b}{\hat{V}}\right)\right) & \text{for } |v_b| \leq \hat{V} \\ \mu_s \text{sgn}(v_b) & \text{for } |v_b| \geq \hat{V}, \end{cases} \tag{4.4}$$

where $\hat{V}$ is the amplitude of the velocity response function at steady state (assuming sliding). In this section, the average friction values calculated numerically for the system in Fig. 4.1, with loading in the tangential direction only, are compared to those obtained analytically using Eq. 4.4.

The first comparisons for excitation frequencies $\Omega = 4$ and $\Omega = 2$ are shown in Fig. 4.2(a) and Fig. 4.2(b), respectively, which, as expected, portray very good matches between the numerical and analytical results. In Fig. 4.3(a) and Fig. 4.3(b), the same comparison is done for $\Omega = 1.5$ and $\Omega = 1$, respectively, with the latter corresponding to the natural frequency of the undamped system in the X_1 direction. As shown in the plots, the agreement between numerical and analytical results is good for these excitation frequencies as well, with small discrepancies observed for the case of $\Omega = 1$. These deviations are attributed to the treatment of the friction force in the analytical approach. In the analytically derived velocity response (see Chapter 3), assuming full sliding, friction is treated as a constant force and does not influence the harmonic velocity response solution. Thus, the latter depends solely on the system (mass, stiffness, viscous damping) and excitation (amplitude and frequency) properties. Since the velocity response does not depend on the friction force, which is a function of the sign of the relative velocity between the mass and the belt, the velocity response remains the same regardless of the belt velocity.

Similarly, in the extended Method of Direct Separation of Motion (MDSM), considering full sliding, the solution for the fast motion (found to correspond to the velocity response

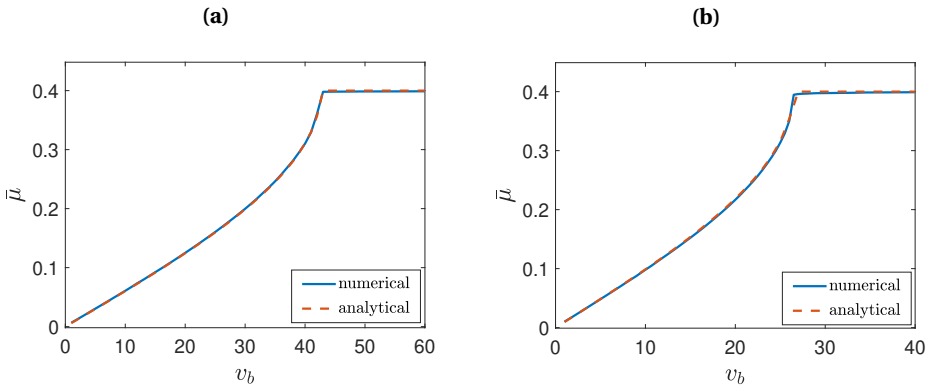

Figure 4.2: Comparison of average friction results obtained numerically (blue line) and analytically (orange line): (a) excitation frequency in tangential direction $\Omega = 4$; (b) excitation frequency in tangential direction $\Omega = 2$. The rest of the parameters are $\beta_1 = 0.1$, $\mu_s = 0.4$, $\alpha = 10$, and $\gamma^2 = 1$.

function and used for the calculation of the average friction) is harmonic and again independent of the friction force term. As a result, the fast motion and the velocity response function yield the same outcomes, but neither captures the damping effect of the friction force observed in the numerical results. This effect is most significant in the damping-dominated region (near and at resonance). Therefore, for $\Omega = 1$, the numerical results that account for this damping effect lead to the observed differences. Nonetheless, the discrepancies remain small because the friction force term is weaker than the viscous damping term as the value of γ^2, which describes the ratio of gravity loading to spring force, is 1 ($\mu_s \gamma^2 = 0.4$). A comparison of these terms in terms of the energy dissipated by each is presented later in this section.

Using a higher γ^2, for example $\gamma^2 = 10$, leads to bigger discrepancies between the numerical and analytical results as shown in Fig. 4.4(a) and Fig. 4.4(b). The plots show that the agreement between numerical and analytical results deteriorates for $\Omega = 1.5$, particularly as v_b increases (except for v_b values where no friction variation is observed); however, the discrepancies are moderate. In contrast, for $\Omega = 1$, the differences between numerical and analytical results are considerably large across all v_b values (apart from cases where no friction variation occurs).

As previously noted, the analytical approach yields a velocity response that is independent of the friction force expression and, therefore, of the belt velocity v_b. For $\gamma^2 = 1$, where the friction force is relatively weak, the numerical results closely match the analytical ones, indicating that the belt velocity has little influence on the velocity response, as shown in Fig.4.5(a). In contrast, for the same excitation frequency $\Omega = 1$ and $\gamma^2 = 10$ where the friction force is stronger, Fig.4.5(b) shows that the numerically obtained velocity responses depend significantly on the belt velocity, leading to larger discrepancies between the numerical and analytical average friction values, as shown in Fig.4.4(b). Therefore, it is important to note that the analytical results for the average friction match with the numerical ones at any excitation frequency when the friction force is weak in

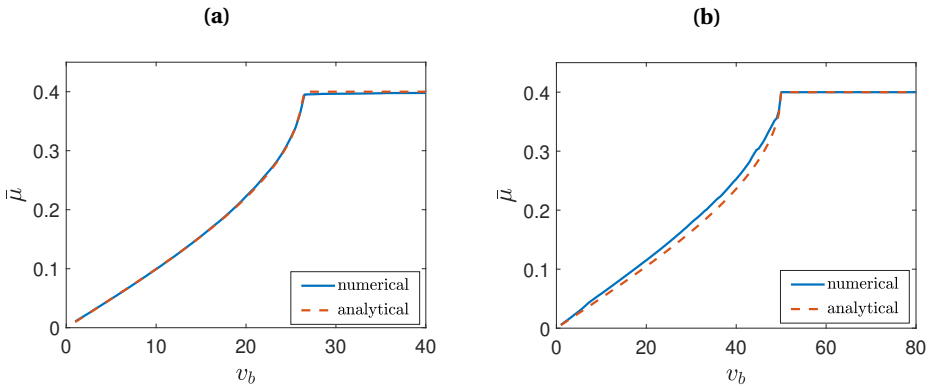

Figure 4.3: Comparison of average friction results obtained numerically (blue line) and analytically (orange line) for $\gamma^2 = 1$: (a) excitation frequency in tangential direction $\Omega = 1.5$; (b) excitation frequency in tangential direction $\Omega = 1$. The rest of the parameters are as in Table 4.1.

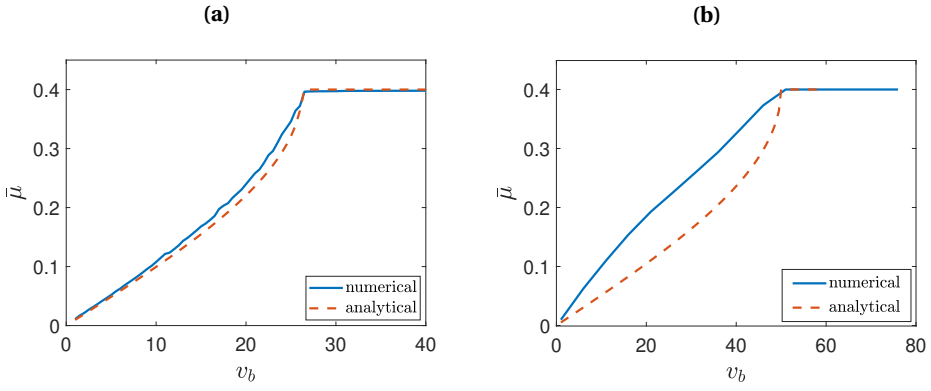

Figure 4.4: Comparison of average friction results obtained numerically (blue line) and analytically (orange line) for $\gamma^2 = 10$: (a) excitation frequency in tangential direction $\Omega = 1.5$; (b) excitation frequency in tangential direction $\Omega = 1$. The rest of the parameters are as in Table 4.1.

comparison to the viscous damping term. However, for stronger friction forces, discrepancies between analytical and numerical results appear, specifically near and at resonance.

Fig. 4.6 illustrates a comparison of the dimensionless energies dissipated by viscous damping, $E_{\text{dis,v}}$, and friction damping, $E_{\text{dis,f}}$, calculated as follows:

$$E_{\text{dis,v}} = \int 2\beta_1 \dot{x}_1^2 \mathrm{d}\tau, \qquad E_{\text{dis,f}} = \int \gamma^2 \mu_s \text{sign}(\dot{x}_1 - v_b)\dot{x}_1 \mathrm{d}\tau \tag{4.5}$$

The comparison is shown for two values of $\gamma^2 = 1$ and $\gamma^2 = 10$ with $\Omega = 1$ for both cases. Fig. 4.6(a), corresponding to $\gamma^2 = 1$, shows that the energy dissipated by viscous

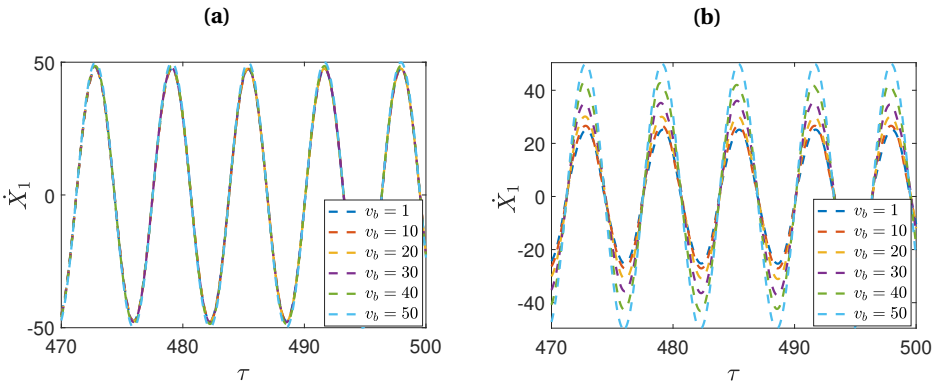

Figure 4.5: Steady-state velocity response in tangential direction for different υ_b values: (a) $\Omega = 1$ and $\gamma^2 = 1$; (b) $\Omega = 1$ and $\gamma^2 = 10$. The rest of the parameters are as in Table 4.1.

damping is at least around 20 times bigger than that dissipated by the friction force. The difference becomes bigger for increasing υ_b values with $E_{\text{dis,v}}$ increasing and $E_{\text{dis,f}}$ approaching zero. Moreover, the variation in the dissipated energy values with respect to υ_b remains relatively small for both cases, which aligns with the observation that the velocity responses are similar across the range of υ_b values. Thus, for this value of γ, the contribution of frictional damping is negligible compared to that of viscous damping, and the influence of the friction force on the amplitude of the velocity response at resonance in X_1 direction is minimal. In contrast, Fig. 4.6(b), which corresponds to $\gamma^2 = 10$, shows that the energies dissipated by viscous and friction damping are more comparable, especially at low υ_b values, even though the difference between the two forms of energy dissipation increases as υ_b increases. This indicates that the influence of friction damping is stronger at higher γ values and as a result, the numerical results that take into account this contribution differ more significantly from analytical solutions that neglect this effect.

Lastly, it is important to note that this section states that, under tangential loading only, the equations of motion reduce to those of a single-degree-of-freedom system, as no vibrations are observed in the X_2 direction. While this holds true for all the scenarios discussed, the presence of nonlinear coupling between the equations of motion implies that the system can still exhibit oscillations in the X_2 direction, even when the excitation is applied in the X_1 direction only. This phenomenon can occur if the system exhibits internal resonance, for example, when the ratio of natural frequencies is 1:2 ($\omega_r = 0.5$). For this case, it can be shown that multimodal solutions (responses in both X_1 and X_2 directions) are often unstable [22, 23]. Even when they do exist and are stable, numerical simulations should be approached with caution, as they are sensitive to initial conditions and the basin of attraction is small. Furthermore, it can be verified that when oscillations in the X_2 direction occur, their amplitudes are very small. Although these oscillations are small in amplitude, the coupling in the system leads to significant changes in the main response in the X_1 direction. Since the response in X_1 direction is affected by the presence of internal resonance, this in turn changes the average friction results.

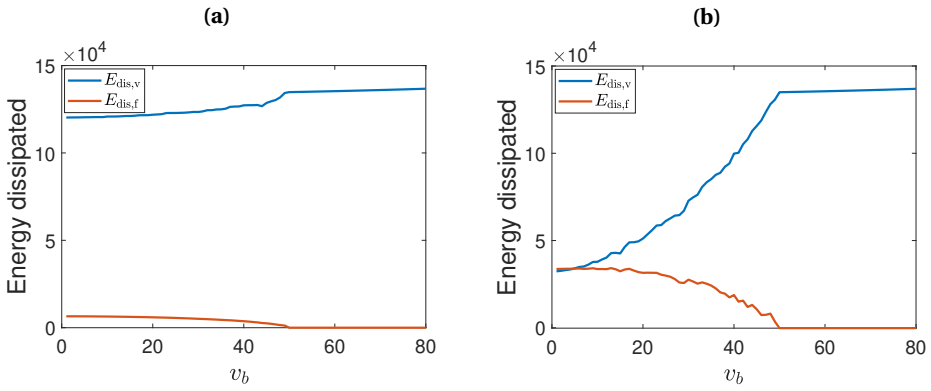

Figure 4.6: Energies dissipated by viscous and friction damping for $\Omega = 1$: (a) $\gamma^2 = 1$; (b) $\gamma^2 = 10$. The rest of the parameters are as in Table 4.1.

However, a parametric analysis of the internal resonances and their exact effect on friction modulation is beyond the scope of this study.

4.3.2. TANGENTIAL AND TRANSVERSE LOADING

In this section, loading acting in both transverse and tangential directions is considered. For different excitation frequencies, the effect of transverse stiffness on the average friction values is investigated by varying the ratio of transverse to tangential natural frequency ω_r. It should be noted that the reported average friction values correspond to changes in the tangential friction force, so in the component of the friction force along the X_1 direction.

First, as done in the previous section, the excitation frequency $\Omega = 4$ is considered, Fig. 4.7(a), with the blue line referring to the tangential-only loading case, which serves as a reference, indicating the average friction behaviour without the influence of the transverse stiffness. The other curves are obtained using loadings in both directions with ω_r values varying from 0.5 ($\omega_2 < \omega_1$) to 4 ($\omega_2 = \Omega_e$) and lastly 10 ($\omega_2 > \omega_1$ and $\omega_2 > \Omega$). For low ω_r values (e.g. $\omega_r = 0.5$, marked with * for a better distinction from other closely present curves), and low V_b values (< 35), the average friction values are higher than those for higher ω_r values and tangential loading only. At higher belt velocities, the presence of transverse loading leads to more friction reduction than tangential loading only, independent of the transverse stiffness values. As the value of the latter increases, the average friction values decrease, reaching their minimum for $\omega_r = 4$, which corresponds to the excitation frequency. Thus, the reduction is the biggest at resonance in the X_2 direction. Then, as the ω_r value increases further, the average friction values increase again, approaching the tangential loading cases as shown, for example, for $\omega_2 = 10$.

Not only the values, but also the shape of average friction plots vary depending on ω_r. For low ω_r values, different from the tangential-only case, the curves have a concave shape. This shape has also been observed in other studies that consider the effect of transverse loading on friction reduction [8, 9, 10, 15], where no transverse stiffness was

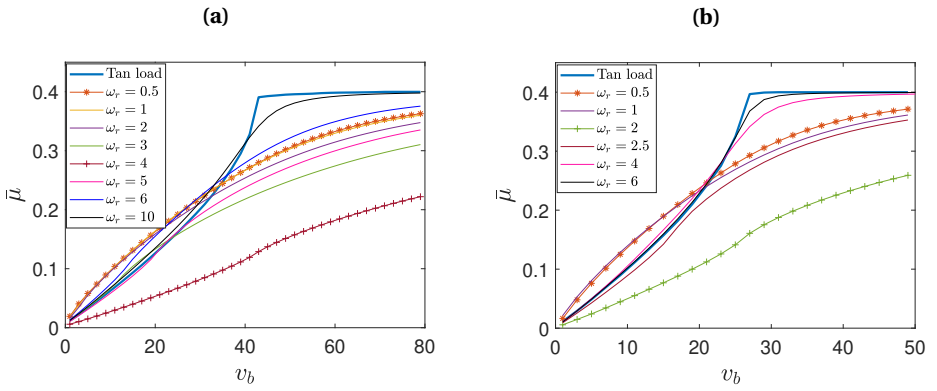

Figure 4.7: Average friction plots for different ω_r values: (a) $\Omega = 4$; (b) $\Omega = 2$. $\beta_2 = 0.1$ and the rest of the parameters are as in Table 4.1.

considered. As the ω_2 increases, the curve gradually transitions to a convex shape. More specifically, for transverse stiffness values corresponding to the excitation frequency, the average friction curve is partially convex and partially concave. As ω_r increases further, the curves approach the tangential-only curve shape but do not exhibit the characteristic kink. Instead, they transition more smoothly, indicating a gradual variation in average friction values. In Fig. 4.7(b), the same plots are obtained for a lower excitation frequency, $\Omega = 2$, showing the same trends in terms of values and shapes as in Fig. 4.7(a). Again, for low ω_r and low v_b values, the average friction values are higher than those for high ω_r values. The average friction values reach their minimum for $\omega_r = 2$, which corresponds to the excitation frequency (resonance in X_2 direction) and increase for increasing ω_r, approaching the tangential loading cases.

Lastly, Fig. 4.8 presents the results for $\Omega = 1$, which corresponds to the natural frequency ω_1, with Fig. 4.8(a) and Fig. 4.8(b) corresponding to results for $\gamma^2 = 1$ and $\gamma^2 = 10$, respectively. In this loading scenario, variations in ω_r lead to smaller changes in the average friction values compared to other excitation frequency cases. Specifically, for $\gamma^2 = 1$, when $\omega_r = \Omega = 1$, ($\Omega_e = \omega_2$ and, differently from before, $\Omega_e = \omega_1$ too, so, resonance in both directions) the average friction curve is no longer the lowest at all v_b values, marking another difference from the behaviour observed at other excitation frequencies, see Fig. 4.8(a). For all the other ω_r values, the plots of average friction are close to each other and to the tangential-only loading case. As the system is now resonating in the X_1 direction, the influence of the response in the X_2 direction is lower than before and the average friction results are closer to the tangential-only loading case. Moreover, as shown in Fig. 4.8(b), for $\gamma^2 = 10$, less friction reduction (compared to $\gamma^2 = 1$) is observed for all ω_r values. This outcome is attributed to lower velocity response amplitude values in this scenario, as shown in Fig. 4.5(b). It is important to highlight that, in this case, the average friction curve exhibits a concave shape even when tangential-only loading is applied. Thus, when the mass is excited at resonance in X_1 direction and the friction force is strong, the system exhibits both less friction reduction, compared to the weak friction case, and a concave average friction curve, even under tangential excitation only.

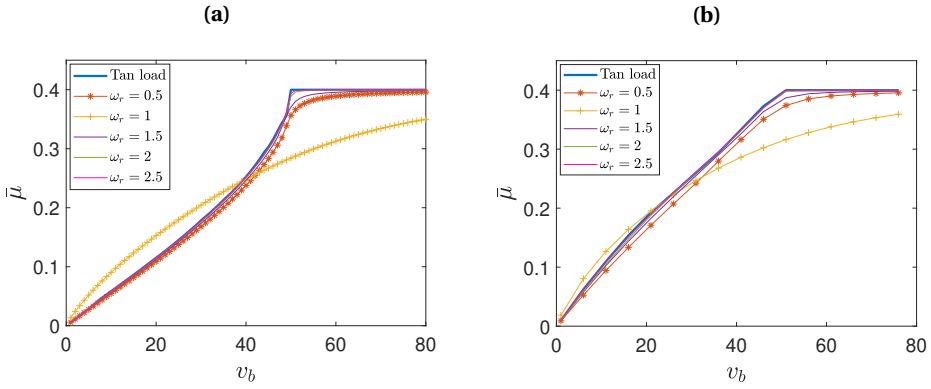

Figure 4.8: Average friction plots for $\Omega = 1$ and for different ω_r values: (a) $\gamma^2 = 1$; (b) $\gamma^2 = 10$. The rest of the parameters are as in Table 4.1.

To better understand the difference in the average friction curve trends between the case of $\Omega = 1$ and other excitation frequencies, Fig. 4.9 and Fig. 4.10 are plotted. These figures illustrate the velocity responses for $\Omega = 2$ and $\Omega = 1$, respectively, considering for each case three ω_r values: below, at, and above resonance. For $\Omega = 2$ and $\omega_r = 1$, Fig. 4.9(a) shows the velocity responses in X_1 and X_2 directions to be in phase with each other and 90° out of phase with the external load F_{ext}. It should be noted that the phase shift analysis presented here is with respect to the velocity response, not the displacement response and the observations in terms of amplitude and phase are in accordance with the linear theory of vibration (as in the velocity response is in phase with the excitation at resonance and approximately 90° out of phase elsewhere). As shown in Fig. 4.7(b), this configuration corresponds to the highest average friction values (at low belt velocities). At resonance in X_2 direction, so for $\omega_r = 2$, Fig. 4.9(b) shows the responses $\dot{x}_1$ and $\dot{x}_2$ to be 90° out of phase. With respect to the external force, $\dot{x}_2$ is in phase, while $\dot{x}_1$ is 90° out of phase. This case results in the lowest average friction, as shown in Fig.4.7(b). For $\omega_r = 3$, Fig. 4.9(c) shows the responses $\dot{x}_1$ and $\dot{x}_2$ to be close to 180° out of phase. Both responses are approximately 90° out of phase with the external force. In this case, the average friction increases again and tends to converge towards the values observed under purely tangential excitation. These observations indicate that the highest average friction occurs when the velocity responses are in phase with each other and out of phase with the external force (e.g., for $\omega_r = 1$), while the lowest average friction is obtained when the responses are 90° out of phase with each other and $\dot{x}_2$ is in phase with the external force. This conclusion holds for higher excitation frequencies as well.

For the case of $\Omega = 1$, the velocity responses are in phase for $\omega_r = 1$. As established in the previous paragraph, this phase relationship leads to the highest average friction values at low belt velocities, which is indeed the case, as shown in Fig. 4.8(a). The other two cases show responses to be 90° out of phase with each other and, with respect to the external force, $\dot{x}_1$ is in phase, while $\dot{x}_2$ is 90° out of phase. This configuration leads to lower average friction values, even though, as already mentioned, the variations from the tangential-only case are small.

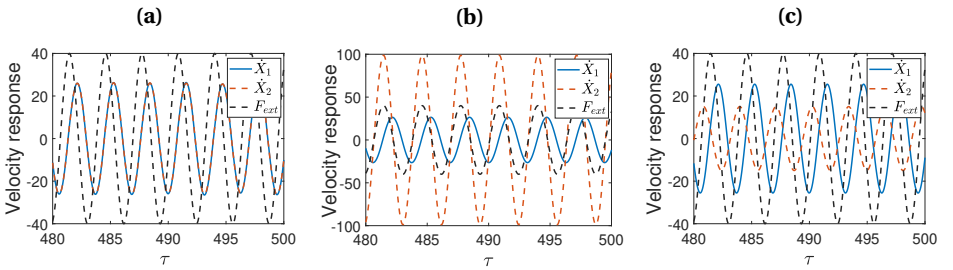

Figure 4.9: Relative velocity plots and external excitation for $\Omega = 2$: (a) $\omega_r = 1$ and velocity responses are in phase; (b) $\omega_r = 2$ and velocity responses are 90° out of phase; (c) $\omega_r = 3$ and velocity responses are close to 180° out of phase. The rest of the parameters are as in Table 4.1.

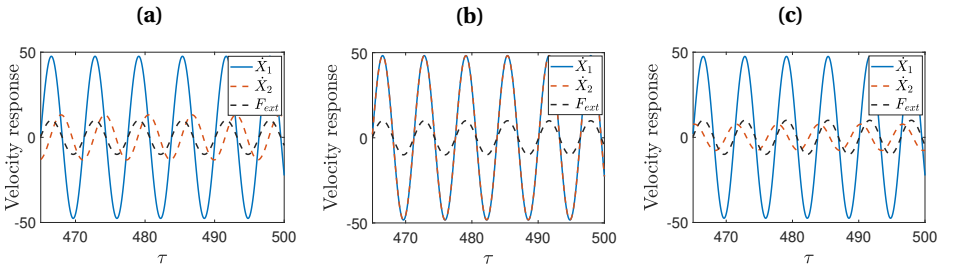

Figure 4.10: Relative velocity plots and external excitation for $\Omega = 1$ and $\gamma^2 = 1$: (a) $\omega_r = 0.5$ and velocity responses are 90° out of phase; (b) $\omega_r = 1$ and velocity responses are in phase; (c) $\omega_r = 1.5$ and velocity responses are 90° out of phase. The rest of the parameters are as in Table 4.1.

4.4. Discussion on related experimental results

Lastly, a discussion is provided between the findings obtained in this study and related experimental works. Several researchers have developed and studied models to investigate the phenomenon of friction force reduction under the effect of loading in tangential, transverse or both directions and compared the results to those obtained in experimental campaigns. These studies have generally shown that much better compliance with experimental results is obtained when, instead of the Amonton-Coulomb law, dynamic friction models such as Dahl and Dupont were considered. These models account for contact compliance, so they assume that the friction force depends on the elastic deflection of the contact zone in the slip direction.

More specifically, Kapelke employed the Dupont model and the Amontons-Coulomb law to compare the experimental results to theoretical ones [24]. The experimental results showed an excellent match to the elasto-plastic Dupont model, for moderate excitation frequencies; however, when high-excitation frequencies were used to catch the behaviour of the friction force accurately, a significantly different value of tangential stiffness was needed for the Dupont model. Gutowski and Leus also developed a model to investigate how vibrations in arbitrary directions affect the friction force [16]. To

capture the resultant friction force, dynamic friction models of Dahl and Dupont were adopted, and assumptions were made regarding the rate of change of elastic deformation of the contact, which depends, among other parameters, on the contact stiffness in the tangential direction. The results of the numerical analysis carried out using the developed models showed very good consistency with the outcomes of the experimental tests for the cases considered in the study.

In the referenced studies, the use of dynamic friction models resulted in average friction curves exhibiting a concave shape. In the present study, a similar concave shape is observed in two cases, one of which occurs when the excitation frequencies are close to or at resonance, as shown in Fig. 4.4(b), under tangential loading only (no transverse stiffness/vibration and high γ^2). This highlights the importance of accounting for the system dynamics. As shown later in Fig. 4.8, for the same excitation frequency (at resonance in X_1 direction), variations in transverse stiffness values have small influence on the resulting average friction plots. The other case in which concave average friction shapes are observed occurs when loading in both directions and low transverse stiffness values are employed, even though the Amonton-Coulomb's law is used, as shown in Fig. 4.7. Thus, the concave shape does not arise exclusively from the use of dynamic friction models but can also result from the presence of transverse stiffness or from resonance occurring in the tangential direction. However, in terms of friction reduction, the findings of Kapelke and Gutowski and Leus demonstrated that Amonton-Coulomb's law tends to overestimate the reduction in friction due to vibrations, leading to predictions that deviate from experimental results. Similarly, in our study, higher average friction values were observed for low transverse stiffness values. The differences in friction reduction between the cases with and without transverse stiffness were less pronounced than those reported in the works of Kapelke and Gutowski and Leus.

These discrepancies indicate that the "true" behaviour of the average friction under an external excitation is probably somewhere in between these modelling approaches. Models such as those of Dahl and Dupont incorporate contact compliance into the friction formulation itself, and as a result, are capable of describing complex behaviours, but may lack generality as their parameters often require tuning based on the excitation frequency and cannot be directly linked to material properties. Alternatively, using the more simplistic Amonton-Coulomb's law and considering the transverse stiffness as a system parameter allows getting a clearer picture of the role of the system stiffness in friction modulation. Ultimately, neither approach alone fully captures the multi-dimensional character of frictional behaviour under external excitation. A more comprehensive understanding may be achieved by combining these perspectives whenever comparisons with experimental data are carried out, to provide more robust and generalizable insights into friction modulation under different excitation conditions.

4.5. CONCLUSIONS

This work investigates the influence of transverse stiffness and resonance condition on the modulation of friction in a two-degree-of-freedom system subjected to tangential and transverse loading. Initially, the case with tangential loading only is considered, and numerical results for average friction are compared with analytical predictions obtained

using the extended MDSM. The average friction results from both approaches match for any excitation frequency when the friction force is weak. However, for stronger friction forces, discrepancies between analytical and numerical results appear, specifically near and at resonance, with the results from the extended MDSM overestimating friction reduction. This discrepancy arises due to the damping effect of friction that is mostly pronounced in the damping-dominated region, an effect not captured by the assumptions made while adopting the extended MDSM.

Then, the effect of transverse stiffness is analysed under combined tangential and transverse loading. The average friction plots reveal that, for transverse stiffness values smaller than the excitation frequencies and at low belt velocities, the average friction values are higher than the reference case of tangential loading only. As the transverse stiffness increases, friction reduction becomes more pronounced, reaching a minimum at resonance in X_2 direction ($\omega_r = \Omega$). Thus, the influence of the transverse motion on the average friction is most significant when resonance occurs in the X_2 direction. However, this influence is less pronounced if resonance occurs in the X_1 direction as well. For higher transverse stiffness values, the average friction curves approach the tangential-only loading case. The average friction plots also exhibit a concave shape under certain parameter values and loading conditions. More specifically, the concave shape is observed when the excitation frequency is near or at resonance (tangential-only loading and strong friction force). For loading in both directions and higher excitation frequencies, the concave shape arises for low transverse stiffness values. In both these cases, Amonton-Coulomb's friction law is used, indicating that the concave shape is not exclusively a result of employing dynamic friction models, as shown in other related studies. These results highlight the importance of properly accounting for the system dynamics.

5

PARAMETRIC EXCITATION AND FRICTION MODULATION FOR A FORCED 2-DOF SYSTEM

This chapter builds on the previous ones by studying a two-degree-of-freedom model, considering this time the effect of nonlinear normal contact properties and external excitation on friction modulation. The parametric excitation resulting from the oscillating normal force and the nonlinear coupling through friction triggers friction-induced vibrations. Through the analysis of this system, the study contributes to the dissertation's objectives: exploring the interactive and coupled relationship of friction and vibrations by investigating the potential of external excitation in destabilising initially stable systems and analysing how such instabilities affect friction modulation. Readers familiar with the background presented in the "State of the art" chapter may skip the introduction section if desired.

This chapter has been published as: Sulollari, E., van Dalen, K.N., and Cabboi, A. (2025). Parametric excitation and friction modulation for a forced 2-DOF system. Nonlinear Dynamics, 113, 12793–12816.

ABSTRACT

A two-degree-of-freedom mass on a moving belt system has been considered to study the effect of friction-induced oscillations, due to nonlinear contact properties and external excitation, on friction modulation. Both tangential and normal excitation are present and the Hertz-Damp model governs the normal contact. The combined presence of the normal–tangential coupling through friction and of the external excitation, results in a parametric excitation and triggers friction-induced oscillations. Using a numerical analysis, the occurrence of such oscillations is explained through the inspection of the friction force versus relative velocity plots, which indicate the presence of a negative damping effect in the tangential direction, despite considering Amontons-Coulomb law. Hence, a linearized stability analysis of the steady sliding state, by taking advantage of the Method of Direct Separation of Motion, is employed to predict the bifurcation point as function of system parameters. It is shown that the linearized stability analysis provides a good qualitative agreement for the occurrence of the friction-induced oscillations for the investigated system, while the quantitative match varies depending on the system parameters and their values. Lastly, the effect of the observed friction-induced oscillations on the friction modulation is studied. Through a numerical analysis, a significant degree of scatteredness in friction force modulation is observed. Such scatteredness is significantly linked to the emergence of friction-induced oscillations, and it also depends on the averaging procedure used to quantify the effective friction reduction.

5.1. INTRODUCTION

Friction-induced oscillations are very common in mechanical systems, and in most cases they are undesirable. Examples include the noise generated by door hinges or car brakes, and the chatter of machine tools or vibrations in slides and seals. One of the most studied mechanisms that leads to friction-induced oscillations is based on the presence of a decreasing friction force or friction coefficient linked to the corresponding increase in relative sliding velocity, naturally triggering a negative damping-like effect [1]. If such "negative damping" is higher than the bulk or structural damping of the system, instability occurs, characterized by the growth of the oscillatory motion during sliding. Friction-induced oscillations may also occur for a constant value of the friction coefficient if phenomena such as sprag-slip [2, 3, 4] or mode coupling [5, 6, 7, 8] characterize the system dynamics. Another mechanism that causes instability is the presence of a follower force for structures resembling the Pflüger or Ziegler column [9].

The role of damping is generally a key factor in friction-induced vibrations. In fact, with reference to the mode-coupling mechanism, Hoffmann and Gaul [5] analyzed a mass on belt system characterized by a vertical and horizontal degree of freedom, and concluded that the presence of non-proportional damping may, counterintuitively, destabilize the system. Similar observations were made by Sinou and Jezequel [6], pointing out that an optimal structural damping ratio and a pulsation ratio are capable of decreasing the unstable region due to mode coupling. Massi and Giannini [10] performed an experimental investigation of the relationship between the distribution of modal damping and the propensity to develop squeal in a beam-on-disk setup. Fritz and coworkers [11] used a finite element model of a whole brake corner and then a stability analysis to study the effects of damping on brake squeal coalescence patterns. Charroyer and coworkers [12]

considered a mass-spring system of three degrees of freedom with friction and carried out parametric studies to evaluate the effects of various system parameters on stability, especially that of damping in mode-coupling instabilities with planar and rectilinear friction assumptions. Besides damping, the presence of a nonlinear contact stiffness has also a leading role in determining unstable regions. Li and coworkers [7] showed that an increase in the nonlinear stiffness, tends to destabilize the nonlinear system, while at certain higher values, a stable regime can be achieved.

Besides mechanisms leading towards friction-induced oscillations, techniques were also developed to mitigate such phenomena. Thomsen [13], for example, considered a mass-on-moving belt system subjected to a high-frequency tangential excitation and showed that the excitation can effectively cancel the negative slope in the friction-velocity relationship, thus preventing self-excited oscillations. Hoffman and coworkers [14] showed that external excitation has a stabilising effect on the mode-coupling instability of a two-degree-of-freedom model. Michaux and coworkers [15] studied the effect of the tangential excitation on the system stability considering the traditional mass-on-moving belt system and using a monotonic and a non-monotonic friction-velocity relation. Their study demonstrated that while excitation is found to always have a stabilizing influence in the case of a Stribeck friction law (non-monotonic friction-velocity relation), the system with the monotonic decreasing friction behaviour can be either stabilised or destabilised by the external excitation. The latter scenario, was already stressed out by Berger and coworkers [16, 17], highlighting that the presence of excitation can also produce locally unstable responses. They considered a two-degree-of-freedom system with linear contact properties, excited by the fluctuations caused by a rough surface, while the tangential direction is excited by the normal-tangential coupling of friction. Arising from the velocity-dependent coupling of the normal and tangential modes and the periodic normal force variations, a parametric resonance was encountered for a ratio between forcing excitation and natural frequency in the normal direction equal to two.

The application of an external excitation has an effect not only on the system stability but also on the friction force, resulting into a friction modulation. In most studies, the effect of an oscillatory load on the friction force has been investigated with an emphasis on the high-frequency forcing [13, 14, 15]. Recently, Sulollari and coworkers [18] showed that the combination of the averaging technique and the velocity response function can be used to determine the vibration-induced effect on the friction force for a general frequency of excitation. Other than theoretical studies, several experimental studies on the influence of oscillatory loads on friction have been conducted. In the '60s, Tolstoi [19] showed experimentally that contact micro-vibrations, acting normal to the sliding plane, strongly affect both the magnitude of the frictional force and the stability of sliding. Later on, Tworzydlo and Becker [20] followed the general line of Tolstoi's experiments and performed a numerical analysis assuming a non-linear normal compliance of the interface, matching the experimental data with a good accuracy. Matunaga and Onoda [21] also investigated the effect of vibration on the friction force, by means of a mass sliding on an in-plane vibrating table. The observed reduction of the friction force, due to oscillatory loads, was also predicted by a simplified model assuming Amontons-Coulomb law. Despite the qualitative match between experiments and model, the measured reduced friction force values also exhibited a non-negligible degree of scatteredness with reference

to the analytical results. The reason for such discrepancy could be due to the omission of system dynamic effects in the theoretical analysis. In later studies, the effect of the contact compliance on the vibration-induced friction modulation mechanism received more attention. For example, Kapelke and Seemann [22], adopted an elasto-plastic friction model (Dupont model [23]) to match their experimental results on friction modulation. However, the friction model parameters needed to be retuned, depending on the excitation frequency used. More recent studies [24, 25] confirmed the need to use a compliant contact model to match experimental results of vibration-induced friction reduction, between various material pairs (e.g. steel, Teflon, PTFE) characterized by different surface roughness. In most of the investigation encountered so far, aimed at quantifying the vibration-induced friction modulation (or reduction) from experiments, an analysis on the stability of the investigated system is often missing.

With reference to the aforementioned background, the aim of this study is to analyze the stability of the continuous sliding state and the friction modulation of a two-degrees-of-freedom mass on belt system. The investigated system is governed by nonlinear contact properties and is harmonically excited in both the tangential and normal direction. The nonlinear contact is characterized by a normal contact force, which is assumed to be governed by the Hertz-Damp model [26]. The nonlinear normal force is then used to define the friction force, which is proportional to a given coefficient of friction. The presence of a harmonic normal excitation and the normal–tangential coupling through friction results in a periodically time-varying dissipative term, representing parametric excitation. Contrary to what shown in [13, 14, 15], the numerical simulations highlight that occurrence of such parametric excitation along the tangential direction can destabilize an otherwise stable steady sliding state of the system. To complement and extend the results presented in [16, 17], it is shown that the parametric excitation in the dissipative term leads to negative slopes in the friction force versus relative velocities relationship, indicating the presence of a negative damping mechanism which can trigger friction-induced vibrations, independently of the ratio between forcing excitation and natural frequencies of the system. Due to such instability mechanism, the harmonically excited system then oscillates not only at the excitation frequency but also at the natural frequency of the tangential mode.

An attempt is made to predict the onset of such friction-induced vibrations through a linearized stability analysis, and taking advantage of the Method of Direct Separation of Motion [18, 27, 28] that allows to incorporate the averaged effects of the friction force. Through a brief numerical validation study, it is demonstrated that, for the investigated model configuration, the results from the linearized stability analysis show a good qualitative agreement with the occurrence of friction-induced oscillations, though the quantitative match varied depending on the system parameters and their values. Further numerical analysis also demonstrates how the occurrence of a friction-induced oscillation can drastically change the outcome of a friction modulation analysis. A significant degree of scatteredness in terms of friction force modulation is observed in the numerical results, mirroring those attained experimentally by Matunaga and Onoda [21] and depending on the averaging procedure used to quantify friction change. Averaging over the vibration period of the tangential mode results in almost no scatteredness.

In this paper, first, the two-degree-of-freedom model with nonlinear contact properties

is introduced in Section 5.2. In Section 5.3, friction-induced vibrations are observed through a numerical analysis and the mechanism triggering these vibrations is found. In Section 5.4, a stability analysis is performed where the eigenvalues of the Jacobian matrix of the linearized harmonically unforced and forced systems are calculated and the Routh-Hurwitz criteria is used to study the influence of system properties and excitation on the stability of the steady sliding state. In Section 5.5, the effect of these vibrations on friction modulation is portrayed. Finally, conclusions are drawn in Section 5.6 and Appendices are added, providing additional details to the discussions and to the results presented in this study.

5.2. THE MODEL SYSTEM

To reveal the effects of system parameters and external excitation on the occurrence of friction-induced vibration and on friction change, the system illustrated in Fig. 5.1 is developed from a classic two-degree-of-freedom (2-DOF) model. The system consists of a mass M positioned on a belt, moving at a constant speed V_b. In the tangential direction, a linear spring with stiffness K_1 and a linear dashpot with damping coefficient C_1 are present. In the vertical direction, the Hertz-Damp contact model is employed [26],

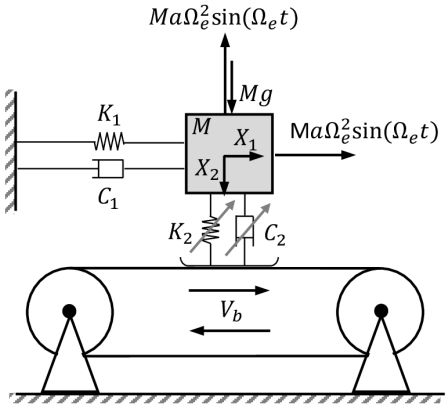

Figure 5.1: Layout of the 2-DOF Hetz-Damp system subject to external harmonic loads in the normal and tangential directions.

whereby a non-linear damper is used in parallel with the Hertz spring [29]. According to this model, the normal force F_n becomes:

$$F_n = \begin{cases} K_2 X_2^{3/2} + C_2 X_2^{3/2} \dot{X}_2 & \text{for } X_2 > 0 \\ 0 & \text{for } X_2 \leq 0, \end{cases} \tag{5.1}$$

where the stiffness $\frac{3}{2}K_2X_2^{1/2}$ and the damping coefficient $C_2X_2^{3/2}$ are respectively considered as the normal nonlinear contact stiffness and the nonlinear damping between the objects in relative sliding motion. Note that the use of the Hertz-Damp model for this study is not dictated by any specific application, but it only serves the purpose of introducing nonlinear terms in the normal direction. For the current study, nonlinear terms related to the tangential contact stiffness are neglected, since a high-level of complexity already arises due to the Hertz-Damp model. To avoid further complexities, the study of the transition between stick and slip through partial slip (see [30, 31]) is also omitted. Throughout the study, and with reference to the stability analysis, only the continuous-sliding regime is considered. While stick-slip may still occur at certain belt velocities, the presence of an external excitation (especially in the horizontal direction) extends the range of velocities where continuous sliding takes place [13, 14]. Additionally, as one of the key objectives of the study is to examine friction modulation, which is calculated by averaging the friction force over one oscillation period during sliding, on the case of stick-slip, this averaging approach is rather questionable, as it involves averaging a "static" and an oscillatory response of the system. Furthermore, throughout the paper, the chosen system parameter values guarantee that the mass is always in contact with the belt (non-jumping condition).

Given the time-varying normal force, the expression of the friction force F_f then becomes

$$F_f = \mu(V_r)F_n = \mu(V_r)(C_2X_2^{3/2}\dot{X}_2 + K_2X_2^{3/2}). \tag{5.2}$$

For the chosen model setup, we consider the kinetic friction to be the same as the static friction. The adopted friction law for this illustrative example, resembles the Amontons-Coulomb's law [32, 33], since the corresponding friction force is directly linked to a constant coefficient of friction, and proportional to the normal force. The direction of the friction force is established through a "signum" function assigned to the coefficient of friction, which reads as follows

$$\mu(V_r) = \mu_s \mathrm{sgn}(V_r), \tag{5.3}$$

where μ_s is the static friction coefficient and V_r is the relative velocity. Regarding the external load, both tangential and normal loading characterized by a frequency Ω_e and amplitude $M\alpha\Omega_e^2$ are applied as shown in Fig. 5.1. The equations of motion of the system then become

$$\begin{aligned}&\begin{bmatrix}1 & 0\\ 0 & 1\end{bmatrix}\begin{pmatrix}\ddot{X}_1\\ \ddot{X}_2\end{pmatrix} + \begin{bmatrix}2\beta_1\omega_1 & 0\\ 0 & 2\beta_2^*\omega_2^*X_2^{3/2}\end{bmatrix}\begin{pmatrix}\dot{X}_1\\ \dot{X}_2\end{pmatrix} + \begin{bmatrix}\omega_1^2 & 0\\ 0 & \omega_2^{*2}\end{bmatrix}\begin{pmatrix}X_1\\ X_2^{3/2}\end{pmatrix}\\ &+\begin{pmatrix}\mu_s\mathrm{sgn}(\dot{X}_1 - V_b)(2\beta_2^*\omega_2^*X_2^{3/2}\dot{X}_2 + \omega_2^{*2}X_2^{3/2})\\ -g\end{pmatrix} = \begin{pmatrix}\alpha\Omega_e^2\sin(\Omega_e t)\\ -\alpha\Omega_e^2\sin(\Omega_e t)\end{pmatrix},\end{aligned} \tag{5.4}$$

where $\beta_1 = \frac{C_1}{2M\omega_1}$, $\beta_2^* = \frac{C_2}{2M\omega_2^*}$, $\omega_1^2 = \frac{K_1}{M}$, $\omega_2^{*2} = \frac{K_2}{M}$ and V_r is written in terms of $\dot{X}_1$ and V_b. Note that while β_1 is dimensionless, β_2^* has the dimension of $\frac{1}{\mathrm{m}^{5/4}}$ and instead of $\frac{\mathrm{rad}}{\mathrm{s}}$, ω_2^* has the dimension of $\frac{\mathrm{rad}}{\mathrm{m}^{1/4}\mathrm{s}}$. Thus, the system described in Eq. (5.4) consists of two nonlinearly one-way coupled subsystems where the first subsystem is coupled to the second one through the friction force.

It is important to note that the tangential and normal excitation applied to the system have the same magnitude and frequency, with no phase shift between them. This type of loading can occur, for example, if an external force is applied at a 45-degree angle relative to the tangential direction of the mass. However, for the sake of analysis, an example with a phase shift of $\pi/2$, as well as an example with different excitation frequencies is examined in Section 5.3, to demonstrate that the investigated mechanism of friction-induced vibrations can still occur under these conditions.

5.3. PRELIMINARY NUMERICAL ANALYSIS

To obtain the numerical solutions of the velocity response for different loading scenarios and system parameters, the equations of motion, Eq. (5.4), are solved numerically using the MATLAB solver ode45. The baseline parameter values used are summarized in Table 5.1. To ensure that the chosen integration scheme appropriately captures the

Table 5.1: Baseline parameter values used.

Symbol	ω_1	ω_2^*	β_1	β_2^*	μ_s	α	Ω_e
Value	1.0	0.5	0.1	0.15	0.4	2	4.0

system's dynamics, for all the cases studied, the system's energy balance is verified, confirming that energy conservation is maintained. Figure 5.2(a) shows the numerical solution of the velocity response along the tangential direction for 3 different values of the belt velocity and for an external excitation driven at 4 rad/s. Note that the chosen time-window in Fig. 5.2(a), is far away from the initial transient part of the response. As illustrated in Fig. 5.2(a), different V_b values lead to variations in the velocity response. Most importantly, oscillations of several periods are present in the dynamic response. To get an overview of the spectral content, the Fast Fourier Transform (FFT) is applied over the entire time span, and the corresponding amplitude spectrum is displayed in Fig. 5.2(b). The figure reveals a distinct peak not only at the excitation frequency, Ω_e = 4 rad/s, but also at ω = 1 rad/s. The latter corresponds to the natural frequency ω_1 of the system along the tangential direction. The peak is present for certain values of belt velocities and vanishes after $V_b \approx 8$ m/s. Thus, the response oscillates not only at the excitation frequency but also at the natural frequency ω_1. Due to the non-linearity, other peaks are observed in the amplitude spectrum. As the nonlinearity is neither purely even nor purely odd, it leads to a mix of even and odd harmonics. However, they have small amplitudes and subsequently small significance on the response. In Fig. 5.2(c), a spectrogram is depicted, visualising how the frequency spectrum varies with time. As indicated in the spectrogram, the peak at ω = 1 rad/s persists throughout the whole duration and is not solely a result of the transient part of the response.

The transition between different dynamical regimes is also shown by the phase space plots in Figure 5.2(d,e). For the belt velocity V_b = 2 m/s, the system settles into a periodic limit cycle, as evidenced by the single closed trajectory in the phase plane. In contrast, at V_b = 6 m/s, the phase portrait reveals a more complex, multi-period response where the

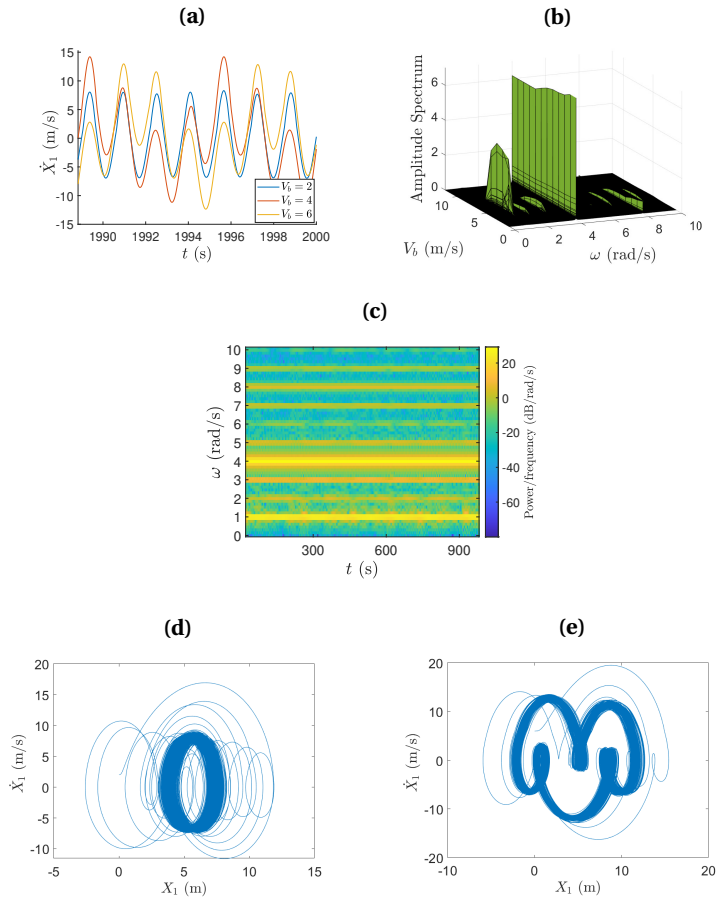

Figure 5.2: (a) Comparison of the velocity response in the tangential direction for different V_b values; (b) Amplitude spectrum of the velocity $\dot{X}_1$; (c) Spectrogram visualising the variation of frequency spectrum with time for $V_b = 4$ m/s; Phase space plots for (d) $V_b = 2$ m/s and (e) $V_b = 6$ m/s. Parameters as in Table 5.1.

trajectory consists of multiple overlapping loops. Thus, the phase space plots confirms the observations from the time-domain and spectral analysis.

In the scenario depicted in Fig. 5.2, the excitation frequency Ω_e is an integer multiple of the natural frequency ω_1. However, even with non-integer multipliers, the peak at ω_1 is still present. For instance, as shown in Appendix B.1, when the excitation frequency is set to 4.5 rad/s, the peak at ω_1 remains evident. Moreover, the peak at ω_1 also occurs for cases when the frequencies of excitation of the tangential and normal forcing are different from each other. As illustrated in Appendix B.1, when the excitation frequencies are 6 rad/s and 4 rad/s for the tangential and normal directions, respectively, the amplitude spectrum of the velocity response $\dot{X}_1$ still exhibits notable peaks at ω_1 alongside the two excitation frequencies and other harmonics. Thus, the oscillations at the natural frequency ω_1

indicate the presence of friction-induced vibrations. In the examples discussed so far, no phase shift has been observed between the tangential and normal loading. However, the friction-induced vibrations can still occur when a phase shift of $\pi/2$ is present, even though the velocity range for which these vibrations appear differs. An additional example illustrating this is provided in Appendix B.1.

To understand the mechanism by which friction can induce vibrations, the time-evolving friction force is investigated, with reference to the change of the corresponding relative sliding velocity. Figure 5.3(a) shows a time-series of the velocity response along the tangential direction, characterized predominately by the forcing frequency and by the natural frequency ω_1. The steady-state part is represented by the blue region, from which corresponding friction force versus relative sliding velocity plots are investigated. Figure 5.3(b) presents such a plot obtained over one full period T_1 ($=\frac{2\pi}{\omega_1}$). The plot starts at

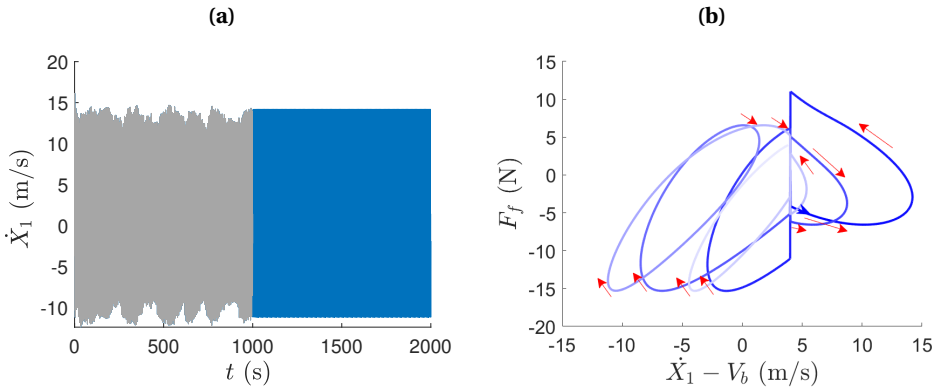

Figure 5.3: (a) Transient (grey) and steady-state (blue) part of the velocity response $\dot{X}_1$; (b) Friction force versus relative velocity. Belt velocity V_b= 4m/s. The rest of the parameters as in Table 5.1.

the point indicated by the blue arrow, with the color transitioning from dark blue to lighter blue as it progresses. The annotated red arrows show regions where the friction force increases while the relative velocity decreases in magnitude, or vice versa, indicating a negative slope in the friction force-velocity relationship. This negative slope corresponds to a negative damping effect along the tangential direction, which triggers the motion of the corresponding vibrational mode. Thus, parametric excitation of the dissipative term leads to the occurrence of negative damping, the net presence of which (from viscous damping and friction force) in the tangential direction (in parts of the oscillation cycles) explains the emergence of the additional peak at ω_1, and is the mechanism causing friction-induced oscillations. The presence of positive net damping in other parts of the oscillation cycles bounds the response.

To predict the onset of friction-induced vibrations, in the next section, a linearized stability analyses of the 2-DOF system is performed, considering both the harmonically unforced and forced scenarios (hereafter referred to simply as unforced and forced for brevity). For the forced cases, the linearized stability analysis is set up by taking advantage of the Method of Direct Separation of Motion.

5.4. STABILITY ANALYSIS OF THE STEADY SLIDING STATE

In this section, the stability analysis at the equilibrium point is carried out for both the unforced and forced systems. To take into account the excitation-induced friction modulation effect, the Method of Direction Separation of Motion (MDSM) is used within the linearized stability framework. First, a linearized eigenvalue analysis is performed to assess the local stability of the steady sliding state of the system. Then, the Routh-Hurwitz stability criterion is applied to examine how various parameters influence the stability.

5.4.1. JACOBIAN LINEARIZATION AND STABILITY ANALYSIS OF THE UNFORCED SYSTEM

The stability analysis of the unforced system is conducted by calculating the complex eigenvalues of the linearized system. To determine such eigenvalues, the Jacobian matrix is used. The initial stage in the Jacobian linearization process involves identifying the equilibrium points of the system. To accomplish this, the equations of motion are expressed in the following state-space form

$$Y_1 = \dot{X}_1 \tag{5.5}$$

$$\dot{Y}_1 = -2\beta_1\omega_1 Y_1 - \omega_1^2 X_1 + \mu_s(2\beta_2^*\omega_2^* X_2^{3/2} Y_2 + \omega_2^{*2} X_2^{3/2}) \tag{5.6}$$

$$Y_2 = \dot{X}_2 \tag{5.7}$$

$$\dot{Y}_2 = -2\beta_2^*\omega_2^* X_2^{3/2} Y_2 - \omega_2^{*2} X_2^{3/2} + g \tag{5.8}$$

equivalent to Eq. (5.4) for $\dot{X}_1 < V_b$ (the mass never overtakes the belt) and $X_2 > 0$ (non-jumping case). Setting the Eqs. (5.5)- (5.8) to zero, the equilibrium points are

$$(X_1^0, Y_1^0) = \left(\frac{\mu_s g}{\omega_1^2}, 0\right), \quad (X_2^0, Y_2^0) = \left(\left(\frac{g}{\omega_2^{*2}}\right)^{2/3}, 0\right). \tag{5.9}$$

By taking the partial derivatives of equations (5)-(8), the Jacobian matrix is obtained

$$\mathbf{J} = \begin{bmatrix} \frac{\partial \dot{X}_1}{\partial X_1} & \frac{\partial \dot{X}_1}{\partial Y_1} & \frac{\partial \dot{X}_1}{\partial X_2} & \frac{\partial \dot{X}_1}{\partial Y_2} \\ \frac{\partial \dot{Y}_1}{\partial X_1} & \frac{\partial \dot{Y}_1}{\partial Y_1} & \frac{\partial \dot{Y}_1}{\partial X_2} & \frac{\partial \dot{Y}_1}{\partial Y_2} \\ \frac{\partial \dot{X}_2}{\partial X_1} & \frac{\partial \dot{X}_2}{\partial Y_1} & \frac{\partial \dot{X}_2}{\partial X_2} & \frac{\partial \dot{X}_2}{\partial Y_2} \\ \frac{\partial \dot{Y}_2}{\partial X_1} & \frac{\partial \dot{Y}_2}{\partial Y_1} & \frac{\partial \dot{Y}_2}{\partial X_2} & \frac{\partial \dot{Y}_2}{\partial Y_2} \end{bmatrix}$$

$$= \begin{bmatrix} 0 & 1 & 0 & 0 \\ -\omega_1^2 & -2\beta_1\omega_1 & \mu_s(3\beta_2^*\omega_2^* X_2^{1/2} Y_2 + \frac{3}{2}\omega_2^{*2} X_2^{1/2}) & 2\mu_s\beta_2^*\omega_2^* X_2^{3/2} \\ 0 & 0 & 0 & 1 \\ 0 & 0 & -3\beta_2^*\omega_2^* X_2^{1/2} Y_2 - \frac{3}{2}\omega_2^{*2} X_2^{1/2} & -2\beta_2^*\omega_2^* X_2^{3/2} \end{bmatrix}, \tag{5.10}$$

and evaluating the Jacobian at the equilibrium points, the linearization reads as follows

$$\mathbf{J}^0 = \begin{bmatrix} 0 & 1 & 0 & 0 \\ -\omega_1^2 & -2\beta_1\omega_1 & \frac{3}{2}\mu_s\omega_2^{*2}\left(\frac{g}{\omega_2^{*2}}\right)^{1/3} & \frac{2\mu_s\beta_2^* g}{\omega_2^*} \\ 0 & 0 & 0 & 1 \\ 0 & 0 & \frac{-3}{2}\omega_2^{*2}\left(\frac{g}{\omega_2^{*2}}\right)^{1/3} & \frac{-2\beta_2^* g}{\omega_2^*} \end{bmatrix}. \tag{5.11}$$

The complex eigenvalues, λ, are found by solving the determinant

$$|\lambda \mathbf{I} - \mathbf{J}^0| = 0. \tag{5.12}$$

The roots of the characteristic equation are computed numerically, and in Fig. 5.4, the real part σ, indicating the growth rate, and the imaginary part ω, representing the oscillation frequencies of the complex eigenvalues λ are depicted. These are plotted for a range of β_1 values, while maintaining all other parameters constant as in Fig. 5.2. The stability of the linearized and unforced system is determined by the sign of σ. If the sign of the sigma of all roots is negative, the unforced system is stable. For $\beta_1 \geq 1$, four negative real

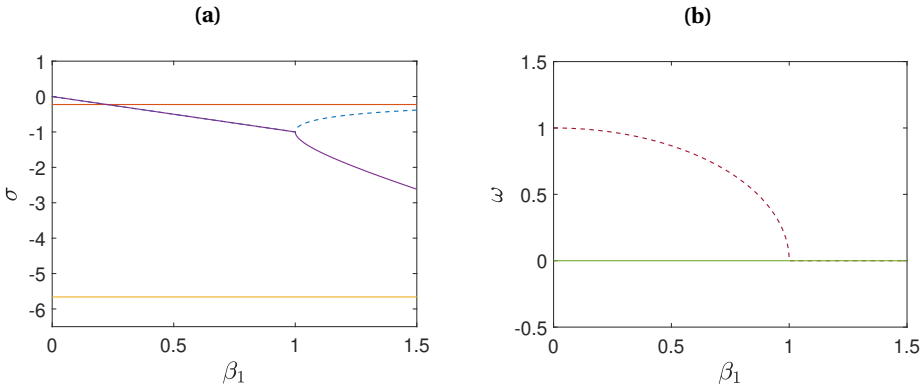

Figure 5.4: (a) Real part σ versus β_1; (b) Imaginary part ω versus β_1. Ω_e =0 (unforced system) and the rest of parameters as in Table 5.1.

σ values are present in Fig. 5.4(a) and the oscillation frequencies ω of the modes merge and equal zero, as shown in Fig. 5.4(b), leading to an overdamped system. For $\beta_1 < 1$, only one mode experiences overdamping. Still, all the σ values are negative, meaning that the unforced linearized system is stable. It is worth highlighting that the adopted system is different from the 2-DOF models considered in [5, 7, 6] where a mode-coupling mechanism due to the presence of a diagonal spring enabled the instability to occur in the corresponding unforced systems, and the effect of systems parameters such as damping, contact nonlinearity or friction coefficient on the instability were studied. It should also be noted that even though the friction coefficient μ_s appears in the Jacobian matrix $\mathbf{J}^0$, Eq. (5.11), it does not appear in the characteristic equation derived from Eq. (5.12). Consequently, contrary to systems with the mode-coupling mechanism enabled by a diagonal spring [5], the stability of the unforced system is not influenced by the friction coefficient. In the following section, the stability analysis of the linearized forced system is investigated.

5.4.2. JACOBIAN LINEARIZATION AND STABILITY ANALYSIS OF THE FORCED SYSTEM

Here, the 2-DOF system in the presence of tangential and normal harmonic excitation is considered, and the effect of excitation on the stability of the steady sliding state is

investigated. To examine this, the Method of Direct Separation of Motion is used which separates the "slow" and "fast" components of the motions [18, 27, 28]. The slow motions, the stability of which is investigated, are those of primary interest, whereas the excitation is accounted for only by its "average" influence. The separation of motions $X_1(\tau)$ and $X_2(\tau)$ into the slow and fast components reads as follows

$$X_1(\tau) = Z_1(\tau) + \Omega^{-1}\Phi_1(\tau, \Omega\tau) \tag{5.13}$$

$$X_2(\tau) = Z_2(\tau) + \Omega^{-1}\Phi_2(\tau, \Omega\tau), \tag{5.14}$$

where $Z_1(\tau)$, $Z_2(\tau)$ describe the slow motions and Φ_1, Φ_2 describe the fast motions at the rate of the external excitation. To make the transformation of variables from $\mathbf{X}$ to $\mathbf{Z}$ and Φ unique, the following constraint is applied

$$\langle \Phi(\tau, \Omega\tau) \rangle = \frac{1}{2\pi} \int_0^{2\pi} \Phi(\tau, \Omega\tau) \mathrm{d}(\Omega\tau) = 0, \tag{5.15}$$

where <> defines the average operator over the period of the rapidly oscillating component.

The application of the MDSM into the equations of motion is greatly complicated by the form of the nonlinearity $X_2^{3/2}$. Therefore, before substituting Eq. (5.13) and Eq. (5.14) into Eq. (5.4), to make the solution process more tractable, the nonlinearity is expressed in the form of a polynomial. Performing a third-order least-squares fit to the nonlinearity over the interval $0 < X_2 < X_{2,\max}$ yields to

$$X_2^{3/2} = c_3 X_2^3 + c_2 X_2^2 + c_1 X_2 + c_0, \tag{5.16}$$

where

$$c_3 = -\frac{8}{33 X_{2,\max}^{3/2}}, c_2 = \frac{72}{77 X_{2,\max}^{1/2}}, c_1 = \frac{24 X_{2,\max}^{1/2}}{77}, c_0 = -\frac{8 X_{2,\max}^{3/2}}{1155}, \tag{5.17}$$

and $X_{2,\max}$ is the maximum value of X_2 encountered. The series approximation has a maximum error of about 10^{-2}. Similar fits for the nonlinearity $X_2^{3/2}$ have been used by Bryant [34] and Hess and Soom [35]. Substituting Eq. (5.16) into Eq. (5.4), separating the motions $[\mathbf{X}] = [X_1 \; X_2]^{\mathrm{T}}$ into the components $[\mathbf{Z}] = [Z_1 \; Z_2]^{\mathrm{T}}$ and $[\Phi] = [\Phi_1 \; \Phi_2]^{\mathrm{T}}$ and making use of the averaging operation, the equations of motion for the components in $\mathbf{Z}$ are obtained

$$\ddot{Z}_1 + 2\beta_1\omega_1\dot{Z}_1 + \omega_1^2 Z_1 + \bar{\mu}(2\beta_2^*\omega_2^*\dot{Z}_2 + \omega_2^{*2})(c_3 Z_2^3 + c_2 Z_2^2 + c_1 Z_2 + c_0) = 0 \tag{5.18}$$

$$\ddot{Z}_2 + (2\beta_2^*\omega_2^*\dot{Z}_2 + \omega_2^{*2})(c_3 Z_2^3 + c_2 Z_2^2 + c_1 Z_2 + c_0) - g = 0, \tag{5.19}$$

where $\bar{\mu}(V_r)$ is the effective friction characteristic (still to be defined). The equations of motion for the components in Φ are shown in Appendix B.2. Equations (5.18) and (5.19) for the slow motions are similar in form to Eq. (5.4) for the total motion, but with the excitation accounted for by the effective friction $\bar{\mu}$ instead of the ordinary μ and the nonlinearity expressed in the form of the polynomial given by Eq. (5.16). The utilization of the polynomial form was needed to simplify the application of the MDSM. Conversely, when applying the Jacobian linearization to the equations of slow motion, Eqs. (5.18)

and (5.19), the polynomial form of the nonlinearity makes the determination of the equilibrium points cumbersome. Hence, it proves more convenient to handle the nonlinearity expressed as $Z_2^{3/2}$. Thus, Eqs. (5.18) and (5.19) are rewritten as

$$\ddot{Z}_1 + 2\beta_1\omega_1\dot{Z}_1 + \omega_1^2 Z_1 + \bar{\mu}(2\beta_2^*\omega_2^*\dot{Z}_2 + \omega_2^{*2})Z_2^{3/2} = 0 \tag{5.20}$$

$$\ddot{Z}_2 + (2\beta_2^*\omega_2^*\dot{Z}_2 + \omega_2^{*2})Z_2^{3/2} - g = 0. \tag{5.21}$$

To determine the Jacobian matrix, Eq. (5.20) and Eq. (5.21) are written in the state-space form and the equilibrum points are found setting the latter to zero, see Appendix B.2. The Jacobian evaluated at the equilibrium points is

$$\mathbf{J}_f^0 = \begin{bmatrix} 0 & 1 & 0 & 0 \\ -\omega_1^2 & -2\beta_1\omega_1 + \bar{\mu}'g & \frac{3}{2}\bar{\mu}^0\omega_2^{*2}\left(\frac{g}{\omega_2^{*2}}\right)^{1/3} & \frac{2\bar{\mu}^0\beta_2^* g}{\omega_2^*} \\ 0 & 0 & 0 & 1 \\ 0 & 0 & \frac{-3}{2}\omega_2^{*2}\left(\frac{g}{\omega_2^{*2}}\right)^{1/3} & \frac{-2\beta_2^* g}{\omega_2^*} \end{bmatrix}, \tag{5.22}$$

where the index f refers to the forced system and $\bar{\mu}'$ denotes the slope of the effective friction at the equilibrium point; note that the linearization of the effective friction expression is necessary for the formulation of the Jacobian of the system. To find the expression of the effective friction $\bar{\mu}$ in the sliding regime, in a previous study where linear contact properties were used [18], it was demonstrated that the velocity response function of the system can be exploited. For that system, the effective friction expression is

$$\bar{\mu}(V_r) = \begin{cases} \mu_s\left(1 - \frac{2}{\pi}\arccos\left(\frac{\dot{Z}_1 - V_b}{\hat{V}}\right)\right) & \text{for } |\dot{Z}_1 - V_b| \le \hat{V} \\ \mu_s \mathrm{sgn}(\dot{Z}_1 - V_b) & \text{for } |\dot{Z}_1 - V_b| \ge \hat{V} \end{cases}, \tag{5.23}$$

where $\hat{V}$ corresponds to the amplitude of the velocity response obtained for linear contact properties. Then, $\bar{\mu}'$ and $\bar{\mu}^0$ are obtained through the linearization process as follows

$$\bar{\mu} = \bar{\mu}^0 + \frac{\partial\bar{\mu}}{\partial\dot{Z}_1}\Big|_{\dot{Z}_1=0}\dot{Z}_1 + O(\dot{Z}_1)^2, \tag{5.24}$$

where

$$\bar{\mu}^0 = \bar{\mu}(\dot{Z}_1^0), \quad \bar{\mu}' = \frac{2\mu_s}{\pi\hat{V}\sqrt{1-(V_b/\hat{V})^2}} \tag{5.25}$$

for $\hat{V} > V_b$.

The complex eigenvalues, λ_f are found from the determinant

$$|\lambda_f\mathbf{I} - \mathbf{J}_f^0| = 0, \tag{5.26}$$

which is solved numerically, and the real part, σ, of the complex eigenvalues, λ_f, is plotted in Fig. 5.5(a) for a range of V_b values and the same parameters used as in Fig. 5.4. While in Fig. 5.4(a), the σ values are all negative, Fig. 5.5(a) depicts positive σ values for V_b belt velocities smaller than approximately 8 m/s. The positive σ values indicate

instability for the corresponding range of V_b values. This range of belt velocities correlates to the one for which the spectral response peak at ω_1 is shown in the amplitude spectrum in Fig. 5.2(b). Thus, $V_b \approx 8$ m/s, is the bifurcation point below which friction-induced vibrations are observed. For V_b values higher than 8 m/s, a sudden drop to negative σ values is depicted. In this range of V_b values, the amplitude of the velocity response $\hat{V}$ is smaller than the belt velocity, indicating that the effective friction is constant and its slope is zero. Consequently, the excitation has no impact on stability, the characteristic equation of the forced system matches that of the unforced system, and the system is stable at the equilibrium point.

Small discrepancies in the value of the bifurcation point predicted by the stability analysis and that observed in the numerical results are due to approximations in the stability analysis. As mentioned above, the expression for effective friction is derived for a system with linear contact properties (which does not experience friction-induced oscillations). However, as will be shown in Section 5.4, since the stability analysis depends on the slope of the effective friction curve, the expression obtained for linear contact properties remains a good approximation. If for a specific parameter space, the slope of the effective friction in the current systems significantly differs from the slope in the system with linear contact properties, the discrepancy in the results obtained through stability and numerical analysis will increase. In the next section, the effect of the slope of effective friction curve on the stability will be discussed in more detail.

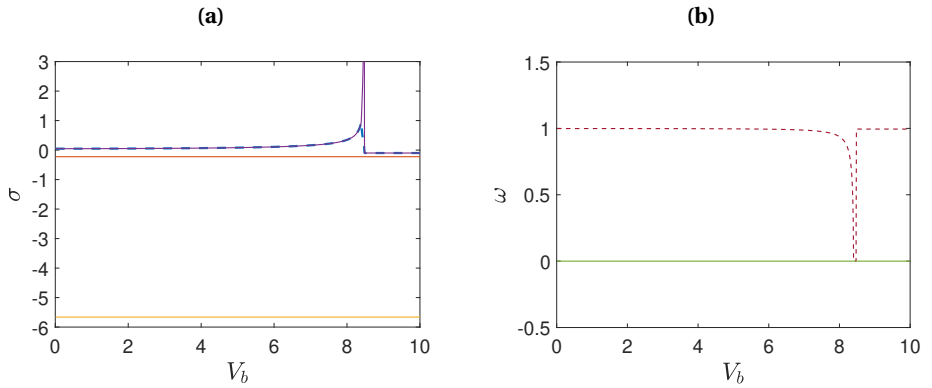

Figure 5.5: (a) Real part σ versus V_b; (b) Imaginary part ω versus V_b. $\Omega_e = 4$ rad/s (forced system) and the rest of parameters as in Table 5.1.

The findings outlined here complement and further extend the domain of investigation explored in Thomsen [13] and Hoffmann [14], in which external excitation was employed to quench the initially unstable system at the equilibrium point. In the current investigated model, the unforced system is stable and the presence of an harmonic excitation may induce instability of the steady sliding state. The current study also extends the results obtained by Michaux and coworkers [15], since their research indicates that an excitation can stabilise or destabilize a single degree of freedom system governed by a decreasing friction law, while in this study, instability is observed despite considering the Amontons-Coulomb law. Moreover, it should be noted that the stability analysis

presented in this study does not provide insights into the stick-slip behavior of the investigated system. Although a negative σ value indicates system stability, it does not offer information on whether the system may exhibit stick-slip or not.

It is important to highlight that even though a value of $\beta_2^* = 0.15$ is utilized, the system is overdamped along the vertical direction due to the presence of the nonlinearity. This holds true for both unforced and forced scenarios, as depicted in Fig. 5.4(b) and Fig. 5.5(b). In the case where linear contact properties are considered, as discussed in [18], a β_2 value greater than 1 would lead to overdamping. For instance, if $\beta_2 = 3$, the system with linear contact properties is overdamped in the X_2 direction and locally unstable along the X_1 direction, leading to friction-induced vibrations for belt velocities lower than the bifurcation belt velocity (see Appendix B.3 for further details). Hence, friction-induced oscillations can occur in an overdamped system with linear contact properties as well. It should be noted that while the effect of damping on friction-induced vibrations is discussed here, systems with both linear and nonlinear contact properties can also experience friction-induced vibrations when they are underdamped by altering the other parameter values. This is shown in the next section, where the Routh-Hurwitz criterion is used to study the effect of the model parameters on the evolution of the bifurcation point of the system.

5.4.3. ROUTH–HURWITZ STABILITY CRITERION

In the previous section, the stability of the steady siding state was determined using the roots of the characteristic equation. Here, the Routh-Hurwitz stability criterion is used as it provides the means for testing the stability without having to obtain the roots of the characteristic equation. Moreover, utilizing this approach enables the derivation of analytical expressions of the Routh-Hurwitz coefficients (in relation to system parameters) that can be employed to determine which parameters govern the stability and how they effect the evolution of the bifurcation point of the system. Considering Eq. (5.26), the 4-th order characteristic polynomial can be written as

$$\lambda^4 + a_1\lambda^3 + a_2\lambda^2 + a_3\lambda + a_4 = 0. \tag{5.27}$$

for which the expressions of a_1, a_2, a_3 and a_4 are shown in Appendix B.4. Moreover, applying the Routh-Hurwitz criterion to this characteristic equation gives the four following coefficients

$$\begin{aligned} H_1 &= a_1 \\ H_2 &= a_1 a_2 - a_3 \\ H_3 &= a_1 a_2 a_3 - a_3^2 - a_4 a_1^2 \\ H_4 &= a_1 a_2 a_3 a_4 - a_1 a_4^2 - a_4 a_3^2. \end{aligned} \tag{5.28}$$

If all these coefficients are positive, the steady sliding state is stable. When at least one of the coefficients is negative, the steady sliding state is unstable.

Figure 5.6(a) portrays the effect of V_b and β_1. Since for the parameters chosen, H_3 governs the stability, only the contour line of H_3 is shown. The shaded area corresponds to negative values of H_3 and, as a result, represents the region in which friction-induced vibration can occur (in the graphs's legend, it is indicated as "unstable"). It can be seen

that as the values of the damping coefficient β_1 increase, the range of belt velocities V_b for which the steady sliding state is unstable decreases. Thus, a higher β_1 value helps in decreasing the range of belt velocities where friction-induced vibrations can occur. This can be explained by the net damping along the tangential direction turning positive once the dissipated energy due to viscosity and due to the friction force exceeds the energy associated with the negative damping effect of the friction force. Considering the approximations introduced for the linearized stability analysis, a numerical validation study of the effect of β_1 on the system stability is presented in Fig. B.4 in Appendix B.5, demonstrating a good qualitative and quantitative agreement between the numerical results and the stability diagram. A comprehensive discussion can be found in Appendix B.5.

The effect of damping ratio in the normal direction β_2^* is shown in Fig. 5.6(b) where the contour line of H_3 is plotted with the shaded area corresponding to the unstable region. This region remains relatively the same for increased β_2^* values (limited to $\beta_2^* = 0.3$ because the system is overdamped even for the value of 0.15 used in this study.) Thus, unlike β_1, variations in β_2^* have little effect on the unstable region. The numerical validation plots in Fig. B.5 show a good qualitative agreement. While the quantitative match is good within the stability region, discrepancies are observed in the unstable region for certain parameter values (see Appendix B.5).

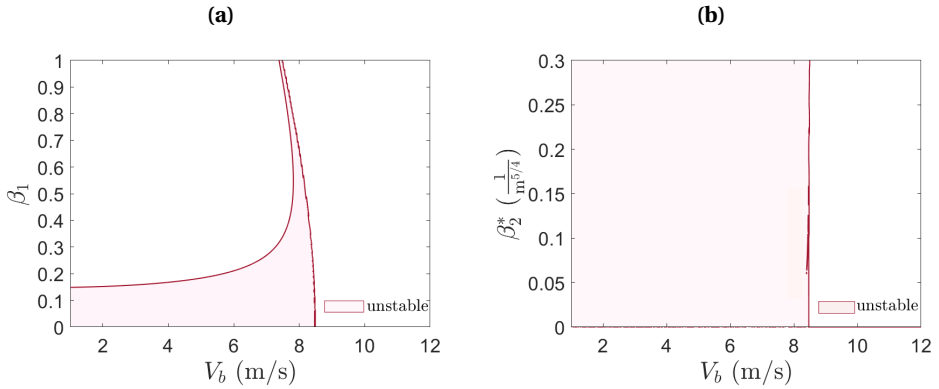

Figure 5.6: Parametric study on the stability of the system: (a) effect of damping ratio β_1; (b) effect of damping ratio β_2^*.

To assess the influence of the excitation frequency Ω_e, Fig. 5.7 shows the contour line of H_3 as a function of Ω_e and V_b. The unstable region decreases for increased Ω_e values. Thus, a higher Ω_e value helps in decreasing the range of belt velocities where friction-induced vibrations occur. As mentioned previously, it is important to note that the unstable region gives no information about the stick-slip behaviour. For the excitation frequency value used in this study, i.e. $\Omega_e = 4$ rad/s, Fig. 5.7 shows that for belt velocities smaller than the bifurcation point of $V_b \approx 8$ m/s, friction-induced oscillations occur and the numerical results, Fig. 5.2, indicate that the system is in the sliding state. For different excitation frequencies, however, the system might exhibit a stick-slip behaviour. For example, for excitation frequencies $\Omega_e = 8$ rad/s and $\Omega_e = 10$ rad/s, the numerical validation plots presented in Fig. B.6 in Appendix B.5 show that stick-slip behavior occurs

within the stable regions depicted in the stability diagram (for V_b values less than 10 m/s and 15 m/s, respectively). These results contradict those by previous studies [13, 14, 15] where high excitation frequencies were used to quench stick-slip motion. The numerical results also indicate that the stability diagram underestimates the size of the unstable region as excitation frequencies increase.

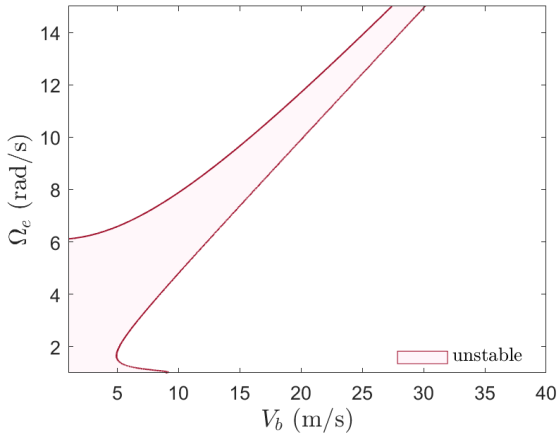

Figure 5.7: Parametric study on the stability of the system: effect of excitation frequency Ω_e. The rest of the parameters as in Table 5.1.

In Fig. 5.8(a) and Fig. 5.8(b), the influence of the stiffness is shown by varying the values of ω_1 and ω_2^*. As the ω_1 value increases, the unstable region decreases, reaching its minimum when $\omega_1 = \Omega_e = 4$ rad/s. However, as ω_1 continues to increase beyond this point, the unstable region begins to expand. The numerical validation plots shown in Fig. B.7 in Appendix B.5 display a good qualitative and quantitative match. Regarding ω_2^*, the numerical results show stick-slip regions for increasing ω_2^* values (the actual frequency being the square root of the linearised stiffness term, i.e., $\frac{3}{2}\omega_2^{*2}\left(\frac{g}{\omega_2^{*2}}\right)^{1/3}$). Therefore, the y-axis of the stability diagram is limited to $\omega_2^* = 2\ \frac{\text{rad}}{\text{m}^{1/4}\text{s}}$. In Fig. 5.8(b), it is shown that the unstable region slightly decreases by varying ω_2^*. In Fig. B.8, a good qualitative and quantitative agreement is shown with the numerical validation plots (Appendix B.5).

Lastly, the influence of $\bar{\mu}'$ is studied. While in the Jacobian matrix of the forced system in Eq. (5.22), both $\bar{\mu}'$ and $\bar{\mu}^0$ are present, in the expressions of a_1, a_2, a_3 and a_4 of the characteristic equation, Eq. (5.27), only $\bar{\mu}'$ remains, meaning that the complex eigenvalues and also the Routh-Hurwitz coefficients, Eq. (5.28), depend only on $\bar{\mu}'$. Thus, the stability is influenced by the slope of the effective friction expression. As shown in Eq. (5.23), the effective friction expression is defined by a piece-wise function. For relative velocities smaller than $\hat{V}$, the average friction takes the shape of an arccosine, the slope of which increases with increasing V_b value and goes to infinity as V_b approaches the $\hat{V}$ value. For relative velocities bigger than $\hat{V}$, the average friction becomes the constant μ_s and its slope is zero. This behaviour is also portrayed in Fig. 5.9. When the slope $\bar{\mu}'$ becomes zero,

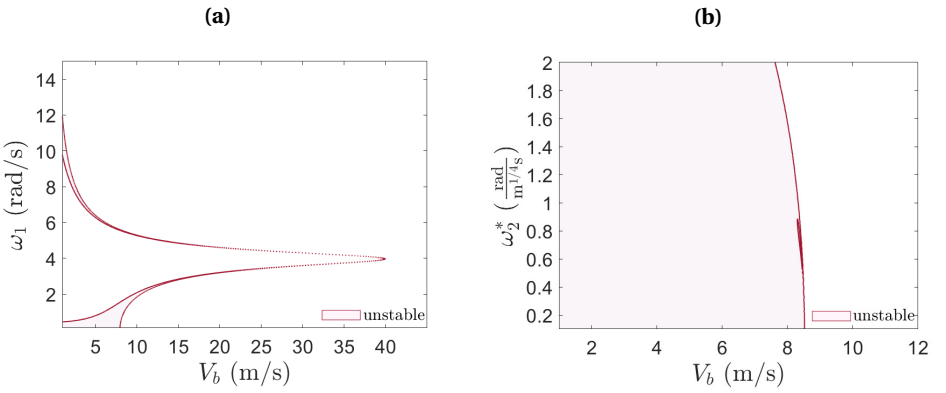

Figure 5.8: Parametric study on the stability of the system: (a) effect of ω_1; (b) effect of ω_2^*. The rest of the parameters are chosen as in Table 5.1.

the characteristic equation of the forced system aligns with that of the unforced system, indicating that the excitation has no influence on the stability. Thus, for V_b exceeding $\hat{V}$, the system is stable, akin to the unforced system. For V_b less than $\hat{V}$, slope values span from nearly zero to positive infinity (based on the parameters determining $\bar{\mu}'$). Hence, the stability is primarily governed by the system parameters such as damping, stiffness and frequency of excitation, as $\bar{\mu}'$ depends on these parameters.

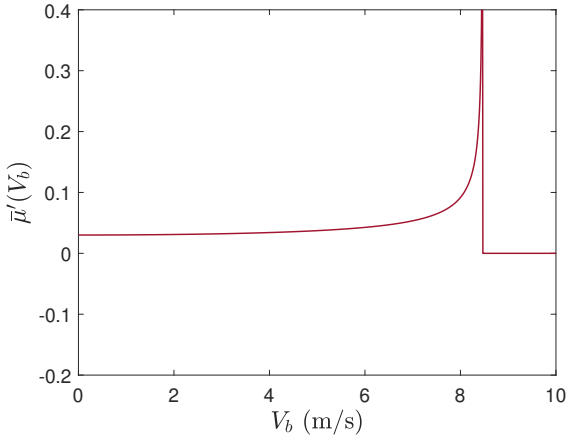

Figure 5.9: Slope of average friction versus belt velocity. Parameters as in Table 5.1.

5.5. Effect on friction modulation

In this section, the aim is to study the effect of friction-induced vibrations on friction modulation. In our previous work [18], it was demonstrated that effective friction expres-

sion is calculated using a cycle of the velocity response of the system in the steady-state regime. The direction of the friction force changes depending on the direction of relative velocity, and the effective friction is calculated by performing an averaging operation on the friction force over one cycle of oscillation. In the case of no friction-induced oscillations, the variation in the cycles of the velocity response (due to higher harmonics) is negligible. For the system considered in this study, however, since oscillations at the natural frequency are also present, the calculation of the friction modulation is not that straightforward. Looking at the graph illustrating the numerically obtained velocity response for $\Omega_e = 4$ rad/s and $V_b = 4$ m/s, see Fig. 5.10(a), the cycles differ from each other, since multiple oscillation periods are present. Consequently, the averaged friction values (averaging over $\frac{2\pi}{\Omega_e}$) derived from different cycles are not the same, as shown in Fig. 5.10(b). The colors of the circles, which illustrate the effective friction values, align with the colors of the cycles employed in computing these effective friction values. As shown in Fig. 5.10(b), there is a scatteredness in the effective friction values for belt velocities less than 8 m/s, corresponding to the bifurcation point (see Fig. 5.5). As a result of this scatteredness, there exist multiple effective friction values for a specific belt velocity.

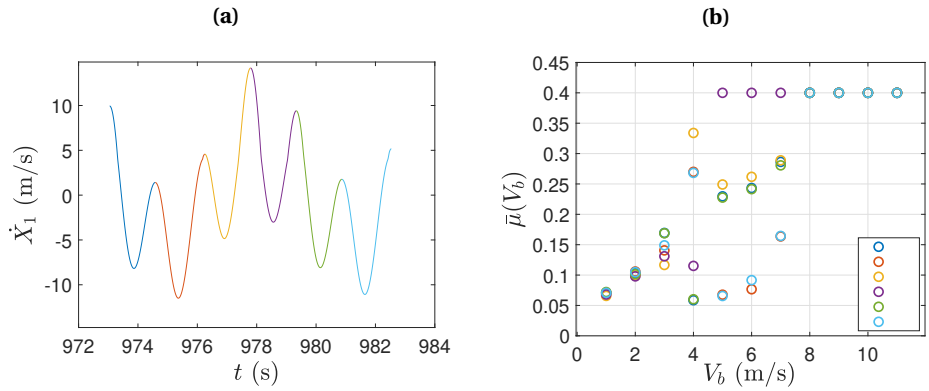

Figure 5.10: (a) Velocity response for $V_b = 4$m/s; (b) Friction modulation obtained averaging over $\frac{2\pi}{\Omega_e}$. The cycle colors in plot (a) correspond to the colored circles in plot (b). Parameters as in Table 5.1.

If instead of using cycles aligning with the period of excitation frequency, as depicted in Fig. 5.10(a), the averaging process is performed over $\frac{2\pi}{\omega_1}$ (associated with the first spectral peak in the amplitude spectrum shown in Fig. 5.2(b)), as illustrated in Fig. 5.11(a), the outcomes presented in Fig. 5.11(b) are obtained, exhibiting a more repeatable trend for the effective friction values at different belt velocities. Additionally, the average friction plot derived using the stable system with linear contact properties (as done in [18]) is depicted by the black line, revealing lower average friction values (for $V_b < 9$ m/s) at a given belt velocity. It is worth mentioning that in this scenario, the excitation frequency is four times the natural frequency. Consequently, in the steady state, after four cycles corresponding to the excitation frequency period (Fig. 5.10(a)), the response repeats itself (Fig. 5.11(a)). Hence, opting for a different time window of at least four cycles and conducting averaging over $\frac{2\pi}{\Omega_e}$, as in Fig. 5.10(b), or over $\frac{2\pi}{\omega_1}$, depicted in Fig. 5.11(b), would

yield the same outcomes.

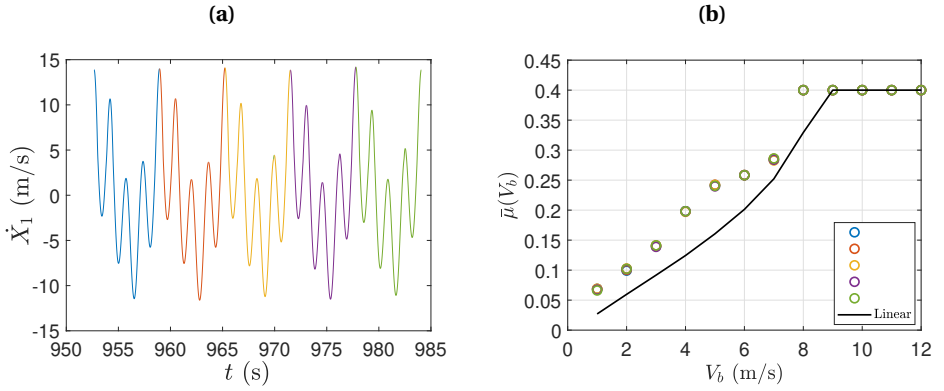

Figure 5.11: (a) Velocity response for $V_b = 4$ m/s; (b) Friction modulation obtained averaging over $\frac{2\pi}{\omega_1}$. The cycle colors in plot (a) correspond to the colored circles in plot (b). Parameters as in Table 5.1.

Increasing the excitation frequency to $\Omega_e = 6$ rad/s, the results depicted in Fig. 5.12(a) are obtained, showing a bigger scatteredness in the effective friction values (the numerical validation plot is shown in Fig. B.6(a) in Appendix B.5). Averaging over $\frac{2\pi}{\omega_1}$ instead, results again in almost no scatteredness, as shown in Fig. 5.12(b). Compared to the stable linear case (see black continuous line in Fig. 5.12(b)), the effective friction values are higher for $V_b < 7$ m/s, lower for 8 m/s $< V_b <$ 15 m/s and equal to the linear case for $V_b >$ 16 m/s. Thus, increasing the excitation frequency leads to an increase in scatteredness in Fig. 5.12(a) and in a variation of the effective friction values that, depending on the belt velocities, might either increase or decrease compared to the ones obtained for the stable system with linear contact properties, Fig. 5.12(b).

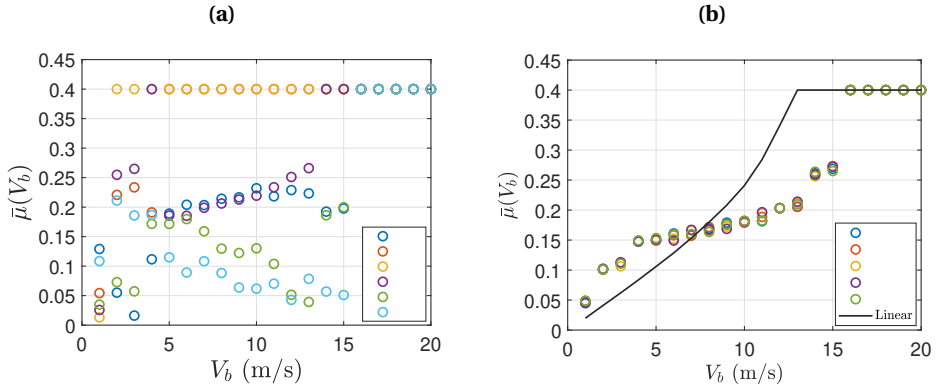

Figure 5.12: (a) Friction modulation obtained averaging over $\frac{2\pi}{\Omega_e}$; (b) Friction modulation obtained averaging over $\frac{2\pi}{\omega_1}$. The cycle colors in plot (a) correspond to the colored circles in plot (b). $\Omega_e = 6$ rad/s and the rest of the parameters as in Table 5.1.

In several theoretical and experimental works conducted on the effect of vibration-induced friction reduction, the measurements did not match the model predictions obtained assuming an Amontons-Coulomb law to model the friction force. Gutowski and Leus [36, 37], for example, analysed the influence on the averaged friction force of an external forcing applied parallel and perpendicular to the sliding direction, respectively. While for the case of longitudinal excitation, the discrepancy of experimental measurements with the theoretical results obtained assuming Amontons-Coulomb friction law was not significantly large, for the case of transverse excitation significant mismatches were observed. To better catch the experimental behaviour, they used the Dahl and the Dupont models [23] that take into account a tangential contact stiffness. The Dahl friction model with different stiffness values was employed by Wang and coworkers as well and a qualitatively good match was obtained with the experimental results [38, 39]. Deviations were still observed for specific material combinations. Kapelke also used the Dupont model and the Amontons-Coulomb law to compare the experimental results to theoretical ones [22]. An excellent match between the experimental results and the elasto-plastic Dupont model was observed. However, to accurately catch the behaviour of the friction force reduction observed for tests carried out with high excitation frequencies, significantly different values of stiffness were needed for the Dupont model compared to the ones used for the low-frequency tests. Figure 5.13 shows the effective friction plots obtained using the Amontons-Coulomb law and both the full and reduced elasto-plastic model as conducted in [22]. The figure indicates that the elasto-plastic friction model yields higher effective friction values than the Amontons-Coulomb law, similar to the results shown in Fig. 5.11(b). Increasing the excitation frequency results in a different trend, Fig. 5.12(b).

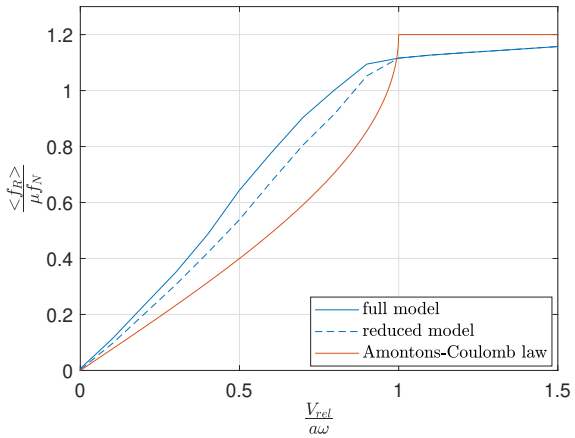

Figure 5.13: Friction–velocity characteristics: Amontons-Coulomb, reduced and full elasto-plastic friction model as in [22].

To summarise, in this study, the friction force is assumed to be proportional to the coefficient of friction and the normal force being time-varying and nonlinear. In other

words, rather than considering a single degree of freedom system coupled to a Dahl and/or Dupont model (which includes a tangential contact stiffness), nonlinear contact properties along the normal direction are incorporated, which, if excited, generate a nonlinear time varying friction force. Hence, attention should be paid to the presence of unexpected dynamic normal force variation during vibration-assisted friction reduction experiments, in which only a deliberate tangential or lateral excitation is applied. An uncontrolled misalignment of such excitation directions with respect to the sliding plane can lead to a time-varying normal force, eventually causing friction-induced vibrations. The combination of nonlinear contact properties along the normal direction and external excitation results in friction modulation graphs which display shapes that qualitatively resemble those obtained experimentally and are different from those derived from systems with no friction-induced oscillations.

5.6. CONCLUSIONS

In this work, the effect of external excitation and nonlinear contact properties on the stability of the steady sliding state and on the friction modulation of a 2-degree-of-freedom mass on a moving belt system is studied. Both tangential and normal excitation are present and the nonlinear contact properties are represented by the Hertz-Damp model. The presence of the time-varying normal contact force and the corresponding friction leads to parametric excitation, triggering friction-induced oscillations. Whenever these oscillations are detected, parts of the friction force versus relative velocity plots reveal negative slopes, even though the Amontons-Coulomb law is assumed. The presence of the parametrically induced negative net damping in the tangential direction is the mechanism behind friction-induced oscillations.

To predict the onset of such oscillations, a linearized stability analysis is performed taking advantage of the Method of Direct Separation of Motion, which allows to incorporate the averaged effects of the friction force modulated through the applied external excitations. While the unforced system is stable at the equilibrium point, the forced system exhibits friction-induced vibration for certain regions of the parameter space. Thus, while external excitation is generally used to quench self-excited oscillation, the presence of an oscillating normal force and the normal–tangential friction coupling can also destabilise an otherwise stable equilibrium state. Additionally, the Routh-Hurwitz criterion is used to study the effect of varying the model parameters on the occurrence of friction-induced vibrations. It is found that a higher damping ratio for β_1 helps in decreasing the region where friction-induced vibrations occur. Similarly, as the natural frequency ω_1 increases, the unstable region decreases, reaching its minimum near resonance. However, as ω_1 continues to increase beyond this point, the unstable region expands again. For the parameter space considered, varying β_2^* and ω_2^* has little impact on the unstable region. A higher excitation frequency Ω_e value increases the stable region. For all cases, the stability analysis does not provide information on whether the system might experience stick-slip behaviour or not. The numerical validation study demonstrated that the results from the linearized stability analysis show a good qualitative agreement with the occurrence of friction-induced oscillations, though the quantitative match varied depending on the system parameters and their values. It is worth mentioning that this study makes use of a

simplified model, with reference to the investigation of parametric excitation. Modifying it could make it more representative of specific real-case scenarios, as shown in [4, 11, 10, 12].

Lastly, the effect of friction-induced vibrations on friction modulation is studied. Whenever friction-induced vibration is present, the cycles in the velocity response differ from each other, since multiple oscillation frequencies are present. This results in a scatteredness in the effective friction values for the range of belt velocities for which instability is observed. Therefore, multiple effective friction values can exist for a specific belt velocity. A similar level of scatteredness can also be observed in related experimental studies. Instead, averaging over the vibration period of the tangential mode results in almost no scatteredness and in effective friction plots with shapes that qualitatively resemble those obtained experimentally or obtained using Dahl and/or Dupont models. Finally, this work calls for further experimental validation, and at the same time, it highlights the need to keep track and measure the presence of normal force oscillations that may occur during the experiments.

6

VIBRATION-INDUCED FRICTION MODULATION FOR AN OSCILLATOR MOVING ON AN ELASTIC ROD

This chapter investigates a moving oscillator in frictional contact with an elastic rod, extending the analysis beyond the discrete systems studied so far. The results are compared with the single-degree-of-freedom system considered in Chapter 3, which considered a rigid rod/belt, in order to illustrate the effect of support flexibility on friction modulation. By analysing this system, this chapter contributes to the dissertation's objectives: increasing the system complexity by considering a flexible supporting structure instead of a rigid one, exploring the effect of the flexibility and load location, applied either on the mass or on the supporting structure, on friction modulation, and comparing the results with existing experiments and real-life application. Readers familiar with the background presented in the "State of the art" chapter may skip the introduction section if desired.

This chapter has been published as: Sulollari, E., van Dalen, K.N., and Cabboi, A. (2025). Vibration-induced friction modulation for an oscillator moving on an elastic rod. International Journal of Solids and Structures, 2025, 113572.

ABSTRACT

Several studies have been dedicated to altering friction forces, with external excitation being one of the approaches explored. When the latter is considered, its influence has primarily been studied within the context of discrete systems. Therefore, in this study, a moving oscillator in frictional contact with an elastic rod of finite length subjected to distributed damping is considered, to study the influence of external excitation in the presence of support flexibility on friction modulation. The modal expansion method is used to derive the modal equations of motion, which are then solved numerically. Two cases are investigated, one with the load acting on the mass and the other with the load acting on the rod. It is found that, for both cases, friction modulation varies along the rod's length, and it differs from that obtained assuming a rigid rod. Moreover, for the load-on-mass scenario, a critical velocity is defined, providing direct insight into the friction modulation differences between flexible and rigid rod cases. For the load-on-rod scenario, large deformations are observed close to and above resonance, and geometric nonlinearity is accounted for to describe the system dynamics accurately. To link theoretical results to applications, the findings are used to qualitatively interpret slip-joint vibration-assisted decommissioning tests, and are compared with experimental results in which friction force reduction is explained through the use of elasto-plastic friction models that account for surface deformability, showing good qualitative agreements between the theoretical and experimental outcomes.

6.1. INTRODUCTION

Controlling the tribological behaviour of interfaces is essential for the satisfactory operation of systems in many fields of applied science. This control is crucial for mitigating energy, efficiency and economic losses and reducing noise pollution [1]. Tribological interface properties encompass various factors, including surface roughness, hardness, wear, and friction. Over the past few decades, extensive research has explored ways to modulate or control friction forces without relying on lubricants. This area of study is particularly relevant in mechanical engineering, as lubrication management –such as timely application, removal, and replacement – can be both challenging and labor-intensive. Additionally, the environmental impact of lubricants further underscores the importance of developing alternative friction-control strategies. A lubricant-like effect at the sliding interface can also be reproduced by a surrounding oscillatory field. The use of a deliberate application of oscillatory forces has already been implemented in metal working [2], decommissioning of joints [3], positioning control in robots [4], pile driving [5] and rendering textures in surface haptics [6]. However, besides the scope of controlling a sliding process, the presence of an oscillatory field at the sliding interface (if uncontrolled or if mistakenly neglected), can also lead to erroneous interpretations of measured friction forces, if the goal is to assess the tribological behaviour of a sliding interface. This may result in an apparent (but misleading) dependency between the friction force and the sliding velocity [7, 8]. The complexity of the friction-vibration interaction increases if the influence of the so-called "inner-dynamics" of the interface is introduced. In fact, in previous studies [9, 10, 11, 12, 13, 14], it has been shown that the small-scale dynamics of a micro-structured interface can have a substantial effect on friction modulation. This means that a desired frictional behavior can also be obtained by optimizing the properties of the microstructure. Besides the application of modulating the friction force, the use of

a deliberate high-frequency microvibration was also investigated to control the adhesion behaviour between two material pairs [15, 16], a topic that lies beyond the remit of this study.

Over the last two decades, researchers have used various models to study friction modulation, with a special focus on developing strategies to quench friction-induced instabilities of a sliding system, the simplest one being represented by a single-degree-of-freedom oscillator sliding over a rigid belt. The effect of a high-frequency tangential excitation on such model was studied by Thomsen [17], who showed that high-frequency excitation can prevent self-excited oscillations by effectively cancelling the negative slope in the assumed friction-velocity relationship. Follow-up studies were carried out by Michaux and coworkers [18] in which monotonic and non-monotonic friction-velocity relations were assumed. An extension to the two-degree-of-freedom system was investigated by Hoffman and coworkers [19]. In their work, they not only investigated the effect of external tangential excitation on the friction force change, but also showed that excitation can stabilise the mode-coupling instability. Other studies used similar systems, emphasizing the focus on the stability rather than friction modulation [20, 21, 22, 23]. In a more recent study, Sulollari and coworkers also considered a similar system to study both the friction modulation and the system stability under the effect of parametric excitation [24].

The above-mentioned studies did not account for the effect caused by microstructured surfaces, whose corresponding stiffness and dynamic properties can significantly affect the friction force. This is shown by Costagliola and coworkers [11], who considered a 1-D elastic surface discretised into mass elements connected by springs, a discretisation representative of the microscopic heterogeneity of the surface roughness. A 2-D spring-block model was studied in a follow-up study [12]. Both models showed that the frictional behaviour depends strongly on the micro-structures' shape, size and orientation. Menga and coworkers also considered a micro-structured 2-D surface modelled through masses connected to radial and torsional elastic elements [13]. It was found that different dynamic regimes that affect friction behaviour can be achieved depending on the supports' elastic properties and static orientation. In a follow-up study, the frictional behaviour of a 3-D lattice structure was studied to account for the effect of the local distribution of the normal load and the in- and out-of-plane self-excited vibrations emergence [14]. These studies show that by optimizing the mechanical properties of the interface microstructure, it would be possible to obtain the desired friction behavior.

Other than theoretical studies examining the effect of external excitation or microstructure dynamics on friction modulation and stability, numerous experimental studies with similar objectives have also been conducted, the results of which have been compared using models (discrete and continuous) akin to those described earlier. Commonly, the experimental tests are conducted on pin-on-disk setups. For instance, Littmann and coworkers [25], Storck and coworkers [26] and Kumar and Hutchings [27] studied the reduction of the friction force due to ultrasonic vibrations applied parallel and perpendicularly to the sliding direction. For each loading case, qualitative agreements between theoretical predictions (e.g., based on single-degree-of-freedom systems) and measurements (e.g., involving a moving ultrasonic vibrator along a track) were obtained. A better consistency of the experimental and theoretical results was obtained by Tsai and

Tseng [28] using the Dahl model [29] which takes into account contact deformability in the tangential direction, or the elasto-plastic friction model proposed by Dupont and coworkers [30]. Kapelke also used the Dupont model and the Amontons-Coulomb law to compare the experimental results to theoretical ones and found an excellent match between the experimental and theoretical results for tests carried out with moderate excitation frequencies [31]. Thus, when comparing experimental results to theoretical studies, the latter are typically focused on 1- or 2-DOF systems, utilizing friction models often coupled with terms accounting for the surface compliance (see the use of the Dahl or Dupont model).

Besides small-scale experiments, the notion of modulating a friction force through a deliberate oscillatory forcing has also been applied to large-scale structures. More specifically, a vibration-assisted technique was tested through laboratory experiments to modulate the friction force, enabling the installation and removal of a scaled slip joint [32]. A follow-up study applied the technique on a full-scale slip joint for a wind turbine connection [3], allowing the decommissioning of the slip joint itself. While the decommissioning operations successfully confirmed the effectiveness of the vibration-assisted technique and correlations were established between the excitation frequencies used and the structural modes of vibration, the actual change of the friction force due to the applied excitation could not be quantified. Moreover, analyzing a more realistic (or high-fidelity) model of the large-scale structure with friction-vibration interaction proved to be too complex for understanding the observed physical behavior.

While previous studies have investigated the effect of external excitation on friction modulation using discrete systems or focused on the influence of microstructure dynamics and geometry without considering external excitation, there remains a gap in understanding how external excitation interacts with the dynamics of continuous systems, which are more representative of the dynamics of real systems. Therefore, this study aims to analyse the effect of external excitation on friction, considering a moving oscillator on an elastic rod of finite length subjected to distributed damping, which allows for a more realistic representation of how external excitation influences frictional behaviour through continuous deformations. Two cases are investigated, one with the external load acting on the mass and the other with the load acting on the rod. For both cases and various excitation frequencies, the values of the effective (or average) friction vary along the rod's length and differ from those obtained assuming a rigid rod. For the load-on-mass scenario, a critical velocity is defined, which reveals direct insight into the differences in friction modulation between the flexible and rigid rod cases. The application of an external excitation to the rod needs particular attention in order to avoid large axial deformation under resonance conditions or high-excitation frequencies. For cases when large deformations are allowed (depending on the material type, properties, loading conditions etc.), geometric nonlinearity is accounted for in the equations of motion. Finally, the results of this study are used to qualitatively explain the vibration-assisted decommissioning tests of the slip joint [3, 32], and allow for a comparative discussion with the friction modulation results obtained using elasto-plastic friction models meant to encapsulate the surface deformability [31].

The paper is structured as follows. First, the description of the moving oscillator on the rod is introduced in Section 6.2. In Section 6.3, the results on friction modulation are

obtained when the oscillatory load acts on the mass. The results for the load acting on the rod are presented in Section 6.4. In Section 6.5, analogies with real-world applications and experimental studies are explored to contextualise the modelling choices. Finally, conclusions are drawn in Section 6.6 and the Appendix is added, providing additional details to the discussions and the results presented in this study.

6.2. THE MODEL SYSTEM

To reveal the effects of axial rod deformations on vibration-induced friction modulation, the system illustrated in Fig. 6.1 is considered. Figure 6.1(a) illustrates the case where the harmonic load is applied on the mass, and Fig. 6.1(b), the case where the load is applied on the rod. The system consists of a moving oscillator composed of a mass m, a spring with stiffness k and a dashpot with damping coefficient c, connected to a massless support. The support is pushed to the right direction with a constant velocity v and the distance from the left end at time t is vt. The initial length of the spring is s_0 and the elongation of the spring from the free length is s. The load N is a constant normal preload acting on the mass. The rod has a cross-sectional area A, density ρ, length L, Young's modulus E and damping coefficient c_b. The axial deformation of the rod at a given position x is $u(x,t)$. The rod has fixed supports on both ends. The external harmonic loading is characterized by a frequency Ω_e and an amplitude $Ma\Omega_e^2$ (e.g., load arising from a horizontally unbalanced mass M at eccentricity a [17]). For the load acting on the rod, Fig. 6.1(b), the application point corresponds to the position defined by the spring's initial length s_0.

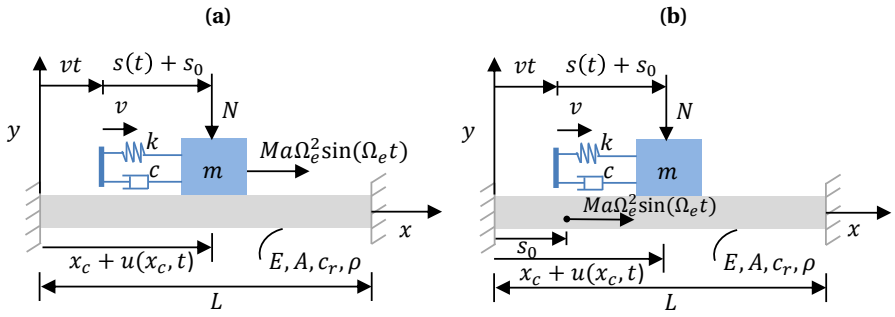

Figure 6.1: Oscillator moving on an axially deforming rod: (a) harmonic load applied on the mass; (b) harmonic load applied on the rod at a position defined by the initial length of the spring s_0.

For the chosen model setup, the kinetic friction is considered to be the same as the static friction. The adopted friction law is the Amontons-Coulomb's law [33, 34], since the corresponding friction force is directly linked to a constant coefficient of friction, and proportional to the normal force. As the aim of this study is to capture the effect of the rod deformation on vibration-induced friction changes, the assumption of Amontons-Coulomb's law is deemed most appropriate, since it avoids the complexity of more realistic friction laws which are case-study and material pair dependent [35, 36]. The

friction force f acting between the mass and the rod is then

$$f = -\mu_s \text{sgn}(v_r) N, \tag{6.1}$$

where μ_s is the static friction coefficient and v_r is the relative velocity. The latter is expressed as

$$v_r = \dot{s} + v - \dot{u}|_{x=x_c}, \tag{6.2}$$

where the overdot represents the total derivative with respect to time and x_c is the position of the point at which the mass contacts the rod.

Under the small deformations theory, so assuming the deformation of the rod and mass to be negligible compared to L and s_0 respectively, the expression of x_c can be written as

$$x_c(t) = vt + s_0. \tag{6.3}$$

It should be noted that on the study of Hong and coworkers [23] where a similar system is considered, the full kinematic expression for the contact point is used, and reads as follows

$$x_c(t) = vt + s_0 + s(t) - u(x_c(t), t). \tag{6.4}$$

According to this expression, u and x_c are coupled, so the x_c expression is implicit. Under small deformations, however, the contributions from the spring elongations and the rod deformation are negligible, and Eq. (6.4) can be approximated by Eq. (6.3). In this study, when small deformations are considered, Eq. (6.3) is used, significantly reducing the computational time.

The equations of motion of the system without considering the external forcing terms then become

$$\rho A \frac{\partial^2 u}{\partial t^2} + c_b \frac{\partial u}{\partial t} - EA \frac{\partial^2 u}{\partial x^2} + f\delta(x - x_c) = 0, \tag{6.5}$$

$$m\frac{d^2 s}{dt^2} + c\frac{ds}{dt} + ks = f. \tag{6.6}$$

with the boundary conditions for a fixed-fixed rod being

$$u = 0 \quad \text{at} \quad x = 0 \quad \text{and} \quad u = 0 \quad \text{at} \quad x = L, \tag{6.7}$$

and the friction force as in Eq. (6.1). In the case of load-on-mass, an additional loading term appears on the right-hand side of Eq. (6.6) as $Ma\Omega_e^2 \sin(\Omega_e t)$. For the load-on-rod case, the loading term appears on the right-hand side of the Eq. (6.5) as $Ma\Omega_e^2 \sin(\Omega_e t)\delta(x - s_0)$. To generalize the results, the following dimensionless parameters are introduced:

$$\begin{gathered} t^* = \omega_n t, \quad \omega_n^2 = \frac{k}{m}, \quad \beta = \frac{c}{2m\omega_n}, \quad x^* = \frac{x}{L}, \quad s^* = \frac{s}{L}, \quad s_0^* = \frac{s_0}{L}, \quad u^* = \frac{u}{L}, \\ v^* = \frac{v}{L\omega_n}, \quad v_r^* = \frac{v_r}{L\omega_n}, \quad \delta^* = L\delta, \quad f^* = \frac{f}{\rho AL^2\omega_n^2}, \quad N^* = \frac{N}{\rho AL^2\omega_n^2}, \\ \beta_b = \frac{c_b}{2\rho A\omega_b}, \quad \omega_b = \frac{\pi}{L}\sqrt{\frac{E}{\rho}}, \quad r_\omega = \frac{\omega_b}{\omega_n}, \quad r_m = \frac{\rho AL}{m}, \quad \Omega_e^* = \frac{\Omega_e}{\omega_n}, \quad \alpha^* = \frac{Ma}{mL}, \end{gathered} \tag{6.8}$$

where r_m is the mass ratio of the rod and the oscillator mass, r_ω is the frequency ratio between the rod's first natural frequency and the oscillator's natural frequency (defined for the separate subsystems when no interaction is present) and the asterisk denotes a dimensionless component. Substituting Eq. (6.8) into Eq. (6.5) and Eq. (6.6), and dropping the asterisks from the dimensionless equation for simplicity, the dimensionless equations of motions of the unforced system are derived

$$\frac{\partial^2 u}{\partial t^2} + 2\beta_b r_\omega \frac{\partial u}{\partial t} - \left(\frac{r_\omega}{\pi}\right)^2 \frac{\partial^2 u}{\partial x^2} + f\delta(x - x_c) = 0, \tag{6.9}$$

$$\frac{d^2 s}{dt^2} + 2\beta \frac{ds}{dt} + s = r_m f. \tag{6.10}$$

To solve the equations of motions, first, the modal expansion method is used to derive the modal equations from the rod equation. Using this method and the mode shapes of a fixed-fixed rod, the response $u(x,t)$ is written as

$$u(x,t) = \sum_{j=1}^{p} T_j(t)\sin(j\pi x), \tag{6.11}$$

where p is the total number of modes considered and $T_j(t)$ is the unknown function of time to be determined. Substituting Eq. (6.11) into Eq. (6.9) and Eq. (6.10), with f and x_c as in Eq. (6.1) and Eq. (6.3) respectively, and using the orthogonality property of the mode shapes, the modal equations are obtained

$$\ddot{T}_j + 2\beta_b r_\omega \dot{T}_j + j^2 r_\omega^2 T_j + 2f_j(\dot{s}, \dot{T}_1, \dot{T}_2 ... \dot{T}_p) = 0, \tag{6.12}$$

$$\ddot{s} + 2\beta\dot{s} + s - r_m f_j(\dot{s}, \dot{T}_1, \dot{T}_2 ... \dot{T}_p) = 0. \tag{6.13}$$

The modal forces f_j are functions of $\dot{s}$, $\dot{T}_1$, $\dot{T}_2$, ..., $\dot{T}_p$ and are given by

$$f_j(\dot{s}, \dot{T}_1, \dot{T}_2 ... \dot{T}_p) = -\mu_s \mathrm{sgn}(v_r|_{x=x_c}) N \sin(j\pi x_c), \tag{6.14}$$

and

$$v_r|_{x=x_c} = \dot{s} + v - \sum_{j=1}^{p} \dot{T}_j \sin(j\pi x_c) - \sum_{j=1}^{p} T_j j\pi \dot{x}_c \cos(j\pi x_c). \tag{6.15}$$

In the v_r expression, the chain rule is used to calculate the total derivative of $\dot{u}$ as x_c is time-dependent. However, the contribution of the last term appeared negligible for the cases considered in this study.

6.3. HARMONIC LOAD ACTING ON THE MASS

This section examines the case of the external harmonic load acting on the mass, Fig. 6.1(a). The equations of motion are solved numerically, and the friction modulation is evaluated as the mass moves along the rod, considering different excitation frequencies. Then, plots of friction modulation for different pushing velocity v values are presented. All results are compared to those obtained for a mass-spring-dashpot system on a rigid rod (analogous to a mass-spring-dashpot on a moving belt system as described in [37]).

6.3.1. FRICTION MODULATION ALONG THE ROD LENGTH

The equations of motion, Eq. (6.12) and Eq. (6.13), are solved using the MATLAB solver ode23s, considering the parameter values shown in Table 6.1 below. The number of

Table 6.1: Dimensionless properties of the rod and the moving oscillator.

Symbol	r_m	r_ω	β_b	β	s_0	ν	μ_s	N	α
Value	4.8	6.0	0.001	0.14	0.25	0.005	0.5	0.002	0.004

modes considered is $p = 10$ (increasing the number of modes can be shown to have a negligible effect on the results). These parameter values are chosen to ensure sliding over a wide range of excitation frequencies. To guarantee that the response adheres to the small deformation assumptions, for the parameters chosen, the solutions obtained are compared to those derived considering a rod with geometric nonlinearity, with the x_c expression as in Eq. (6.4). The comparison shows negligible differences between both cases, as demonstrated in Appendix C.1, complying the small deformation assumption.

The mass and rod responses (obtained from Eq. (6.12) and Eq. (6.13)) are used to calculate the average friction, $\bar{\mu}(v_r)$, by integrating the friction force over the excitation period as follows

$$\bar{\mu}(v_r) = \langle \mu_s \text{sgn}(v_r|_{x=x_c}) \rangle = \langle \mu_s \text{sgn}(\dot{s} + \nu - \sum_{j=1}^{p} \dot{T}_j(t) \sin(j\pi x_c)) \rangle \,, \tag{6.16}$$

where <> defines the average operator over the excitation period $\frac{2\pi}{\Omega_e}$. In Fig. 6.2, the continuous lines represent the average friction values obtained for different excitation frequencies as the mass moves along the rod length, ranging from 0.25 to 1, as $s_0 = 0.25$ is chosen. The dot markers represent the average friction values obtained analytically for a mass-spring-dashpot system on a rigid rod/belt as done in [37], where the approach for calculating the average friction through the velocity response function is described. These modulated friction values are constant and do not vary along the length of the rod. The colours of the dot markers correspond to the colours of the continuous lines, indicating that the same parameter values are used for each pair. It should be noted that the initial parts of the continuous lines correspond to oscillation cycles of the transient response as the averaging process is carried out on the entire relative velocity response, whereas the dot markers are obtained analytically considering the steady-state response only.

The results shown in Fig. 6.2 are obtained for $r_\omega = 6$, meaning that the natural frequency of the rod's first mode is 6 (i.e. $\omega_b = 6$ rad/s and $\omega_n = 1$ rad/s). Figure 6.2(a) depicts the average friction plots for excitation frequencies smaller than and equal to the rod's first natural frequency, and Fig. 6.2(b) illustrates results for excitation frequencies exceeding the rod's first natural frequency. Both plots demonstrate that the continuous lines are not constant, indicating that, unlike the rigid rod case, the rod's flexibility leads to variations in the average friction along its length. Depending on the position along the rod length, these values can be smaller or larger than the ones obtained for the rigid rod. Towards the end of the rod, the values of the continuous lines approach those of the dot markers,

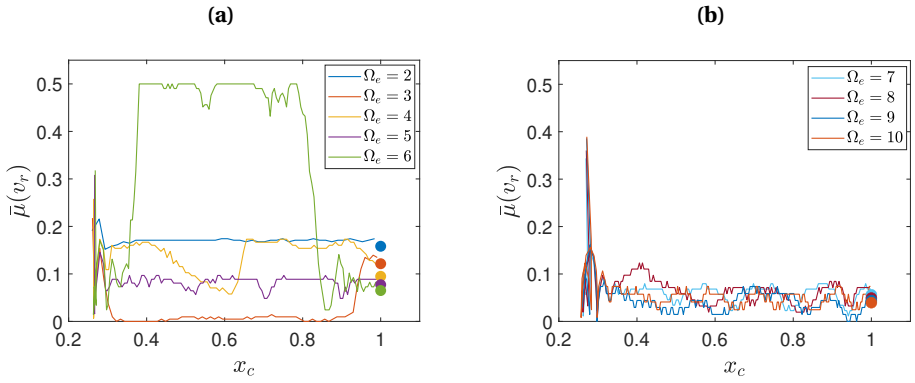

Figure 6.2: Average friction results along the rod length for $\nu = 0.005$. Continuous lines refer to the case of the flexible rod, and dot markers refer to the rigid rod. Dot marker colours match those of the continuous lines for the same excitation frequency: (a) results for excitation frequencies smaller than and equal to 6; (b) results for excitation frequencies bigger than 6.

since the axial deformation at both rod's ends approaches zero. Differences in values are from rod oscillations in the proximity of the support due to the change in (perceived) stiffness giving rise to transition-radiation effects [38]. While all the continuous lines show variations, the most significant differences relative to the rigid case are observed at excitation frequencies $\Omega_e = 3$ and $\Omega_e = 6$.

To better highlight the influence of the deformable rod with respect to the rigid one, Fig. 6.3 shows boxplots for different excitation frequencies, highlighting the statistical distribution of the average friction values while the mass slides over the rod. For each boxplot, the median is indicated by the central red line. The bottom and top edges of the box represent the 25th percentile (Q1) and 75th percentile (Q3), respectively, while the whiskers extend to the most extreme data points within 1.5 times the interquartile range below Q1 and above Q3. All other observed data points outside the boundary of the whiskers are plotted as outliers using the "+" grey marker and are mainly a result of averaging over the oscillation cycles of the transient response.

The green dot markers indicate the average friction values obtained considering the rigid rod and they show a clear trend as their values decrease for increasing excitation frequencies, and for frequencies bigger than the frequency of the rod's first mode, they are close to the median and mean (middle of the box) values of the boxes. For lower excitation values, the green dot markers display significant deviations from the mean and median values represented in the boxes, with the largest discrepancies occurring at excitation frequencies $\Omega_e = 3$ and $\Omega_e = 6$, as already shown in Fig. 6.2(a).

Figure 6.4 and Fig. 6.5 show the velocity responses of the mass (blue line) and of the rod (red line), for $\Omega_e = 3$ and $\Omega_e = 6$, respectively. The velocity responses are obtained at the moving contact point and allow us to explain the large deviations observed at these excitation frequencies compared to the rigid rod scenario. The amplitude of the velocity response of the rod in Fig. 6.5(a) is higher than in Fig. 6.4(a), as in the former, the

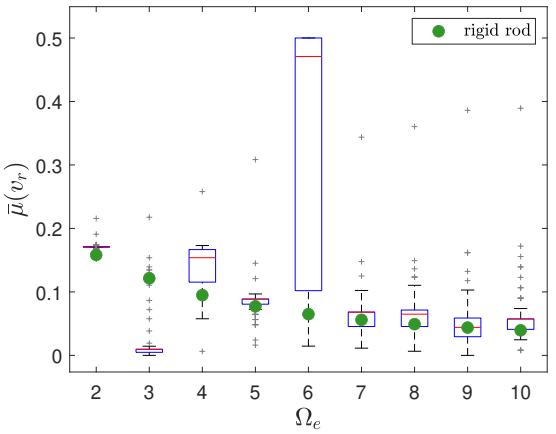

Figure 6.3: Comparison between the statistics of the average friction distributions along the rod length (represented by box plots) and the average friction coefficients for the rigid rod. The assumed pushing velocity is $v = 0.005$.

excitation frequency corresponds to the frequency of the first mode of the rod. Although the velocity responses have a lower amplitude in Fig. 6.4(a), the zoom-in in Fig. 6.4(b) shows the responses to be out of phase with each other. The resulting relative velocity response, v_r, then exhibits a high amplitude, and the friction force reverses direction during each oscillation period. Consequently, this results in low average friction values as shown in Fig. 6.2(a) and Fig. 6.3.

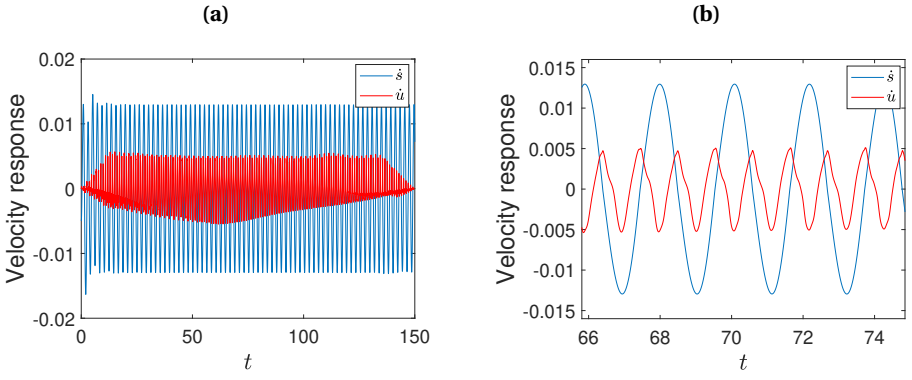

Figure 6.4: (a) Mass and rod velocity response in blue and red lines, respectively; (b) Zoom-in on the response. $\Omega_e = 3$ and $v = 0.005$.

Figure 6.5(b), however, shows the responses to be in phase. The resulting relative velocity has low amplitudes, preventing the friction force from changing direction during certain oscillation cycles. Without a change in direction, the friction force remains

constant. This explains why in Fig. 6.2(a), the average friction tends to the originally imposed friction coefficient $\mu_s = 0.5$. Figure 6.6(a) illustrates this statement, visualizing the relative velocity obtained for $\Omega_e = 6$. Indeed, the amplitudes of the relative velocity response are low and for the time window from ~ 25 - 110, the values are mostly positive, meaning the friction force does not change sign. Figure 6.6(b), provides a zoom-in where the minimum velocity response value approaches zero, resulting in stick-slip behaviour.

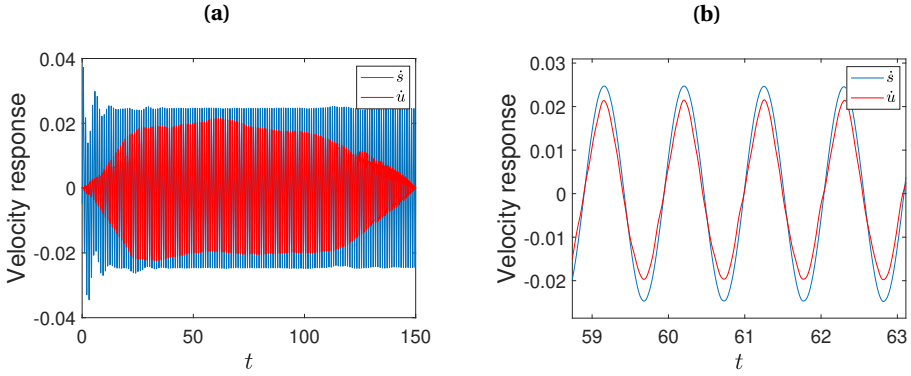

Figure 6.5: (a) Mass and rod velocity response in blue and red lines, respectively; (b) Zoom-in on the response. $\Omega_e = 6$ and $v = 0.005$.

Thus, exciting the mass at an excitation frequency corresponding to the first mode of the rod results in stick-slip behaviour at parts along the rod length, and in a negligible change of the average friction value. Note that for the rigid rod case, stick-slip is not observed. In previous studies [24, 37], the average operation was performed when considering continuous sliding as they were focused on analyzing friction modulation during sliding only. In this case, however, for $\Omega_e = 6$, the averaging process is performed numerically, and it is important to note that this is done over a stick-slip region.

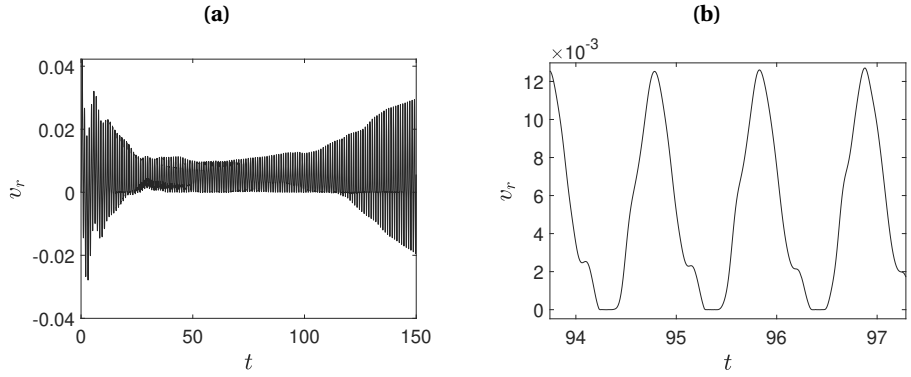

Figure 6.6: (a) Relative velocity response for $\Omega_e = 6$ and $v = 0.005$; (b) Zoom-in on the relative velocity response indicating stick-slip behaviour.

It is worth noting that higher harmonics are present in the rod's velocity response, as shown in Fig. 6.4 and Fig. 6.5, which arise from the moving nature of the load rather than from the nonlinear contact. It can be verified that in addition to these higher harmonics, which correspond to oscillations at the rod's natural frequencies, the influence of the higher harmonics due to the external excitation is also present (when these do not coincide with the rod's natural frequencies), albeit with a small effect. The presence of all higher harmonics also explains the large variations in the average friction values along x_c, for each excitation frequency, as indicated in Fig. 6.2. These average friction values are computed by averaging over the oscillation period, $2\pi/\Omega_e$. However, due to the presence of many harmonics, whose relevance varies depending on the x_c positions, the relative velocity response used to calculate the average friction exhibits quasi-periodic behaviour, causing significant variations in the average friction values when averaged over $2\pi/\Omega_e$. While in this study, the averaging is always performed over the period corresponding to the excitation frequency, as discussed in a previous study [24], when multiple oscillation periods are present in the relative response, the choice of the period is important as it affects the resulting average friction values and their variability.

Before concluding this part, it should be highlighted that the structural response and the resulting average friction depend on the chosen boundary conditions. In this study, fixed-fixed supports were selected to ensure that axial deformation and consequently the rod's velocity contribution to the relative velocity v_r approach zero at the supports. As a result, the average friction values for the flexible rod converge to the rigid-rod solution at $x = 0$ and $x = 1$. Alternative boundary conditions would significantly shift these nodes, resulting in friction modulation even at the rod's boundaries. In a fixed-free (cantilever) scenario, for example, the rod's response in terms of both displacement and velocity reaches its global maximum at the free end (at different times), provided the first vibration mode dominates the response. This would fundamentally alter the relative velocity v_r and, eventually, the friction modulation. Depending on whether the mass and the rod velocities are in-phase or out-of-phase, the friction reduction could be amplified or diminished compared to the fixed-fixed case.

While the figures in this section primarily focus on the response at the contact point x_c, as the objective is to characterize friction modulation at that interface, Appendix C.2 provides a broader visualization of the rod's response along its entire length. These figures illustrate how the deflection shapes deviate from the simple theoretical $\sin(j\pi x)$ mode shapes. Specifically, Appendix C.2 details the rod's vibration for a mass oscillating at its initial position $x_c = 0.25$ with constant velocity $v = 0$, as well as the evolution of the rod's profile as the mass travels across the span at $v = 0.005$ for positions $x_c = 0.25, 0.5$, and 0.75.

6.3.2. Friction modulation versus pushing velocity

This subsection compares the average friction obtained for various pushing velocities v, with reference to the excitation frequencies for which the most significant difference between the flexible and rigid rod case is observed, i.e. $\Omega_e = 3$ and $\Omega_e = 6$. Figure 6.7 depicts the results for $\Omega_e = 3$ for v values ranging from 0.005 to 0.02. As shown in the figure, for low v values (≤ 0.008), the average friction results obtained for the flexible rod are generally smaller than those obtained for the rigid rod, while for bigger v values,

the opposite trend holds. For v values exceeding the amplitude of the relative velocity response (not presented here), the friction force does not change sign and no friction change is observed ($v \geq 0.014$) for both rigid and flexible rod cases. The figure also suggests the existence of a velocity below which the average friction values for the flexible rod are lower than that of the rigid case, while above it, the opposite is true. To better understand the differences in the average friction values between the flexible and rigid rod cases and to investigate the presence of such transition at a specific velocity, Fig. 6.8(a) presents the maximum amplitude of the rod velocity at the contact point for each v value. The choice of the rod velocity is based on the fact that the largest difference in relative velocities between the flexible and rigid rods arises from its contribution.

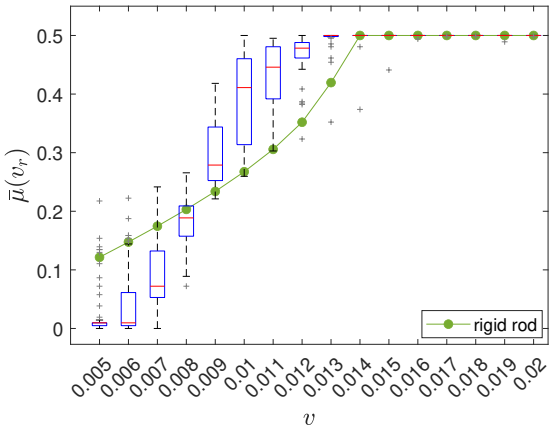

Figure 6.7: Comparison of average friction results for different velocity v values obtained for the flexible and rigid rod case for $\Omega_e = 3$.

Figure 6.8(a) shows that the maximum amplitude of the rod's velocity response is observed at $v = 0.008$, which corresponds to the velocity for which the trend in the average friction values in Fig. 6.7 shifts. This value at which the maximum rod velocity occurs is defined as the "critical" velocity and marks the point where the average friction values obtained for the flexible and rigid rod systems are closest to each other. It is worth highlighting that the average friction values being close does not imply that the responses are identical (in fact, they are not, as the rod response is at its maximum while the belt is rigid). It simply means that the change in sign of the relative velocities is similar, resulting in average friction values that are close to each other. For pushing velocities below the critical one, the system with the flexible rod exhibits lower average friction, whereas, for pushing velocities above it, the same system displays higher average friction values (until the velocity for which no friction modulation is observed for both flexible and rigid rod cases). Therefore, identifying the critical velocity offers direct qualitative insight into how the average friction differs between the system with a rigid rod (assuming its average friction is known) and the one with a flexible rod, without the need to explicitly compute the average friction for the latter. Moreover, to explain the increase in average friction

values with increasing velocity v and to find the pushing velocity beyond which no friction change is observed, Fig. 6.8(b) illustrates the minimum relative velocity response value for each v. The $v_{r,\min}$ values decrease, reaching almost zero at $v = 0.014$, meaning that beyond this pushing velocity, the relative velocity values are strictly positive, resulting in a friction force that does not change sign. Consequently, no friction modulation occurs, consistent with the behaviour portrayed in Fig. 6.7.

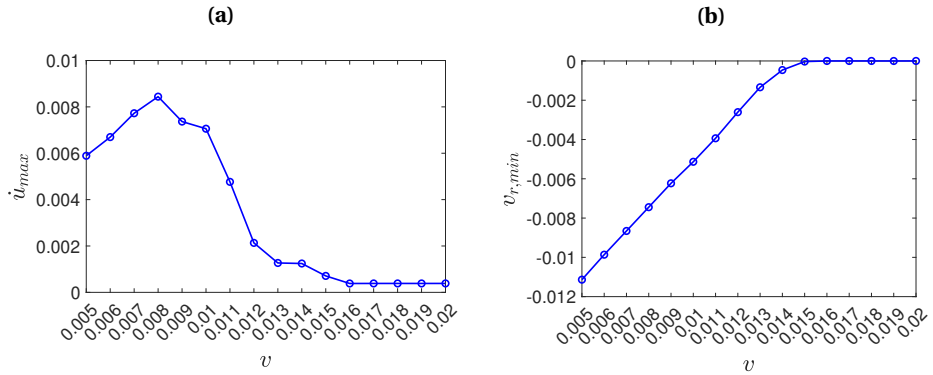

Figure 6.8: (a) The maximum amplitude of the rod's velocity response at the contact point for different velocity v values and for $\Omega_e = 3$; (b) The minimum amplitude of the relative velocity response for the same parameter values.

Figure 6.9 depicts the results for $\Omega_e = 6$ corresponding to the rod's first mode frequency. At low v values, the boxplots show a noticeable difference between the mean (middle of the box) and the median as well as a higher spread in the variability of the values. This variability in distribution decreases as v values increase. For all v values, other than the ones for which no friction change is observed, the average friction results for the flexible rod (except for extremes and outliers) are higher than those for the rigid rod case. Thus, independent of the v value, exciting the mass at an excitation frequency corresponding to the rod's first mode results in less friction reduction. In Fig. 6.9(b), a plot of $\dot{u}_{\max}$ versus v values is presented for this excitation frequency. Unlike Fig. 6.8(a), no distinct critical velocity is observed within this velocity range, as the $\dot{u}_{\max}$ values continuously decrease. This behaviour is similar to the portion of Fig. 6.8(a) where the velocities are greater than 0.008; there, $\dot{u}_{\max}$ also decreases. In Fig. 6.7, this region is associated with average friction values higher than those of the rigid rod, a pattern consistent with the behaviour shown in Fig. 6.9(a). Therefore, even for this excitation frequency, the plot of $\dot{u}_{\max}$ provides qualitative insights into the differences in average friction values between the systems with flexible and rigid rods. Notably, it can be verified that the critical velocity defined and calculated in this section is much smaller than the conventional critical velocity corresponding to the resonance of the rod as induced by a moving oscillatory load of frequency Ω_e (see [39]).

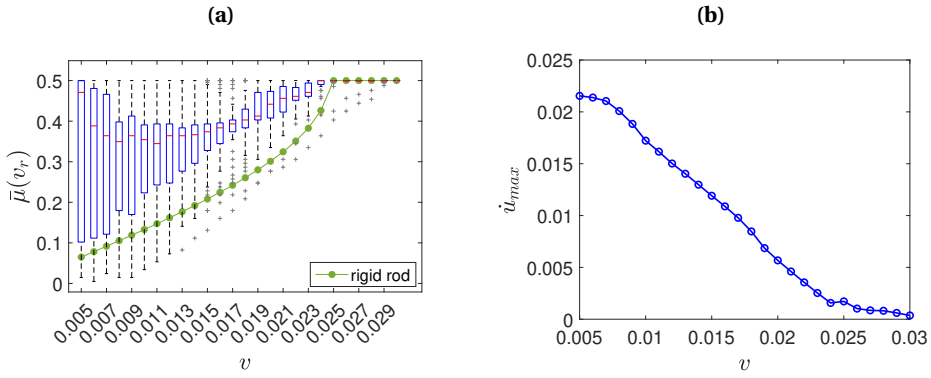

Figure 6.9: (a) Comparison of average friction results for different velocity v values obtained for the flexible and rigid rod case for $\Omega_e = 6$; (b) Maximum amplitude of the rod's velocity response at the contact point.

6.4. HARMONIC LOAD ACTING ON THE ROD

This section examines the case of the external harmonic load acting on the rod at location $x = s_0$, Fig. 6.1(b). Following the methodology and steps outlined in the preceding section, the equations of motion are solved numerically, and the friction modulation is evaluated for different excitation frequencies Ω_e and velocities v. All results are compared to those obtained from a mass-spring-dashpot system on a rigid rod, with the load acting on the mass.

6.4.1. FRICTION MODULATION ALONG THE ROD LENGTH

Using the equations of motion, Eq. (6.12) and Eq. (6.13), with the external harmonic loading applied on the rod, first, the average friction values along the rod length are obtained for different excitation frequencies, employing the x_c expression in Eq. (6.3). The results are depicted in Fig. 6.10(a) where, like in Fig. 6.2, the continuous lines represent the results of the flexible rod and the dot markers correspond to those of the rigid rod. Again, similarly to Fig. 6.2, Fig. 6.10(a) shows large variations in the average friction values along x_c, for each excitation frequency (other than the ones for which no change in the frictional behaviour is observed, such as for $\Omega_e = 2$ and $\Omega_e = 3$). For this case as well, with the load acting on the rod, due to the moving load, the beam velocity response exhibits oscillations not only at the excitation frequency but also at additional frequencies, leading to a quasi-periodic response, causing significant variations in the average friction values when averaged over $2\pi/\Omega_e$. The plots in Fig. 6.10(a)indicate that for $\Omega_e = 2$ and $\Omega_e = 3$ (shown with a dashed line for distinction), no friction change is observed. For $\Omega_e = 4$, the average friction values vary along the rod length, and no change is observed after $x_c \approx 0.7$. To explain the unchanged friction values after $x_c \approx 0.7$, in Fig. 6.10(b), the relative velocity for $\Omega_e = 4$ is plotted as a function of time. As illustrated in the figure, the relative velocity is at its highest near the location of the applied load and decreases towards the fixed end on the right, eventually reaching zero. As the relative velocity decreases, it becomes strictly positive, indicating the absence of sign changes and, consequently, no friction

modulation. For $\Omega_e = 2$ and $\Omega_e = 3$, the relative velocity values remain strictly positive at all times, explaining the absence of friction modulation at any point x_c, Fig. 6.10(a).

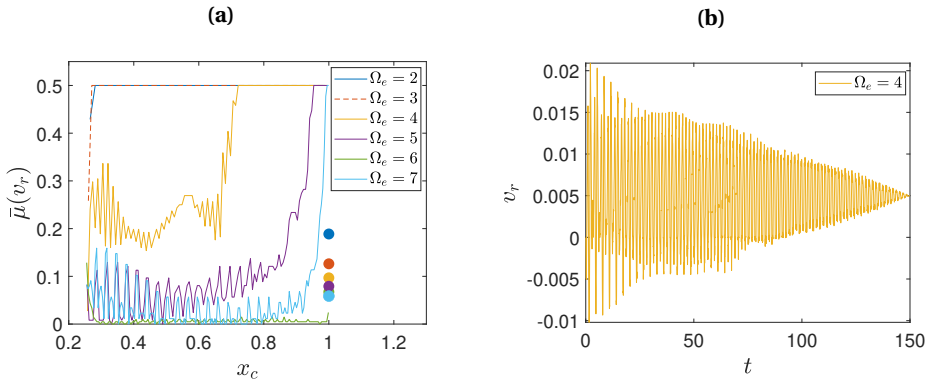

Figure 6.10: (a) Average friction results along the rod length for different Ω_e values and $\nu = 0.005$. Continuous lines represent the results of the flexible rod and the dot markers those of the rigid rod. Dot marker colours match the lines for the same excitation frequency; (b) Relative velocity response for $\Omega_e = 4$.

When compared to the rigid rod case (load acting on the mass which oscillates on a rigid rod), the dot markers indicate lower average friction values for the rigid rod for all three Ω_e values (2, 3, and 4). Although the load in the rigid rod case is applied directly to the mass, while this section examines the scenario where the load is applied to the flexible rod, these cases are compared not only to highlight their differences but also because the rigid rod with the load on the mass serves as a benchmark for evaluating the effects of load application on the mass versus on the rod in flexible rod systems. For instance, as shown in Fig. 6.2(a), for $\Omega_e = 4$, when the load is applied to the mass in the flexible rod case, the average friction values are closer to those in the rigid rod case (with the load on the mass) and are even smaller along parts of the rod's length. In contrast, when the load is applied on the rod in the flexible rod case, Fig. 6.10(a), for $\Omega_e = 4$, the average friction values are consistently higher than those in the rigid rod case (with the load on the mass). Thus, applying the load directly to the mass can result in greater friction modulation than applying it to the rod. The friction reduction increases as Ω_e increases to 5, 6 and 7, with the highest reduction for $\Omega_e = 6$, corresponding to the natural frequency of the rod's first mode, as shown in Fig. 6.10(a). For the latter case, the friction reduction associated with the flexible rod (green line) is greater than that of the rigid rod (green dot) and also greater than that of the load-on-mass case, where almost no friction reduction was observed (see subsection 6.3.1). As already explained, for the load-on-mass case and for an excitation frequency of $\Omega_e = 6$, the rod velocity response is high and comparable to the mass response, but the two responses are in phase. This results in a low-magnitude relative velocity, predominantly positive, causing no change in the friction force's sign and, consequently, no friction modulation. In contrast, for the load-on-rod case described here, the rod's response is high while the mass response is minimal. As a result, the relative velocity is dominated by the rod's motion, leading to a

change in the friction force's sign and a reduction in the average friction. For $\Omega_e = 5$ and $\Omega_e = 7$, the comparison varies depending on the position along the rod length.

It should be noted that for Ω_e values of 5, 6 and 7, the responses of the rod are high and do not comply with the small deformation theory. To accurately describe the system dynamics, geometric nonlinearity should be accounted for (see Appendix C.1). However, as large deformations are not desirable, another approach is to vary the excitation amplitude value, α, to identify the maximum α value that ensures the response complies with the small deformation theory. To achieve this, the results from Eq. (6.12) and Eq. (6.13) using x_c as in Eq. (6.3) are compared to those from Eq. (C.4) and Eq. (C.5) with x_c as in Eq. (6.4). Figure 6.11(a) presents the average friction values corresponding to α values for which the results obtained from the equations of motions with and without geometric nonlinearity agree. As shown in the figure, for the results to agree, the α value is reduced from 0.004, used so far in this study, to 0.0015, 0.00004 and 0.001 for Ω_e values of 5, 6 and 7, respectively. For $\Omega_e = 5$ and $\Omega_e = 7$, the average friction changes along the beam length. The average friction values are smaller for the higher excitation frequency, but still bigger than those corresponding to the same Ω_e value in Fig. 6.10(a), as in the latter a greater α value is used. The reduction in α is most prominent for $\Omega_e = 6$, as this excitation frequency results in the highest rod displacement response. While the α reduction leads to small deformations, it also results in a relative velocity response with oscillation cycles having amplitudes smaller than the velocity v. Consequently, no friction change is present in sections along the rod length for $\Omega_e = 6$.

To provide an indication of the displacement values, Fig. 6.11(b) presents the maximum values of the displacement response across a range of velocities v for $\Omega_e = 6$ and the reduced $\alpha = 0.00004$. Within this velocity range, the peak displacement value is approximately 0.0022, corresponding to 0.22% of the rod's length L. This shows that as the excitation amplitude value is decreased, the strain value remains small and does not lead to failure phenomena. For comparison, in the next subsection, the scenario of maintaining the original α value while accounting for geometric nonlinearity is presented, along with the corresponding maximum deformation values.

To sum up, when the load is acting on the rod, the velocity response of the rod is higher than that of the mass and it increases as the excitation frequency increases, significantly contributing to friction reduction. This response changes along the rod length and exhibits oscillations at different frequencies leading to large variations in average friction values and in no variations towards the end of the rod. High responses also imply a potential deviation from the small deformations theory. To address this, either geometric nonlinearity should be incorporated into the model, or the amplitude of the harmonic load needs to be adjusted. A reduction of the α value implies less friction reduction. When the excitation frequency matches the natural frequency of the rod's first mode under reduced α, this results in no friction reduction occurring in some sections along the length of the rod.

6.4.2. FRICTION MODULATION VERSUS PUSHING VELOCITY

The average friction values for a range of velocities v are presented and compared for both the flexible and rigid rod cases. In subsection 6.3.1, the comparison was made for excitation frequencies $\Omega_e = 3$ and $\Omega_e = 6$ for which the most significant differences

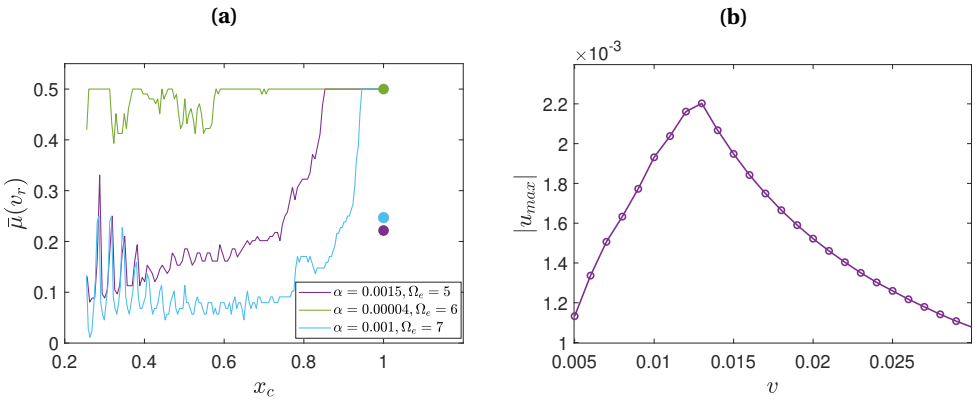

Figure 6.11: (a) Average friction results along the rod length using α values for which the results from the equations of motion with and without geometric nonlinearity agree; (b) Maximum amplitude of the rod's displacement response for $\Omega_e = 6$ and $\alpha = 0.00004$.

between the flexible and rigid rod cases were observed. Looking at Fig. 6.10(a), for $\Omega_e = 2$ and $\Omega_e = 3$, no friction change is observed for $v = 0.005$ and that holds for higher velocities as well since friction reduction lessens with increasing v. Therefore, no average friction plots are shown for these excitation frequencies. In Fig. 6.12(a), results for $\Omega_e = 4$ are illustrated. As shown in the figure, the average friction values for the system with the flexible rod, except for some extremes, are higher than those for the rigid rod system for any velocity v value. For the rigid rod, no change in friction is observed for $v \geq 0.018$, whereas for the flexible rod, this behaviour occurs at a lower $v = 0.014$. The latter observation can be explained by revisiting the relative velocity response shown in Fig.6.10(b) for $v = 0.005$. As previously mentioned, the relative velocity decreases and becomes strictly positive as the mass approaches the fixed end of the rod, indicating no friction sign change and no friction modulation towards the rod's end. Increasing the velocity incrementally to $v = 0.006, 0.007, ...$, up to $v = 0.02$, as shown in Fig.6.12(a), reduces the time required for the mass to reach the rod's end. For example, while the rod's end is reached at $t = 150$ for $v = 0.005$, it is reached at $t = 75$ for $v = 0.01$. With this shorter time frame and higher v values, the relative velocity response becomes strictly positive more rapidly, occurring at $x_c \approx 0.5$ instead of approximately 0.7 (observed for $v = 0.005$). Therefore, as the velocity v increases, no friction change is observed from lower x_c values.

In Fig.6.12(b), the same plot is illustrated for the load-on-mass case, as studied in Section 6.3, with the boxplots showing again the results for the flexible rod system and the green markers the results for the rigid one (the latter being the same in Fig.6.12(a) and Fig.6.12(b)). As shown in the figure, the results align more closely with those of the rigid rod case as the mass governs the response, and the rod's contribution is minimal. Consequently, for this excitation frequency, applying the load directly to the mass yields average friction values similar to the rigid rod. In contrast, applying the load to the rod results in less reduction in friction, which diminishes rapidly as the velocity v increases.

Using the same parameters and higher excitation frequencies, for the deformations

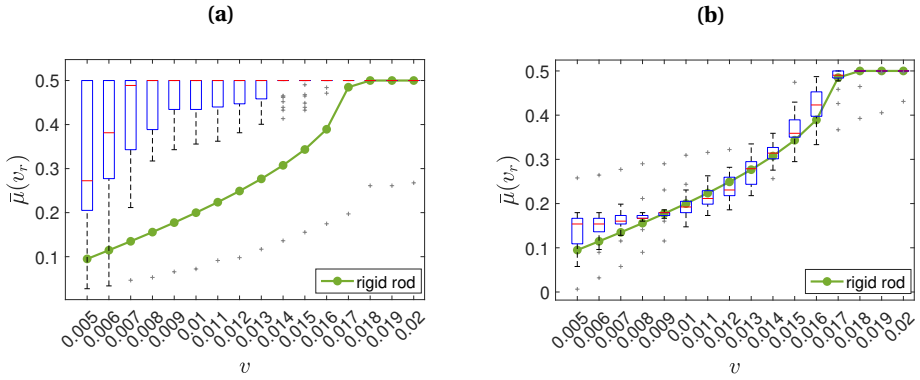

Figure 6.12: Comparison of average friction results for different velocity v values obtained for the flexible and rigid rod case for $\Omega_e = 4$: (a) load acting on the rod; (b) load acting on the mass.

to remain small, either the amplitude of the excitation α should get reduced, as shown in Fig. 6.11(a), or nonlinearity should be considered in the equations of motion. Using a smaller α, the reduction in friction for $\Omega_e = 6$ is not that significant (see Fig. 6.11(a)). Therefore, as shown in Fig. 6.13(a), the average friction is illustrated for the original value of $\alpha = 0.004$, $\Omega_e = 6$ and including the geometric nonlinearity in the rod. Since the excitation frequency matches the first mode of the rod, the velocity response amplitude of the rod becomes significantly higher ($\dot{u}_{\max} \approx 1$) compared to the constant velocity v. This leads to substantial friction reduction, as illustrated in Fig. 6.13(a). In contrast, for the rigid rod case, the average friction values are higher and no friction reduction is observed when $v \geq 0.025$. For the flexible rod, the average friction values remain low (due to the velocity amplitude of the rod being very large) with only small variations along each other for all the v values considered. Only for $v > \dot{u}_{\max}$, no changes in friction will be observed for this case. To provide an indication of the displacement values, Fig. 6.13(b) presents the maximum values of the displacement response for the same range of velocities v as in Fig. 6.13(a). Within this velocity range, the peak displacement value is approximately 0.21, which is around 100 times larger than the one in Fig. 6.11(b) for the same excitation frequency but smaller amplitude α. This displacement is 21% L, and depending on factors such as material type, geometric properties (e.g., cross-sectional shape and size), loading conditions (e.g., magnitude, direction, and duration), boundary conditions and more, it can lead to failure phenomena such as buckling, permanent plastic deformation and crushing or fracture.

Overall, using an excitation frequency corresponding to the first mode results in greater friction reduction compared to the rigid case for any velocity v, but this comes with large deformations experienced by the flexible rod, where the material type and its properties play a crucial role.

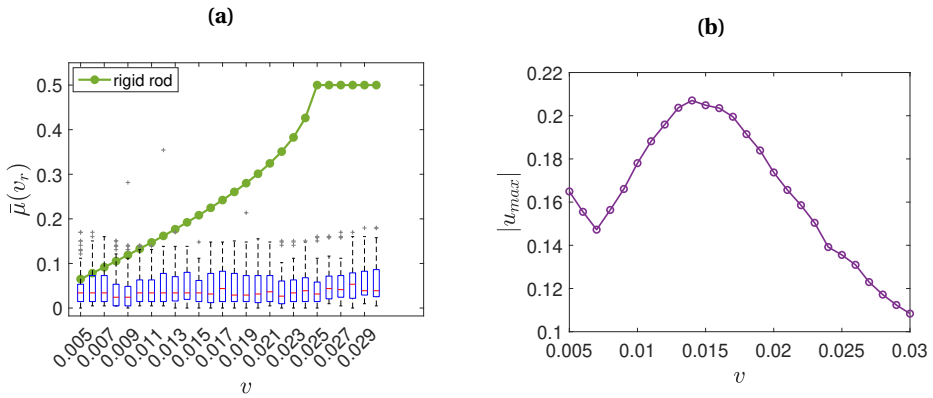

Figure 6.13: (a) Comparison of average friction results for different velocity v values obtained for the flexible rod with geometrical nonlinearity and rigid rod with the load acting on the mass; (b) Maximum amplitude of the rod's displacement response. Results obtained for $\Omega_e = 6$ and $\alpha = 0.004$.

6.5. CONNECTION TO REAL-LIFE SCENARIOS

In this section, connections are drawn to slip joints in offshore wind turbines and related experimental studies to contextualise the model system within the scope of applications and real-life scenarios.

6.5.1. DISCUSSION ON THE SLIP JOINT APPLICATION

In the first study of Cabboi and coworkers on the slip joint application [32], the effectiveness of applying a harmonic excitation during the installation and decommissioning procedure was experimentally investigated using a 1:10 scaled model of the slip joint. In essence, a slip joint for wind turbines enables the connection between the monopile and the transition piece by simply overlapping the two cylindrical structures. The entire connection relies on the frictional forces between the two surfaces in contact. In their study, two cones, one representing the monopile (MP) and one the transition piece (TP), were used for the designed test setup. The TP was excited in either horizontal or vertical direction utilizing a shaker, whereas the static pushing load was applied at the top cone representing the MP. Both cones were made of the same steel type (S355), and had the same total length, mass and wall thickness. The TP cone had a top and bottom outer diameter of 0.01 m thicker than the MP cone. Due to its larger diameter, the TP cone was stiffer.

The results of the tests performed during the experimental campaign showed that settlement occurred when applying a harmonic load at specific forcing frequencies (results hold for both loading directions). To provide some insights concerning which structural modes should be excited to effectively obtain a stable settlement, hammer tests on the testing specimens and experimental modal analysis were performed. One of the identified natural frequencies, specifically at 120 Hz (whenever excited by means of the shakers), was effective in reducing the friction force for both the installation and

dismounting of the cones, regardless of the different amplitudes of the vibratory load. However, settlements were observed for other frequencies as well, and in general, most of the settlement frequencies corresponded well with the identified natural frequencies.

Compared to our system, for the parameters considered, it can be verified that the rod has higher stiffness than the mass ($k_r = EA/L > k$), allowing the rod to serve as a simplified representation of the TP. Similarly, the mass represents the MP for the considered test setup. While this setup simplifies the dynamics of the slip joint, it provides a foundational framework for analysis. As the excitation is applied on the TP, the corresponding case in our study is that of the load applied on the rod, as shown in Section 6.4. One of the conclusions of this section was that loading the rod with an excitation frequency corresponding to the rod's first mode leads to the highest friction reduction. The conclusion is similar to that drawn from the slip joint study as exciting the TP at resonance frequencies was the most effective way to install and decommission the connection.

In a follow-up study [3], the vibration-assisted decommissioning of the slip joint was applied to a full-scale wind turbine, where the lower tower of the wind turbine (WT) was directly connected to the monopile (MP) without the use of a transition piece. The wall thickness of the steel plates forming the monopile and the wind turbine tower decreased with increasing height, from 65 mm to 10 mm, making the MP the stiffer component. The shaker devices were mounted at the base of the wind turbine tower, so the vibratory load was applied to the WT. The decommissioning tests showed that the slip joint detachment was triggered once the circumferential local mode at 53 Hz was excited. An experimental modal analysis was conducted to identify the modes of the structure, and the results were compared to modal properties extracted from a developed FE model. This analysis showed that the mode at 53 Hz only referred to the dynamic of the wind turbine tower, while the monopile foundation almost acted as a rigid body. Thus, the excitation of this mode in combination with a vertical pulling force facilitated the detachment between the two contacting surfaces.

Following the same line of reasoning as described above, compared to our system, the rod has higher stiffness, making it representative of the MP, and the mass representative of the WT, as the excitation is applied on the WT. The corresponding case in our study is of the load applied on the mass, see Section 6.3. This section concluded that exciting the mass at an excitation frequency corresponding to the rod's first mode results in less friction reduction. Thus, to reduce friction forces (i.e. to facilitate decommissioning), it is more effective to excite the mass at frequencies which do not correspond to the rod's first mode. In these cases, the rod response is generally small. This is in line with the result drawn by the study on the slip joint, as the decommissioning was effective at a frequency at which the monopile foundation, represented by the rod in our system, acted almost as a rigid body.

It should be noted that while our study and the slip joint application share conceptual similarities, the agreement between their results is purely qualitative. The slip joint primarily involves bending and circumferential shell modes, making an axially deforming rod not the most representative structure for comparison. Additionally, the dynamic loading in the slip joint study involves a stepwise or linear frequency increase, contrasting with the loading type used in our work. Differences in stiffness, damping ratios, and other parameters also show the distinct nature of the two systems, yet the qualitative

agreements remain, highlighting the broader applicability of the findings.

6.5.2. Discussion on pin-on-disk experimental results

Lastly, a connection is drawn between the findings obtained in this study and related experimental works. In several experimental investigations conducted on the effect of vibration-induced friction reduction, the measurements did not match the model predictions obtained assuming the Amontons-Coulomb law to model the friction force. Different friction models were used to better catch the experimental behaviour, for example, the Dahl and the Dupont models [30] that embed a tangential contact stiffness. In this regard, Kapelke employed the Dupont model and the Amontons-Coulomb law to compare the experimental results to theoretical ones [31]. A pin-on-disk type experimental setup was developed, exhibiting a dominant eigenmode at approximately 100 Hz (corresponding to the motion of the dynamometer in the tangential direction). For moderate excitation frequencies (40 Hz), the experimental results showed an excellent match to the elasto-plastic Dupont model, for which the contact stiffness $k_0 = 5.6 \times 10^5$ N/m was chosen. However, when high-excitation frequencies were used (350 Hz), to catch the behaviour of the friction force accurately, a significantly different value of tangential stiffness was needed for the Dupont model, i.e., $k_0 = 12 \times 10^5$ N/m.

Since this model incorporates a tangential contact stiffness, and our system considers deformations in the tangential direction, a comparison can be made between the results obtained from both systems. As shown in Kapelke's work [31], the elasto-plastic friction model yields higher effective friction values than the Amontons-Coulomb law. The shape of the plots and the results are qualitatively similar to those shown in Fig. 6.7 (for $v > 0.008$) and in Fig. 6.9(a) (for any v), as these results are also higher than those obtained using the Amontons-Coulomb law. The comparison is made with these plots because they correspond to the scenario in which the harmonic load is applied to the mass, aligning with the experimental loading condition. It is important to note that a direct one-to-one comparison between the results from our mass-on-a-rod system and the system with the Dahl/Dupont models cannot be made, as additional information is needed regarding the relationship between the excitation frequency and the system modes, as well as consistent amplitude and velocity values. However, despite these limitations, our system demonstrates that using a rod with the Amontons-Coulomb law provides friction change results that qualitatively resemble those obtained from the Dahl/Dupont models.

An attempt to explain the need for a change in the contact stiffness value k_0, as the excitation frequency increases, is made by calculating a "dynamic stiffness" (as perceived by the moving contact force throughout the transient process) of the rod in our system, K_ω. To compute K_ω, for a given excitation frequency, the force acting on the rod and the displacement at the contact point are transformed to the frequency domain. Due to the quasi-periodic nature of the system response, K_ω, which is the ratio of force to displacement amplitudes, also exhibits multiple frequency components. The K_ω value is then chosen based on the component that matches the given excitation frequency. The same procedure is repeated for other excitation frequencies, and the results are illustrated in Fig. 6.14. As shown in the figure, K_ω is at its lowest at the rod's modal frequencies and higher between them. Moreover, the peaks in the plot of K_ω increase with increasing frequency. This behaviour could explain why higher contact stiffness values are needed

at higher excitation frequencies in the work of Kapelke and colleagues, assuming that the excitation frequency used in their study lies between the disk modes.

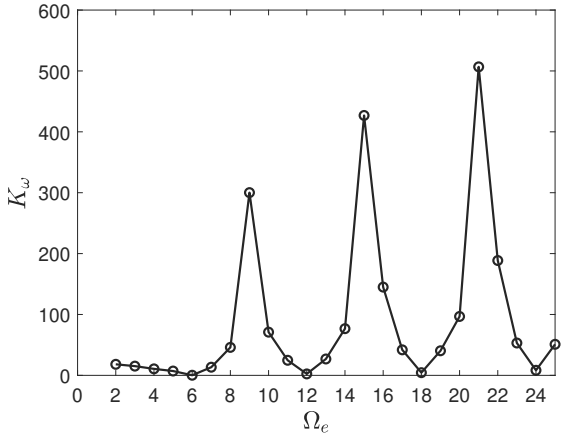

Figure 6.14: "Dynamic stiffness" of the rod.

6.6. CONCLUSIONS

In this work, the effect of external excitation in the presence of support flexibility on the friction modulation of a moving oscillator on an elastic rod of finite length is investigated. Two loading scenarios are analysed. In the first, a harmonic tangential load is applied on the moving mass, while in the second, the same load is applied on the rod. The modal expansion method is employed to derive the modal equations of the rod, which are then used to obtain the numerical solutions for the system's response.

In the case where the load acts on the mass, it is observed that, unlike the rigid rod scenario where the average friction is a constant value, the deformation of the rod introduces variations in average friction values along its length. Depending on the position along the rod length, these values are smaller or bigger than the ones obtained for the rigid rod system. Deviations are observed across excitation frequencies, with the most prominent ones occurring at half the rod's first mode frequency and at the first mode frequency itself. For the latter case, unlike the rigid rod scenario, no friction modulation and stick-slip behaviour is observed along parts of the rod. For both cases, it is also found that the critical velocity, i.e. the velocity for which maximum rod velocity response is observed, provides direct qualitative insight into the differences in average friction between the rigid and flexible rod cases without explicitly computing the average friction values for the latter scenario. For pushing velocities smaller than the critical velocity, the average friction values for the flexible rod are lower than those of the rigid case, while above it, the opposite is true.

Even when the load acts on the rod, variations in average friction values along the rod length are observed, but they differ from the results from the load-on-mass scenario.

For excitation frequencies close to and above the rod's first natural frequency, the rod's response increases and does not comply with the small deformation theory. To address this, either the amplitude of the excitation value α is reduced, or, if large deformations are permitted, geometric nonlinearity is incorporated into the model. A lower α value leads to less friction reduction for all excitation frequencies and to no friction reduction along parts of the rod for the excitation frequency equal to the rods' first natural frequency. For the same excitation frequency, introducing geometric nonlinearity results in very high friction reduction compared to the rigid case for any velocity v. Again, this comes with large deformations experienced by the flexible rod.

The presence of support flexibility allows for comparisons with real-life applications as well. Regarding the slip joint application, the system's behaviour is used to represent a simplified version of the dynamics of the tower and the monopile. The findings from our study regarding the choice of excitation frequencies for which the highest friction reduction is obtained in the load-on-mass and load-on-rod scenarios support the results of the experiments on the full scale and on the 1:10 scaled model of the slip joint, respectively. Regarding experimental studies, the average friction results from our study are used to provide an alternative interpretation of the results of published works using the Dahl and Dupont models. Using these models, higher average friction values than those predicted by Amontons-Coulomb law are observed. Similarly, in our study, according to a comparable loading scenario, higher average friction values are also observed (depending on the excitation frequency and pushing velocities). Thus, modelling the system with a flexible rod yields friction change results that qualitatively align with those from the Dahl and Dupont models and related experimental studies, even though the Amontons-Coulomb law is used.

7

CONCLUSIONS AND RECOMMENDATIONS

There is a mysterious charm in
things not quite finished.

Unknown

In this final chapter, this dissertation's conclusions are summarised and practical guidelines and recommendations for future research are outlined. The first section begins with general conclusions that synthesise the main findings from each chapter, providing an overarching perspective on the work as a whole. This is followed by more detailed findings highlighting the individual chapters' specific contributions, insights, and implications. Together, these reflections highlight how the research objectives have been met and suggest potential paths for extending the study in terms of theoretical advancement and potential applications.

7.1. CONCLUSIONS

This dissertation investigated the effect of external excitation on friction modulation by adopting a modelling strategy that increases system complexity without resorting to overly complex friction laws. This objective is achieved by examining the problem from multiple perspectives, focusing on both the properties of the applied excitation and the effect of system dynamics on average friction while also considering the relevance of these effects in practical scenarios. More specifically, this work investigated how different excitation properties (phase, location, frequency) affect friction change. Additionally, the effect of incorporating system dynamic effects, including system stiffness (e.g., directional stiffnesses in discrete models) and flexibility (deformability in continuous models), on average friction was analysed. Furthermore, the friction-vibration interaction in terms of instability and its subsequent influence on friction modulation was explored. Finally, the results were interpreted in the context of real-life scenarios.

In this chapter, the conclusions are presented. First, the main high-level conclusions are given: 1.1-1.2 correspond to the highlights from Chapter 3, 2.1-2.2 to Chapter 4, 3.1-3.2

to Chapter 5 and 4.1-4.2 to Chapter 6. These highlights are followed by more detailed conclusions.

1.1 Friction modulation by external excitation depends on both the excitation properties and system dynamics. Increasing the excitation frequency leads to more friction reduction, but this trend does not hold near and at resonance. Viscous and friction damping play a key role in shaping the system's behaviour and eventually friction modulation in this region.

1.2 Friction modulation under the presence of more than one external load depends on the interaction between the load phases. An additional load does not necessarily lead to more friction reduction, and its effect is determined by how the load properties affect the system's dynamic response.

2.1 The presence of transverse stiffness and oscillation significantly affects friction modulation, especially near resonance (in the transverse direction). Under certain combinations of stiffness and excitation parameters, the averaged friction curve exhibits a shape that qualitatively resembles that typically associated with dynamic friction models, even though the classical Amonton–Coulomb law is employed. This observation suggests that such behaviour can arise from the system dynamics rather than from the specific choice of friction law.

2.2 Increasing the system complexity by accounting for transverse stiffness may lead to instability phenomena, and attention should be paid to their possible occurrence.

3.1 The presence of external excitation and normal tangential coupling through friction in a 2-DOF system induces parametric excitation and leads to self-excited oscillations driven by the negative damping mechanism, even under Amontons-Coulomb law.

3.2 When friction-induced oscillations occur, the presence of multiple frequency components causes scattered average friction values.

4.1 The presence of support flexibility (accounting for vibrational modes in one of the structures in contact), rather than rigid support, influences friction modulation by causing special variation in average friction values. Different results are observed when the load is applied to the moving mass versus the flexible support, with large deviation from the rigid case occurring for excitation frequencies near modal frequencies.

4.2 Considering one of the structures in contact as flexible allows for qualitative interpretation of slip-joint vibration-assisted decommissioning tests and comparison of average friction values to experimental results in which friction force reduction is explained using elasto-plastic friction models. The theoretical predictions showed good qualitative agreement with experimental outcomes.

From this point onward, detailed conclusions are presented. The initial set of conclusions emphasises the role of excitation, while the latter focuses on the role of the system dynamics. However, these two aspects cannot always be treated independently. The

influence of excitation on friction modulation often depends on the specific properties of the system, and many of the observed phenomena arise from the interplay between excitation and system characteristics. As such, some conclusions reflect this coupled behavior rather than isolating one factor alone.

Excitation, applied at arbitrary frequencies and along different directions, was considered to evaluate its effect on friction change. To this end, the Method of Direct Separation of Motion (MDSM) was extended to quantify the vibration-induced modulation of the friction force in both single- and multi-degree-of-freedom systems. The extension enabled the identification of a threshold, $\Omega_e = 5\omega_n$, which serves to distinguish what is commonly referred to in the literature as "high-frequency" regime for vibration-induced friction modulation. In this high-frequency regime, increasing the excitation frequency leads to more friction reduction (assuming all other parameters remain unchanged). However, increasing the excitation frequencies does not always result in greater friction reduction. Specifically, this trend does not hold near resonance. In the high-frequency regime, the amplitude of the velocity response function increases linearly with the excitation frequency, and since a higher velocity amplitude correlates with greater friction reduction, the relationship is straightforward. However, the behaviour is more nuanced near resonance (damping-dominated region). The amplitude of the velocity response reaches its peak at the resonant excitation frequency and decreases for frequencies slightly above or below it. As a result, an excitation frequency of, for example, $\Omega_e = 1.2\omega_n$ may lead to more friction reduction than a higher frequency such as $\Omega_e = 2\omega_n$. In the vicinity of resonance, however, the damping effect of the friction force becomes more pronounced, which can reduce the amplitude of the velocity response and thus counteract the expected friction reduction. Therefore, both viscous damping and friction damping must be considered when analysing the system's response near resonance.

The presence of an additional load—such as a normal or transverse force—in combination with a tangential load leads to friction reduction values that differ from those observed under tangential loading alone. An additional load, however, does not necessarily lead to more friction reduction. For instance, in the case of combined tangential and normal loading, a 180° phase change in the tangential load (a switch from an initial positive $+X_1$ to an initial negative direction $-X_1$ with respect to the considered reference system) alters the stick-slip boundary, the velocity response function, and eventually the effective friction. Whether the friction reduction is smaller or greater than in the case of tangential loading alone depends on the interplay of factors, including not only the loading phase, but also the excitation frequency, system characteristics (mass, stiffness, damping), the static friction coefficient, and the nature of the normal contact force (compliant or rigid). Specifically, for excitation frequency $\Omega_e = 1$ which is equal to the natural frequency of the undamped system in X_1 direction, the normal-tangential loading case with the 180° phase change results in a higher amplitude of the velocity response function, leading to a slightly larger parameter space for friction decrease compared to tangential loading only or normal-tangential loading with an initial tangential load in $+X_1$ direction.

Furthermore, the nature of the normal contact force (compliant vs. inertial) affects the velocity response functions and, consequently, the average friction. When the normal force is primarily driven by inertial effects (rigid contact), the velocity response functions for the normal-tangential loading with and without a 180° phase shift do not coincide

at higher frequencies. In contrast, when the normal force is governed by damping and stiffness (compliant contact), the response functions closely match. Among all scenarios, the greatest reduction in friction is achieved when the normal force is inertial and there is no phase shift between the normal and tangential loading.

In terms of increasing system complexity, the role of a transverse system in friction modulation was investigated. It was found that for transverse stiffness values (expressed in terms of the ratio of the natural frequencies ω_r) smaller than the excitation frequency and at low belt velocities, average friction values are higher than the reference case with tangential loading only. As transverse stiffness increases, friction reduction becomes more pronounced, reaching a minimum at resonance when ω_r equals the excitation frequency ($\omega_r = \Omega_e$). Thus, the influence of the transverse motion on the average friction is most significant when resonance occurs in the X_2 direction. However, this influence is less pronounced if resonance occurs in the X_1 direction as well. For transverse stiffness values higher than the excitation frequency, the average friction curves approach those of the tangential-only loading case. The average friction curves also exhibit a concave shape under certain parameter values and loading conditions. More specifically, the concave shape is observed when the excitation frequency is near or at resonance (tangential-only loading and strong friction force). For loading in both directions and higher excitation frequencies, the concave shape arises for low transverse stiffness values. In both these cases, Amonton-Coulomb's friction law is used, indicating that the concave shape is not exclusively a result of employing dynamic friction models, as shown in other related studies. These results underscore the importance of properly accounting for system dynamics (including transverse stiffness effects) in analysing vibration-assisted friction modulation.

To enhance the model, the role of normal linear and nonlinear contact properties was also investigated. It was observed that the combination of normal contact properties and external harmonic excitation in a two-degree-of-freedom mass-on-belt system leads to parametric excitation. This parametric excitation, arising from the time-varying normal force and friction coupling, can trigger friction-induced oscillations. The mechanism driving the friction-induced oscillations was identified as negative damping, as negative slopes were observed in parts of the friction force versus relative velocity relationship, even though the Amontons-Coulomb law was assumed. A linearised stability analysis of the steady sliding state, utilising the MDSM to account for the averaged friction expression, was used to predict the onset of friction-induced oscillation. It was found that while the unforced system was stable at the equilibrium point, the forced system can become unstable, highlighting a case where external excitation, rather than stabilising, can destabilise an otherwise stable equilibrium state, particularly due to the oscillating normal force and its coupling with tangential friction.

The Routh-Hurwitz criterion was used to analyse the effect of various system parameters on stability. More specifically, it was found that an increased damping ratio (β_1) in the tangential direction helps reduce the range of belt velocities where friction-induced vibrations occur. Increasing the natural frequency (ω_1) initially decreases the instability region, reaching a minimum near resonance, but as ω_1 increases further, the unstable region expands again. Variations in the damping ratio (β_2^*) and stiffness (ω_2^*) in the normal direction have a limited effect on the unstable region. A higher excitation frequency

(Ω_e) increases the stable region, thereby reducing the occurrence of friction-induced vibrations. Through a brief numerical validation study, it was demonstrated that, for the investigated model configuration, the linearised stability analysis reliably predicted the onset of friction-induced oscillations across a range of parameter variations. While qualitative agreements were consistently observed, the quantitative match depended on the specific parameter values. In particular, good qualitative and quantitative agreements with the stability diagrams were observed for variations in β_1 and ω_1 values. However, when varying β_2 and ω_2, quantitative agreement was limited in certain regions, particularly at low belt velocities and in unstable zones. The presence of friction-induced vibrations significantly impacts friction modulation. When these oscillations are present, the velocity response cycles differ due to multiple oscillation frequencies, leading to scatteredness in the effective friction values for the unstable range of belt velocities. Averaging over the vibration period of the tangential mode, however, yields a more consistent trend in effective friction values, which qualitatively aligns with existing related experimental results and models like Dahl and Dupont.

Apart from discrete systems, to capture additional physical effects, the effect of external excitation on friction modulation was investigated for a moving oscillator in frictional contact with a finite-length elastic rod subjected to distributed damping. Two loading scenarios were examined: a harmonic tangential load applied to the moving mass, and the same load applied to the rod itself. In the scenario where the load was applied to the mass, it was observed that the rod's deformation introduced variations in friction along its length. This contrasts with a rigid rod scenario, where average friction remains constant. Deviations were observed across excitation frequencies, with the most prominent ones occurring at half the rod's first mode frequency (the biggest friction reduction) and at the first mode frequency itself (the least friction reduction). For the latter case, unlike the rigid rod scenario, no friction modulation and stick–slip behaviour is observed along parts of the rod.

For both loading scenarios, a "critical velocity" was identified. This velocity, corresponding to the maximum rod velocity response, offered direct qualitative insight into the differences in average friction between flexible and rigid rod systems without requiring explicit computation of the average friction for the flexible rod. Specifically, for velocities below this critical point, the flexible rod exhibited lower average friction compared to a rigid rod, while above it, the flexible rod showed higher average friction.

When the load was applied directly to the rod, variations in average friction along the rod's length were also observed, though these differed from the load-on-mass scenario. For excitation frequencies near or above the rod's first natural frequency, the rod's response intensified, violating the small deformation assumptions. To address this, either the excitation amplitude needed to be reduced, or geometric nonlinearity had to be incorporated into the model. Reducing the excitation amplitude led to smaller deformations but also less or no friction reduction along parts of the rod length. Conversely, incorporating geometric nonlinearity resulted in substantial friction reduction but also significant deformations that may lead to failure phenomena depending on material and geometric properties.

Parallels were drawn to real-life applications, such as slip joints in offshore wind turbines. The findings regarding optimal excitation frequencies for friction reduction in the

load-on-mass and load-on-rod scenarios supported experimental results from scaled and full-scale slip joint applications. Furthermore, the friction modulation results from this study were used to provide an alternative interpretation for published experimental works that utilised Dahl and Dupont friction models that account for surface deformability. Using these models, in existing studies, higher average friction values than those predicted by Amontons-Coulomb law are observed. Similarly, in our study, according to a comparable loading scenario, higher average friction values are also observed (depending on the excitation frequency and pushing velocities). Thus, modelling the system with a flexible rod yields friction change results that qualitatively align with those from the Dahl and Dupont models and related experimental studies, even though the Amontons-Coulomb law is used.

7.2. PRACTICAL GUIDELINES

Based on the conclusions of this work, the following practical guidelines are provided:

- Exploiting Tangential Resonance: Targeting the tangential natural frequency results in higher friction reduction. However, caution must be exercised in "strong friction" scenarios, where the response decreases due to friction damping, resulting in less pronounced friction modulation compared to "weak friction" cases. (Chapter 3 and Chapter 4)
- Exploiting Transverse Resonance: Targeting the resonance condition where the excitation frequency matches the system's natural frequency in the transverse direction consistently yields the most significant friction reduction across belt velocities. (Chapter 4)
- Exploiting Modal Excitation: In continuous structures like slip joints, exciting a structural mode can be either beneficial or not depending on the load's location. If the vibration is applied to the stiffer part of the system, such as the elastic rod, resonance maximizes relative motion and friction reduction. Conversely, if the vibration is applied to the less stiff component, exciting the structural mode can cause the parts to move in phase, which minimizes relative velocity and leads to stick-slip behaviour. (Chapter 6)
- Awareness of Parametric Instabilities: It is important to recognize that instabilities can occur even under tangential excitation. Due to normal-tangential coupling, tangential motion can trigger normal force oscillations and result in self-excited vibrations and the "scattered" average friction values often observed in experiments. Precise alignment between the excitation force and the sliding plane is necessary to minimize the coupling that triggers these uncontrolled oscillations. (Chapter 5)
- Designing for Predictability via High-Frequency Excitation: In complex structures where resonances are difficult to manage, operating in the high-frequency regime is recommended. In this zone, the system response becomes more predictable because the influence of specific structural resonances and the effects of different damping mechanisms become less significant, allowing for more predictable friction control. (Chapter 3)

7.3. RECOMMENDATIONS FOR FUTURE WORK

Based on the discussions and findings in this work, the following recommendations for future work are made:

(1) Studying the effect of different loading types and conditions: The current work considers sinusoidal harmonic excitation, while in applications like slip joints, for example, different excitation patterns, such as stepwise or frequency-sweeping loads, are applied. Investigating these alternative excitation patterns, along with variations in phase shifts and initial load positions, could provide a deeper understanding of friction modulation under more general and application-oriented excitation scenarios.

(2) Combining system dynamics and complex friction models: This dissertation showed that the classic Amonton-Coulomb law or the dynamic friction models like Dahl and Dupont alone may not fully capture the complex frictional behaviour under external excitation. Future work could aim to create models that include both contact compliance (as in dynamic friction models) and system dynamics. This approach can help in providing generalizable insights into friction modulation across different excitation conditions. Additionally, extending the models to account for wear, surface roughness, and temperature effects could improve the predictive capability and relevance to practical applications.

(3) Developing more realistic structural models: The current study considers a 1-D axial rod, limiting the capture of multi-directional vibrations present in real applications such as slip joints. Since the slip joint involves complex bending and circumferential shell modes, future work should focus on using more sophisticated structural models that can capture these modes. For example, modeling the slip joint components as shell or cylindrical structures instead of simple axial rods would offer a better representation of the physical system and yield more accurate predictions of friction-vibration interactions.

(4) Conducting experimental validation: While the dissertation provides numerical and analytical insights on the influence of excitation and system properties and makes comparisons to existing experimental studies, further experimental studies are recommended to validate these findings and quantify the role of excitation parameters and system dynamics across different materials. This would help better tune the parameters, improve model accuracy and identify an eventual slip length or the surface dynamics that govern the initiation of macroscopic sliding.

(5) Assessing energy efficiency: While this study investigates the effect of vibrations on friction modulation, the amount of energy required from the additional power source generating these vibrations is not quantified. A comprehensive energy balance analysis would help determine conditions under which net energy savings can be achieved. This analysis would enable efficient implementations that minimise energy consumption while ensuring friction change.

REFERENCES

REFERENCES CHAPTER 1

[1] B. Feeny, A. Guran, N. Hinrichs, and K. Popp. "A historical review on dry friction and stick-slip phenomena". In: *Applied Mechanics Reviews* 51.5 (1998), pp. 321–341.

[2] H. Liu, B. Yang, C. Wang, Y. Han, and D. Liu. "The mechanisms and applications of friction energy dissipation". In: *Friction* 11.6 (2022), pp. 839–864.

[3] K. Holmberg and A. Erdemir. "Global impact of friction on energy consumption, economy and environment". In: *FME Transactions* 43 (2015), pp. 181–185.

[4] K. Holmberg and A. Erdemir. "Influence of tribology on global energy consumption, costs and emissions". In: *Friction* 5.3 (2017), pp. 263–284.

[5] R. Shah, M. Woydt, and S. Zhang. "The economic and environmental significance of sustainable lubricants". In: *Lubricants* 9.2 (2021), p. 21.

[6] D. M. Tolstoi. "Significance of the normal degree of freedom and natural normal vibrations in contact friction". In: *Wear* 10.3 (1967), pp. 199–213.

[7] H. D. Fridman and P. Levesque. "Reduction of Static Friction by Sonic Vibrations". In: *Journal of Applied Physics* 30.10 (1959), pp. 1572–1575.

[8] S. Matunaga and J. Onoda. "New gravity compensation method by dither for low-g simulation". In: *Journal of Spacecraft and Rockets* 32.2 (1995), pp. 364–369.

[9] H. Storck, W. Littmann, J. Wallaschek, and M. Mracek. "The effect of friction reduction in presence of ultrasonic vibrations and its relevance to travelling wave ultrasonic motors". In: *Ultrasonics* 40.1 (2002), pp. 379–383.

[10] M. A. Michaux, A. A. Ferri, and K.A. Cunefare. "Effect of Waveform on the Effectiveness of Tangential Dither Forces to Cancel Friction-Induced Oscillations". In: *Journal of Sound and Vibration* 311.3 (2008), pp. 802–823.

[11] K. Siegert and A. Möck. "Wire drawing with ultrasonically oscillating dies". In: *Journal of Materials Processing Technology.* 60.1-4 (1996), pp. 657–660.

[12] W. Wu, J. Zhou, P. Huang, C. Pan, Z. Huang, and C. Xu. "Antifriction Mechanism of Longitudinal Vibration-Assisted Insertion in DBS". In: *Annals of Biomedical Engineering* 49.9 (2021), pp. 2057–2065.

[13] M. A. Atalla, J. J. Tuijp, M. Wiertlewski, and A. Sakes. "Toward Variable-Friction Catheters Using Ultrasonic Lubrication". In: *IEEE Transactions on Medical Robotics and Bionics* 6.4 (2024), pp. 1375–1381.

[14] A. Tsetas, A. Tsouvalas, and A. V. Metrikine. "The mechanics of the Gentle Driving of Piles". In: *International Journal of Solids and Structures* 282 (2023), p. 112466.

[15] A. Cabboi, M. Segeren, H. Hendrikse, and A. Metrikine. “Vibration-assisted installation and decommissioning of a slip-joint”. In: *Engineering Structures* 209 (2020), p. 109949. ISSN: 0141-0296.

[16] H. Gong, X. Ding, J. Liu, and H. Feng. “Review of research on loosening of threaded fasteners”. In: *Friction* 10.3 (2021), pp. 335–359.

[17] R. A. Ibrahim. “Friction-Induced Vibration, Chatter, Squeal, and Chaos—Part I: Mechanics of Contact and Friction”. In: *Applied Mechanics Reviews* 47.7 (1994), pp. 209–226.

[18] R. A. Ibrahim. “Friction-Induced Vibration, Chatter, Squeal, and Chaos—Part II: Dynamics and Modeling”. In: *Applied Mechanics Reviews* 47.7 (1994), pp. 227–253.

[19] R. T. Spurr. “A Theory of Brake Squeal”. In: *Proceedings of the Institution of Mechanical Engineers: Automobile Division* 15.1 (1961), pp. 33–52.

[20] L. Gaul and R. Nitsche. “The Role of Friction in Mechanical Joints”. In: *Applied Mechanics Reviews* 54.2 (2001), pp. 93–106.

[21] N. Hoffmann, M. Fischer, R. Allgaier, and L. Gaul. “A minimal model for studying properties of the mode-coupling type instability in friction induced oscillations”. In: *Mechanics Research Communications* 29.4 (2002), pp. 197–205.

[22] V. L. Popov, J. Starcevic, and A.E. Filippov. “Influence of Ultrasonic In-Plane Oscillations on Static and Sliding Friction and Intrinsic Length Scale of Dry Friction Processes”. In: *Tribology Letters* 39 (2010), pp. 25–30.

[23] W. Littmann, H. Storck, and J. Wallaschek. “Proceedings of the SPIE, Volume 4331, p. 302-311”. In: *SPIE Proceedings*. Vol. 4331. 2001, pp. 302–311.

References Chapter 2

[1] J. Tautz, F. Roces, and B. Hölldobler. “Use of a Sound-Based Vibratome by Leaf-Cutting Ants”. In: *Science* 267.5194 (1995), pp. 84–87.

[2] D. Wang and H. Liu. “Dolphin-Inspired Skin Microvibrations Offer a Novel Pressure-Dominated Drag Reduction Mechanism”. In: *Journal of Bionic Engineering* 22.2 (2025), pp. 793–804.

[3] V. V. Pavlov. “Dolphin skin as a natural anisotropic compliant wall”. In: *Bioinspiration & Biomimetics* 1.2 (2006), pp. 31–40.

[4] M. G. Strahan, D. S. Houser, J. J. Finneran, J. Mulsow, and D. E. Crocker. “Behaviorally measured tactile sensitivity in the common bottlenose dolphin, *Tursiops truncatus*”. In: *Marine Mammal Science* 36.3 (2020), pp. 802–812.

[5] W. W. L. Au. “Echolocation signals of wild dolphins”. In: *Acoustical Physics* 50.4 (2004), pp. 454–462.

[6] V. A. Ryabov. “Acoustic signals and echolocation system of the dolphin”. In: *Biophysics* 59.1 (2014), pp. 135–147.

[7] H. J. Melosh. “Acoustic fluidization: A new geologic process?” In: *Journal of Geophysical Research: Solid Earth* 84.B13 (1979), pp. 7513–7520.

[8] H. J. Melosh. “Dynamical weakening of faults by acoustic fluidization”. In: *Nature* 379.6566 (1996), pp. 601–606.

[9] F. Huber. “Central nervous control of sound production in crickets and some speculations on its evolution”. In: *Evolution* 16.4 (1962), pp. 429–442.

[10] K. Kowalski and R. Lakes-Harlan. “Sounds, behaviour, and auditory receptors of the armoured ground cricket, Acanthoplus longipes”. In: *Journal of Insect Science* 10.59 (2010), pp. 1–15. DOI: 10.1673/031.010.5901.

[11] J. Sueur, D. Mackie, and J. F. C. Windmill. “So small, so loud: Extremely high sound pressure level from a pygmy aquatic insect (Corixidae, Micronectinae)”. In: *PLoS ONE* 6.6 (2011), e21089.

[12] R. D. Alexander and D. Otte. “Crickets”. In: *Encyclopedia of Insects*. Elsevier, 2009, pp. 232–236.

[13] M. Polo. *The Description of the World*. Ed. by A. C. Moule and P. G. Pelliot. Available online. London: Routledge, 1938.

[14] C. Darwin. *The Voyage of the Beagle*. 4th. London: Ward, Lock & Co. Ltd, 1889.

[15] P. Sholtz, M. Bretz, and F. Nori. “Sound-producing sand avalanches”. In: *Contemporary Physics* 38.5 (1997), pp. 329–342.

[16] K. Siegert and A. Möck. “Wire drawing with ultrasonically oscillating dies”. In: *Journal of Materials Processing Technology*. 60.1-4 (1996), pp. 657–660.

[17] F. K. Garskii and V. I. Efromov. “Effect of ultrasound on the decomposition of solid solutions”. In: *Izv Akad Nauk Beloroussk SSR* 3 (1953), pp. 176–179.

[18] F. Blaha and B. Langenecker. “Dehnung von Zink-Kristallen unter Ultraschalleinwirkung”. In: *Die Naturwissenschaften* 42.20 (1955), pp. 556–556.

[19] K. F. Graff. “Ultrasonic metal forming”. In: *Power Ultrasonics*. Elsevier, 2015, pp. 377–438.

[20] W. Wu, J. Zhou, P. Huang, C. Pan, Z. Huang, and C. Xu. “Antifriction Mechanism of Longitudinal Vibration-Assisted Insertion in DBS”. In: *Annals of Biomedical Engineering* 49.9 (2021), pp. 2057–2065.

[21] A. Cabboi, M. Segeren, H. Hendrikse, and A. Metrikine. “Vibration-assisted installation and decommissioning of a slip-joint”. In: *Engineering Structures* 209 (2020), p. 109949. ISSN: 0141-0296.

[22] A. Cabboi, T. Kamphuis, E. van Veldhuizen, M. Segeren, and H. Hendrikse. “Vibration-assisted installation and decommissioning of a slip-joint: Application to an offshore wind turbine”. In: *Engineering Structures* 76 (2021).

[23] A. Tsetas, A. Tsouvalas, and A. V. Metrikine. “The mechanics of the Gentle Driving of Piles”. In: *International Journal of Solids and Structures* 282 (2023), p. 112466.

[24] K. Tashiro, Y. Shiokawa, T. Aono, and T. Maeno. “Realization of button click feeling by use of ultrasonic vibration and force feedback”. In: *3rd Joint EuroHaptics Conference and Symposium on Haptic Interfaces for Virtual Environment and Teleoperator Systems*. Salt Lake City, UT, USA: IEEE, 2009, pp. 1–6.

[25] J. Monnoyer, E. Diaz, C. Bourdin, and M. Wiertlewski. “Ultrasonic friction modulation while pressing induces a tactile feedback”. In: *Eurohaptics 2016*. Ed. by F. Bello, H. Kajimoto, and Y. Visell. Vol. 9774. Lecture Notes in Computer Science. Cham, Switzerland: Springer, 2016, pp. 171–179.

[26] J. Monnoyer, E. Diaz, C. Bourdin, and M. Wiertlewski. “Optimal skin impedance promotes perception of ultrasonic switches”. In: *2017 IEEE World Haptics Conference (WHC)*. Munich, Germany: IEEE, 2017, pp. 130–135.

[27] D. J. Meyer, M. Wiertlewski, M. A. Peshkin, and J. E. Colgate. “Dynamics of ultrasonic and electrostatic friction modulation for rendering texture on haptic surfaces”. In: *2014 IEEE Haptics Symposium (HAPTICS)*. Houston, TX, USA: IEEE, 2014, pp. 63–67.

[28] H. Gong, X. Ding, J. Liu, and H. Feng. “Review of research on loosening of threaded fasteners”. In: *Friction* 10.3 (2021), pp. 335–359.

[29] R. A. Ibrahim. “Friction-Induced Vibration, Chatter, Squeal, and Chaos—Part II: Dynamics and Modeling”. In: *Applied Mechanics Reviews* 47.7 (1994), pp. 227–253.

[30] H. D. Fridman and P. Levesque. “Reduction of Static Friction by Sonic Vibrations”. In: *Journal of Applied Physics* 30.10 (1959), pp. 1572–1575.

[31] D. M. Tolstoi. “Significance of the normal degree of freedom and natural normal vibrations in contact friction”. In: *Wear* 10.3 (1967), pp. 199–213.

[32] D. Godfrey. “Vibration Reduces Metal to Metal Contact and Causes an Apparent Reduction in Friction”. In: *ASLE Transactions* 10.2 (1967), pp. 183–192.

[33] W. Lenkiewicz. “The sliding friction process—effect of external vibrations”. In: *Wear* 13.2 (1969), pp. 99–108.

[34] H. Nolle and R.S.H. Richardson. “Static friction coefficients for mechanical and structural joints”. In: *Wear* 28.1 (1974), pp. 1–13.

[35] Z. Broniec and W. Lenkiewicz. “Static friction processes under dynamic loads and vibration”. In: *Wear* 80.3 (1982), pp. 261–271.

[36] A. Lehtovaara. “Influence of vibration on the kinetic friction between plastics and ice”. In: *Wear* 115.1 (1987), pp. 131–138.

[37] T. Skåre and J. E. Ståhl. “Static and dynamic friction processes under the influence of external vibrations”. In: *Wear* 154.1 (1992), pp. 177–192.

[38] S. Matunaga and J. Onoda. “New gravity compensation method by dither for low-g simulation”. In: *Journal of Spacecraft and Rockets* 32.2 (1995), pp. 364–369.

[39] I. I. Blekhman. *Vibrational Mechanics – Nonlinear Dynamic Effects, General Approach, Applications*. World Scientific, Singaopre, 2000.

[40] H. Storck, W. Littmann, J. Wallaschek, and M. Mracek. “The effect of friction reduction in presence of ultrasonic vibrations and its relevance to travelling wave ultrasonic motors”. In: *Ultrasonics* 40.1 (2002), pp. 379–383.

[41] V. C. Kumar and I. M Hutchings. “Reduction of the sliding friction of metals by the application of longitudinal or transverse ultrasonic vibration”. In: *Tribology International* 37.10 (2004), pp. 833–840.

[42] M. A. Chowdhury and Helali. M. "The effect of frequency of vibration and humidity on the coefficient of friction". In: *Tribology International* 39.9 (2006), pp. 958–962.

[43] M. A. Chowdhury and M. Helali. "The effect of amplitude of vibration on the coefficient of friction for different materials". In: *Tribology International* 41.4 (2008), pp. 307–314.

[44] M. A. Chowdhury, M. Helali, and T. Hasan. "The frictional behavior of mild steel under horizontal vibration". In: *Tribology International* 42.6 (2009), pp. 946–950.

[45] M. A. Chowdhury and M. Helali. "The frictional behavior of materials under vertical vibration". In: *Industrial Lubrication and Tribology* 61.3 (2009), pp. 154–160.

[46] V. L. Popov, J. Starcevic, and A.E. Filippov. "Influence of Ultrasonic In-Plane Oscillations on Static and Sliding Friction and Intrinsic Length Scale of Dry Friction Processes". In: *Tribology Letters* 39 (2010), pp. 25–30.

[47] E. Teidelt, V. Popov, and J. Starcevic. "Influence of In-Plane and Out-of-Plane Ultrasonic Oscillations on Sliding Friction". In: *SAE International Journal of Passenger Cars – Mechanical Systems* 4.3 (2011), pp. 1387–1393.

[48] E. Teidelt, J. Starcevic, and V. L. Popov. "Influence of Ultrasonic Oscillation on Static and Sliding Friction". In: *Tribology Letters* 48.1 (2012), pp. 51–62.

[49] M. Popov, V. L. Popov, and N. V. Popov. "Reduction of friction by normal oscillations. I. Influence of contact stiffness". In: *Friction* 5.1 (2017), pp. 45–55.

[50] X. Mao, V. L. Popov, J. Starcevic, and M. Popov. "Reduction of friction by normal oscillations. II. In-plane system dynamics". In: *Friction* 5.2 (2017), pp. 194–206.

[51] P. Gutowski and M. Leus. "The effect of longitudinal tangential vibrations on friction and driving forces in sliding motion". In: *Tribology International* 55 (2012), pp. 108–118.

[52] P. Gutowski and M. Leus. "Computational model for friction force estimation in sliding motion at transverse tangential vibrations of elastic contact support". In: *Tribology International* 90 (2015), pp. 455–462.

[53] P. Wang, H. Ni, R. Wang, Zh. Li, and Y. Wang. "Experimental investigation of the effect of in-plane vibrations on friction for different materials". In: *Tribology International* 99 (2016), pp. 237–247.

[54] P. Wang, H. Ni, R. Wang, W. Liu, and Sh. Lu. "Research on the mechanism of in-plane vibration on friction reduction". In: *Materials* 10.9 (2017).

[55] S. Kapelke and W. Seemann. "On the Effect of Longitudinal Vibrations on Dry Friction: Modelling Aspects and Experimental Investigations". In: *Tribology Letters* 66.3 (2018).

[56] P. Gutowski and M. Leus. "Computational model of friction force reduction at arbitrary direction of tangential vibrations and its experimental verification". In: *Tribology International* 143 (2020), p. 106065.

[57] M. Leus and P. Gutowski. "Friction Force Reduction Efficiency in Sliding Motion Under Tangential Vibrations of Elastic Support". In: *Acta Mechanica et Automatica* 18.1 (2024), pp. 101–109.

[58] J. J. Thomsen. “Using fast vibrations to quench friction-induced oscillations”. In: *Journal of Sound and Vibration* 228.5 (1999), pp. 1079–1102.

[59] I. I. Blekhman and V. S. Sorokin. “Effects produced by oscillations applied to nonlinear dynamic systems: a general approach and examples”. In: *Nonlinear Dynamics* 83.4 (Mar. 2016), pp. 2125–2141.

[60] M. A. Michaux, A. A. Ferri, and K.A. Cunefare. “Effect of Waveform on the Effectiveness of Tangential Dither Forces to Cancel Friction-Induced Oscillations”. In: *Journal of Sound and Vibration* 311.3 (2008), pp. 802–823.

[61] N. Hoffmann, N. Wagner, and L. Gaul. “Quenching mode-coupling friction-induced instability using high-frequency dither”. In: *Journal of Sound and Vibration* 279.1 (2005), pp. 471–480.

[62] D. P. Hess and A. Soom. “Normal Vibrations and Friction Under Harmonic Loads: Part I-—Hertzian Contacts”. In: *Journal of Tribology* 113.1 (1991), pp. 80–86.

[63] D. P. Hess and A. Soom. “Normal Vibrations and Friction Under Harmonic Loads: Part II—-Rough Planar Contacts”. In: *Journal of Tribology* 113.1 (1991), pp. 87–92.

[64] D. P. Hess, A. Soom, and C. H. Kim. “Normal vibrations and friction at a Hertzian contact under random excitation: Theory and experiments”. In: *Journal of Sound and Vibration* 153.3 (1992), pp. 491–508.

[65] M. Leus and P. Gutowski. “Analysis of longitudinal tangential contact vibration effect on friction force using Coulomb and Dahl models”. In: *Journal of Theoretical and Applied Mechanics* 46.1 (2008), pp. 171–184.

[66] R. P. Dahl. “Solid Friction Damping of Mechanical Vibrations”. In: *AIAA Journal* 14.12 (1976), pp. 1675–1682.

[67] K. Grudzinsky and R. Kostek. “Influence of Normal Micro-Vibrations in Contact on Sliding Motion of Solid Body”. In: *Journal of Theoretical and Applied Mechanics* 43.1 (2005), pp. 37–49.

[68] S. Kapelke, W. Seemann, and H. Hetzler. “The effect of longitudinal high-frequency in-plane vibrations on a 1-DoF friction oscillator with compliant contact”. In: *Nonlinear Dynamics* 88.4 (2017), pp. 3003–3015.

[69] R. A. Ibrahim. “Friction-Induced Vibration, Chatter, Squeal, and Chaos—Part I: Mechanics of Contact and Friction”. In: *Applied Mechanics Reviews* 47.7 (1994), pp. 209–226.

[70] L. Gaul and R. Nitsche. “The Role of Friction in Mechanical Joints”. In: *Applied Mechanics Reviews* 54.2 (2001), pp. 93–106.

[71] V. P. Sergienko, S. N. Bukharov, and A. V. Kupreev. “Noise and vibration in brake systems of vehicles. Part 1: Experimental procedures”. In: *Journal of Friction and Wear* 29.3 (2008), pp. 234–241.

[72] V. P. Sergienko and S. N. Bukharov. “Vibration and noise in brake systems of vehicles. Part 2: Theoretical investigation techniques”. In: *Journal of Friction and Wear* 30.3 (2009), pp. 216–226.

[73] M. Yokoi and M. Nakai. “A Fundamental Study on Frictional Noise: 1st Report, The generating mechanism of rubbing noise and squeal noise”. In: *Bulletin of JSME* 22.173 (1979), pp. 1665–1671.

[74] R. T. Spurr. “A Theory of Brake Squeal”. In: *Proceedings of the Institution of Mechanical Engineers: Automobile Division* 15.1 (1961), pp. 33–52.

[75] D. Bigoni and G. Noselli. “Experimental evidence of flutter and divergence instabilities induced by dry friction”. In: *Journal of the Mechanics and Physics of Solids* 59.10 (2011), pp. 2208–2226.

[76] N. Hoffmann, M. Fischer, R. Allgaier, and L. Gaul. “A minimal model for studying properties of the mode-coupling type instability in friction induced oscillations”. In: *Mechanics Research Communications* 29.4 (2002), pp. 197–205.

[77] N. Hoffmann and L. Gaul. “Effects of damping on mode-coupling instability in friction induced oscillations”. In: *ZAMM - Journal of Applied Mathematics and Mechanics / Zeitschrift für Angewandte Mathematik und Mechanik* 83.8 (2003), pp. 524–534.

[78] Z. Li, H. Ouyang, and Z. H. Wei. “Insights into instability of friction-induced vibration of multi-degree-of-freedom models”. In: *Journal of Sound and Vibration* 503 (2021), p. 116107.

[79] J. Juel Thomsen and A. Fidlin. “Analytical approximations for stick–slip vibration amplitudes”. In: *International Journal of Non-Linear Mechanics* 38.3 (2003), pp. 389–403.

[80] G. Fritz, J. J. Sinou, J. M. Duffal, and L. Jézéquel. “Effects of damping on brake squeal coalescence patterns – application on a finite element model”. In: *Mechanics Research Communications* 34.2 (2007), pp. 181–190.

[81] J. Sinou and L. Jezequel. “Mode coupling instability in friction-induced vibrations and its dependency on system parameters including damping”. In: *European Journal of Mechanics - A/Solids* 26 (2007), pp. 106–122.

[82] L. Charroyer, O. Chiello, and J. J. Sinou. “Parametric study of the mode coupling instability for a simple system with planar or rectilinear friction”. In: *Journal of Sound and Vibration* 384 (2016), pp. 94–112.

[83] S. K. Rhee, P. H. S. Tsang, and Y. S. Wang. “Friction-induced noise and vibration of disc brakes”. In: *Wear* 133.1 (1989), pp. 39–45.

[84] H. Ouyang and J. E. Mottershead. “Dynamic Instability of an Elastic Disk Under the Action of a Rotating Friction Couple”. In: *Journal of Applied Mechanics* 71.6 (2004), pp. 753–758.

[85] Z. Zhang, S. Oberst, and J. C. S. Lai. “A non-linear friction work formulation for the analysis of self-excited vibrations”. In: *Journal of Sound and Vibration* 443 (2019), pp. 328–340.

[86] E. J. Berger, C. M. Krousgrill, and F. Sadeghi. “Friction-induced sliding instability in a multi-degree-of-freedom system with oscillatory normal forces”. In: *Journal of Sound and Vibration* 266.2 (2003), pp. 369–387.

REFERENCES CHAPTER 3

[1] S. L. Ipri and H. Asada. “Tuned dither for friction suppression during force-guided robotic assembly”. In: *Proceedings of the 1995 IEEE/RSJ International Conference on Intelligent Robots and Systems: Human Robot Interaction and Cooperative Robots*. 1 (1995), pp. 310–315.

[2] A. Cabboi, T. Kamphuis, E. van Veldhuizen, M. Segeren, and H. Hendrikse. “Vibration-assisted installation and decommissioning of a slip-joint: Application to an offshore wind turbine”. In: *Engineering Structures* 76 (2021).

[3] A. Tsetas, A. Tsouvalas, and A. V. Metrikine. “The mechanics of the Gentle Driving of Piles”. In: *International Journal of Solids and Structures* 282 (2023), p. 112466.

[4] W. Wu, C. Xu, C. Pan, Z. Huang, J. Zhou, and P. Huang. “Effect of vibration frequency on frictional resistance of brain tissue during vibration-assisted needle insertion”. In: *Medical Engineering & Physics*. 86 (2020), pp. 35–40.

[5] J. Fu, Zh. Ren, J. Bai, F. Qin, and B. Li. “The friction-reducing principle and application of the drill string with a hydro-oscillator”. In: *Journal of Petroleum Science and Engineering* 165 (2018), pp. 453–461.

[6] K. Siegert and A. Möck. “Wire drawing with ultrasonically oscillating dies”. In: *Journal of Materials Processing Technology*. 60.1-4 (1996), pp. 657–660.

[7] A. Socoliuc, E. Gnecco, S. Maier, O. Pfeiffer, A. Baratoff, R. Bennewitz, and Meyer E. “Atomic-scale control of friction by actuation of nanometer-sized contacts.” In: *Science* 313.5784 (2006).

[8] D. J. Meyer, M. Wiertlewski, M. A. Peshkin, and J. E. Colgate. “Dynamics of ultrasonic and electrostatic friction modulation for rendering texture on haptic surfaces”. In: *2014 IEEE Haptics Symposium (HAPTICS)*. Houston, TX, USA: IEEE, 2014, pp. 63–67.

[9] N. A. Muhammad and C. S. Wu. “Ultrasonic vibration assisted friction stir welding of aluminium alloy and pure copper”. In: *J. Manuf. Process.* 39 (2019), pp. 114–127.

[10] H. D. Fridman and P. Levesque. “Reduction of Static Friction by Sonic Vibrations”. In: *Journal of Applied Physics* 30.10 (1959), pp. 1572–1575.

[11] D. M. Tolstoi. “Significance of the normal degree of freedom and natural normal vibrations in contact friction”. In: *Wear* 10.3 (1967), pp. 199–213.

[12] D. P. Hess and A. Soom. “Normal Vibrations and Friction Under Harmonic Loads: Part I-—Hertzian Contacts”. In: *Journal of Tribology* 113.1 (1991), pp. 80–86.

[13] D. P. Hess and A. Soom. “Normal Vibrations and Friction Under Harmonic Loads: Part II—-Rough Planar Contacts”. In: *Journal of Tribology* 113.1 (1991), pp. 87–92.

[14] D. P. Hess, A. Soom, and C. H. Kim. “Normal vibrations and friction at a Hertzian contact under random excitation: Theory and experiments”. In: *Journal of Sound and Vibration* 153.3 (1992), pp. 491–508.

[15] S. Matunaga and J. Onoda. “New gravity compensation method by dither for low-g simulation”. In: *Journal of Spacecraft and Rockets* 32.2 (1995), pp. 364–369.

[16] H. Storck, W. Littmann, J. Wallaschek, and M. Mracek. “The effect of friction reduction in presence of ultrasonic vibrations and its relevance to travelling wave ultrasonic motors”. In: *Ultrasonics* 40.1 (2002), pp. 379–383.

[17] V. C. Kumar and I. M Hutchings. “Reduction of the sliding friction of metals by the application of longitudinal or transverse ultrasonic vibration”. In: *Tribology International* 37.10 (2004), pp. 833–840.

[18] M. Leus and P. Gutowski. “Analysis of longitudinal tangential contact vibration effect on friction force using Coulomb and Dahl models”. In: *Journal of Theoretical and Applied Mechanics* 46.1 (2008), pp. 171–184.

[19] R. P. Dahl. “Solid Friction Damping of Mechanical Vibrations”. In: *AIAA Journal* 14.12 (1976), pp. 1675–1682.

[20] K. Grudzinsky and R. Kostek. “Influence of Normal Micro-Vibrations in Contact on Sliding Motion of Solid Body”. In: *Journal of Theoretical and Applied Mechanics* 43.1 (2005), pp. 37–49.

[21] V. L. Popov, J. Starcevic, and A.E. Filippov. “Influence of Ultrasonic In-Plane Oscillations on Static and Sliding Friction and Intrinsic Length Scale of Dry Friction Processes”. In: *Tribology Letters* 39 (2010), pp. 25–30.

[22] E. Teidelt, V. Popov, and J. Starcevic. “Influence of In-Plane and Out-of-Plane Ultrasonic Oscillations on Sliding Friction”. In: *SAE International Journal of Passenger Cars – Mechanical Systems* 4.3 (2011), pp. 1387–1393.

[23] E. Teidelt, J. Starcevic, and V. L. Popov. “Influence of Ultrasonic Oscillation on Static and Sliding Friction”. In: *Tribology Letters* 48.1 (2012), pp. 51–62.

[24] M. Popov, V. L. Popov, and N. V. Popov. “Reduction of friction by normal oscillations. I. Influence of contact stiffness”. In: *Friction* 5.1 (2017), pp. 45–55.

[25] X. Mao, V. L. Popov, J. Starcevic, and M. Popov. “Reduction of friction by normal oscillations. II. In-plane system dynamics”. In: *Friction* 5.2 (2017), pp. 194–206.

[26] J. J. Thomsen. “Using fast vibrations to quench friction-induced oscillations”. In: *Journal of Sound and Vibration* 228.5 (1999), pp. 1079–1102.

[27] I. I. Blekhman. *Vibrational Mechanics – Nonlinear Dynamic Effects, General Approach, Applications*. World Scientific, Singaopre, 2000.

[28] I. I. Blekhman and V. S. Sorokin. “Effects produced by oscillations applied to nonlinear dynamic systems: a general approach and examples”. In: *Nonlinear Dynamics* 83.4 (Mar. 2016), pp. 2125–2141.

[29] V. S. Sorokin. “Analysis of motion of inverted pendulum with vibrating suspension axis at low-frequency excitation as an illustration of a new approach for solving equations without explicit small parameter”. In: *International Journal of Non-Linear Mechanics*. 63 (2014), pp. 1–9.

[30] M. A. Michaux, A. A. Ferri, and K.A. Cunefare. “Effect of Waveform on the Effectiveness of Tangential Dither Forces to Cancel Friction-Induced Oscillations”. In: *Journal of Sound and Vibration* 311.3 (2008), pp. 802–823.

[31] N. Hoffmann, N. Wagner, and L. Gaul. “Quenching mode-coupling friction-induced instability using high-frequency dither”. In: *Journal of Sound and Vibration* 279.1 (2005), pp. 471–480.

[32] S. Kapelke, W. Seemann, and H. Hetzler. “The effect of longitudinal high-frequency in-plane vibrations on a 1-DoF friction oscillator with compliant contact”. In: *Nonlinear Dynamics* 88.4 (2017), pp. 3003–3015.

[33] S. Kapelke and W. Seemann. “On the Effect of Longitudinal Vibrations on Dry Friction: Modelling Aspects and Experimental Investigations”. In: *Tribology Letters* 66.3 (2018).

[34] S.W. Shaw. “On the dynamic response of a system with dry friction”. In: *Journal of Sound and Vibration* 108.2 (1986), pp. 305–325.

[35] U. Andreaus and P. Casini. “Dynamics of friction oscillators excited by a moving base and/or driving force”. In: *Journal of Sound and Vibration* 245.4 (2001), pp. 685–699.

[36] K. Nakano. “Two dimensionless parameters controlling the occurrence of stick-slip motion in a 1-DOF system with Coulomb friction”. In: *Tribology Letters* 24.2 (2006), pp. 91–98.

[37] J. H. Dieterich. “Modeling rock friction: 1. Experimental results and constitutive equations”. In: *Journal of Geophysical Research* 84 (1979), pp. 2161–68.

[38] C. Canudas deWit, H. Olsson, K. Astrom, and P. Lischinsky. “A new model for control of systems with friction”. In: *IEEE Transactions on Automatic Control* 40.3 (1995), pp. 419–425.

[39] V. S. Sorokin and Thomsen. J. J. “Vibration suppression for strings with distributed loading using spatial cross-section modulation”. In: *Journal of Sound and Vibration* 335 (2015), pp. 66–77.

[40] J. P. Den Hartog. “LXXIII. Forced vibrations with combined viscous and Coulomb damping”. In: *The London, Edinburgh, and Dublin Philosophical Magazine and Journal of Science* 9.59 (1930), pp. 801–817.

References Chapter 4

[1] M. Murakawa and M. Jin. “The utility of radially and ultrasonically vibrated dies in the wire drawing process”. In: *Journal of Materials Processing Technology.* 113.1-3 (2001), pp. 81–86.

[2] G. Eggers, J. Klein, J. Blank, and S. Hassfeld. “Piezosurgery: An ultrasound device for cutting bone and its use and limitations in maxillofacial surgery”. In: *British Journal of Oral and Maxillofacial Surgery* 42.5 (2004), pp. 451–453.

[3] Y. Ashida and H. Aoyama. “Press forming using ultrasonic vibration”. In: *Journal of Materials Processing Technology* 187 (2007), pp. 118–122.

[4] A. Cabboi, M. Segeren, H. Hendrikse, and A. Metrikine. “Vibration-assisted installation and decommissioning of a slip-joint”. In: *Engineering Structures* 209 (2020), p. 109949. ISSN: 0141-0296.

[5] A. Cabboi, T. Kamphuis, E. van Veldhuizen, M. Segeren, and H. Hendrikse. "Vibration-assisted installation and decommissioning of a slip-joint: Application to an offshore wind turbine". In: *Engineering Structures* 76 (2021).

[6] A. Tsetas, A. Tsouvalas, and A. V. Metrikine. "The mechanics of the Gentle Driving of Piles". In: *International Journal of Solids and Structures* 282 (2023), p. 112466.

[7] J. Monnoyer, E. Diaz, C. Bourdin, and M. Wiertlewski. "Optimal skin impedance promotes perception of ultrasonic switches". In: *2017 IEEE World Haptics Conference (WHC)*. Munich, Germany: IEEE, 2017, pp. 130–135.

[8] S. Matunaga and J. Onoda. "New gravity compensation method by dither for low-g simulation". In: *Journal of Spacecraft and Rockets* 32.2 (1995), pp. 364–369.

[9] H. Storck, W. Littmann, J. Wallaschek, and M. Mracek. "The effect of friction reduction in presence of ultrasonic vibrations and its relevance to travelling wave ultrasonic motors". In: *Ultrasonics* 40.1 (2002), pp. 379–383.

[10] V. C. Kumar and I. M Hutchings. "Reduction of the sliding friction of metals by the application of longitudinal or transverse ultrasonic vibration". In: *Tribology International* 37.10 (2004), pp. 833–840.

[11] J. J. Thomsen. "Using fast vibrations to quench friction-induced oscillations". In: *Journal of Sound and Vibration* 228.5 (1999), pp. 1079–1102.

[12] M. A. Michaux, A. A. Ferri, and K.A. Cunefare. "Effect of Waveform on the Effectiveness of Tangential Dither Forces to Cancel Friction-Induced Oscillations". In: *Journal of Sound and Vibration* 311.3 (2008), pp. 802–823.

[13] M. Leus and P. Gutowski. "Analysis of longitudinal tangential contact vibration effect on friction force using Coulomb and Dahl models". In: *Journal of Theoretical and Applied Mechanics* 46.1 (2008), pp. 171–184.

[14] P. Gutowski and M. Leus. "The effect of longitudinal tangential vibrations on friction and driving forces in sliding motion". In: *Tribology International* 55 (2012), pp. 108–118.

[15] P. Gutowski and M. Leus. "Computational model for friction force estimation in sliding motion at transverse tangential vibrations of elastic contact support". In: *Tribology International* 90 (2015), pp. 455–462.

[16] P. Gutowski and M. Leus. "Computational model of friction force reduction at arbitrary direction of tangential vibrations and its experimental verification". In: *Tribology International* 143 (2020), p. 106065.

[17] E. Sulollari, K. N. van Dalen, and A. Cabboi. "Vibration-induced friction modulation for a general frequency of excitation". In: *Journal of Sound and Vibration* 573 (2024), p. 118200.

[18] G. Amontons. "De la resistance cause'e dans les machines (About resistance and force in machines)". In: *Mem l'Acedemie R A* (1699), pp. 257–282.

[19] C. A. Coulomb. *Theorie des machines simple (Theory of simple machines)*. Paris: Bachelier, 1821.

[20] A. Cabboi and J. Woodhouse. “Validation of a constitutive law for friction-induced vibration under different wear conditions”. In: *Wear* 396-397 (2018), pp. 107–125.

[21] A. Cabboi and J. Woodhouse. “Identifying short-term variation of dynamic friction by means of its frequency response function”. In: *Journal of Sound and Vibration* 472.115212 (2020).

[22] J. J. Thomsen. *Vibrations and Stability: Advanced Theory, Analysis, and Tools*. English. Germany: Springer Verlag, 2003. ISBN: 3540401407.

[23] F. Clementi, S. Lenci, and G. Rega. “1:1 internal resonance in a two d.o.f. complete system: a comprehensive analysis and its possible exploitation for design”. In: *Meccanica* 55.6 (May 2020), pp. 1309–1332.

[24] S. Kapelke and W. Seemann. “On the Effect of Longitudinal Vibrations on Dry Friction: Modelling Aspects and Experimental Investigations”. In: *Tribology Letters* 66.3 (2018).

REFERENCES CHAPTER 5

[1] R. A. Ibrahim. “Friction-Induced Vibration, Chatter, Squeal, and Chaos—Part II: Dynamics and Modeling”. In: *Applied Mechanics Reviews* 47.7 (1994), pp. 227–253.

[2] R. T. Spurr. “A Theory of Brake Squeal”. In: *Proceedings of the Institution of Mechanical Engineers: Automobile Division* 15.1 (1961), pp. 33–52.

[3] N. Hoffmann and L. Gaul. “A sufficient criterion for the onset of sprag-slip oscillations”. In: *Archive of Applied Mechanics* 73.9-10 (2004), pp. 650–660.

[4] J. J. Sinou, O. Dereure, G. B. Mazet, F. Thouverez, and L. Jezequel. “Friction-induced vibration for an aircraft brake system—Part 1: Experimental approach and stability analysis”. In: *International Journal of Mechanical Sciences* 48.5 (2006), pp. 536–554.

[5] N. Hoffmann and L. Gaul. “Effects of damping on mode-coupling instability in friction induced oscillations”. In: *ZAMM - Journal of Applied Mathematics and Mechanics / Zeitschrift für Angewandte Mathematik und Mechanik* 83.8 (2003), pp. 524–534.

[6] J. Sinou and L. Jezequel. “Mode coupling instability in friction-induced vibrations and its dependency on system parameters including damping”. In: *European Journal of Mechanics - A/Solids* 26 (2007), pp. 106–122.

[7] Z. Li, H. Ouyang, and Z. Guan. “Nonlinear Friction-Induced Vibration of a Slider–Belt System.” In: *Journal of Vibration and Acoustics* 138 (2016).

[8] Z. Li, H. Ouyang, and Z. H. Wei. “Insights into instability of friction-induced vibration of multi-degree-of-freedom models”. In: *Journal of Sound and Vibration* 503 (2021), p. 116107.

[9] D. Bigoni, O. N. Kirillov, D. Misseroni, G. Noselli, and M. Tommasini. “Flutter and divergence instability in the Pflüger column: Experimental evidence of the Ziegler destabilization paradox”. In: *Journal of the Mechanics and Physics of Solids* 116 (2018), pp. 99–116.

[10] F. Massi and O. Giannini. “Slight effect of damping on the propensity of squeal instability: An experimental investigation”. In: *Journal of the Acoustical Society of America* 123.4 (2008), pp. 2017–2023.

[11] G. Fritz, J. J. Sinou, J. M. Duffal, and L. Jézéquel. “Effects of damping on brake squeal coalescence patterns – application on a finite element model”. In: *Mechanics Research Communications* 34.2 (2007), pp. 181–190.

[12] L. Charroyer, O. Chiello, and J. J. Sinou. “Parametric study of the mode coupling instability for a simple system with planar or rectilinear friction”. In: *Journal of Sound and Vibration* 384 (2016), pp. 94–112.

[13] J. J. Thomsen. “Using fast vibrations to quench friction-induced oscillations”. In: *Journal of Sound and Vibration* 228.5 (1999), pp. 1079–1102.

[14] N. Hoffmann, N. Wagner, and L. Gaul. “Quenching mode-coupling friction-induced instability using high-frequency dither”. In: *Journal of Sound and Vibration* 279.1 (2005), pp. 471–480.

[15] M. A. Michaux, A. A. Ferri, and K. A. Cunefare. “Effect of Tangential Dither Signal on Friction Induced Oscillations in an SDOF Model”. In: *Journal of Computational and Nonlinear Dynamics* 2 (2007), pp. 201–210.

[16] E. J. Berger, C. M. Krousgrill, and F. Sadeghi. “Stability of Sliding in a System Excited by a Rough Moving Surfaces”. In: *Journal of Tribology* 119.4 (1997), pp. 672–680.

[17] E. J. Berger, C. M. Krousgrill, and F. Sadeghi. “Friction-induced sliding instability in a multi-degree-of-freedom system with oscillatory normal forces”. In: *Journal of Sound and Vibration* 266.2 (2003), pp. 369–387.

[18] E. Sulollari, K. N. van Dalen, and A. Cabboi. “Vibration-induced friction modulation for a general frequency of excitation”. In: *Journal of Sound and Vibration* 573 (2024), p. 118200.

[19] D. M. Tolstoi. “Significance of the normal degree of freedom and natural normal vibrations in contact friction”. In: *Wear* 10.3 (1967), pp. 199–213.

[20] W. W. Tworzydlo and E. Becker. “Influence of forced vibrations on the static coefficient of friction — numerical modeling.” In: *Wear* 143.1 (1991), pp. 175–196.

[21] S. Matunaga and J. Onoda. “New gravity compensation method by dither for low-g simulation”. In: *Journal of Spacecraft and Rockets* 32.2 (1995), pp. 364–369.

[22] S. Kapelke and W. Seemann. “On the Effect of Longitudinal Vibrations on Dry Friction: Modelling Aspects and Experimental Investigations”. In: *Tribology Letters* 66.3 (2018).

[23] P. Dupont, V. Hayward, B. Armstrong, and F. Altpeter. “Single state elastoplastic friction models”. In: *IEEE Transactions on Automatic Control* 47.5 (2002), pp. 787–792.

[24] M. Leus, P. Gutowski, and M. Rybkiewicz. “Effectiveness of Friction Force Reduction in Sliding Motion Depending on the Frequency of Longitudinal Tangential Vibrations, Sliding Velocity and Normal Pressure”. In: *Acta Mechanica et Automatica* 17.4 (2023), pp. 490–498.

[25] M. Leus, P. Gutowski, and E. Bachtiak-Radka. “The effect of contact compliance of sliding pair on friction force reduction at longitudinal tangential vibrations”. In: *Tribolology International* 187 (2023), p. 108701. ISSN: 0301-679X.

[26] K. H. Hunt and F. R. E. Crossley. “Coefficient of restitution interpreted as damping in vibroimpact”. In: *Journal of Applied Mechanics* 42.2 (1975), pp. 440–445.

[27] I. I. Blekhman. *Vibrational Mechanics – Nonlinear Dynamic Effects, General Approach, Applications*. World Scientific, Singaopre, 2000.

[28] I. I. Blekhman and V. S. Sorokin. “Effects produced by oscillations applied to nonlinear dynamic systems: a general approach and examples”. In: *Nonlinear Dynamics* 83.4 (Mar. 2016), pp. 2125–2141.

[29] H Hertz. “On the contact of elastic solids”. In: *Miscellaneous Papers, Chapter V* (1896), pp. 146–162.

[30] C. Cattaneo. “Sul contatto di due corpi elastici: distribuzione locale degli sforzi”. In: *Rendiconti della Accademia Nazionale dei Lincei* 27 (1938), pp. 342–248, 434–436, 474–478.

[31] R. P. Dahl. “Solid Friction Damping of Mechanical Vibrations”. In: *AIAA Journal* 14.12 (1976), pp. 1675–1682.

[32] G. Amontons. “De la resistance cause’e dans les machines (About resistance and force in machines)”. In: *Mem l’Acedemie R A* (1699), pp. 257–282.

[33] C. A. Coulomb. *Theorie des machines simple (Theory of simple machines)*. Paris: Bachelier, 1821.

[34] M. D. Bryant. “Non-linear forced oscillation of a beam coupled to an actuator via Hertzian contact”. In: *Journal of Sound and Vibration* 99 (1985), pp. 403–414.

[35] D. P. Hess and A. Soom. “Normal Vibrations and Friction Under Harmonic Loads: Part I-—Hertzian Contacts”. In: *Journal of Tribology* 113.1 (1991), pp. 80–86.

[36] P. Gutowski and M. Leus. “The effect of longitudinal tangential vibrations on friction and driving forces in sliding motion”. In: *Tribology International* 55 (2012), pp. 108–118.

[37] P. Gutowski and M. Leus. “Computational model for friction force estimation in sliding motion at transverse tangential vibrations of elastic contact support”. In: *Tribology International* 90 (2015), pp. 455–462.

[38] P. Wang, H. Ni, R. Wang, Zh. Li, and Y. Wang. “Experimental investigation of the effect of in-plane vibrations on friction for different materials”. In: *Tribology International* 99 (2016), pp. 237–247.

[39] P. Wang, H. Ni, R. Wang, W. Liu, and Sh. Lu. “Research on the mechanism of in-plane vibration on friction reduction”. In: *Materials* 10.9 (2017).

References Chapter 6

[1] H. Liu, B. Yang, C. Wang, Y. Han, and D. Liu. “The mechanisms and applications of friction energy dissipation”. In: *Friction* 11.6 (2022), pp. 839–864.

[2] K. Siegert and A. Möck. “Wire drawing with ultrasonically oscillating dies”. In: *Journal of Materials Processing Technology*. 60.1-4 (1996), pp. 657–660.

[3] A. Cabboi, T. Kamphuis, E. van Veldhuizen, M. Segeren, and H. Hendrikse. “Vibration-assisted installation and decommissioning of a slip-joint: Application to an offshore wind turbine”. In: *Engineering Structures* 76 (2021).

[4] S. L. Ipri and H. Asada. “Tuned dither for friction suppression during force-guided robotic assembly”. In: *Proceedings of the 1995 IEEE/RSJ International Conference on Intelligent Robots and Systems: Human Robot Interaction and Cooperative Robots*. 1 (1995), pp. 310–315.

[5] A. Tsetas, A. Tsouvalas, and A. V. Metrikine. “The mechanics of the Gentle Driving of Piles”. In: *International Journal of Solids and Structures* 282 (2023), p. 112466.

[6] D. J. Meyer, M. Wiertlewski, M. A. Peshkin, and J. E. Colgate. “Dynamics of ultrasonic and electrostatic friction modulation for rendering texture on haptic surfaces”. In: *2014 IEEE Haptics Symposium (HAPTICS)*. Houston, TX, USA: IEEE, 2014, pp. 63–67.

[7] D. M. Tolstoi. “Significance of the normal degree of freedom and natural normal vibrations in contact friction”. In: *Wear* 10.3 (1967), pp. 199–213.

[8] A. Soom and C. Kim. “Interactions between Dynamic Normal and Frictional Forces during Unlubricated Sliding”. In: *Journal of Lubrication Technology* 105.2 (1983), pp. 221–229.

[9] D. P. Hess, A. Soom, and C. H. Kim. “Normal vibrations and friction at a Hertzian contact under random excitation: Theory and experiments”. In: *Journal of Sound and Vibration* 153.3 (1992), pp. 491–508.

[10] K. Grudziński and R. Kostek. “An analysis of nonlinear normal contact microvibrations excited by a harmonic force”. In: *Nonlinear Dynamics* 50.4 (2007), pp. 809–815.

[11] G. Costagliola, F. Bosia, and N.M. Pugno. “Hierarchical spring-block model for multiscale friction problems”. In: *ACS Biomaterials Science & Engineering* 3.11 (2017), pp. 2845–2852.

[12] G. Costagliola, F. Bosia, and N.M. Pugno. “A 2-D model for friction of complex anisotropic surfaces”. In: *Journal of the Mechanics and Physics of Solids* 112 (2018), pp. 50–65.

[13] N. Menga, F. Bottiglione, and G. Carbone. “Dynamically induced friction reduction in micro-structured interfaces”. In: *Nature* 11.1 (2021), pp. 171–184.

[14] N. Menga, F. Bottiglione, and G. Carbone. “Exploiting surface textures dynamics for dry friction control”. In: *Nonlinear Dynamics* 111 (2023), pp. 3099–3112.

[15] M. Tricarico, M. Ciavarella, and A. Papangelo. “Enhancement of adhesion strength through microvibrations: Modeling and experiments”. In: *Journal of the Mechanics and Physics of Solids* 196 (2025), p. 106020.

[16] I. Argatov, A. Papangelo, and M. Ciavarella. “An asymptotic model of vibroadhesion”. In: *International Journal of Non-Linear Mechanics*. 136 (2025), p. 105089.

[17] J. J. Thomsen. “Using fast vibrations to quench friction-induced oscillations”. In: *Journal of Sound and Vibration* 228.5 (1999), pp. 1079–1102.

[18] M. A. Michaux, A. A. Ferri, and K. A. Cunefare. “Effect of Tangential Dither Signal on Friction Induced Oscillations in an SDOF Model”. In: *Journal of Computational and Nonlinear Dynamics* 2 (2007), pp. 201–210.

[19] N. Hoffmann, N. Wagner, and L. Gaul. “Quenching mode-coupling friction-induced instability using high-frequency dither”. In: *Journal of Sound and Vibration* 279.1 (2005), pp. 471–480.

[20] H. Ouyang, J.E. Mottershead, M.P. Cartmell, and D.J. Brookfield. “Friction-induced vibration of an elastic slider on a vibrating disc”. In: *International Journal of Mechanical Sciences* 41 (1999), pp. 325–336.

[21] J. Sinou and L. Jezequel. “Mode coupling instability in friction-induced vibrations and its dependency on system parameters including damping”. In: *European Journal of Mechanics - A/Solids* 26 (2007), pp. 106–122.

[22] Z. Li, H. Ouyang, and Z. Guan. “Nonlinear Friction-Induced Vibration of a Slider–Belt System.” In: *Journal of Vibration and Acoustics* 138 (2016).

[23] J.G. Hong, J. Kim, and J. Chung. “Stick-slip vibration of a moving oscillator on an axially flexible beam”. In: *Journal of Mechanical Science and Technology* 34 (2020), pp. 541–553.

[24] E. Sulollari, K. N. van Dalen, and A. Cabboi. “Parametric excitation and friction modulation for a forced 2-DOF system”. In: *Nonlinear Dynamics* (2025), pp. 12793–12816.

[25] W. Littmann, H. Storck, and J. Wallaschek. “Proceedings of the SPIE, Volume 4331, p. 302-311”. In: *SPIE Proceedings*. Vol. 4331. 2001, pp. 302–311.

[26] H. Storck, W. Littmann, J. Wallaschek, and M. Mracek. “The effect of friction reduction in presence of ultrasonic vibrations and its relevance to travelling wave ultrasonic motors”. In: *Ultrasonics* 40.1 (2002), pp. 379–383.

[27] V. C. Kumar and I. M Hutchings. “Reduction of the sliding friction of metals by the application of longitudinal or transverse ultrasonic vibration”. In: *Tribology International* 37.10 (2004), pp. 833–840.

[28] C. C. Tsai and C.H. Tseng. “The effect of friction reduction in the presence of in-plane vibrations”. In: *Archive of Applied Mechanics* 75.2-3 (2006), pp. 164–176.

[29] R. P. Dahl. “Solid Friction Damping of Mechanical Vibrations”. In: *AIAA Journal* 14.12 (1976), pp. 1675–1682.

[30] P. Dupont, V. Hayward, B. Armstrong, and F. Altpeter. “Single state elastoplastic friction models”. In: *IEEE Transactions on Automatic Control* 47.5 (2002), pp. 787–792.

[31] S. Kapelke and W. Seemann. “On the Effect of Longitudinal Vibrations on Dry Friction: Modelling Aspects and Experimental Investigations”. In: *Tribology Letters* 66.3 (2018).

[32] A. Cabboi, M. Segeren, H. Hendrikse, and A. Metrikine. "Vibration-assisted installation and decommissioning of a slip-joint". In: *Engineering Structures* 209 (2020), p. 109949. ISSN: 0141-0296.

[33] G. Amontons. "De la resistance cause'e dans les machines (About resistance and force in machines)". In: *Mem l'Acedemie R A* (1699), pp. 257–282.

[34] C. A. Coulomb. *Theorie des machines simple (Theory of simple machines)*. Paris: Bachelier, 1821.

[35] A. Cabboi and J. Woodhouse. "Validation of a constitutive law for friction-induced vibration under different wear conditions". In: *Wear* 396-397 (2018), pp. 107–125.

[36] A. Cabboi and J. Woodhouse. "Identifying short-term variation of dynamic friction by means of its frequency response function". In: *Journal of Sound and Vibration* 472.115212 (2020).

[37] E. Sulollari, K. N. van Dalen, and A. Cabboi. "Vibration-induced friction modulation for a general frequency of excitation". In: *Journal of Sound and Vibration* 573 (2024), p. 118200.

[38] A. B. Fărăgău, T. Mazilu, A. V. Metrikine, T. Lu, and K. N. van Dalen. "Transition radiation in an infinite one-dimensional structure interacting with a moving oscillator—the Green's function method". In: *Journal of Sound and Vibration* 492 (2021), p. 115804.

[39] Ladislav Frýba. *Vibration of Solids and Structures Under Moving Loads*. Vol. 1. Springer, 1973.

REFERENCES APPENDICES

[1] E. Sulollari, K. N. van Dalen, and A. Cabboi. "Vibration-induced friction modulation for a general frequency of excitation". In: *Journal of Sound and Vibration* 573 (2024), p. 118200.

[2] R. de Borst, M.A. Crisfield, J.J.C. Remmers, and C.V. Verhoosel. *Non-linear finite element analysis of solids and structures*. 2nd. Chichester: Wiley, 2012, p. 544.

A

A.1. Extended MDSM for 2 DOF system; general harmonic loading

Following the discussion in Section 3.4, the motions $[\mathbf{X}] = [X_1\ X_2]^\top$ are separated into components $[\mathbf{Z}] = [Z_1\ Z_2]^\top$ and $[\Phi] = [\Phi_1\ \Phi_2]^\top$. By applying the averaging operation and subtracting the equation of motion for $\mathbf{Z}$ from the total motion, the equations for Φ are obtained for the general case as follows

$$\begin{aligned}\Omega_e\Phi_1'' + 2\dot{\Phi}_1' + \Omega_e^{-1}\ddot{\Phi}_1 + 2\beta_1\omega_1(\Phi_1' + \Omega_e^{-1}\dot{\Phi}_1) + \omega_1^2\Omega_e^{-1}\Phi_1 \\ +\mu(-V_b + \Phi_1' + \Omega_e^{-1}\dot{\Phi}_1)(\omega_2^2\Omega_e^{-1}\Phi_2 + 2\beta_2\omega_2(\Phi_2' + \Omega_e^{-1}\dot{\Phi}_2)) \\ +(\omega_2^2 Z_2 + 2\beta_2\omega_2\dot{Z}_2)\left(\mu(-V_b + \Phi_1' + \Omega_e^{-1}\dot{\Phi}_1) - \langle\mu(-V_b + \Phi_1' + \Omega_e^{-1}\dot{\Phi}_1)\rangle\right) = \alpha\Omega_e^2\sin(\Omega_e\tau)\end{aligned} \tag{A.1}$$

and

$$\Omega_e\Phi_2'' + 2\dot{\Phi}_2' + \Omega_e^{-1}\ddot{\Phi}_2 + 2\beta_2\omega_2(\Phi_2' + \Omega_e^{-1}\dot{\Phi}_2) + \omega_2^2\Omega_e^{-1}\Phi_2 = -\alpha\Omega_e^2\sin(\Omega_e\tau). \tag{A.2}$$

Note that Eq. (A.1) and Eq. (A.2) are coupled, and the solution for Φ_1 is needed to find $\bar{\mu}(V_b)$. The solutions are sought in the form of the harmonic series presented below

$$\Phi_1 = B_{11}(\tau)\sin(\Omega_e\tau) + B_{12}(\tau)\cos(\Omega_e\tau) \tag{A.3}$$

$$\Phi_2 = B_{21}(\tau)\sin(\Omega_e\tau) + B_{22}(\tau)\cos(\Omega_e\tau). \tag{A.4}$$

Inserting Eq. (A.3) and Eq. (A.4) into Eq. (A.1) and Eq. (A.2) and gathering the coefficients of the involved harmonics $\sin(\Omega_e\tau)$ and $\cos(\Omega_e\tau)$, results in expressions for $\ddot{B}_{11}$, $\ddot{B}_{12}$, $\ddot{B}_{21}$ and $\ddot{B}_{22}$. After some mathematical manipulations, the equations of motion for Φ can be solved analytically. All expressions of $B_{11}(\tau)$, $B_{12}(\tau)$, $B_{21}(\tau)$ and $B_{22}(\tau)$ approach to a constant value as τ increases reaching a steady-state condition. This behavior is shown in Fig. A.1 where all the plots are presented for the case of combined normal and tangential loading (2-DOF system).

A.2. Velocity response function for 2 DOF system; general harmonic loading

Here, with reference to subsection 3.4.4, the derivation of the velocity response function for the 2-DOF system is illustrated. For the 2DOF system, the assumed solution is

$$\mathbf{X} = \Im[\hat{\mathbf{X}}(\Omega_e)e^{i\Omega_e t}], \tag{A.5}$$

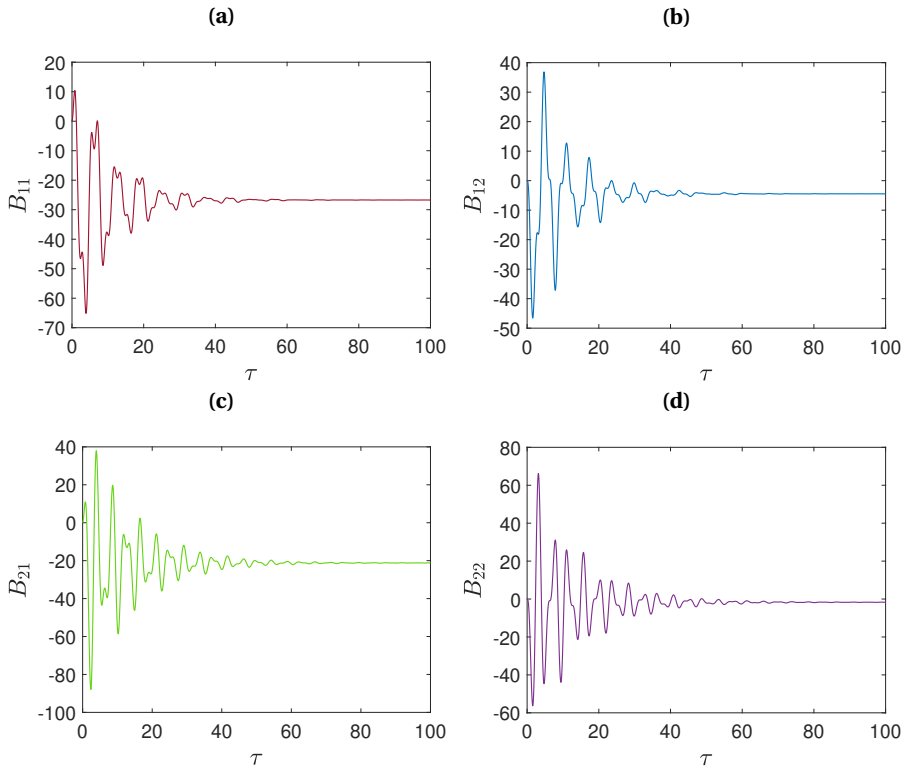

Figure A.1: Transient and steady-state behaviour of (a) $B_{11}(\tau)$ (red), (b) $B_{12}(\tau)$ (blue), (c) $B_{21}(\tau)$ (green), and (d) $B_{22}(\tau)$ (purple). $\Omega_e = 2$ and other parameters as in Figure 3.11.

since the external force is $F_{ext}(t) = \Im[\hat{F}_{ext}(\Omega_e)e^{i\Omega_e t}]$. The frequency-dependent displacement response is then given by

$$\hat{\mathbf{X}}(\Omega_e) = \mathbf{H}(\Omega_e)\hat{\mathbf{F}}_{\mathbf{ext}}(\Omega_e), \tag{A.6}$$

where $\mathbf{H}(\Omega_e)$ is the transfer function, and its inverse reads as follows

$$\mathbf{H}(\Omega_e)^{-1} = \begin{bmatrix} -\Omega_e^2 + i\Omega_e 2\beta_1\omega_1 + \omega_1^2 & \mu_s(\omega_2^2 + i\Omega_e 2\beta_2\omega_2) \\ 0 & -\Omega_e^2 + i\Omega_e 2\beta_2\omega_2 + \omega_2^2 \end{bmatrix}. \tag{A.7}$$

The displacement response function $\hat{X}_1(\Omega_e)$ becomes

$$\begin{aligned} \hat{X}_1(\Omega_e) &= \frac{H_{22}(\Omega_e)\hat{F}_{1,ext}(\Omega_e) - H_{12}(\Omega_e)\hat{F}_{2,ext}(\Omega_e)}{H_{11}(\Omega_e)H_{22}(\Omega_e) - H_{12}(\Omega_e)H_{21}(\Omega_e)} \\ &= \frac{(-\Omega_e^2 + i\Omega_e 2\beta_2\omega_2 + \omega_2^2)\hat{F}_{1,ext}(\Omega_e) - \mu_s(\omega_2^2 + i\Omega_e 2\beta_2\omega_2)\hat{F}_{2,ext}(\Omega_e)}{|\mathbf{H}(\Omega_e)|}, \end{aligned} \tag{A.8}$$

where $\hat{F}_{1,ext}(\Omega_e) = \alpha\Omega_e^2$, $\hat{F}_{2,ext}(\Omega_e) = -\alpha\Omega_e^2$ and $|\mathbf{H}(\Omega_e)|$ is the determinant of $\mathbf{H}(\Omega_e)$. The velocity response function can be easily found as

$$\hat{Y}_1(\Omega_e) = i\Omega_e \hat{X}_1(\Omega_e), \tag{A.9}$$

with the amplitude being

$$|\hat{Y}_1(\Omega_e)| = \sqrt{(\Im[\hat{Y}_1(\Omega_e)])^2 + (\Re[\hat{Y}_1(\Omega_e)])^2}. \tag{A.10}$$

B

B.1. NUMERICAL SOLUTION: RESPONSES FOR DIFFERENT EXCITATION FREQUENCIES

In Section 5.3, the excitation frequency Ω_e used is an integer multiple of the natural frequency ω_1. As shown in Fig. B.1(a), setting the excitation frequency to 4.5 rad/s still produces a noticeable spectral peak at ω_1. Moreover, the spectral peak at ω_1 is also evident even when the excitation frequencies applied in the tangential and normal directions differ from each other. As illustrated in Fig. B.1(b), when the excitation frequencies are 6 rad/s and 4 rad/s for the tangential and normal directions, respectively, the amplitude spectrum of the velocity response $\dot{X}_1$ still exhibits a notable spectral peak at ω_1. The primary spectral peak aligns with the tangential excitation frequency of 6 rad/s, while the spectral peak corresponding to the normal excitation frequency of 4 rad/s is also notable. It is worth highlighting that a strong response emerges at the second harmonic $\omega = 2\omega_1$. Hence, different excitation frequencies may induce strong higher harmonics. In comparison, the amplitudes at other harmonics are negligible.

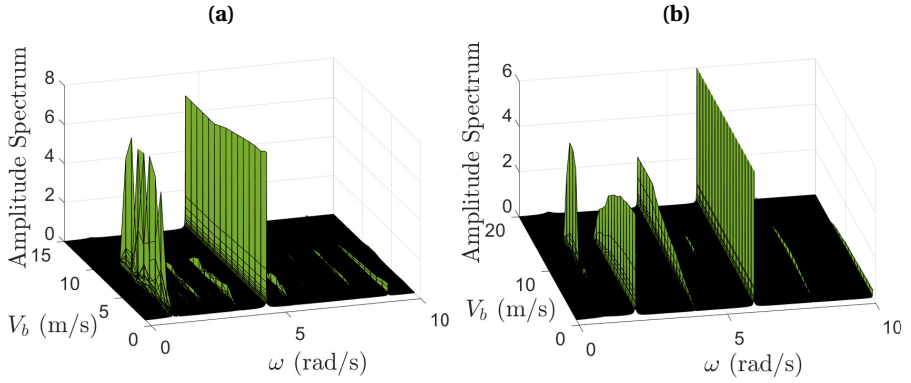

Figure B.1: (a) Amplitude spectrum of the velocity $\dot{X}_1$ for $\Omega_e = 4.5$ rad/s; (b) Amplitude spectrum of the velocity $\dot{X}_1$ for excitation frequencies 6 rad/s and 4 rad/s for the tangential and normal directions, respectively. The rest of the parameters as in Fig. 5.2.

In Fig. B.2, the amplitude spectrum of the velocity response $\dot{X}_1$ is displayed for the case where the excitation in the tangential direction has a phase shift of $\pi/2$ relative to the

excitation in the normal direction. The spectral peak at ω_1 is again evident, meaning that friction-induced vibrations occur even when a phase shift is present. However, compared to the case of no phase shift, the velocity range for which these vibrations appear is different. Thus, the phase shift has an influence on the range of belt velocities for which friction-induced vibrations occur.

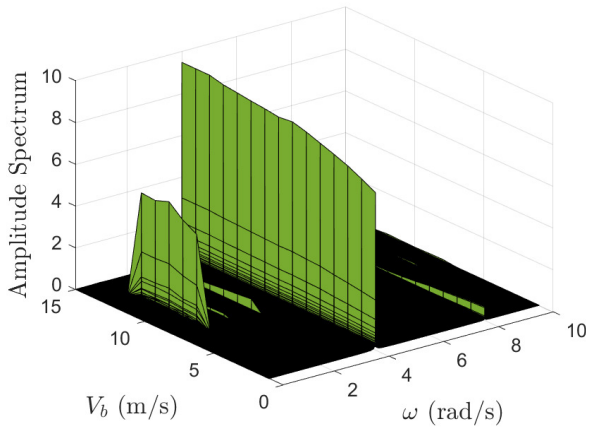

Figure B.2: Amplitude spectrum of the velocity $\dot{X}_1$ for $\Omega_e = 4$ rad/s and phase shift $\pi/2$; The rest of the parameters as in Fig. 5.2.

B.2. STABILITY ANALYSIS: JACOBIAN LINEARISATION FOR THE FORCED SYSTEM

Here, for sake of completeness, the equations of motion Φ are obtained. As written in subsection 5.4.2, separating the motions $[\mathbf{X}] = [X_1\ X_2]^{\mathrm{T}}$ into the components $[\mathbf{Z}] = [Z_1\ Z_2]^{\mathrm{T}}$ and $[\Phi] = [\Phi_1\ \Phi_2]^{\mathrm{T}}$, making use of the averaging operation and subtracting the equation of motion for $\mathbf{Z}$ from the total one, the equations of motion for the components of Φ are obtained

$$\begin{aligned}\Omega_e\Phi_1'' + 2\dot{\Phi}_1' + \Omega_e^{-1}\ddot{\Phi}_1 + 2\beta_1\omega_1(\Phi_1' + \Omega_e^{-1}\dot{\Phi}_1) + \omega_1^2\Omega_e^{-1}\Phi_1 \\ +\mu(\dot{Z}_1 - V_b + \Phi_1' + \Omega_e^{-1}\dot{\Phi}_1)(2\beta_2^*\omega_2^*(\dot{Z}_2 + \Phi_2' + \Omega_e^{-1}\dot{\Phi}_2) + \omega_2^{*2})(c_3(Z_2 + \Omega_e^{-1}\Phi_2)^3 \\ +c_2(Z_2 + \Omega_e^{-1}\Phi_2)^2 + c_1(Z_2 + \Omega_e^{-1}\Phi_2) + c_0) \\ -\bar{\mu}(2\beta_2^*\omega_2^*\dot{Z}_2 + \omega_2^{*2})(c_3Z_2^3 + c_2Z_2^2 + c_1Z_2 + c_0) = \alpha\Omega_e^2\sin(\Omega_e\tau)\end{aligned} \tag{B.1}$$

and

$$\begin{aligned}\Omega_e\Phi_2'' + 2\dot{\Phi}_2' + \Omega_e^{-1}\ddot{\Phi}_2 + (2\beta_2^*\omega_2^*(\dot{Z}_2 + \Phi_2' + \Omega_e^{-1}\dot{\Phi}_2) + \omega_2^{*2})(c_3(Z_2 + \Omega_e^{-1}\Phi_2)^3 \\ +c_2(Z_2 + \Omega_e^{-1}\Phi_2)^2 + c_1(Z_2 + \Omega_e^{-1}\Phi_2) + c_0) \\ -(2\beta_2^*\omega_2^*\dot{Z}_2 + \omega_2^{*2})(c_3Z_2^3 + c_2Z_2^2 + c_1Z_2 + c_0) = -\alpha\Omega_e^2\sin(\Omega_e\tau).\end{aligned} \tag{B.2}$$

In a previous work [1], it was stated that the motions can be separated for all frequencies of the excitation. Therefore, in this work, no restrictions are imposed on the order of magnitude of Ω_e.

Referring again to subsection 5.4.2, writing the equations of slow motion, Eq. (5.18) and Eq. (5.19), in the state-space form results in

$$S_1 = \dot{Z}_1 \tag{B.3}$$

$$\dot{S}_1 = -2\beta_1\omega_1 S_1 - \omega_1^2 Z_1 + \bar{\mu}(2\beta_2^*\omega_2^* S_2 + \omega_2^{*2}) Z_2^{3/2} \tag{B.4}$$

$$S_2 = \dot{Z}_2 \tag{B.5}$$

$$\dot{S}_2 = -(2\beta_2^*\omega_2^* S_2 + \omega_2^{*2}) Z_2^{3/2} + g \tag{B.6}$$

Setting the Eqs. (B.3)–(B.6) to zero, the equilibrium points are

$$(Z_1^0, S_1^0) = \left(\frac{\bar{\mu}^0 g}{\omega_1^2}, 0\right), \quad (Z_2^0, S_2^0) = \left(\left(\frac{g}{\omega_2^{*2}}\right)^{2/3}, 0\right). \tag{B.7}$$

B.3. NUMERICAL SOLUTION: LINEAR CONTACT PROPERTIES

Referring to the discussion in subsection 5.4.2, here, a 2 DOF system with linear contact properties is considered, as detailed in [1]. For $\beta_2 = 3$, the system is overdamped in the normal direction and has an unstable equilibrium, as illustrated in Fig. B.3(a). Thus, friction-induced oscillations occur (see the peak at ω_1 in the amplitude spectrum, Fig. B.3(b)) for V_b values less than the bifurcation point, $V_b \approx 10$ m/s, despite the assumption of linear contact properties. As in the case of nonlinear contact properties, the presence of a positive net damping in parts of the oscillation cycles bounds the response. In general, a better correlation (than in Fig. 5.2(b)) in the range of belt velocities between the stability analysis and the numerical results is observed, since the effective friction expression used corresponds to the system with linear contact properties.

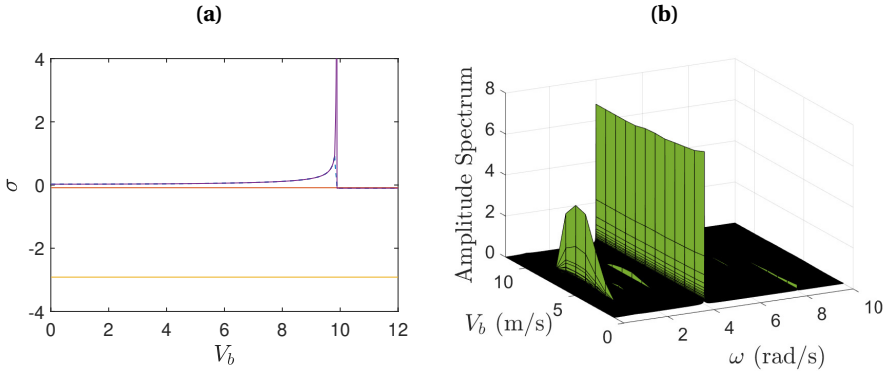

Figure B.3: (a) Real part σ versus V_b for linear contact properties; (b) Amplitude spectrum of the velocity $\dot{X}_1$. ($\omega_1 = 1$ rad/s, $\omega_2 = 0.5$ rad/s, $\beta_1 = 0.1$, $\beta_2 = 3$, $\alpha = 2$m, $\Omega_e = 4$ rad/s and $\mu_s = 0.4$).

B.4. ROUTH–HURWITZ CRITERION: a_1, a_2, a_3 AND a_4 EXPRESSIONS

Here, the expressions for a_1, a_2, a_3, and a_4 utilized in deriving the Routh–Hurwitz coefficients in subsection 5.4.3 are displayed:

$$
\begin{aligned}
a_1 &= 2\beta_1\omega_1 - \bar{\mu}' g + \frac{2\beta_2^* g}{\omega_2^*} \\
a_2 &= \omega_1^2 + (-2\beta_1\omega_1 + \bar{\mu}' g)\left(\frac{-2\beta_2^* g}{\omega_2^*}\right) + \frac{3}{2}\omega_2^{*2}\left(\frac{g}{\omega_2^{*2}}\right)^{1/3} \\
a_3 &= \frac{2\beta_2^* g\omega_1^2}{\omega_2^*} + (-2\beta_1\omega_1 + \bar{\mu}' g)\left(\frac{-3}{2}\omega_2^{*2}\left(\frac{g}{\omega_2^{*2}}\right)^{1/3}\right) \\
a_4 &= \frac{3}{2}\omega_1^2\omega_2^{*2}\left(\frac{g}{\omega_2^{*2}}\right)^{1/3}.
\end{aligned}
\tag{B.8}
$$

B.5. NUMERICAL VALIDATION OF STABILITY DIAGRAMS

Referring to the discussion in subsection 5.4.3, here, numerical results of the amplitude spectrum are displayed to validate parts of the stability diagrams. The stability diagram in Fig. 5.6(a) shows that a higher β_1 value helps in decreasing the range of belt velocities where friction-induced vibrations occur. The amplitude spectra in Fig. B.4 show that, indeed, as β_1 value increases from 0.05 in Fig. B.4(a), to 0.2 in Fig. B.4(b) and 0.4 in Fig. B.4(c), the range of belt velocities for which friction-induced vibrations are observed decreases.

The stability diagram of β_2^* displayed in Fig. 5.6(b) shows that the unstable region remains relatively the same as β_2^* values are varied. The amplitude spectra in Fig. B.5 illustrate that as the value of β_2^* increases from $0.1\frac{1}{\mathrm{m}^{5/4}}$ in Fig. B.5(a) to $0.2\frac{1}{\mathrm{m}^{5/4}}$ in Fig. B.5(b), and further to $0.3\frac{1}{\mathrm{m}^{5/4}}$ in Fig. B.5(c), the range of belt velocities for which friction-induced oscillation occur decreases. In all cases, no friction-induced vibrations are observed for $V_b > 8$ m/s, which matches the stability diagram. However, the quantitative match is not good for smaller V_b and high β_2^* values, as the numerical results show a decrease in the range of belt velocities for which friction-induced oscillations are triggered.

The stability diagram of Ω_e, Fig. 5.7, show that the instability region decreases for increased Ω_e values. Figure B.6(a) displays the amplitude spectrum for $\Omega_e = 6$ rad/s which shows a good qualitative and quantitative match to the stability diagram. For excitation frequencies $\Omega_e = 8$ rad/s and $\Omega_e = 10$ rad/s, the numerical results indicate that stick-slip behavior occurs within the stability regions shown in the stability diagram, specifically for V_b values below 10m/s and 15 m/s, respectively. Therefore, the amplitude spectra in Fig. B.6(b) and Fig. B.6(c) start at belt velocities V_b higher than these values. The numerical results also show that the stability diagram underestimates the size of the unstable region as the excitation frequencies rise, since they show friction-induced vibrations over a broader range of belt velocities.

The stability diagram in Fig. 5.8(a) shows that as ω_1 value increases, the instability region decreases, reaching its minimum when $\omega_1 = \Omega_e = 4$ rad/s. The numerical results

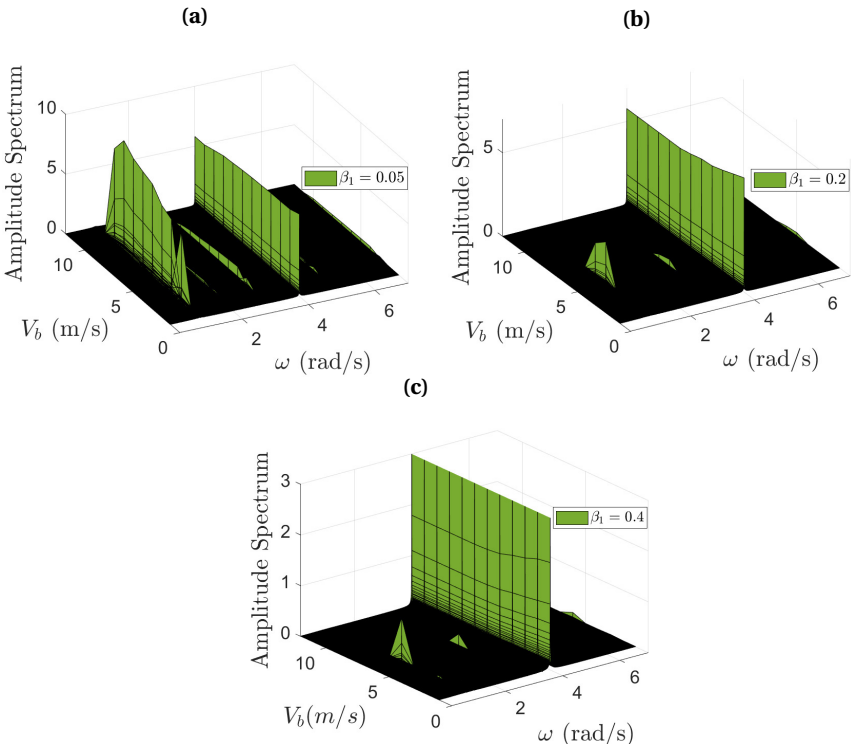

Figure B.4: Amplitude spectrum of the velocity $\dot{X}_1$: (a) $\beta_1 = 0.05$; (b) $\beta_1 = 0.2$; (c) $\beta_1 = 0.4$. The rest of the parameters as in Fig. 5.2.

confirm that as ω_1 increases from 0.3 rad/s in Fig. B.7(a) to 3 rad/s in Fig. B.7(b), the range of belt velocities exhibiting friction-induced oscillations narrows. At even higher ω_1 values, such as $\omega_1 = 12$ rad/s, no peak is seen in the amplitude spectrum, as shown in Fig. B.7(c), aligning with the stability diagram. Thus, there is good qualitative and quantitative agreement between the stability diagram and the numerical results.

Regarding the influence of ω_2^* , the stability diagram in Fig. 5.8(b) shows that varying ω_2^* slightly decreases the instability region. The amplitude spectra in Fig. B.8 show a good quantitative match to the stability diagram for $V_b > 8$ m/s. At lower belt velocities, the quantitative match deteriorates, as the reduction in the belt velocity ranges where friction-induced oscillations occur is more pronounced in the numerical results. This indicates that the stability diagrams overestimate the extent of the unstable region.

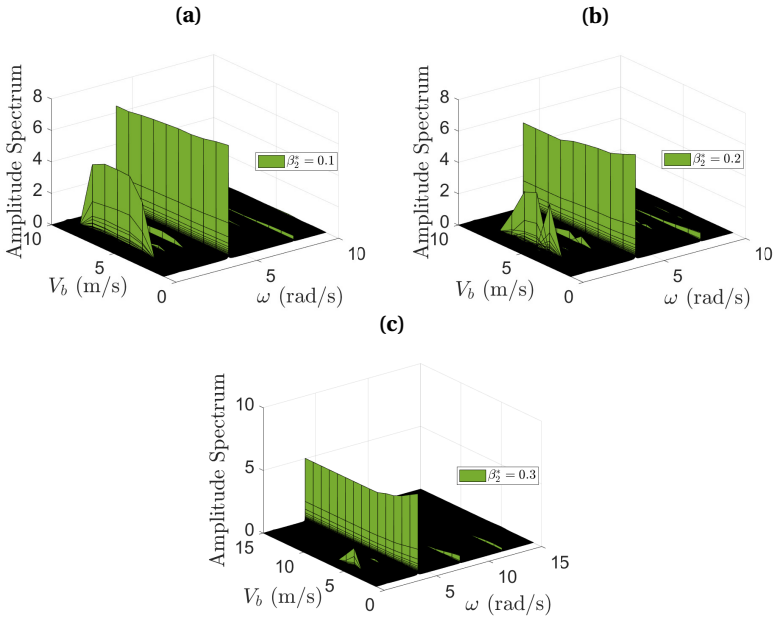

Figure B.5: Amplitude spectrum of the velocity $\dot{X}_1$: (a) $\beta_2^* = 0.1\frac{1}{\mathrm{m}^{5/4}}$; (b) $\beta_2^* = 0.2\frac{1}{\mathrm{m}^{5/4}}$; (c) $\beta_2^* = 0.3\frac{1}{\mathrm{m}^{5/4}}$. The rest of the parameters as in Fig. 5.2.

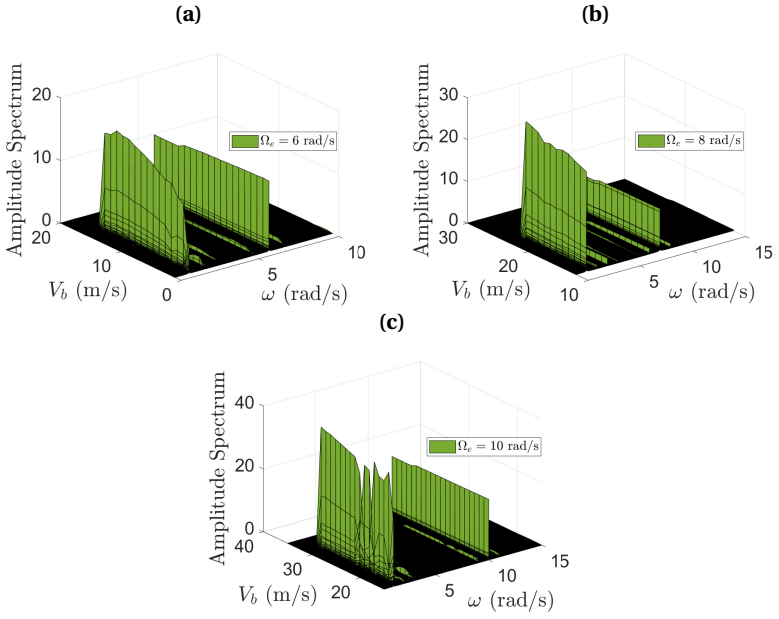

Figure B.6: Amplitude spectrum of the velocity $\dot{X}_1$: (a) $\Omega_e = 6$ rad/s; (b) $\Omega_e = 8$ rad/s; (c) $\Omega_e = 10$ rad/s. The rest of the parameters as in Fig. 5.2.

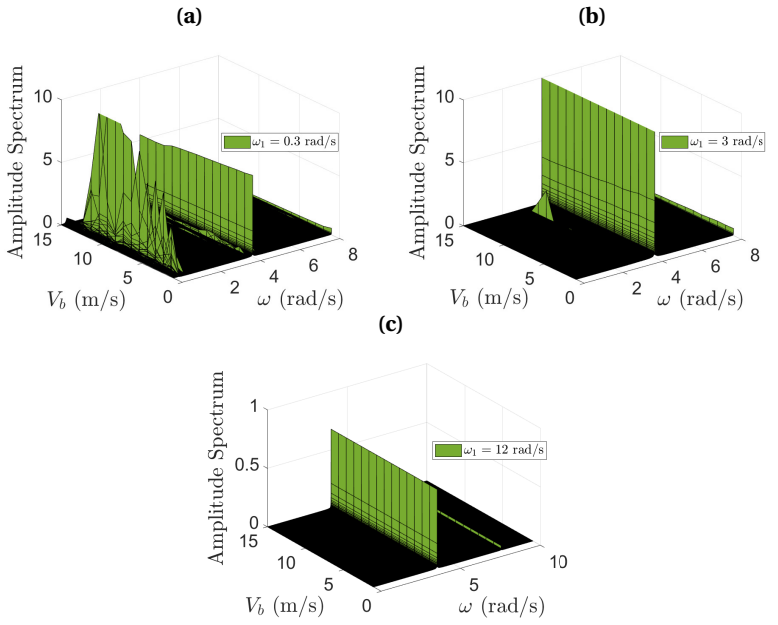

Figure B.7: Amplitude spectrum of the velocity $\dot{X}_1$: (a) $\omega_1 = 0.3\ \frac{\text{rad}}{\text{s}}$; (b) $\omega_1 = 3\ \frac{\text{rad}}{\text{s}}$; (c) $\omega_1 = 12\ \frac{\text{rad}}{\text{s}}$. The rest of the parameters as in Fig. 5.2.

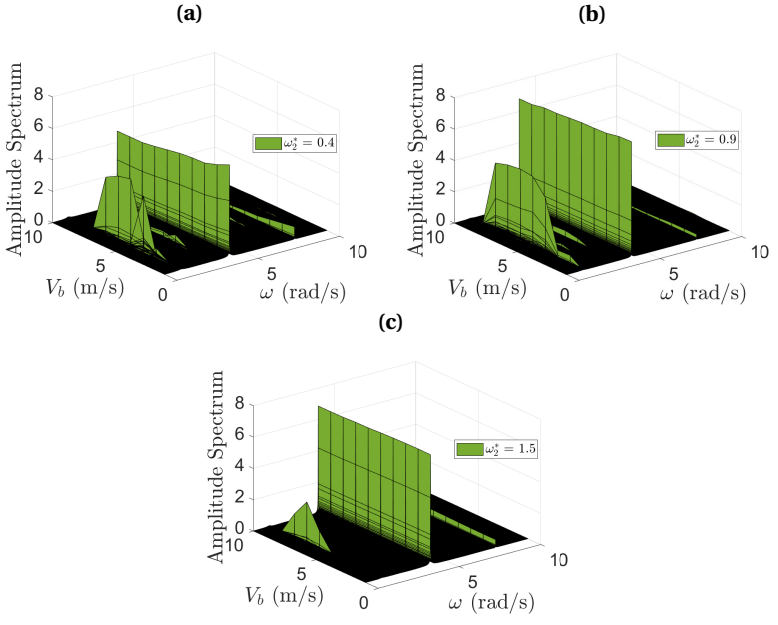

Figure B.8: Amplitude spectrum of the velocity $\dot{X}_1$: (a) $\omega_2^* = 0.4\ \frac{\text{rad}}{\text{m}^{1/4}\text{s}}$; (b) $\omega_2^* = 0.9\ \frac{\text{rad}}{\text{m}^{1/4}\text{s}}$; (c)$\omega_2^* = 1.5\ \frac{\text{rad}}{\text{m}^{1/4}\text{s}}$. The rest of the parameters as in Fig. 5.2.

C

C.1. GEOMETRICALLY NONLINEAR ROD

With reference to subsection 6.3.1, to ensure that the response of the rod adheres to the small deformation assumptions, the solutions obtained are compared to those derived considering a rod with geometric nonlinearity with x_c expression as in Eq. (6.4). For the geometrically nonlinear rod, the displacement-strain relation [2] and the strain-stress relation are given by

$$\varepsilon_x = \frac{\partial u}{\partial x} + \frac{1}{2}\left(\frac{\partial u}{\partial x}\right)^2, \quad \sigma_x = E\varepsilon_x. \tag{C.1}$$

Thus, the displacement-strain relation has an additional quadratic term. The equations of motion then become

$$\rho A\frac{\partial^2 u}{\partial t^2} + c_b\frac{\partial u}{\partial t} - EA\frac{\partial^2 u}{\partial x^2} - EA\frac{\partial u}{\partial x}\frac{\partial^2 u}{\partial x^2} + f\delta(x - x_c) = 0, \tag{C.2}$$

$$m\frac{d^2 u}{dt^2} + c\frac{du}{dt}s + ks = f, \tag{C.3}$$

Using the same dimensionless parameters as in Eq. (6.9), the dimensionless equation of motion are derived

$$\frac{\partial^2 u}{\partial t^2} + 2\beta_b r_w\frac{\partial u}{\partial t} - \left(\frac{r_\omega}{\pi}\right)^2\frac{\partial^2 u}{\partial x^2} - \left(\frac{r_\omega}{\pi}\right)^2\frac{\partial u}{\partial x}\frac{\partial^2 u}{\partial x^2} + f\delta(x - x_c) = 0, \tag{C.4}$$

$$\frac{d^2 u}{dt^2}s + 2\beta\frac{du}{dt} + s = r_m f, \tag{C.5}$$

The modal equations of the rod are derived using the same solution method as in subsection 6.3.1 and are solved numerically using the MATLAB solver ode23s.

In Fig. C.1, the results of the rod displacement u obtained using the equations of motion with (dashed orange line) and without (continuous blue line) geometric nonlinearity of the rod are presented for two different excitation frequencies. As shown in Fig. C.1(a) for $\Omega_e = 3$, the differences between the lines are negligible. The differences become more pronounced at higher time values for $\Omega_e = 6$, as shown in Fig. C.1(b). This case is particularly noteworthy since $\Omega_e = 6$ corresponds to the first natural frequency of the rod, leading to a higher response. Nevertheless, the maximum relative error in the responses

is approximately 6.7%, and this occurs only within a narrow time range. As a result, the error has no significant impact on the relative velocity and, consequently, on the average friction.

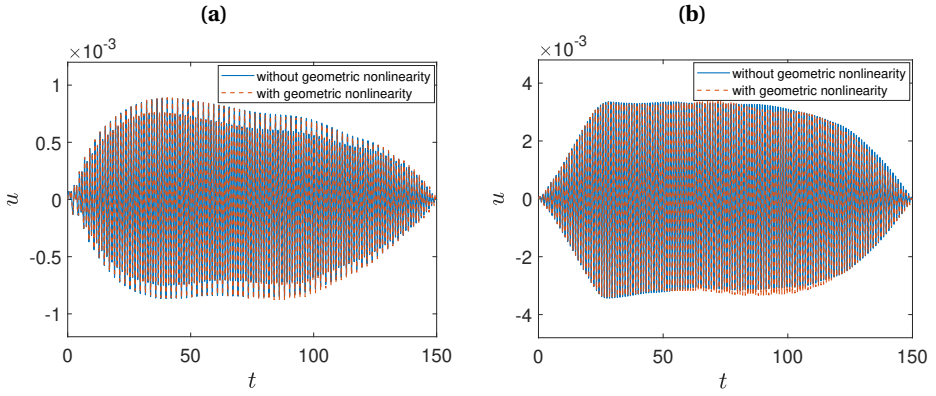

Figure C.1: Comparison of rod displacement u obtained using the equations of motion with (dashed orange line) and without (continuous blue line) geometric nonlinearity in the rod: (a) for excitation frequency $\Omega_e = 3$; (b) for excitation frequency $\Omega_e = 6$.

C.2. ROD DEFLECTION SHAPES

With reference to subsection 6.3.1, the deflection shapes of the rod are presented here to illustrate the rod's profile under localized harmonic loading and friction force. Figure C.2(a) shows the rod's profile for a mass at $x_c = 0.25$ with $v = 0$. This distortion of the

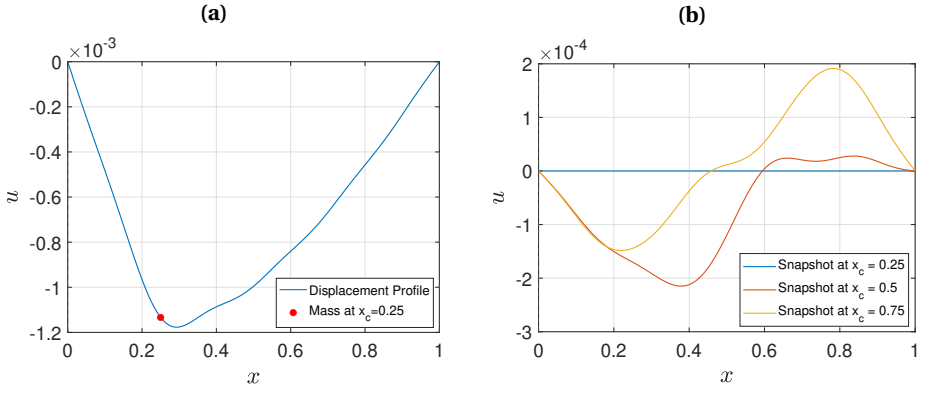

Figure C.2: Deflection shapes of the flexible rod: (a) mass oscillating at $x_c = 0.25$ ($v = 0, t = 100$, $\Omega_e = 4$); (b) moving mass with $v = 0.005$ at three spatial snapshots ($x_c = 0.25, 0.5, 0.75$) and $\Omega_e = 4$.

fundamental sine wave confirms that the mass influences the rod's response even without

translational motion. The displacement becomes zero at the supports, validating the fixed-fixed constraints.

Figure C.2(b) illustrates the rod profile during the moving mass scenario ($v = 0.005$) at snapshots where the mass reaches $x_c = 0.25$, $x_c = 0.5$, and $x_c = 0.75$. As the simulation begins at $x_c = 0.25$ (at $t = 0$), the rod is initially undeformed. For the subsequent instances, the moving load introduces a characteristic asymmetry, where the deformation peak is shown to lag slightly behind the mass position due to the system's travel history. The appearance of secondary oscillations indicates the excitation of higher harmonics. These profiles illustrate why friction modulation varies along the rod, as the changing response governs the relative velocity at the interface.

ACKNOWLEDGEMENTS

I believe that every meaningful achievement is the result of intelligence, hard work, some other things and a touch of fairy dust. I am happy to say I have received plenty of the last one, especially regarding the people I have worked and lived with over the last four years. Beginning with my supervisors, I have been fortunate to know **Karel** for almost nine years now, dating back to when I was a Master's student sitting in on his lectures. Like so many other students, I appreciated Karel —and yes, I was among those who voted for him as Teacher of the Year— not only for his willingness to teach and his desire to see us succeed, but for being approachable, genuinely caring, and supportive. These are the same qualities he brought to his roles as the chair of my thesis committee and as my PhD promoter. Thank you, Karel, for always being interested and involved throughout this entire process, for your enthusiasm, and for your ideas and feedback that were always constructive, prompt, and vital to my progress. Thank you also for your investment in my development as a researcher and for always wanting to celebrate my achievements.

Unlike my promoter, I did not know **Alessandro** before starting the PhD, so the amount of "fairy dust" sprinkled here was truly abundant. As I have jokingly told my friends whenever they asked how my PhD was going, having you as a supervisor felt like redemption for every challenge I have ever faced in my life (and there were a lot). As I struggle now to put my appreciation into words, I find myself amazed that I found such an ideal supervisor and mentor, someone I could talk to openly and wholeheartedly about research or any obstacle I encountered in academia and beyond. I am grateful for everything I have learned from you Alessandro; it has helped me grow both as a researcher and as a person. Thank you for the knowledge shared, the advice and motivation given, for truly caring about my progress during and after the PhD, for the conversations during coffee breaks, lunches, and dinners, conference attendances and travels. Thank you for all the laughs and the cries (on my part) where you had to act as my therapist, and for having to deal with my shenanigans in general (sorry!). While I am happy to complete this work, it is sad to no longer have you as my supervisor, though knowing we will continue on as friends makes it better. I want you to know that every success in my life will also be thanks to you (while every failure will be my own).

I would also like to thank the independent members of my doctoral committee, **Alain Le Bot**, **Michaël Wiertlewski**, **Norbert Hoffmann**, and **Peter Steeneken**, for taking the time to read my thesis, for their valuable comments, and for their willingness to participate in the defense. Your insights helped shape the final version of this work, significantly enhancing its quality and clarity.

My thanks go to the **MPS family**, both the original and V2.0. Starting with **Luca**, my first officemate, with whom I monitored nonlocalized nonlinearities and studied acoustic levitation (a joke only Luchino will understand), learned valuable Italian phrases, and drew and scribbled on the whiteboard that I still don't dare to erase. Continuing with **Yi**,

who taught me during one of our yearly summaries each December, where we discussed what we did and didn't do during the year, that we don't always have to regret not doing more, and that what we did was enough. Thank you for always encouraging my gym visits despite my frequent failures, for being the only one who knows my favorite manga genre, and for the promise of my future visit to China (which I cannot delve into further here).

To **Theo**, who blessed us with his youthful energy, to **Christos**, one of the smartest and kindest people I have had the chance to share an office with, and to **Jan**, for providing the calmest vibes just by being in your presence. To **Sijia**, my current, longest-standing, and loveliest officemate, who makes me happy every time I enter the office; thank you for showing me the best bubble tea places, sharing a love for fragrances, and for going to great lengths to bring me a bag from China. To **Nora**, for all the deep conversations we shared about self-care and self-learning; and to **Nicholas**, one of the kindest people I have ever met, who does so much for others behind the scenes (I'm thinking of the archery course and the science fair, Nicholas). I feel grateful for all the coffee breaks, dinners, games, town visits, and dance-offs I shared over the years with all of you, and, of course, for simply sitting and working alongside one another.

My thanks also go to someone who was unofficially part of the MPS family, and much more than that to me, **Julie**, with whom I felt comfortable enough to cry while sipping Aperol on the streets of Italy. I am grateful for all the memories we made across different countries, offices, libraries, Bijenkorfs, and Skins; for the courses we started but never finished at X; and for our not-so-successful gym efforts but very successful, heart-opening talks. I would also like to thank **Avni**, one of the strongest and smartest people I have met, for all the conversations we shared, for the business we will one day create (manifesting), and for bearing with me despite my shortcomings (Avni knows what I mean).

Additionally, I would like to thank my postdoc supervisor, **Peter**. Even though I have only gotten to know him better since finishing my four-year PhD, he is already continuing my streak of wonderful, supportive, and caring supervisors. Speaking of mentors and supervisors, I would also like to thank my professor from my Bachelor studies, **Yalin Arici**, who is part of the reason I started this PhD. He was likely the first person I shared the position with, and just as he did during my undergraduate years, he supported, encouraged, and motivated me to apply for this journey. *Teşekkür ederim, Hocam!*

I would like to extend my thanks to everyone on the ES and faculty PhD councils for your time, dedication, and the sense of community you helped build. In particular, I want to thank **Angeliki**, **Yuanchen**, **Julie**, **Shozab**, **Michele**, **Ali**, **Abishek**, **Giorgio**, **Max**, **Luuk**, **Roberto**, **Til**, **Ian**, **Weilun**, **Lisa**, **Sijmen**, **Wei**, **Nirvana**, and **Entela** for your commitment and collaboration, and for the wonderful conversations we shared during our meetings, dinners, and drinks. I would also like to thank the Visibility team, especially **Trayana**, **Angelique**, **Angeliki**, **Willem**, and **Lukas**, for our fun meetings and for our shared work in highlighting and celebrating our department's achievements.

I am grateful to the people with whom I have shared these four years outside the walls of the CITG building, even though our connections first formed within those same walls almost nine years ago during our Master's studies. My heartfelt thanks to **Anmol** and **Sanya**, **Andrew** and **Anqi** (and of course Hanhan), **Knut**, **David**, and **Guili**; I could easily write long paragraphs for each of you. While the Netherlands is not the first country I have lived in abroad, it is the first place where I met such a diverse international community.

Thanks to all of you, I realized there is hope and that the world is a beautiful place. Thank you for all the moments we have shared, for letting me be part of your families and cultures across different countries, and for keeping me hopeful about the world.

The same thanks go to the artistic, cool, and caring **Hazal**, whom I have known and shared memories with for thirteen years since starting my studies in Turkey. Finally, to my lifelong best friend **Fjona**, whom I have known since birth and with whom I have shared every achievement and failure ever since.

Many thanks to **Felicia**, **Maurice**, **Anastasia**, **Jim**, and **Jaap** for all the fun dinners and incredible food, especially the meals cooked by Jim and the Ukrainian desserts from Anastasia. I also want to thank you for the board games; while I don't usually like them, I have always enjoyed playing with all of you (except, perhaps, for the times when I lose). Thank you for the karaoke nights, the different city and country visits, and the playful bickering (mostly with Jaap).

To **Jord**, my partner and the person who has seen me in every form, from the moments I walked through our front door after work, whether I was happy or sad, excited or annoyed, full of energy or completely exhausted, complaining or celebrating. Thank you for being there through it all. I will not say that I couldn't have made it through these four years without you, but I can certainly say that without you, they would have been much sadder, emptier, and far less successful. Your advice and opinions (even the ones I don't always agree with), your goofiness, your silliness, and your cuteness overload have made this journey so much more fulfilling. Your desire to celebrate my achievements even more than I do, the peace and love you provide, your genuine interest in the people I work with, and even your relatively deep understanding of my research have made this all worthwhile. You aren't the fairy dust, Jord; you are the fairy. My thanks also go to your amazing and supportive parents and brother, **Els**, **Tjabe**, and **Victor**, for being my family here in the Netherlands. *Dank jullie wel!*

My deepest gratitude goes to my big family, my entire **fisi**: my uncles, aunts, and close and distant cousins. To everyone who raised me up, to those that I helped raise up and those who grew up alongside me, *faleminderime pa fund.*

Vëllai im i vogël, **Adli**, you grew up so fast that instead of me being the supportive big sister, you became the person I know I can turn to if everything falls apart, whether emotionally or financially (no pressure!). Every success of mine is truly thanks to you; since we were children, despite all the dreams I have had and changed, pursued or not, the only consistent one has been to be an inspiring big sister, someone you can hopefully feel proud of and look up to. *Babi im*, **Adriatik**, still the wisest person I know, the one who always advocated for a good education, and didn't necessarily advocate for a PhD, thank you for letting me feel "rebellious" by going for it anyway. *Mami im*, **Dritë**, the most optimistic, motivated, and full of energy person I have ever known, regardless of the situation, and the one who didn't even advocate for Civil Engineering (mother knows best), thank you for always trying to pass that energy on to me and for being my constant source of strength. **To the three of you**, needless to say, none of the wonderful people I have met, the experiences I have had, the studies I have pursued, and the life I have lived would have been possible without your support, your teachings, your love, and your tremendous sacrifices.

To my grandparents, *gjyshërit e mi*, **Sefigjer**, **Nevrus**, **Servete**, and **Hekuran**, who could

attend at most four years of school, who lived their lives entirely for their children and grandchildren. Completing this PhD is, through and through, thanks to you and in honor of your memory, especially yours, *Nëne*.

And finally, to myself.

CURRICULUM VITAE

Enxhi Sulollari

07-06-1995 Born in Pogradec, Albania.

ACADEMIC EXPERIENCE

2013–2017 Bachelor of Science
Civil Engineering
Middle East Technical University, Turkey

2017–2019 Master of Science
Structural Engineering
Delft University of Technology, the Netherlands
Thesis: Study of nonlinear dynamic soil response to harmonic excitation using semi-analytical and numerical methods
Supervisors: A. Faragau, F. Pisano, K. N. van Dalen and A. Metrikine

2021–2025 Doctor of Philosophy
Delft University of Technology, the Netherlands
Dissertation: Vibration-induced friction force modulation
Promoters: A. Cabboi and K. N. van Dalen

2025–2026 Postdoc researcher
Delft University of Technology, the Netherlands

PROFESSIONAL EXPERIENCE

2019–2021 Structural Engineer
Advanced Technology and Research
Haskoning, the Netherlands

LIST OF PUBLICATIONS

JOURNAL PUBLICATIONS

1. E. Sulollari, K.N. van Dalen, and A. Cabboi. "On the effect of planar dynamics and resonance on vibration-induced friction modulation". In: *International Journal of Non-Linear Mechanics* 187 (2026), p. 105362
2. E. Sulollari, K. N. van Dalen, and A. Cabboi. "Vibration-induced friction modulation for an oscillator moving on an elastic rod". In: *International Journal of Solids and Structures* 321 (2025), p. 113572
3. E. Sulollari, K. N. van Dalen, and A. Cabboi. "Parametric excitation and friction modulation for a forced 2-DOF system". In: *Nonlinear Dynamics* (2025), pp. 12793–12816
4. E. Sulollari, K. N. van Dalen, and A. Cabboi. "Vibration-induced friction modulation for a general frequency of excitation". In: *Journal of Sound and Vibration* 573 (2024), p. 118200
5. J. Zhang, E. Sulollari, A. B. Fărăgău, F. Pisanò, P. van der Male, M. Martinelli, A. V. Metrikine, and K. N. van Dalen. "Harmonic Balance Method for the Stationary Response of Finite and Semi-infinite Nonlinear Dissipative Continua: Three Canonical Problems". In: *Advanced Structured Materials* 139 (2021), pp. 255–274